National Library of Canada
Bibliothèque nationale du Canada

Canadian Theses Service
Service des thèses canadiennes

Ottawa, Canada
K1A 0N4

NOTICE

The quality of this microform is heavily dependent upon the quality of the original thesis submitted for microfilming. Every effort has been made to ensure the highest quality of reproduction possible.

If pages are missing, contact the university which granted the degree.

Some pages may have indistinct print especially if the original pages were typed with a poor typewriter ribbon or if the university sent us an inferior photocopy.

Reproduction in full or in part of this microform is governed by the Canadian Copyright Act, R.S.C. 1970, c. C-30, and subsequent amendments.

AVIS

La qualité de cette microforme dépend grandement de la qualité de la thèse soumise au microfilmage. Nous avons tout fait pour assurer une qualité supérieure de reproduction.

S'il manque des pages, veuillez communiquer avec l'université qui a conféré le grade.

La qualité d'impression de certaines pages peut laisser à désirer, surtout si les pages originales ont été dactylographiées à l'aide d'un ruban usé ou si l'université nous a fait parvenir une photocopie de qualité inférieure.

La reproduction, même partielle, de cette microforme est soumise à la Loi canadienne sur le droit d'auteur, SRC 1970, c. C-30, et ses amendements subséquents.

NL-339 (r. 88/04) c

Canada

ELECTRON PARAMAGNETIC RESONANCE AND OPTICAL-ABSORPTION STUDIES ON Cu^{2+} IMPURITY IN SINGLE/POLY CRYSTALS OF HYDRATED MONOPYRAZINE ZINC SULPHATE, (CADMIUM, NICKEL, MAGNESIUM)-AMMONIUM SULPHATE, AND MAGNESIUM ACETATE

Chunzheng Wang

A Thesis
in
The Department
of
Physics

Presented in Partial Fulfillment of the Requirements
for the Degree of Doctor of Philosophy at
Concordia University
Montreal, Quebec, Canada

March 1990

ISBN 0-315-64677-2

ABSTRACT

Electron Paramagnetic Resonance and Optical-Absorption Studies on Cu^{2+} Impurity in Single/Poly Crystals of Hydrated Monopyrazine zinc sulphate, (Cadmium, Nickel, Magnesium)-Ammonium Sulphate, and Magnesium Acetate

CHUNZHENG WANG, Ph.D.
Concordia University, 1990

X-band electron paramagnetic resonance (EPR) measurements on both, single crystal and polycrystalline, specimen of Cu^{2+}-doped monopyrazine zinc sulphate trihydrate, cadmium ammonium sulphate hexahydrate, and magnesium ammonium sulphate hexahydrate have been made at room, and below and above room temperatures, as well as on single-crystal specimen of Cu^{2+}-doped nickel ammonium sulphate hexahydrate and magnesium acetate tetrahydrate at room and lower temperatures. The Cu^{2+} spin-Hamiltonian parameters, including the quadrupole interaction tensor, are estimated from EPR line positions by the use of appropriate least-square fitting. The room temperature optical-absorption spectrum of magnesium acetate tetrahydrate, recorded in the 190-820 nm wavelength range, is exploited to study the crystal-field and charge-transfer transitions of the Cu^{2+} ion.

The principal values of the $\tilde{g}^2$- and $\tilde{A}^2$- tensors for Cu^{2+}-doped monopyrazine zinc sulphate trihydrate indicate that the Cu^{2+} ion is situated at a site of octahedral symmetry with orthorhombic distortion in this lattice. The EPR data indicate the occurrence of both the static and

dynamic Jahn-Teller effects over the temperature range of investigation, the transition from static to dynamic Jahn-Teller effect occurring at 334 ± 1 K.

The temperature dependence of the principal values of $\tilde{g}$ matrix for Cu^{2+}-doped cadmium ammonium sulphate hexahydrate and magnesium ammonium sulphate haxahydrate are explained by taking into account the pseudo Jahn-Teller effect experienced by the $Cu(H_2O)_6^{2+}$ complex. The differences in the energies of the three Jahn-Teller configurations of the $Cu(H_2O)_6^{2+}$ complex in the two hosts have been estimated.

The EPR spectra of Cu^{2+}-doped paramagnetic host nickel ammonium sulphate haxahydrate are considerably different from those in the isostructural diamagnetic hosts cadmium and magnesium ammonium sulphate haxahydrate. No Cu^{2+} hyperfine structure could be observed in the former at room and liquid-nitrogen temperatures; even at liquid-helium temperature the hyperfine structure was not well resolved, it could only be observed at lower Zeeman magnetic fields. It can be attributed to the dipole-dipole and exchange interactions between the paramagnetic impurity ion Cu^{2+} and the host Ni^{2+} ions, which broaden the EPR lines.

Both the room temperature optical-absorption and EPR data of magnesium acetate tetrahydrate are used to estimate the core polarization contribution (K_0) and the molecular orbital coefficients for the Cu^{2+} ion doping magnesium acetate tetrahydrate.

Acknowledgements

The author is indebted deeply to Professor S.K. Misra for suggesting the research problems presented in this thesis. He expresses sincere appreciation for his continued availability and active guidance, necessary for the completion of this thesis.

The author is grateful to Concordia University for the David J. Azrieli and the Concordia University Graduate Fellowships. He acknowledges thankfully receiving partial financial support from Dr. Misra's NSERC Grant (No. A4485). He is grateful for the teaching assistanship received from the Department of Physics, and the research assistanship received from the action-structure grant, offered by the Government of Quebec to Dr. Misra along with nine other professors (Responsable Administratif: Professor C. Langford).

The author is thankful to the Concordia University Computer Center for providing their facilities to analyze the data, and to the Department of Chemistry for allowing him to record the optical-absorption spectrum.

Finally, the author expresses his appreciation to his wife, Shiying Pan, and his sons Zhi and Xi for their patient and continued encouragement in all of his endeavors.

TABLE OF CONTENTS

SYMBOLS

cal.	calculated
CASH	cadmium ammonium sulphate haxahydrate
DPPH	α, α′ diphenyl-β-picryl hydrazyl
D_q	octahedral crystal field parameter
D_s	second-order tetragonal field parameter
D_t	fourth-order tetragonal field parameter
E_0	energy level of the ground state
E_o, E_a, E_b, E_c, E_s	the five energy levels for Cu^{2+} ion in an orthorohmbic symmetry; E_o for $d_{3z^2-r^2}$, E_a for d_{xy}, E_b and E_c for overlaps of d_{xz} and d_{yz}, E_s for $d_{x^2-y^2}$
E_n	energy level of excited state
E_g, $\mathcal{E}_g$	electronic & vibrational functions of an octahedral complex
ΔE_i	calculated energy difference between energy levels participating in resonance
EPR	electron paramagnetic resonance
g_e	free electron g factor
g_n	nuclear g factor
h	Planck's constant
$\hbar$	$h/2\pi$
$\mathcal{H}$	Hamiltonian operator
$\mathcal{H}_{cf}$	crystal field Hamiltonian
$\mathcal{H}_{hf}$	hyperfine-structure-energy Hamiltonian

$\mathcal{H}_{Q}$	quadrupole-energy Hamiltonian
$\mathcal{H}_{ss}$	spin-spin-energy Hamiltonian
$\mathcal{H}_{Ze}$	electronic Zeeman energy Hamiltonian
$\mathcal{H}_{Zn}$	nuclear Zeeman energy Hamiltonian
h.f.	hyperfine
JT	Tahn-Teller
JTE	Tahn-Teller effect
k	Boltzmann constant
K_o	core polarization contribution
L	electronic orbital-angular momentum
$\hat{L}_x, \hat{L}_y, \hat{L}_z$	electronic orbital-angular momentum operators
$\hat{L}_-$	$\hat{L}_x - i\hat{L}_y$
$\hat{L}_+$	$\hat{L}_x + i\hat{L}_y$
LSF	least-squares fitting
MASH	magnesium ammonium sulphate haxahydrate
MAT	magnesium acetate tetrahydrate
MO	molecular orbital
NASH	nickel ammonium sulphate haxahydrate
obs.	observed
PZST	monopyrazine zinc sulphate trihydrate
Q_ε, Q_θ	distortion modes of an octahedron
R_e	distance between ligands in the equatorial plane and the central metal ion
R_a	distance between ligands located upon the axis perpendicular to the equatorial plane and the central metal ion

$\langle r^2 \rangle$	mean-square-power radius of the Cu^{2+} ion orbital
$\langle r^4 \rangle$	mean-fourth-power radius of the Cu^{2+} ion orbital
$\langle r^{-3} \rangle$	average of the inverse-cube radius of the Cu^{2+} ion
SHP	spin Hamiltonian parameter
UV	ultraviolet
Ze	nuclear charge
α_i; $i = 0,1,2$	MO coefficients of antibonding levels $3b_{1g}$, $2b_{2g}$, $2e_g$ for the Cu^{2+} ion$^+$ ion
α'_i; $i = 1,2$	MO coefficients of antibonding levels $2b_{2g}$ and $2e_g$ for the Cu^{2+} ion
β_i; $i = 0,1,2$	MO coefficients of antibonding levels $3b_{1g}$, $2b_{2g}$, $2e_g$ for the ligandsgands
β'_i; $i = 1,2$	MO coefficients of antibonding levels $2b_{2g}$ and $2e_g$ for the ligands
Δ	$= 10D_q$
Δ_1, Δ_2	energies of $d_{xy} \longleftrightarrow d_{x^2-y^2}$ and $d_{xz,yz} \longleftrightarrow d_{x^2-y^2}$ d-d transitions
Δ'_1, Δ'_2	energies corresponding to the charge-transfer transitions $1b_{2g} \longleftrightarrow 3b_{1g}$ and $1e_g \longleftrightarrow 3b_{1g}$
$\delta_{1,2}$	energy-splitting between potential valleys 1 and 2
$\delta_{1,3}$	energy-splitting between potential valleys 1 and 3
σ_i	effective weight factor

λ	spin-orbital coupling constant (= ξ_M) of the metal ion
μ	coefficient of p electron orbital of oxygen ligands in the $3b_{1g}$ configuration
μ_B	Bohr magneton
μ_n	nuclear magneton
ν_1	Klystron frequency
ξ	constant for Cu^{2+} (= 2/21)
ξ_l	spin-orbital coupling constant of ligands
ξ_M	spin-orbital coupling constant (= λ) of the metal ion
ω	frequency of lattice phonons
$\|0>$	electronic ground-state wave function
$\|n>$	electronic excited-state wave function

CHAPTER I

INTRODUCTION

A large number of investigations on electron paramagnetic resonance (EPR) of Cu^{2+} ion have been reported [39]. Bleaney et al. [8] and Penrose [45] were, respectively, the first to discover the fine structure in undiluted copper Tutton salts, and the hyperfine (h.f.) structure in magnetically-dilute salts by means of EPR. Soon after, Bleaney et al. [9, 10, 11] made the interpretation of EPR spectra of both the allowed and forbidden h.f. transitions of the Cu^{2+} ion in magnetically-diluted salts, and they estimated the relative strengths of the quadrupole interactions from their EPR data.

The paramagnetism of the Cu^{2+} ion, which has $3d^9$, or $3d^1$-hole, configuration, arises from a single unpaired electron spin, because the orbital angular momentum is quenched by the crystal field, i.e., the matrix elements of $\hat{L}_x$, $\hat{L}_y$, $\hat{L}_z$ between the ground state wavefunctions are zero. On account of such a simple configuration of the outer electron shell, the ground state of the Cu^{2+} ion in different local symmetries has been investigated in much detail. The ground state of the free Cu^{2+} ion is $^2D_{5/2}$. This five-fold degenerate state is split by the ligand field. When a Cu^{2+} ion is in a crystal field, often, the ground orbital levels are not split by the crystal field, e.g., in crystal fields with cubic, octahedral, or tertahedral symmetry. On the other hand, they are incompletely split in crystal fields with orthorhombic, or lower, symmetries. The resulting two- or three- fold degenerate (partially degenerate) orbitals can be, further, split by a Jahn-Teller (JT) distortion. This fact makes EPR a powerful tool to observe the Jahn-Teller (JT) effect. The ground-state wave function of the Cu^{2+} ion in crystal lattices depends upon the local symmetry of the Cu^{2+}-complex, which can be predicted by the crystal-field theory, or more accurately, by the molecular-orbital theory. The principal values of the $\tilde{g}$ matrix, which can be directly obtained from EPR data, provide information on the symmetry of the Cu^{2+}-complex. In the case of the $Cu(H_2O)_6^{2+}$ complex, with an orthorhombic symmetry, the principal axes of the orthorhombic $\tilde{g}$ tensor are within experimental errors, oriented parallel to the three inequivalent Cu-O bond pairs [53]. The ground-state wave function is strongly influenced by the anisotropy of the $\tilde{g}$ matrix. Thus, a study of ligand field, which determines the ground-state wave function, is essential in the understanding of EPR data of Cu^{2+}-doped single crystals. This thesis is focused on the Cu^{2+}-complex, its ground state wave function and the JT effect, as studied from the EPR measurements in the X-band (≈ 9.5 GHz) microwave range.

The following EPR studies of the Cu^{2+} ion are included in this thesis:

(i) EPR measurements on a single crystal of Cu^{2+}-doped manopyrazine zinc sulphate trihydrate (hereafter PZST), $Zn(C_4H_4N_2)SO_4.3H_2O$, were performed over an extended temperature range (4.2-375 K). Existence of three physically equivalent, but magnetically inequivalent, Cu^{2+} complexes was confirmed. The principal values of the $\tilde{g}$ and $\tilde{A}$ matrices indicated that the Cu^{2+} ion experienced an octahedral symmetry with an orthorhombic distortion in PZST. The data were used to deduce the occurrence of both the static and dynamic JT effects over the temperature range of investigation, the transition from static to dynamic JT effect occurring at 334 ± 1 K.

(ii) The EPR measurements of both single and polycrystalline specimens of Cu^{2+}-doped cadmium ammonium sulphate hexahydrate $Cd(NH_4)_2(SO_4).6H_2O$ (hereafter CASH), and magnesium ammonium sulphate haxahydrate $Mg(NH_4)_2(SO_4).6H_2O$ (hereafter MASH), have been made over the temperature range from 4.2 K to a temperature above the room temperature. The hyperfine forbidden transitions of Cu^{2+} were observed only at 4.2 K for CASH, while only at 77 and 4.2 K for MASH. In these two diamagnetic hosts, the temperature dependence of the principal values of the $\tilde{g}$ matrix are explained by taking into account the pseudo JT effect experienced by the $Cu(H_2O)_6^{2+}$ complex. The differences in the energies of the three JT configurations of the $Cu(H_2O)_6^{2+}$ complex have been estimated.

(iii) EPR measurements of Cu^{2+}-doped nickel ammonium salphate haxahydrate $Ni(NH_4)_2(SO_4).6H_2O$ (hereafter NASH), have been made at 295, 77, and 4.2 K. Only the Cu^{2+} fine structure was observed in these EPR spectra. At liquid-helium temperature the hyperfine structure of Cu^{2+} was observed only at the lower magnetic field values. It can be attributed to the dipole-dipole and exchange interactions between the paramagnetic impurity Cu^{2+} ion and the host Ni^{2+} ions, which result in decreasing the spin-lattice relaxation time. The principal values of the $\tilde{g}$ matrix show that Cu^{2+}ion is in a complex with orthorhombic symmetry at 295, 77, and 4.2 K.

(iv) EPR measurements on a single-crystal sample of Cu^{2+}-doped magnesium acetate tetrahydrate $Mg(CH_3COO)_2.4H_2O$, (hereafter MAT), have been made at 295, 77 and 4.2 K. The optical-absorption spectrum study of Cu^{2+}-doped MAT single crystal at room temperature shows that there are six absorption bands in the wavelength range 190 to 820 nm. They have been assigned as d-d transition and charge-transfer transition bands. These provide the energy levels of the Cu^{2+} ion in a tetragonal symmetry. Further, the coefficient of molecular orbital and the core polarization contribution, K_o, were estimated.

(v) The estimation of the spin-Hamiltonian parameters, i.e., the $\tilde{g}$ and $\tilde{A}$ matrices, for all single-crystal specimens, and the quadrupole-interaction matrix $\tilde{Q}$ in the case of Cu^{2+}-doped $Cd(NH_4)_2(SO_4).6H_2O$ and $Mg(NH_4)_2(SO_4).6H_2O$ at 4.2 K, have been made from EPR line positions by the use of a rigorous least-square fitting (LSF) procedure. The principal values of the $\tilde{g}$ matrix for a polycrystalline specimen in the case of Cu^{2+}-doped CASH are estimated from the average EPR line positions from the EPR spectra recorded three times at the same temperature.

The organization of the thesis is as follows. The experimental arrangement is described in chapter II. The spin Hamiltonian of the Cu^{2+} ion is discussed in chapter III. Chapter IV deals with the theoretical calculations, and the estimation of spin Hamiltonian parameters from EPR data. The details of EPR measurements and experimental results are given in chapter V. In chapter VI is included the optical-absorption study of Cu^{2+}-doped magnesium acetate tetrahydrate. The details of observations of Jahn-Teller effects of Cu^{2+} ions in single-crystals, and the estimation of molecular-orbital coefficients of Cu^{2+} in magnesium acetate tetrahydrate are described in chapter VII and VIII, respectively. The conclusions are summarized in chapter IX. The copies of the three published papers "*Low and high-temperature electron paramagnetic resonance studies on* Cu^{2+}*-doped monopyrazine zinc sulphate trihydrate single crystal: observation of the Jahn-Teller effect*", "*EPR and optical-absorption studies of* Cu^{2+}*-doped* $Mg(CH_3COO)_2.4H_2O$ *single crystal*", and "*EPR of* Cu^{2+}*-doped cadmium ammonium sulphate: Pseudo-Jahn-Teller effect*", as well as the LSF computer program, for the estimation of the $\tilde{g}^2$, $\tilde{A}^2$ and $\tilde{Q}$ tensors, are included in Appendices I and II, respectively.

CHAPTER II

EXPERIMENTAL ARRANGEMENT

All the EPR spectra discussed in the present thesis were recorded on a homodyne X-band Varian V4502 spectrometer. A block diagram of the spectrometer is shown in Figure II.1.

The microwive bridge is Varian V-4500-42 X-band microbridge. The magnet is Varian V3900 series 12" low-impedance electromagnet, along with a Bruker B-MN50/200 power supply. The magnetic field is controlled by a Bruker field controller B-H15. Magnetic field measurements were made with a Bruker (B-NM20) gaussmeter, with an accuracy of 0.001 gauss. A small amount of α, α' diphenyl-β-picryl hydrazyl (DPPH), for which $g = 2.0036 \pm 0.0002$, was used as a reference to check the accuracy of the magnetic field values.

The EPR spectrometer is equipped with a 100 kHz field modulation for measurements at room and above-room temperatures, and a 400 Hz field modulation for measurements at liquid-nitrogen and liquid-helium temperatures.

The cavity arm of the spectrometer is of rectangular type, resonating in the TE_{102} mode, at a frequency of approximately 9.5 GHz at room temperature. It is designed for use inside a commercial cryostat; the top flange is sealed off for evacuation purposes by means of a mica sheet. The cavity arm is evacuated in order to reduce condensation

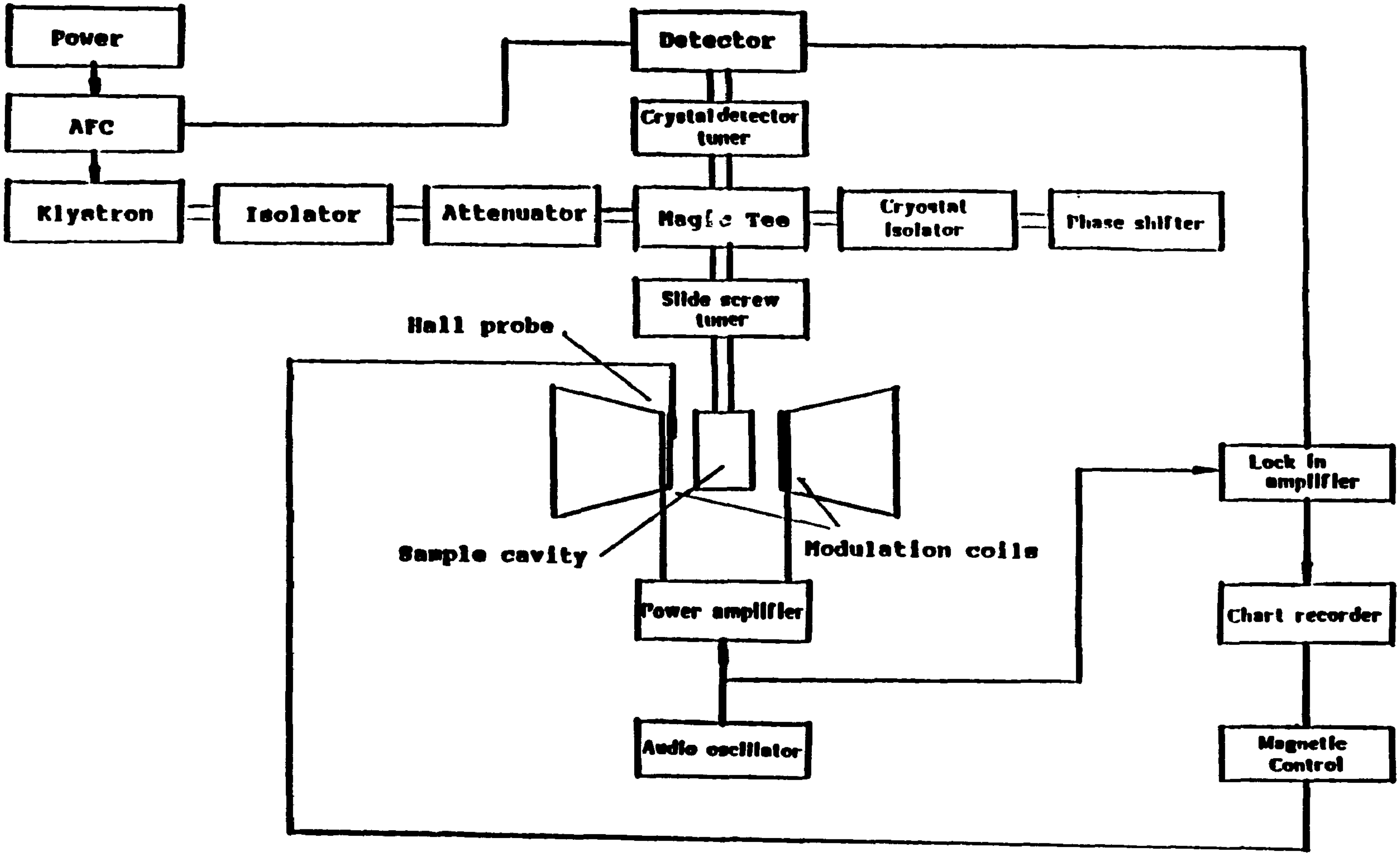

Figure II.1. Block diagram of the X-band spectrometer that would, otherwise, disturb the tuning of the sample cavity at low temperatures. Full description of the metallic variable-temperature cryostat is given in Ref. [52].

The temperature is varied by the use of a heater resistor inside the low-temperature cryostat. The temperatures in the liquid-nitrogen and liquid-helium temperature ranges were determined by measuring the resistances of the platinum and germanium resistors, respectively, using appropriate calibration charts. For high-temperature measurements, a Varian Associates variable-temperature controller (model No. E4540), attached to a microprocessor digital thermometer, manufactured by Omega (model No. 870), was employed.

The following details apply to all the crystals discussed in this thesis. The angular variations of EPR line positions were recorded for the orientation of $\vec{B}$, the external magnetic field, in three mutually perpendicular planes at all temperatures of measurement for all single-crystal specimens. The spectra were recorded for the orientation of $\vec{B}$ at every 4° interval at room and high temperatures, and at every 5° interval at liquid-nitrogen and liquid-helium temperatures. The experimental laboratory frame (x,y,z) was defined as follows. The largest flat plane of the specimen was chosen to be the zx plane. The direction of $\vec{B}$, in this plane, for which the positions of the hyperfine (h.f.) lines were at the minimum values of $\vec{B}$, was chosen to be the z axis, while the direction at 90° to this direction was defined the x axis. The y axis is, of course, perpendicular to the zx plane. For EPR measurements in the zy and xy planes at room temperature the single-crystal specimen was rotated about the x and z axes, respectively, keeping the direction of $\vec{B}$ fixed. At liquid-nitrogen and liquid-helium temperatures, when the low-temperature csyostat was used, $\vec{B}$ was rotated about the x and z axes keeping the single-crystal specimen fixed.

Optical-absorption spectrum was recorded on a Hewlett-Packard spectrometer (model 8452A) in the wavelength range 190-820 nm. The absorption spectrum and the wavelengths of the absorbed peaks, were directly recorded using a microcomputer.

CHAPTER III

SPIN HAMILTONIAN OF THE Cu^{2+} ION

The energy of an atom, or radical, containing unpaired electrons and nuclei with non-zero spins, can be expressed in terms of the Hamiltonian operator. The EPR spectra of Cu^{2+} ion (electron spin S = 1/2, nuclear spin I = 3/2 for each of the 69.09%-abundant ^{63}Cu and the 30.91%-aboundant ^{65}Cu isotopes) can be fitted to the spin Hamiltonian [48]:

$$\mathcal{H} = \mathcal{H}_{Ze} + \mathcal{H}_{ss} + \mathcal{H}_{hf} + \mathcal{H}_{Zn} + \mathcal{H}_{Q} \ . \qquad \text{(III.1)}$$

The first term, $\mathcal{H}_{Ze}$, in eq. III.1 is the electronic Zeemann term, of the explicit form

$$\mathcal{H}_{Ze} = \mu_B \vec{B}.\tilde{g}.\vec{S} \ , \qquad \text{(III.2)}$$

where the $\tilde{g}^2$ tensor is symmetric, μ_B the Bohr magneton, and $\vec{B}$ is the external Zeeman field.

In the second term

$$\mathcal{H}_{ss} = \vec{S}.\tilde{D}.\vec{S} \ , \qquad \text{(III.3)}$$

represents the spin-spin interaction called the zero-field splitting term. It is valid only for those special cases where there are present Cu^{2+}-Cu^{2+} pairs with effective spin S = 1, or four Cu^{2+} ions aggregated with effective spin S =

2. In the present cases the Cu^{2+} ions present $S = 1/2$. In that case the spin-spin interaction is zero.

The third term in eq. III.1 is the hyperfine (h.f.) interaction term. It can, in general, be expressed as

$$\mathcal{H}_{hf} = \vec{S}.\tilde{A}.\vec{I} + \sum_{\imath} \vec{S}.\tilde{A}_{\imath}.\vec{I}_{\imath} \, , \qquad \text{(III.4)}$$

where the h.f. interaction energy $\tilde{A}^2$ and $\tilde{A}^2_{\imath}$ tensors are symmetric, and the summation over $\imath$ covers the interaction with N ligand nuclei. The first term in eq. III.4 is due to the interaction of the unpaired electron spin with the nuclear spin of the Cu^{2+} ion, called h.f. interaction, while the second term is due to the interaction of the unpaired electron spin of Cu^{2+} ion with its ligand nuclear spins, called the ligand-h.f. or superhyperfine, interaction. The superhyperfine structure was not observed in the present work.

The fourth term in eq. III.1 expresses the nuclear-Zeeman term

$$\mathcal{H}_{Zn} = -\sum_{\imath} \mu_n g_{n\imath} \tilde{H}.\vec{I}_{\imath} \, , \qquad \text{(III.5)}$$

where μ_n is the nuclear magneton. This term is, usually, not taken into account to interpret EPR data, for, its energy is rather small, being about $0\text{-}10^{-3}$ cm^{-1}.

The last term in eq. III.1 stands for the energy of the interaction of the nuclear electric-quadrupole moment with the electric-field gradient

$$\mathcal{H}_Q = \vec{I}.\tilde{Q}.\vec{I} \ , \qquad \text{(III.6)}$$

where the quadrupole energy tensor $\tilde{Q}$ is symmetric and traceless, i.e.,

$$Q_{ij} = Q_{ji} \qquad \text{(III.7)}$$

and

$$Q_{xx} + Q_{yy} + Q_{zz} = 0 \ . \qquad \text{(III.8)}$$

Thus, there are only five, rather than six, independent components of the $\tilde{Q}$ tensor.

The components of $\tilde{g}^2$, $\tilde{D}$, $\tilde{A}^2$, and $\tilde{Q}$ tensors are the spin Hamiltonian parameters (SHP). The problem of interpreting EPR spectra consists of (i) identification of EPR lines corresponding to the various transitions, (ii) calculation of SHP, and (iii) calculation of other physical quantities of interest depending upon SHP, e.g., the molecular-orbital coefficients.

CHAPTER IV

SPIN HAMILTONIAN PARAMETERS

IV.1. Estimation of SHP from EPR data

The evaluation of SHP from EPR data of Cu^{2+}-doped single crystals is important for further analysis. The perturbation expressions for the eigenvalues of the spin Hamiltonian are used to express the theoretical dependence of resonant line positions on SHP. Thus, the EPR line positions can be used to estimate SHP.

The computer evaluation of SHP by the use of least-square fitting (LSF) technique is widely used. For the case of Cu^{2+} the eigenvalues of the spin Hamiltonian can be calculated by second-order perturbation [32, 33]. Using these, one can estimate the individual values of all SHP, provided that EPR line positions for allowed transitions ($\Delta M = \pm 1$, $\Delta m = 0$; where M, m are, respectively, the electron and nuclear magnetic quantum numbers) corresponding to several orientations of the external magnetic field are simultaneously fitted in a rigorous LSF. In the estimation of parameters by LSF, the "chi-squared" value (χ^2) is defined as [30, 31]

$$\chi^2 = \Sigma\ (|\Delta E_i| - h\nu_i)^2/\sigma_i^2\ , \qquad \text{(IV.1)}$$

where ΔE_i is the calculated energy difference between the energy levels participating in resonance, ν_i is the klystron frequency, h is the Planck's constant and $\sigma_\imath$ is an effective weight factor. The index $\imath$ covers all the resonant line positions (data points) used simultaneously in the fitting.

The elements of the $\tilde{Q}$ tensor can be evaluated from the forbidden h.f. line positions, employing another LSF procedure, using the computer program, which was used to calculate the $\tilde{Q}$ tensor in the case of VO^{2+}-doped $K_2C_2O_4.H_2O$ [34], considering only the forbidden h.f. transitions $\Delta M = \pm1$, $\Delta m = \pm1$, modified to take into account the forbidden h.f. transitions $\Delta M = \pm1$, $\Delta m = \pm2$ for the present cases. In this program, the previously-determined values of the $\tilde{g}^2$ and the $\tilde{A}^2$ tensors are used as input constants, only the components of the $\tilde{Q}$ tensor are varied. The $\tilde{Q}$ tensor was determined by inputting all the observed forbidden h.f. transition line positions, observed for $\vec{B}$ in three mutually perpendicular planes zx, zy and xy, in the LSF program. Diagonalization of the $\tilde{Q}$ tensor yields the principal values of the $\tilde{Q}$ tensor, as well as its direction cosines with respect to the principal axes of the $\tilde{g}^2$ tensor.

IV.2. Theoretical calculation of SHP

Perturbation theory is usually applied to calculate the SHP. For the calculation of the $\tilde{g}$ matrix, the spin-orbit interaction of the electron is considered as a perturbation. On the other hand, the electron-nuclear spin interaction and the nuclear-spin-orbital interaction are considered as perturbations for the calculation of the h.f. matrix $\tilde{A}$.

Owing to the particular electron configuration of the Cu^{2+} 3d-shell, these calculations are relatively simple.

First, the ground state wavefunction of the Cu^{2+} ion is determined from the local symmetry, then the components of the $\tilde{g}$ and $\tilde{A}$ matrices are calculated by the use of perturbation theory. The expressions for the components of the $\tilde{g}$ and $\tilde{A}$ matrices, denoting the wavefunctions of the ground and excited states as $|0>$ and $|n>$, are as follows [1, 29]:

$$g_{pq} = g_e - 2\bar{\Lambda}_{pq} \tag{IV.2}$$

and

$$A_{pq} = -P[K_o\delta_{pq} + 3\xi\ell_{pq} + \bar{\Lambda}_{pq} - 3\xi\bar{\Lambda}'_{pq}] \tag{IV.3}$$

In eq. IV.2 g_e (= 2.0023) is the free electron g value, $P = 2g_n\mu_B\mu_n<r^{-3}>_M = 0.036\ cm^{-1}$ [24] and $\xi = 2/21$ [1] for Cu^{2+} ion, where g_n and $<r^{-3}>_M$ are, respectively, the nuclear g factor and the average of the inverse-cube radius of the Cu^{2+} ion, K_o is the core-polarization contribution.

The various quantities appearing on the right-hand side of eq. IV.2 and IV.3 are defined as follows:

$$\ell_{pq} = \frac{1}{2} <0|L_pL_q + L_qL_p|0> - 2\delta_{pq}\ , \tag{IV.4}$$

$$\Lambda_{pq} = \frac{\sum_n{}' <0|L_p|n><n|T_q|0>}{E_0 - E_n}\ , \tag{IV.5}$$

$$\bar{\Lambda}'_{pq} = -\frac{i}{2}\sum_{rt}\varepsilon_{ptr}\sum_{n}{}' \frac{\langle 0|T_r|n\rangle\langle n|L_tL_q + L_qL_t|0\rangle}{E_0 - E_n} . \qquad \text{(IV.6)}$$

In eqs. IV.3 p, q, t, and r are the coordinates, each one can be chosen as x, y, z; L_i is the *i*th component of the electronic orbital angular momentum; E_0 and E_n the energy level of the ground state and the excited state n, respectively. $T = \xi_M L$ when the calculation is based on the crystal-field model, on the other hand, when the ligand ions are taken into account by the use of the molecular orbital theory $T = \xi_M L + \Sigma\xi_l \ell$. (Here ξ_M and ξ_l are, respectively, the spin-orbital coupling constants of the central metal ion (Cu^{2+}) and its ligand ions in the complex.) In this way, the expressions for the principal values of the $\tilde{g}$ and $\tilde{A}$ matrices consist of the core-polarization constant (K_o) and the molecular-orbital coefficients, which can be estimated by solving the equations using the values of the SHP estimated from EPR data, and the energy splitting due to the crystal field, estimated from the optical-absorption data.

CHAPTER V

EPR MEASUREMENTS AND EXPERIMENTAL RESULTS

V.1. Cu^{2+}-doped $Zn(C_4H_4N_2)SO_4.3H_2O$ (PZST) single crystal

The crystal structure of PZST has been reported by Tenhunen [57] to be triclinic (space group P1); the unit cell dimensions are a = 10.734 Å, b = 4.427 Å, c = 6.927 Å, $\alpha = 121.15^\circ$, $\beta = 82.57^\circ$, $\gamma = 104.02^\circ$. There is one formula unit per unit cell (Z = 1), only. So for no structure-analysis data have provided the exact positions of Zn^{2+} ions in the lattice of PZST crystal. That the water molecules are not structural water, can be concluded from experimental data: the infra red spectrum of PZST reveals that there is no band that confirms water coordination in PZST [20]; as well, the thermogravimetric curve [44] indicates that the three water molecules of PZST are rapidly removed at 115°C.

Cu^{2+}-doped PZST single crystals were grown by slow evaporation of an aqueous solution, consisting of stoichiometric amounts of pyrazine $C_4H_4N_2$ and $ZnSO_4.7H_2O$, to which was added a sufficient quantity of $CuSO_4.5H_2O$ so that there was one Cu^{2+} ion for every 100 Zn ions. The grown crystals look like parallelepipeds.

EPR spectra of Cu^{2+}-doped single crystals of PZST were recorded over an extended temperature range (4.2-375 K) [37]. The EPR spectra for Cu^{2+}-doped PZST at liquid-nitrogen and liquid-helium temperatures are quite similar. This can be seen from Figure V.1.1, which exhibits

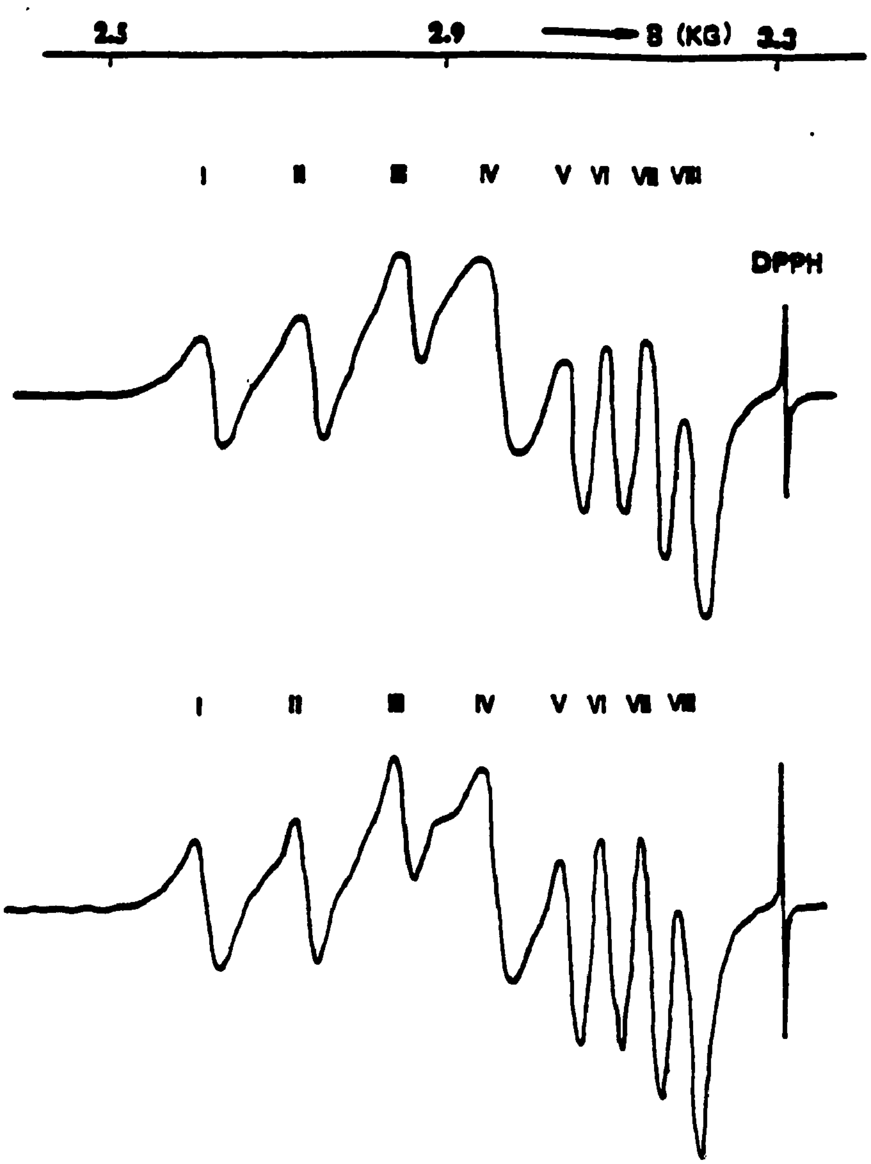

Figure V.1.1. EPR spectra of Cu^{2+}-doped $Zn(C_4H_4N_2)SO_4.3H_2O$ (PZST) at low temperatures. The upper spectrum is recorded at liquid-nitrogen temperature, while the lower at liquid-helium temperature for $\vec{B}$ at 75° from the z axis in the zy plane.

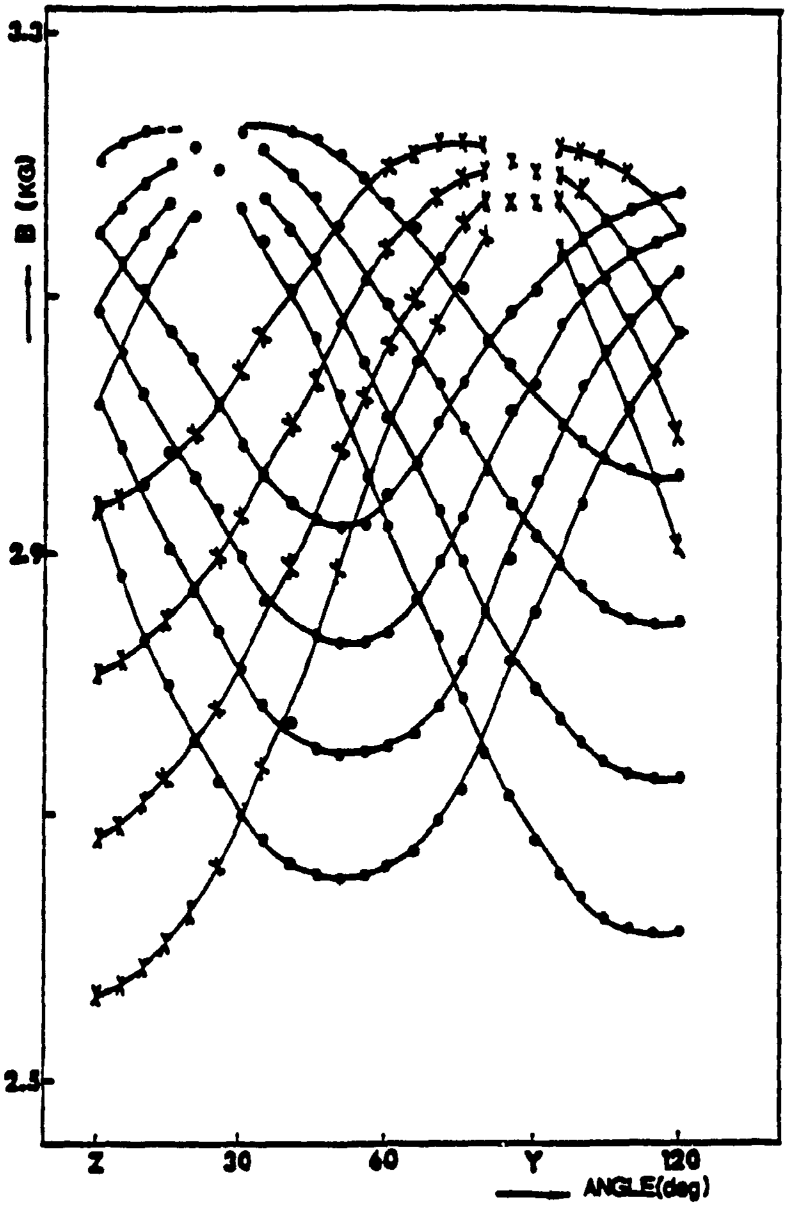

Figure V.1.2. Angular variation of Cu^{2+} EPR spectra in $Zn(C_4H_4N_2)SO_4.3H_2O$ (PZST) at 4.2 K for the orientation of $\vec{B}$ in the zx plane. The solid lines connect data points, observed for the same transition. Empty circles, solid circles, and crosses represent three different sets of spectra, corresponding to the three magnetically inequivalent Cu^{2+} ions.

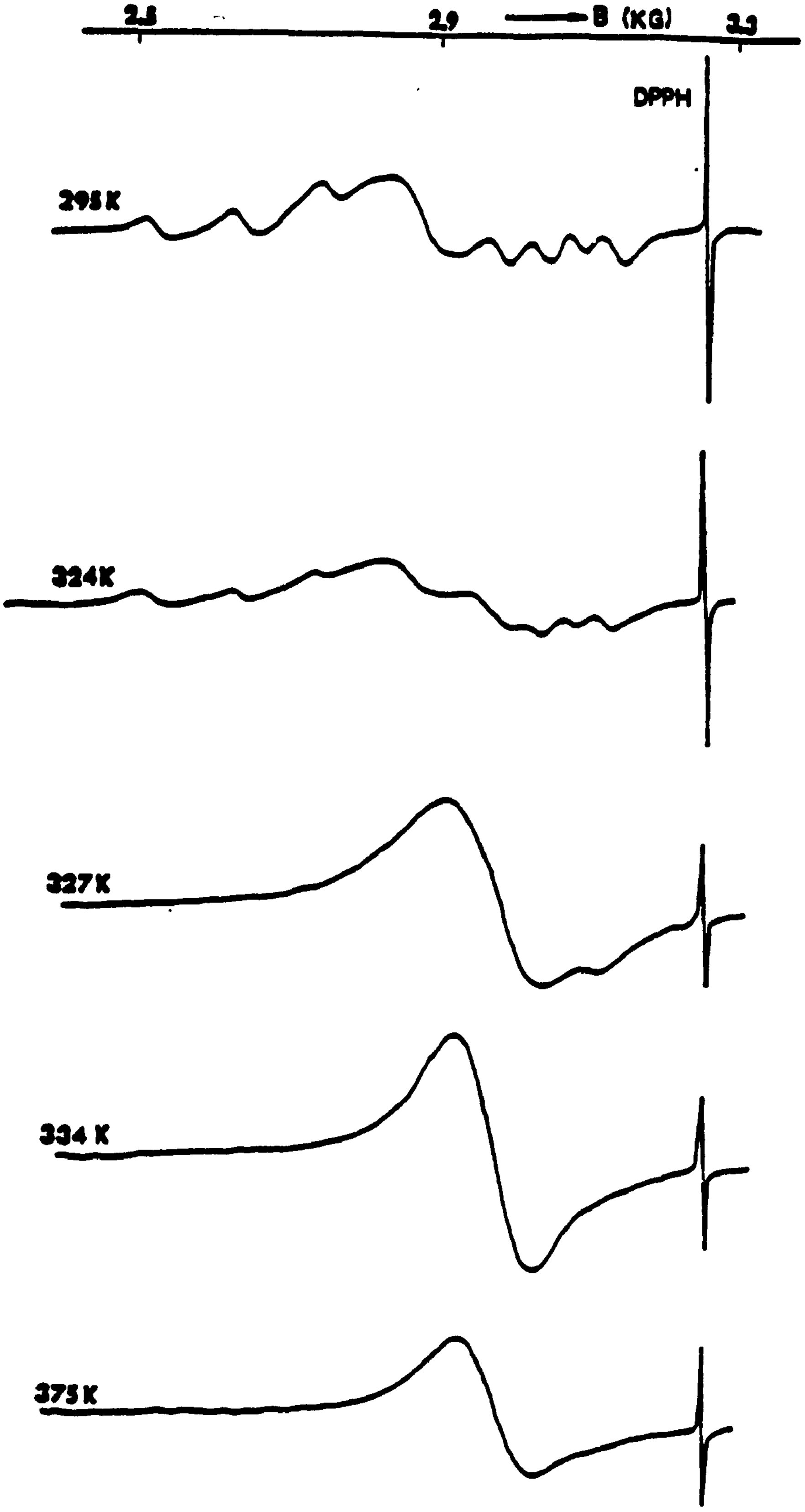

Figure V.1.3. EPR spectra of Cu^{2+}-doped $Zn(C_4H_4N_2)SO_4 \cdot 3H_2O$ (PZST) for $\vec{B}$ at 75° from the z axis in the zy plane at 295, 324, 327, 334, and 375 K.

the EPR spectrum for the magnetic-field orientation at 75° from the z-axis in the zy plane, at liquid-nitrogen and liquid-helium temperatures. These spectra are not much different from that at room temperature. It can be seen by comparing the spectra in Figure V.1.1 with those of Figure V.1.3, which displays spectra with the same orientation of the external magnetic-field at 295 K, that they consist of three sets of four h.f. lines, typical of the Cu^{2+} ion. The lines corresponding to the less-abundant isotope of the Cu^{2+} could not be clearly seen. The three sets of h.f. lines belong to the three physically equivalent, but magnetically inequivalent Cu^{2+} complexes; because their variations of EPR line positions with $\vec{B}$ (angular variations) are different from each other. This can be seen from Figure V.1.2, exhibiting the angular variations of spectra in the zy plane at liquid-helium temperature. The peak-to-peak first derivative linewidths do not change significantly, as one lowers the temperature from room- to liquid-helium temperature. They are 25, 22, 22, 34, 26, 25, 26, 21 gauss, respectively, for the eight clearly-resolved EPR lines, in order of increasing $\vec{B}$, as seen from Figure V.1.1; one actually sees only eight clearly-resolved single EPR lines (indicated as I, II, III, IV, V, VI, VII, VIII). The lowest-field four lines belong to the Cu^{2+} ion occupying site I, while the highest-field four lines belong to the Cu^{2+} ion occupying site II; the four lines belonging to Cu^{2+} ion occupying site III overlap the lowest-field line of site

I and the three highest-field lines of site II, i.e., they overlap the lines IV, V, VI, VII.

The spin Hamiltonian appropriate to the present sample is

$$\mathcal{H} = \mu_B \vec{B}.\tilde{g}.\vec{S} + \vec{S}.\tilde{A}.\vec{I} \ , \qquad \text{(V.1.1)}$$

where the notations have been defined in chapter II.

The principal values of the $\tilde{g}$ and $\tilde{A}$ matrices were evaluated at various temperatures and listed in Table V.1.1. It is noted here that the principal values of the $\tilde{g}$ and $\tilde{A}$ matrices are the same, within experimental error, for the three magnetically inequivalent Cu^{2+} complexes. The direction cosines of the principal axes of the $\tilde{g}$ and $\tilde{A}$ matrices are listed in Tables V.1.2 - V.1.4 at 295, 77 and 4.2 K respectively.

It is seen from Table V.1.1 that the principal values of the $\tilde{g}$ and $\tilde{A}$ matrices remain the same, within experimental error, over the temperature range 77-295 K, while Tables V.1.2 and V.1.3 reveal that the principal axes of the $\tilde{g}$ and the $\tilde{A}$ matrices remain coincident over this temperature range. Although the principal values of the $\tilde{g}$ and the $\tilde{A}$ matrices at 4.2 K, as given in Table V.1.1, were found to be the same as those at room and liquid-nitrogen temperatures, within experimental error, the principal axes of the $\tilde{A}$ matrix are now no longer coincident with those of the $\tilde{g}$ matrix, as seen from Table V.1.4.

TABLE V.1.1. Principal values of the $\tilde{g}$ and $\tilde{A}$ matrices (square roots of the principal values of the $\tilde{g}^2$ and $\tilde{A}^2$ tensors, respectively for Cu^{2+} in $Zn(C_4H_4N_2)SO_4.3H_2O$ (PZST) at different temperatures (T). The $\tilde{g}$ principal values are dimensionless, while the $\tilde{A}$ principal values (A_1,A_2,A_3) are in GHz. (The values in Refs. b, and c are in Gauss.) The labelling is such that $g_3 > g_1 > g_2$.

Temperature	g_3	g_1	g_2	A_3	A_1	A_2	Ref.
295 K	2.3875	2.1924	2.0205	0.324	0.181	0.104	a
295 K	2.414	2.216	2.109	107 G	66 G	41 G	b
77 K	2.3876	2.1923	2.0200	0.326	0.182	0.105	a
77 K	2.42			110 G			c
4.2 K	2.3868	2.1929	2.0190	0.328	0.185	0.105	a
334 K	2.191	2.191	2.191				a

a. Present work.

b. Krishnan, Ref. [25], for a single-crystal specimen.

c. Krishnan, Ref. [25], for a polycrystalline specimen.

TABLE V.1.2. Direction cosines of the principal axes of the $\tilde{g}$ and $\tilde{A}$ matrices of Cu^{2+} in $Zn(C_4H_4N_2)SO_4.3H_2O$ (PZST) at 295 K. (The same as those of the $\tilde{g}^2$ and $\tilde{A}^2$ tensors, respectively.) The direction cosines of the $\tilde{g}^2$ tensor are given with respect to the laboratory axes (x,y,z), while those of the $\tilde{A}$ matrix are expressed relative to (x',y',z'), the principal axes of the $\tilde{g}^2$ tensor.

	Direction cosines of the $\tilde{g}^2$ tensor		
	z	x	y'
Z'	0.4510	0.2010	0.8696
X'	-0.6486	0.7431	0.1647
Y'	-0.6131	-0.6383	0.4655
	Direction cosines of the $\tilde{A}^2$ tensor		
	z'	x'	y'
Z"	0.9999	0.0062	0.0140
X"	-0.0064	0.9998	0.0191
Y"	-0.0103	-0.0192	0.9998

Table V.1.3. Same details as in the caption of Table V.1.2. The values are those found at 77 K.

Direction cosines of the $\tilde{g}^2$ tensor

	z	x	y
Z′	0.4192	0.2720	0.8662
X′	-0.6498	0.7562	0.0770
Y′	-0.6341	-0.5952	0.4937

Direction cosines of the $\tilde{A}^2$ tensor

	z′	x′	y′
Z"	0.9999	0.0062	0.0100
X"	-0.0064	0.9999	0.0156
Y"	-0.0099	-0.0158	0.9998

Table V.1.4. Same details as in the caption of Table II. The values are those found at 4.2 K.

Direction cosines of the $\tilde{g}^2$ tensor

	z	x	y
Z'	0.3649	0.2468	0.8978
X'	-0.6372	0.7692	0.0476
y'	-0.6788	-0.5895	0.4379

Direction cosines of the $\tilde{A}^2$ tensor

	z'	x'	y'
Z"	0.9969	0.0788	0.0058
X"	-0.0698	0.9126	-0.4028
Y"	-0.3700	0.4011	0.9153

As the temperature is raised above the room temperature, the EPR spectra were found to be significantly different from those at room and lower temperatures. The h.f. lines of Cu^{2+} become broader and weaker with increasing temperature. Finally, at 334 ± 1 K, only one single broad, isotropic line, is observed. Both the position of the line centre and the linewidth become independent of the orientation of the external magnetic field. There is no significant change in the linewidth as the temperature is raised to 375 K, the temperature at which the dehydration of the crystal begins to takes place. Upon lowering the temperature again below 334 K, after having raised the temperature above 334 K, the same features of the EPR spectra were obtained, as those observed before. This was repeated three times, and each time the features of the EPR spectra were recaptured. Figure V.1.3 shows the temperature variation of EPR spectra of Cu^{2+}-doped PZST over the range 295-374 K for the external magnetic field orientation at 75° from the z-axis in the zy plane. The single isotropic line corresponds to $g = 2.191$, as listed in Table V.1.1.

EPR study of Cu^{2+}-doped PZST has been previously reported by Krishnan [25] at 295 K on a single crystal specimen, and at 77 K on a polycrystalline specimen. His EPR spectra also revealed the existence of three magnetically different sites for Cu^{2+}, although there is only one substitutional site available to Cu^{2+} in the unit cell of PZST. The principal values of the $\tilde{g}$ and the $\tilde{A}$

matrices reported by Krishnan [25] are also included in Table V.1.1 for comparison.

V.2. Cu^{2+}-doped $Cd(NH_4)_2(SO_4).6H_2O$ (CASH) single and poly crystals

The crystal structure of CASH is monoclinic, with the space group $P_{21/a}$ [42]; the unit-cell dimensions at 300 K are: a = 9.43 Å, b = 12.82 Å, c = 6.29 Å, β = 106°52′. There are two formula units per unit cell (Z = 2); each Cd^{2+} ion is surrounded by six water molecules. The bond lengths between the central ion Cd^{2+} and the ligand atoms are 2.298 Å, 2.297 Å, and 2.241 Å for Cd-O(7)(H_2O), Cd-O(8)(H_2O), and Cd-O(9)(H_2O), respectively; while the bond angles are 89.1° for O(7)-Cd-O(8), 92.6° for O(7)-Cd-O(9), and 91.3° for O(8)-Cd-O(9). These data indicate that the Cd^{2+} ion in CASH is approximately in a compressed tetragonally-distorted octahedral crystal field, as shown in Figure V.2.1.

Cu^{2+}-doped CASH single crystal were grown by slow evaporation of an aqueous solution, consisting of stoichiometric amounts of $3CdSO_4.8H_2O$ and $(NH_4)_2SO_4$, to which was added a sufficient quantity of $CuSO_4.5H_2O$, so that there was one Cu^{2+} ion for every 100 Cd^{2+} ions.

The EPR spectra of Cu^{2+}-doped CASH single crystal were reported at 295, 77, and 4.2 K [38]. The spectra were found to be quite different from each other in their profiles, as seen from Figure V.2.2, which exhibits EPR spectra for the orientation of the Zeeman field ($\vec{B}$) at 10° from z-axis in

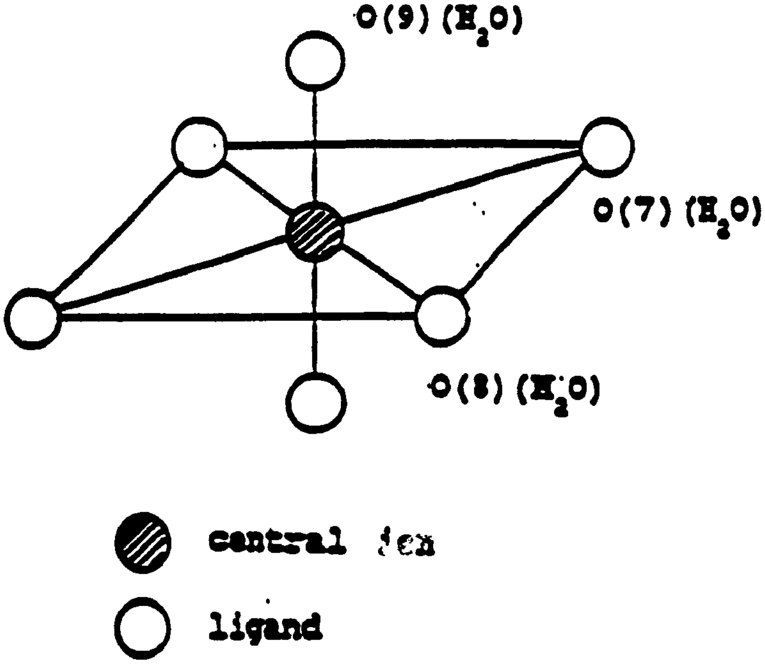

Figure V.2.1. Relationship of the oxygens to bivalent atoms in the structure of $M(NH_4)_2(SO_4)_2 \cdot 6H_2O$, M = Cd, Cu, Mg, Ni (After Refs. [12, 28, 40, 41, 42]) the zx plane. The spectrum at 295 K consists of two broad lines, which indicate the presence of two physically equivalent, but magnetically inequivalent Cu^{2+} complexes in the unit cell of CASH. At 77 K these two broad lines split, due to the Cu^{2+} h.f. interaction, into two sets of tetrads due to the more abundant isotope ^{63}Cu; the lines corresponding to the less-abundant isotope ^{65}Cu could not be clearly seen. At 4.2 K some satellite lines, corresponding to the h.f. forbidden transitions, were also observed.

The EPR spectra of Cu^{2+} ion in CASH are fitted to the following spin Hamiltonian:

$$\mathcal{H} = \mu_B\vec{S}.\tilde{g}.\vec{B} + \vec{S}.\tilde{A}.\vec{I} + \vec{I}.\tilde{Q}.\vec{I} - \mu_n\vec{I}.\tilde{g}_n.\vec{B} , \qquad (V.2.1)$$

where the notations have been defined in chapter II.

The estimation of the principal values and direction cosines of the $\tilde{g}$ and the $\tilde{A}$ matrices show that the directions of the principal axes of the $\tilde{g}$ matrix did not change with temperature, the principal axes of the $\tilde{A}$ matrix were coincident with those of the $\tilde{g}$ matrix at liquid-nitrogen and liquid-helium temperatures, within experimental errors. The principal values of the $\tilde{g}$ and the $\tilde{A}$ matrices at various temperatures are listed in Table V.2.1. Table V.2.2 gives the direction cosines of the principal axes of the $\tilde{g}$ and the $\tilde{A}$ matrices.

The evaluation of the elements of the $\tilde{Q}$ tensor was accomplished by the use of the another LSF computer program,

Table V.2.1. Principal values of the $\tilde{g}$ and $\tilde{A}$ matrices (square roots of the principal values of the $\tilde{g}^2$ and $\tilde{A}^2$ tensors, respectively), and the $\tilde{Q}$-tensor for Cu^{2+} in the $Cd(NH_4)_2(SO_4).6H_2O$ (CASH) single crystal specimen at different temperatures. The principal $\tilde{g}$ values are dimensionless, while the principal values of the $\tilde{A}$ matrix and the $\tilde{Q}$ tensor are in GHz.

Temperature	$g_{z'}$	$g_{y'}$	$g_{x'}$	$A_{z''}$	$A_{y''}$	$A_{x''}$	$Q_{z''}$	$Q_{y''}$	$Q_{x''}$	Ref.
295K	2.3373	2.2111	2.0712							a
295K	2.331	2.202	2.073							b
77 K	2.3613	2.1721	2.0522	0.333	0.074	0.151				a
77 K	2.355	2.172	2.054	0.333	0.078	0.157				b
4.2K	2.4290	2.1594	2.0513	0.335	0.077	0.156	0.013	-0.012	-0.001	a

a Present work.

b Data from Ref. [50].

Table V.2.2. Direction cosines of the $\tilde{g}$, $\tilde{A}$ matrices (the same as those for the $\tilde{g}^2$, $\tilde{A}^2$ tensors), and those of the $\tilde{Q}$ tensor for Cu^{2+} in the $Cd(NH_4)_2(SO_4).6H_2O$ (CASH) single-crystal specimen at 4.2 K. The principal axes of the $\tilde{g}$ matrix are expressed with respect to the laboratory axes (x,y,z), defined in Sec. 3.1. The principal axes of the $\tilde{A}$ matrix are coincident with those of the $\tilde{g}$ matrix, and the principal axes of the $\tilde{Q}$ tensor are expressed relative to (x′,y′,z′), the principal axes of the $\tilde{g}$ matrix.

	z	x	y
$g_{z'}$	0.996	0.091	-0.022
$g_{x'}$	-0.042	0.227	-0.973
$g_{y'}$	-0.084	0.970	0.230

	z′	x′	y′
$Q_{z''}$	0.970	0.242	0.032
$Q_{x''}$	-0.195	0.848	-0.493
$Q_{y''}$	-0.147	0.472	0.869

described in chapter IV. There were only six forbidden transition lines observed in the best-resolved EPR spectrum. At liquid-helium temperature, the allowed and forbidden line positions for any orientation of the external magnetic field, $\vec{B}$, were calculated using the SHP evaluated previously, in order that the observed h.f. forbidden transition lines could be identified. Both the allowed and forbidden transition-line positions for $\vec{B}$ at 10° from the z-axis in the zx plane for the set at lower magnetic fields are indicated in Figure V.2.2. It is clear that the two remaining forbidden transitions lines, not clearly resolved, lie extremely close to the allowed h.f. lines. The principal values of the $\tilde{Q}$ tensor are listed in Table V.2.1, while the direction cosines of its principal axes are included in Table V.2.2.

In order to study the temperature dependence of the principal g-values the EPR spectra of a CASH polycrystalline specimen were recorded in the temperature range 4.2 - 354 K. Some of these are plotted in Figure V.2.3. As can be seen from Figure V.2.3, a single, broad EPR line is observed at high temperatures, at about T > 120 K, which consists of three components, corresponding to the three principal values g_{zz}, g_{yy} and g_{xx} [48]. At low temperatures, at about T < 120 K, the component corresponding to g_{zz}, lying at the lowest values of the magnetic field exhibits h.f. structure, while the h.f. structure corresponding to the other two components (g_{xx} and g_{yy}) remains unresolved, even at 4.2 K.

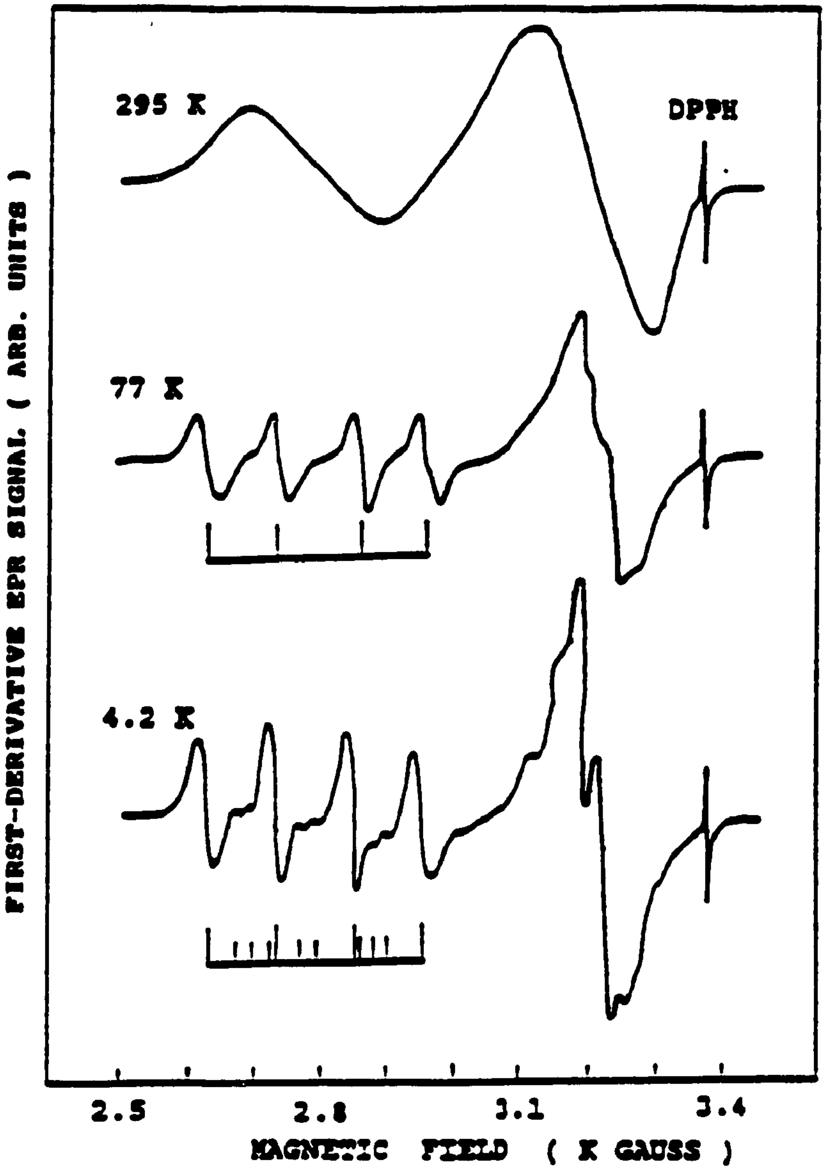

Figure V.2.2. Single-crystal EPR spectra of Cu^{2+}-doped $Cd(NH_4)_2(SO_4).6H_2O$ (CASH) single crystal for $\vec{B}$ at 10° from the z axis in the zx plane at various temperatures; the allowed hf lines at 77 and 4.2 K are indicated by longer bars, the eight short bars indicate the forbidden-transition line positions, corresponding to the transitions $\Delta m = -1, +1, -2, +2, +2, -2, +1, -1$ respectively, as expressed in order of increasing magnetic field values.

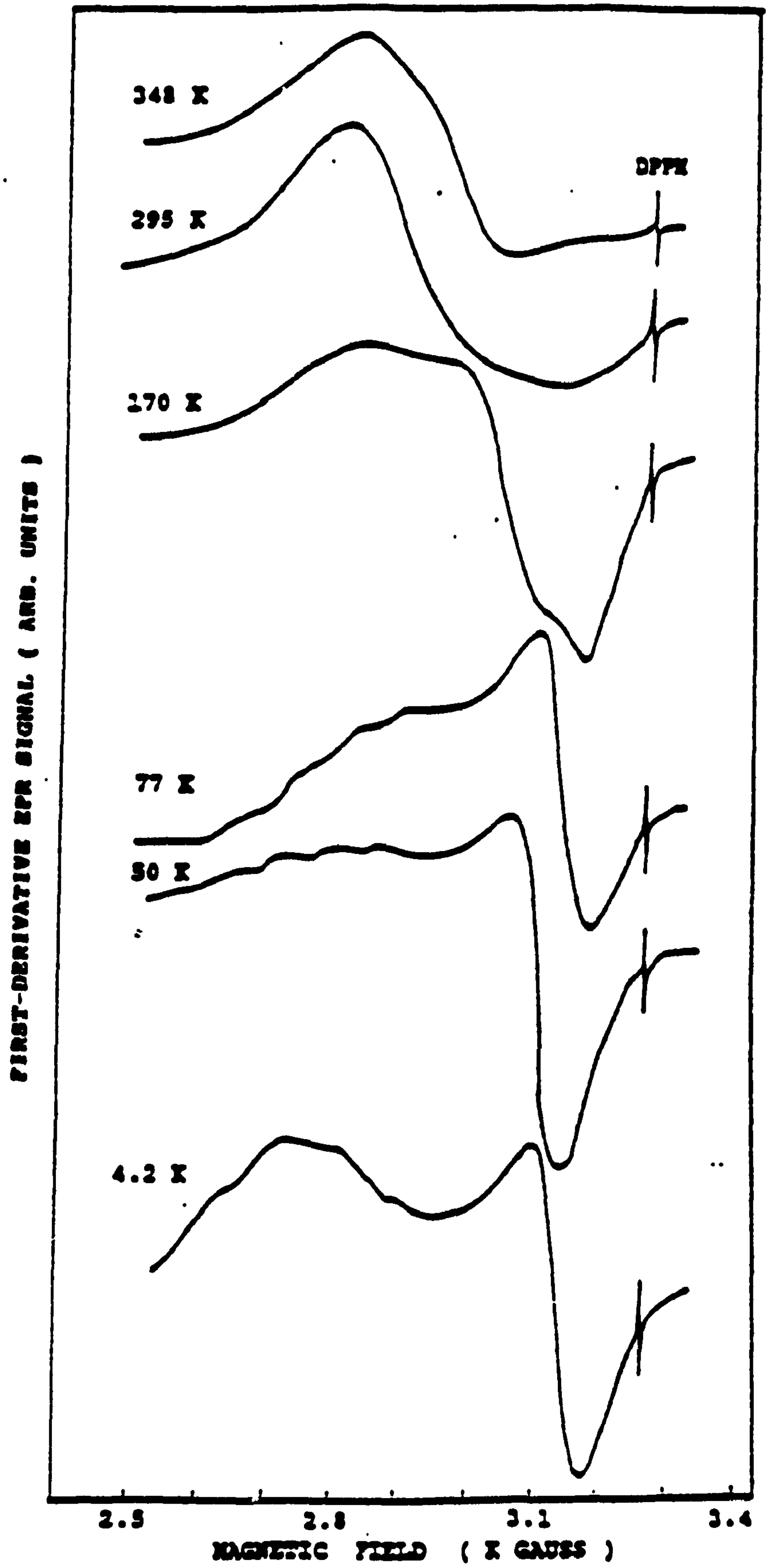

Figure V.2.3. Polycrystalline EPR spectra of Cu^{2+}-doped $Cd(NH_4)_2(SO_4)\cdot 6H_2O$ (CASH) at various temperatures.

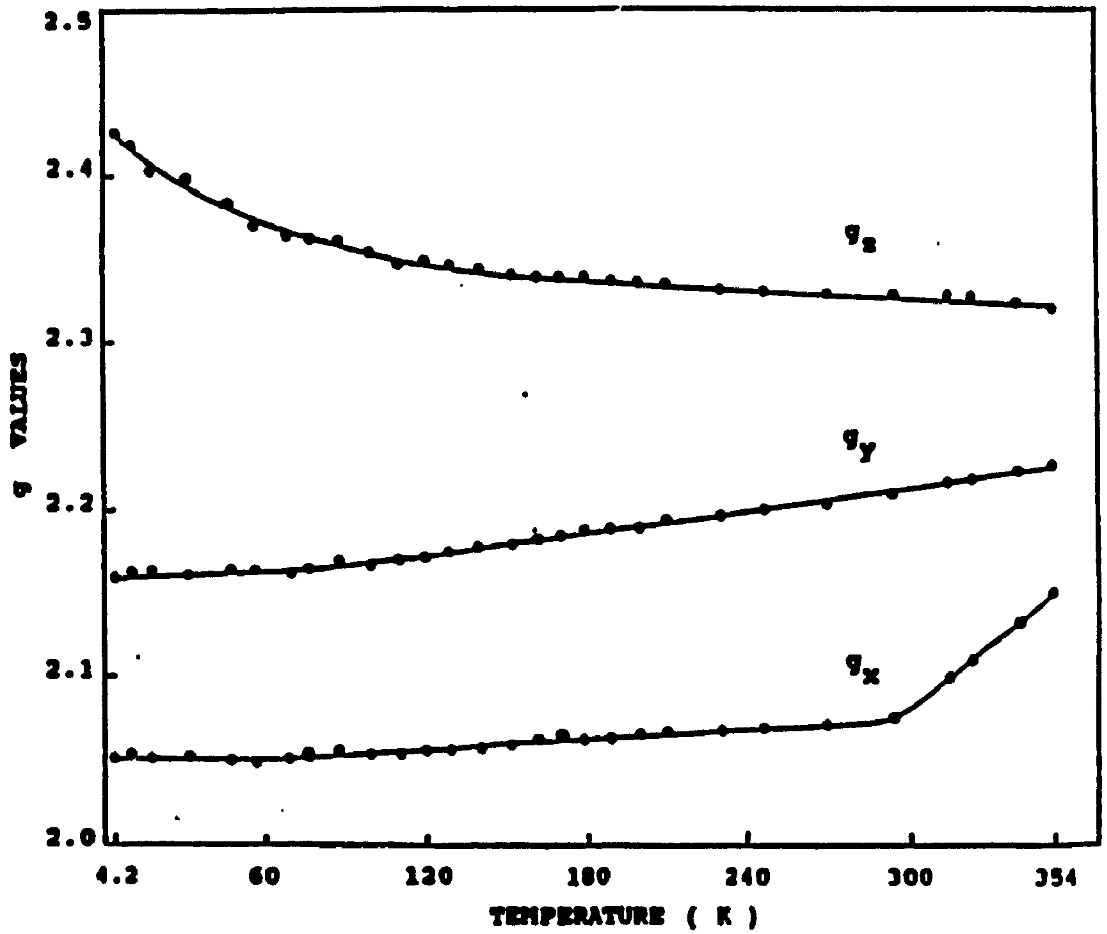

Figure V.2.4. Temperature variation of the principal g-values of Cu^{2+} in $Cd(NH_4)_2(SO_4).6H_2O$ (CASH). The values at 4.2, 77, and 295 K are those estimated from a single-crystal EPR lines, while those at other temperatures are estimated from the line positions due to a polycrystalline specimen.

This is different from the cases of Cu^{2+}-doped Zn Tutton salts, where the three components of h.f. structure were well resolved, even at temperatures slightly above 77 K [53]. This indicates that the Cu^{2+} spins have a rather strong interaction with the CASH lattice compared to that with the lattices of Zn Tutton salts [50]. The principal g values, as estimated for the polycrystalline CASH specimen at various temperatures, are plotted in Figure V.2.4.

The experimental data, described above, for either single-crystal, or the polycrystalline, specimen reveal the following features: (i) All the principal values of the Cu^{2+} $\tilde{g}$ and $\tilde{A}$ matrices ($g_{\alpha\alpha}$, $A_{\alpha\alpha}$; α = x, y, z) are temperature dependent, except that g_{xx} does not change appreciably in the temperature range 4.2 - 77 K. The directions of the principal axes of the $\tilde{g}$ and $\tilde{A}$ matrices are coincident at all temperatures within experimental error. (ii) The average of the principal values of the $\tilde{g}$ matrix at various temperatures is close to 2.2. (iii) The widths of the EPR lines are temperature dependent.

In the EPR study of Cu^{2+} ion in CASH reported by Satyanarayana [50], the EPR spectra of a single-crystal specimen in the 77-300 K range indicated that the impurity ion substituted for a Cd^{2+} ion in the CASH host lattice. The SHP reported by him are listed in Table V.2.1 for comparison. EPR spectra of a powder specimen at 300 and 77 K were also reported by him.

V.3. Cu^{2+}-doped $Mg(NH_4)_2(SO_4).6H_2O$ (MASH) single and poly crystals

The crystal structure of MASH has been reported by Montgomery and Lingafelter [41] to be the same as that of CASH; the unit-cell dimensions at 300 K are: a = 9.383 Å, b = 12.669 Å, c = 6.220 Å, β = 107°03′. The bond lengths between the central ion Mg^{2+} and the ligand atoms were reported [28] as 2.083 Å, 2.073 Å and 2.051 Å for Mg-O(7) (H_2O), Mg-O(8) (H_2O), and Mg-O(9) (H_2O), respectively, while the bond angles are 90.3° for O(7)-Mg-O(8), 90.0° for O(7)-Mg-O(9), and 91.5° for O(8)-Mg-O(9). These data indicate that the symmetry of the Mg^{2+} complex in MASH is approximately tetragonally-distorted octahedral, as shown in Figure V.2.1.

Cu^{2+}-doped MASH single crystals were grown by the same procedure as that for CASH, except for the aqueous solution consisting of $MgSO_4.7H_2O$, instead of $3CdSO_4.8H_2O$. No EPR study on Cu^{2+}-doped MASH has been reported so far.

The single-crystal EPR spectra of Cu^{2+}-doped MASH at 295, 77, and 4.2 K were found to be quite different in their profiles, as seen from Figure V.3.1, which exhibits EPR spectra for the orientation of $\vec{B}$ at 20° form the z axis in the zx plane. The spectrum at 295 K consists of two broad lines, which indicate the presence of two physically-equivalent, but magnetically- inequivalent, Cu^{2+} complexes in the unit-cell of MASH lattice. At low temperatures (LNT and LHT) these two broad lines split due

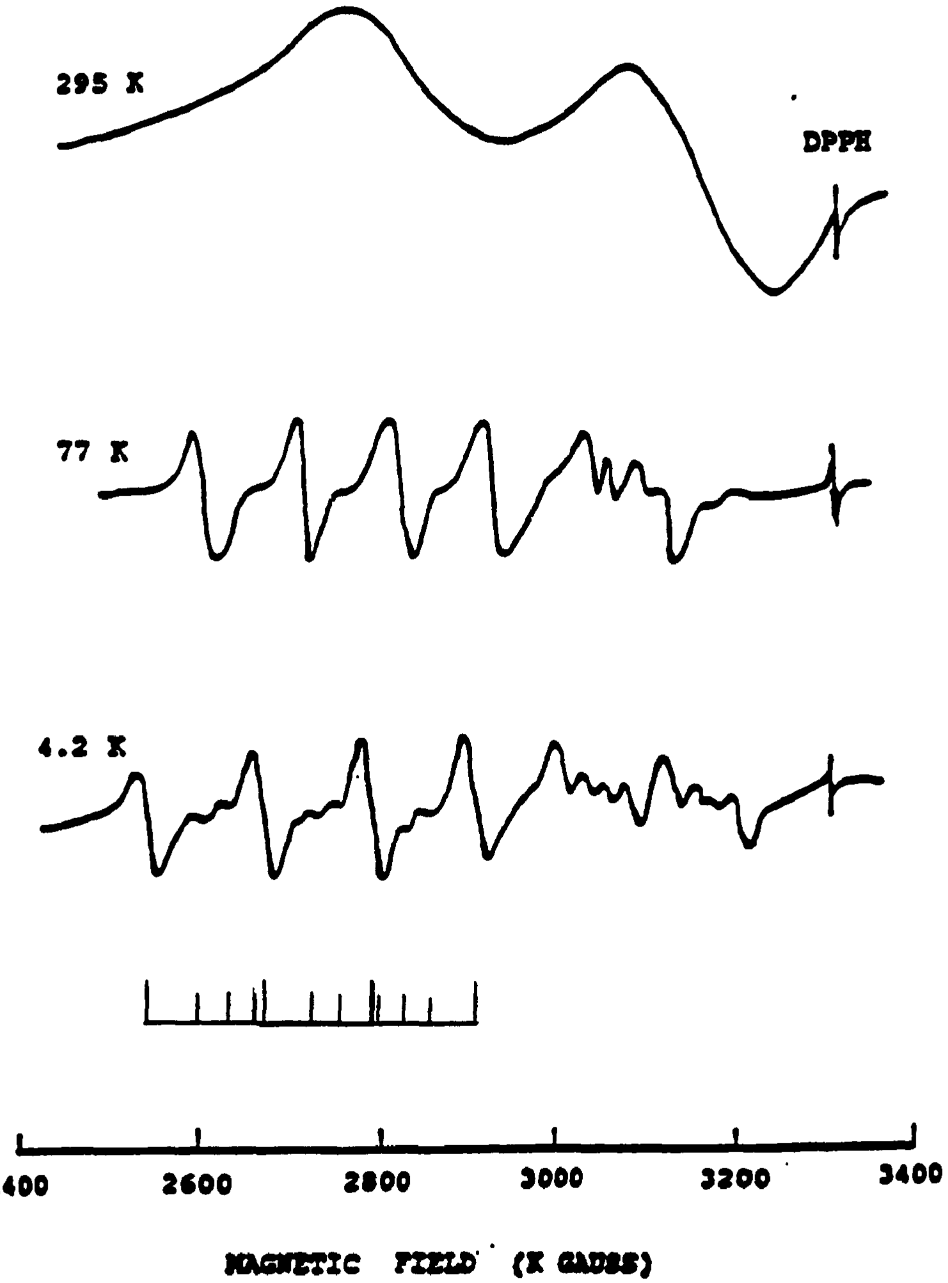

Figure V.3.1. Single-crystal EPR spectra of Cu^{2+}-doped $Mg(NH_4)_2(SO_4).6H_2O$ (MASH) for $\vec{B}$ at 20° from the z axis in the zx plane at various temperatures; the allowed hf lines at 77 and 4.2 K are indicated by longer bars, the eight short bars indicate the forbidden-transition line positions, corresponding to the transitions $\Delta m = -1, +1, -2, +2, +2, -2, +1, -1$ respectively, as expressed in order of increasing magnetic field values.

Table V.3.1. Principal values of the $\tilde{g}$ and $\tilde{A}$ matrices (square roots of the principal values of the $\tilde{g}^2$ and $\tilde{A}^2$ tensors, respectively), and the $\tilde{Q}$-tensor for Cu^{2+} in the $Mg(NH_4)_2(SO_4).6H_2O$ (MASH) single-crystal specimen at different temperatures. The principal $\tilde{g}$ values are dimensionless, while the principal values of the $\tilde{A}$ matrix and the $\tilde{Q}$ tensor are in GHz.

Temperature	$g_{z'}$	$g_{y'}$	$g_{x'}$	$A_{z''}$	$A_{y''}$	$A_{x''}$	$Q_{z''}$	$Q_{y''}$	$Q_{x''}$
295K	2.3422	2.2560	2.0811						
77 K	2.4168	2.1281	2.0715						
4.2K	2.4263	2.1151	2.0706	0.366	0.114	0.079	0.021	-0.017	-0.003

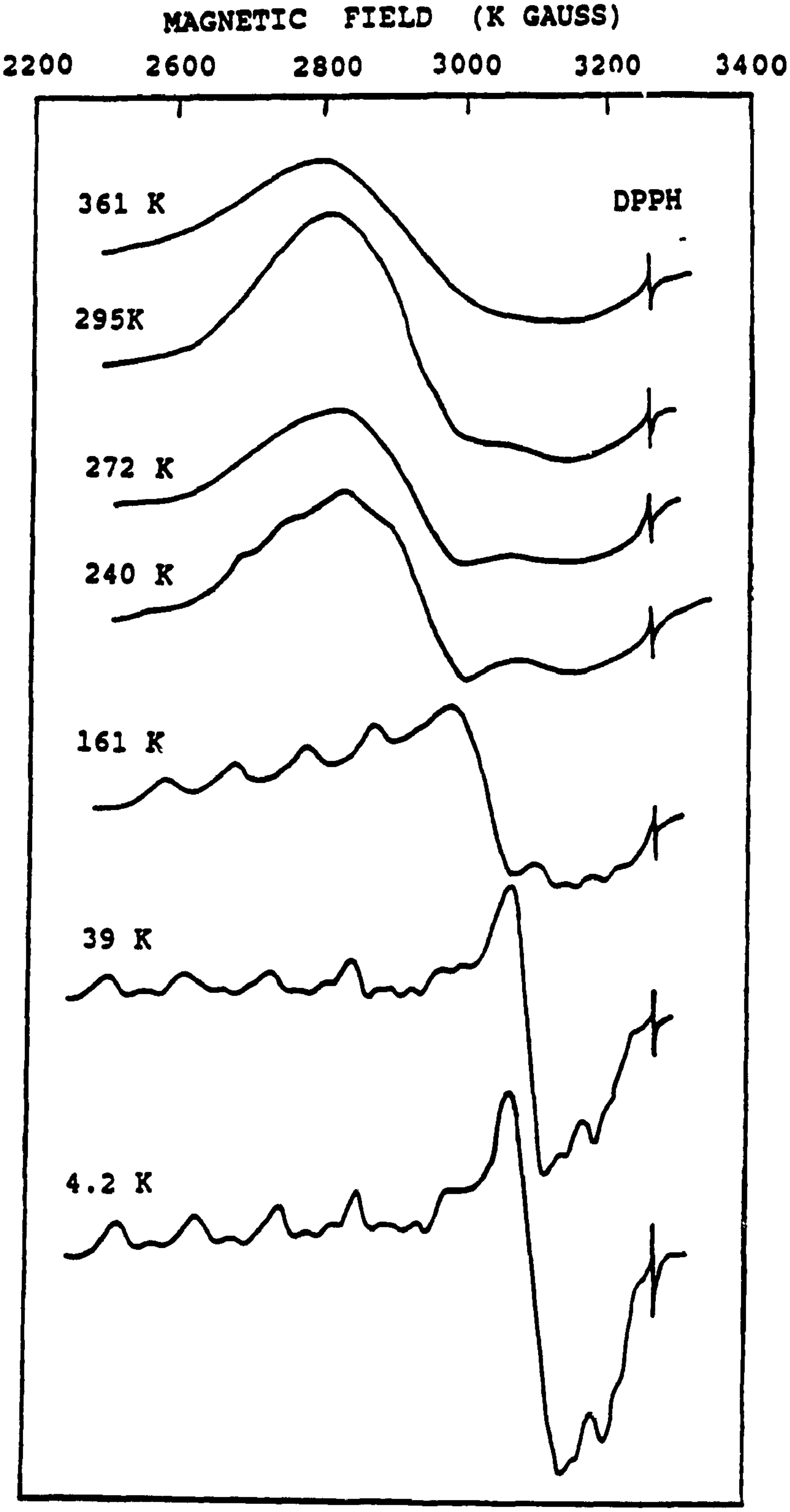

Figure V.3.2. Polycrystalline EPR spectra of Cu^{2+}-doped $Mg(NH_4)_2(SO_4).6H_2O$ (MASH) at various temperatures.

to Cu^{2+} h.f. interaction, into two sets of tetrads due to the more abundant isotope (^{63}Cu) ion; the lines corresponding to the less-abundant isotope (^{65}Cu) ion could not be clearly seen. The EPR spectra at LNT and LHT are almost the same in profile, except for the separations between the lines at high magnetic field. The satellite lines between the four h.f. lines can be seen in one of the two sets of EPR lines located at low magnetic fields. These satellite lines corresponding to the h.f. forbidden transitions. There is a total of eight lines in the higher magnetic field range. They are overlaps of the allowed and forbidden h.f. transitions due to the other set of Cu^{2+} EPR lines. The Cu^{2+} EPR spectra of MASH are described by the spin Hamiltonian as eq. V.2.1.

The analysis of EPR data indicates that the directions of the principal axes of the $\tilde{g}^2$ tensor do not change with temperature, while the principal axes of the $\tilde{A}^2$ tensor remain coincident with those of the $\tilde{g}^2$ tensor at LNT and LHT, within experimental errors. The principal values of the $\tilde{g}$ and $\tilde{A}$ matrices at various temperatures are listed in Table V.3.1. Table V.3.2. lists the direction cosines of the principal axes of the $\tilde{g}$ and $\tilde{A}$ matrices. The principal values and direction cosines of the $\tilde{Q}$ tensor, at 4.2 K, estimated by the use of the same computer program as that used for CASH, are list in Table V.3.1. The $\tilde{Q}$ tensor at 77 K could not be estimated from EPR spectra due to the poor resolution of EPR lines. The identification of the six forbidden h.f. transitions, shown in Figure V.3.1, was accomplished by the same computer program, that used for CASH, for calculating line positions of the allowed and forbidden h.f. transitions.

EPR spectra of a MASH polycrystalline specimen were recorded in the temperature range 4.2-361 K, to study the temperature dependence of the principal g-values. Some of these are shown in Figure V.3.2. The powder EPR spectra are much like those observed for CASH. A single broad, huge EPR line was observed at high temperatures, $T > 240$ K. At $T < 240$ K, the component corresponding to g_z, lying at the lowest values of the magnetic field exhibited h.f. structure, while the h.f. structure corresponding to the g_x component was only resolved at $T < 200$ K; the h.f. structure corresponding to the g_y component is not at all resolved, even at 4.2 K. This observation is different from that of the cases of Cu^{2+}-doped Zn Tutton salts [53], and Cu^{2+}-doped CASH (Sec. V.2.). It indicates the Cu^{2+} spins have a stronger interaction with the MASH lattice, as compared to that with the lattices of Zn Tutton salts [53]. On the other hand, this interaction is weak as compared to that with the lattice of CASH. The principal g-values estimated from powder specimen of MASH at various temperatures are plotted in Figure V.3.3.

The experimental data, for either the single-crystal, or the polycrystalline, specimen reveal the same feature as those in the case of CASH, except that the g_x component of

Table V.3.2. Direction cosines of the $\tilde{g}$, $\tilde{A}$ matrices (the same as those for the $\tilde{g}^2$, $\tilde{A}^2$ tensors), and those of the $\tilde{Q}$ tensor for Cu^{2+} in the $Mg(NH_4)_2(SO_4).6H_2O$ (MASH) single-crystal specimen at 4.2 K. The principal axes of the $\tilde{g}$ matrix are expressed with respect to the laboratory axes (x,y,z), defined in Sec. 3.1. The principal axes of the $\tilde{A}$ matrix are coincident with those of the $\tilde{g}$ matrix, and the principal axes of the $\tilde{Q}$ tensor are expressed relative to (x',y',z'), the principal axes of the $\tilde{g}$ matrix.

	z	x	y
$g_{z'}$	0.931	-0.202	0.304
$g_{x'}$	-0.123	0.609	0.784
$g_{y'}$	-0.343	-0.767	0.542

	z'	x'	y'
$Q_{z''}$	0.917	0.397	0.048
$Q_{x''}$	-0.226	0.613	-0.757
$Q_{y''}$	-0.330	0.683	0.651

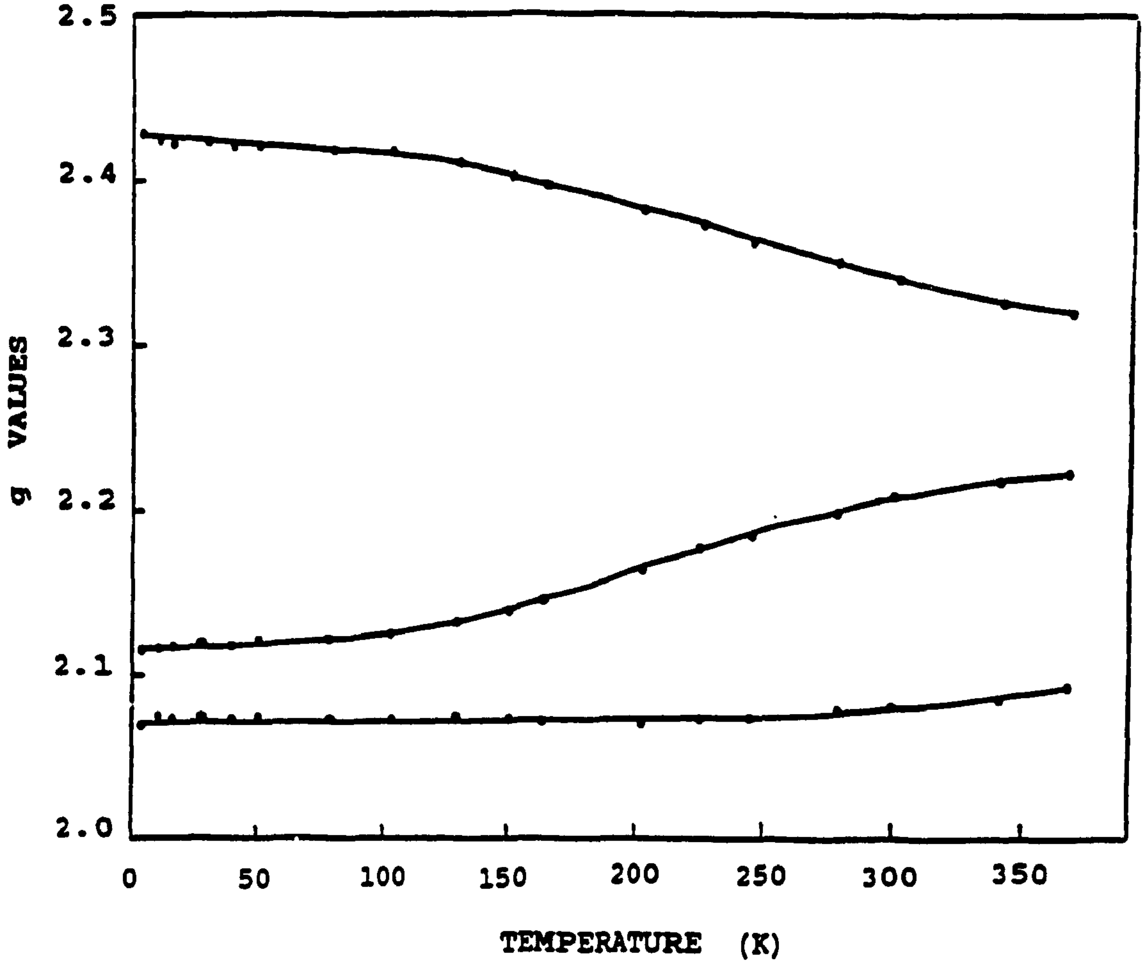

Figure V.3.3. Temperature variation of the principal g-values of Cu^{2+} in $Mg(NH_4)_2(SO_4).6H_2O$ (MASH). The values at various temperatures are estimated from line positions of a polycrystalline specimen.

the $\tilde{g}$ matrix does not change in the temperature range 4.2 - 240 K, where it did not change in the range 4.2 - 77 K for CASH.

V.4. Cu^{2+}-doped $Ni(NH_4)_2(SO_4).6H_2O$ (NASH) single crystal

The crystal structure of NASH has been reported [41] to be the same as that for CASH; the unit-cell dimensions at 300 K are: a = 2.241 Å, b = 12.544 Å, c = 6.243 Å, β = 106°58′. The bond lengths between $Ni-O_7(H_2O)$, $Ni-O_8(H_2O)$, and $Ni-O_9(H_2O)$ are 2.085 Å, 2.083 Å and 2.036 Å, respectively. The bond angles are 90.4° for O_9-Ni-O_7, 88.5° for O_8-Ni-O_7 and 89.3° for O_8-Ni-O_9, as shown in Figure V.2.1.

Cu^{2+}-doped NASH single crystals were grown by the same procedure as that for CASH, except that here the aqueous solution consists of $NiSO_4.7H_2O$, rather than $3CdSO_4.8H_2O$. No EPR study on Cu^{2+}-doped NASH has been reported so far.

The profiles of the single-crystal EPR spectra of Cu^{2+}-doped NASH at 295, 77, and 4.2 K were found to be quite different from those for CASH and MASH, as seen from Figure V.4.1, which exhibits EPR spectra for the orientation of $\vec{B}$ at 25° from the z axis in the zx plane. The spectra at 295 and 77 K consist of two broad EPR lines, which indicate the presence of two physically-equivalent, but magnetically-inequivalent Cu^{2+} complexes in the unit-cell of NASH lattice. At 4.2 K, only the line located at lower magnetic field, of these two broad lines, splits into one

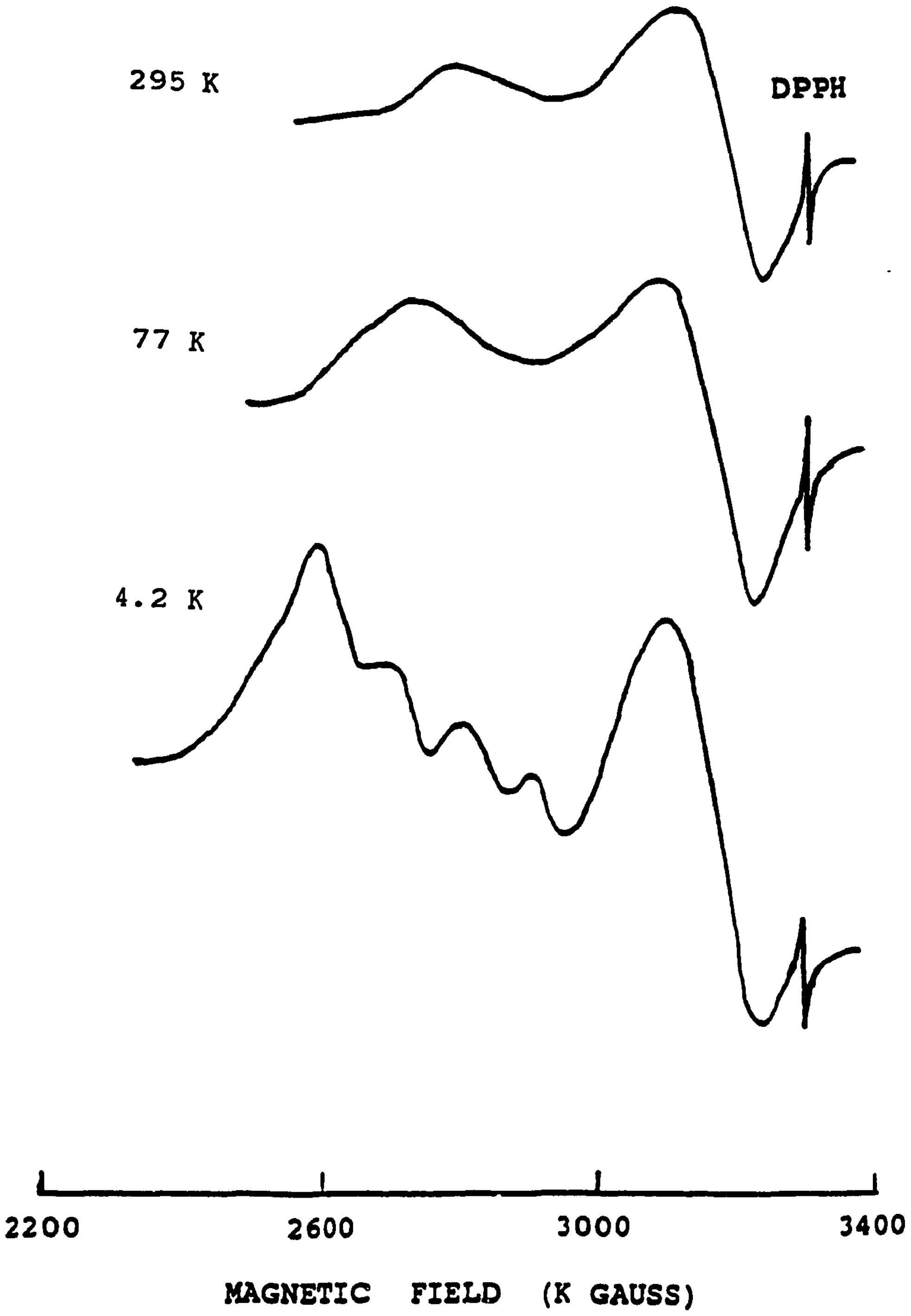

Figure V.4.1. Single-crystal EPR spectra of Cu^{2+}-doped $Ni(NH_4)_2(SO_4).6H_2O$ (NASH) for $\vec{B}$ at 25° from the z axis in the zx plane at various temperatures.

Table V.4.1. Principal values of the $\tilde{g}$ and $\tilde{A}$ matrices (square roots of the principal values of the $\tilde{g}^2$ and $\tilde{A}^2$ tensors, respectively), for Cu^{2+} in the $Ni(NH_4)_2(SO_4) \cdot 6H_2O$ (NASH) single-crystal specimen at different temperatures. The principal $\tilde{g}$ values are dimensionless, while the principal values of the $\tilde{A}$ matrix in GHz.

Temperature	$g_{z'}$	$g_{y'}$	$g_{x'}$	$A_{z''}$	$A_{y''}$	$A_{x''}$
295K	2.3504	2.2080	2.1082			
77 K	2.3818	2.1843	2.0775			
4.2K	2.4110	2.1765	2.1041	0.316	0.017	0.063

Table V.4.2 Direction cosines of the $\tilde{g}$, $\tilde{A}$ matrices (the same as those the $\tilde{g}^2$, $\tilde{A}^2$ tensors) for Cu^{2+} in the $Ni(NH_4)_2(SO_4).6H_2O$ (NASH) single-rystal specimen at 4.2 K. The principal axes of the $\tilde{g}$ matrix are expressed with respect to the laboratory axes (x,y,z), defined in Sec. 3.1. The principal axes of the $\tilde{A}$ matrix are coincident while those of the $\tilde{g}$ matrix are expressed relative to (x′,y′,z′), the principal axes of the $\tilde{g}$ matrix.

	z	x	y
$g_{z'}$	0.941	0.001	0.337
$g_{x'}$	0.278	0.566	-0.776
$g_{y'}$	-0.191	0.825	0.532

tetrad due to h.f. interaction of the more abundant isotope (^{63}Cu); the h.f. lines corresponding to the less-abundant isotope (^{65}Cu) ion could not be seen. The EPR spectra of Cu^{2+} ion in NASH were fitted to the spin Hamiltonian described by eq. V.1.1.

The EPR line positions were used to evaluate the $\tilde{g}$ matrix at 295 and 77 K, while both the $\tilde{g}$ and $\tilde{A}$ matrices at 4.2 K. The principal values of the $\tilde{g}$ and $\tilde{A}$ matrices at 295, 77, and 4.2 K are listed in Table V.4.1. Table V.4.2 gives the direction consines of the principal axes of the $\tilde{g}$ and $\tilde{A}$ matrices. The principal axes of the $\tilde{g}$ matrix are independent of temperature. Further, the principal axes of the $\tilde{A}$ matrix and those of the $\tilde{g}$ matrix are coincident at 4.2 K within experimental errors.

The difference in the profiles of the EPR spectrua for CASH and MASH can be attributed to the magnetic properties of the host ions. In the case of Cu^{2+}-doped NASH, the host ion is Ni^{2+} ion which is paramagnetic, while in the cases of Cu^{2+}-doped CASH and MASH, the host ions are the diamagnetic Cd^{2+} and Mg^{2+} ions. In the paramagnetic host lattice of NASH, the dipole-dipole and exchange interactions between the host Ni^{2+} ion and impurity Cu^{2+} ion play important roles in determining the EPR linewidths [1, 35].

V.5. Cu^{2+}-doped $Mg(CH_3COO)_2.4H_2O$ (MAT) single crystal

The crystal structure of MAT, as determined from X-ray data, has been reported by Shankar et al. [51]. It is

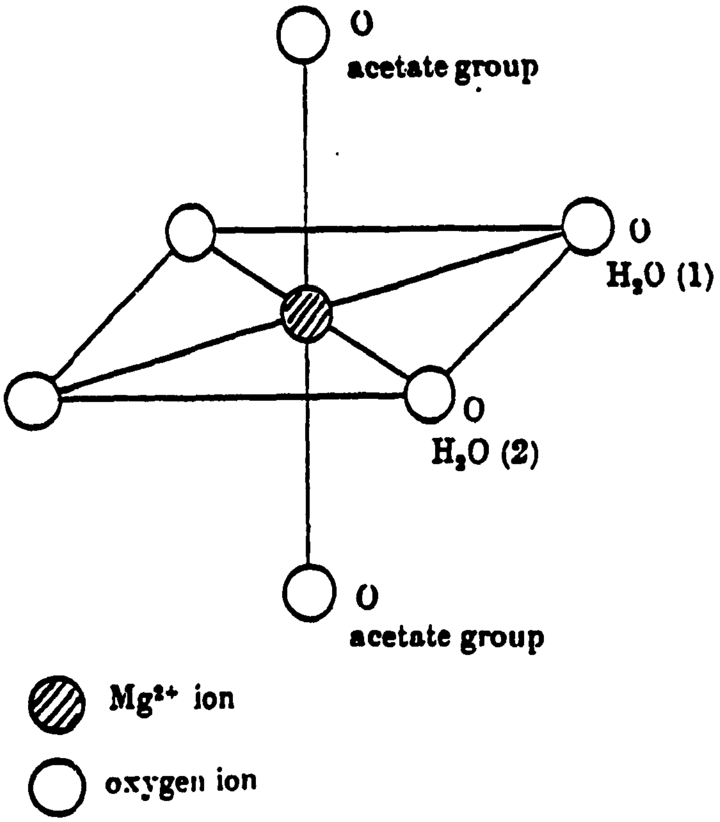

Figure V.5.1. Relationship of the oxygen atoms to Mg atom in the structure of $Mg(CH_3COO)_2.4H_2O$ (MAT).

monoclinic (space group $C_{2h}^{5}-P_{21/c}$); the unit cell dimensions are: a = 4.75 Å, b = 11.79 Å, c = 8.52 Å and β = 94°54′. There are two formula units per unit cell (Z = 2); each Mg^{2+} ion is surrounded by four water molecules, two $H_2O(1)$ and two $H_2O(2)$, in the equatorial plane, and by two oxygen ions belonging to the two acetate groups situated on the axis perpendicular to the equatorial plane. The distances between the Mg^{2+} ion and the oxygen ions of the $H_2O(1)$ and $H_2O(2)$ molecules are 2.07 Å and 2.08 Å, respectively, and those between the Mg^{2+}ion and the two oxygen ions, which belong to the two acetate groups, are 2.11 Å each, as shown in Figure V.5.1. The local site symmetry of the Mg^{2+} ion is, thus, approximately tetragonal (elongated octahedron).

Cu^{2+}-doped single crystals of MAT were grown by the same procedure as that followed for PZST. Here, a sufficient quantity of $Cu(CH_3COO)_2.2H_2O$ was added to an aqueous solution of $Mg(CH_3COO)_2.4H_2O$ so that there was one Cu^{2+} ion per 100 Mg^{2+} ions.

The EPR spectrum for Cu^{2+}-doped MAT single crystal was recorded at 295, 77, and 4.2 K [36]. The spectrum at room temperature consists of two sets of four h.f. lines each, indicating that there exist two magnetically inequivalent, but physically equivalent, Cu^{2+} centres in the unit cell of MAT, as expected from the crystal structure of MAT. Each Cu^{2+} centre is characterized by four h.f. lines, since its electron spin S = 1/2 and nuclear spin I = 3/2 for the two stable isotopes of copper, Cu^{63} (69.09% abundant) and Cu^{65}

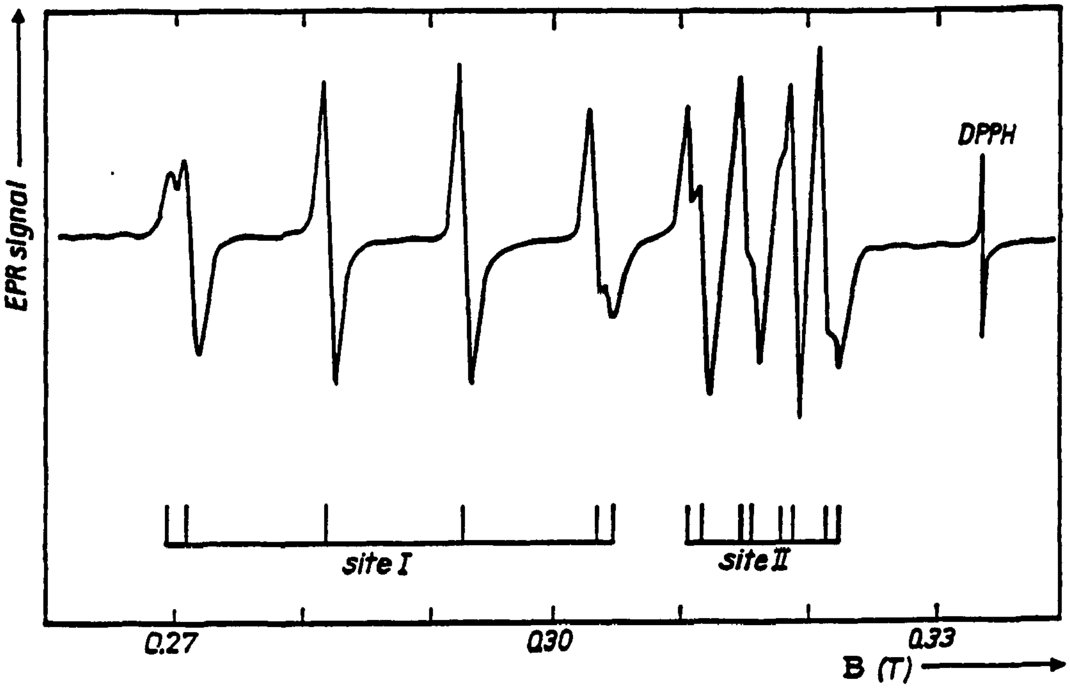

Figure V.5.2. First-derivative X-band EPR spectrum of Cu^{2+}-doped $Mg(CH_3COO)_2.4H_2O$.(MAT) at liquid-helium temperature for the orientation of $\vec{B}$ at 28° from the z axis in the zx plane. The h.f. lines corresponding to the magnetic isotopes Cu^{63} and Cu^{65}, as well as the two spectra corresponding to the two sites (I and II) for Cu^{2+}, have been indicated. The two central h.f. lines for site I due to the two isotopes overlap each other.

Table V.5.1. Principal values of the $\tilde{g}$ and $\tilde{A}$ matrices (square roots of the principal values of the $\tilde{g}^2$ and $\tilde{A}^2$ tensors respectively) for Cu^{2+} in $Mg(CH_3COO)_2.4H_2O$ (MAT) at different temperatures. The g principal values are dimensionless, while the A principal values are in cm^{-1}. The labelling is such that $g_{\parallel} > g_{\perp}$. The errors of the presently-estimated $\tilde{g}$ principal values are ± 0.0018 and those for the $\tilde{A}$ principal values are ± 0.0002 cm^{-1}.

Temperature	isotope	$g_{\parallel}$	$g_{\perp}$	$A_{\parallel}$	$A_{\perp}$	Ref.
295 K	$Cu^{63,65}$	2.3738	2.0960	0.0108	0.0027	[a]
300 K	$Cu^{63,65}$	2.347	2.095	0.0108	0.0026	[27]
77 K	Cu^{63}	2.3882	2.0962	0.0121	0.0031	[a]
	Cu^{65}	2.3882	2.0962	0.0130	0.0034	[a]
77 K	Cu^{63}	2.347	2.095	0.0121	0.0031	[27]
	Cu^{65}	2.347	2.095	0.0130	0.0034	[27]
4.2 K	Cu^{63}	2.3884	2.0963	0.0121	0.0031	[a]
	Cu^{65}	2.3884	2.0963	0.0130	0.0034	[a]

a. Present work.

(30.95% abundant), with non-zero nuclear magnetic moments. The EPR spectra at both the liquid-nitrogen and liquid-helium temperatures are different from those at room temperature, insofar as the h.f. linewidth and the splittings of EPR lines due to the Cu^{63} and Cu^{65} isotopes are concerned. The h.f. lines corresponding to Cu^{63} and Cu^{65} split clearly from each other at liquid-helium temperature, as can be seen from the spectrum, recorded for the orientation of $\vec{B}$ at 28° from the z axis in the zx plane, displayed in Figure V.5.2. Figure V.5.2 exhibits two sets of h.f. lines corresponding to the two impurity sites for Cu^{2+} ions in the unit cell of MAT; the set occurring at lower magnetic field is designated as that belonging to site I, while the other one belonging to site II. For site I, only the outer h.f. lines for Cu^{65} and Cu^{63}, i.e., those corresponding to the allowed transitions $M = 1/2$, $m = \pm 3/2 \leftrightarrow M = -1/2$, $m = \pm 3/2$ split completely from each other (Figure V.5.2). (Here M and m refer to the electronic and nuclear magnetic quantum numbers, respectively.) On the other hand, for site II all the four h.f. lines, i.e., those corresponding to the transitions $1/2, m \leftrightarrow -1/2, m$; $m = 3/2, 1/2, -1/2, -3/2$ for the two isotopes split completely (Figure V.5.2). The EPR linewidth for any h.f. transition at both the liquid-nitrogen and liquid-helium temperatures is 13 ± 1 gauss, while at room temperature it is 34 ± 1 gauss; these linewidths are independent of the orientation and magnitude of $\vec{B}$.

The observed EPR line positions of Cu^{2+} in MAT , for each of the Cu^{63} and Cu^{65} isotopes, were fitted to the spin Hamiltonian, described by eq. (V.1.1).

The principal values of the $\tilde{g}$ and $\tilde{A}$ matrices at 295, 77, and 4.2 K are listed in Table V.5.1. Two principal values of the $\tilde{g}$ and the $\tilde{A}$ matrices were found to be the same, i.e. $g_1 = g_2 = g_\perp$ and $A_1 = A_2 = A_\perp$, these being smaller than the third principal value of the $\tilde{g}$ matrix ($g_3 = g_\parallel$) and the $\tilde{A}$ matrix ($A_3 = A_\parallel$), respectively.

An EPR study of Cu^{2+}-doped MAT at 295 and 77 K has been previously reported by Manakkil [27]. The principal values of the $\tilde{g}$ and the $\tilde{A}$ matrices, as reported in his thesis are also listed in Table V.5.1 for comparison.

CHAPTER VI

OPTICAL-ABSORPTION STUDY OF Cu^{2+}-DOPED $Mg(CH_3COO)_2.4H_2O$ (MAT)

The optical-absorption spectrum provides information on the energy separations between the excited states and the ground state and the energy of charge-transfer bands of the Cu^{2+} ion in crystal lattice. They can be used to estimate the molecular-orbital coefficients, as dicussed in chapter VIII. The crystal-field theory has usually been used to explain the d-d transfer bands, which appear in optical-absorption spectra due to transitions between the excited states and the ground state.

VI.1. Crystal-field Hamiltonian

The ground state of the free Cu^{2+} ion is $^2D_{5/2}$. This five-fold degenerate state splits in a crystal field. The sequence of the energy levels depends on the symmetry of the crystal field in which the Cu^{2+} ion is situated. In the case of MAT, there exists a tetragonally-distorted octahedral symmetry (D_{4h}) at the site of the Cu^{2+} ion. The energy of the Cu^{2+} ion in a distorted-octahedral symmetry can be expressed in terms of the Hamiltonian operator as [3]:

$$\mathcal{H}_{cf} = D_q\left[\frac{35}{12}\,\hat{L}_z^4 - \frac{155}{12}\,\hat{L}_z^2 + 6 + \frac{5}{24}\left(\hat{L}_+^4 + \hat{L}_-^4\right)\right] + D_s(\hat{L}_z^2 - 2) - D_t\left(\frac{35}{12}\,\hat{L}_z^4 - \frac{155}{12}\,\hat{L}_z^2 + 6\right), \qquad \text{(VI.1)}$$

where $\hat{L}_z$, $\hat{L}_+$ (= $\hat{L}_x + i\,\hat{L}_y$) and $\hat{L}_-$ (= $\hat{L}_x + i\,\hat{L}_y$) are the elecron orbital-angular momentum operators. The parameters D_q, D_s, and D_t are referred to as the octahedral, and the second- and fourth-order tetragonal field parameters, respectively. They are expressed, using the point-charge model, as [21]:

$$D_q = -\frac{1}{6} Ze^2 \frac{\langle r^4 \rangle}{R_e^5} ,$$

$$D_s = -\frac{2}{7} Ze^2 \frac{\langle r^2 \rangle}{R_e^3} \left(1 - \frac{R_e^3}{R_a^3}\right) ,$$

and

$$D_t = -\frac{2}{7} Ze^2 \frac{\langle r^4 \rangle}{R_e^5} \left(1 - \frac{R_e^5}{R_a^5}\right) . \qquad \text{(VI.2)}$$

where Ze, $\langle r^2 \rangle$, $\langle r^4 \rangle$, R_e, and R_a are, respectively, the charge of the ligands, the mean-square and mean-fourth-power radii of the Cu^{2+} ion orbitals, and the distances of the ligands in the equatorial plane and those situated upon the axis perpendicular to the equatorial plane and the Cu^{2+} ion.

VI.2. Energy level scheme of the Cu^{2+} ion in a tetragonally-distorted octahedral symmetry

The energy levels of the Cu^{2+} ion in a tetragonally-distorted octahedral symmetry (D_{4h}), as determined from the crystal-field Hamitonian $\mathcal{H}_{cf}$, are shown

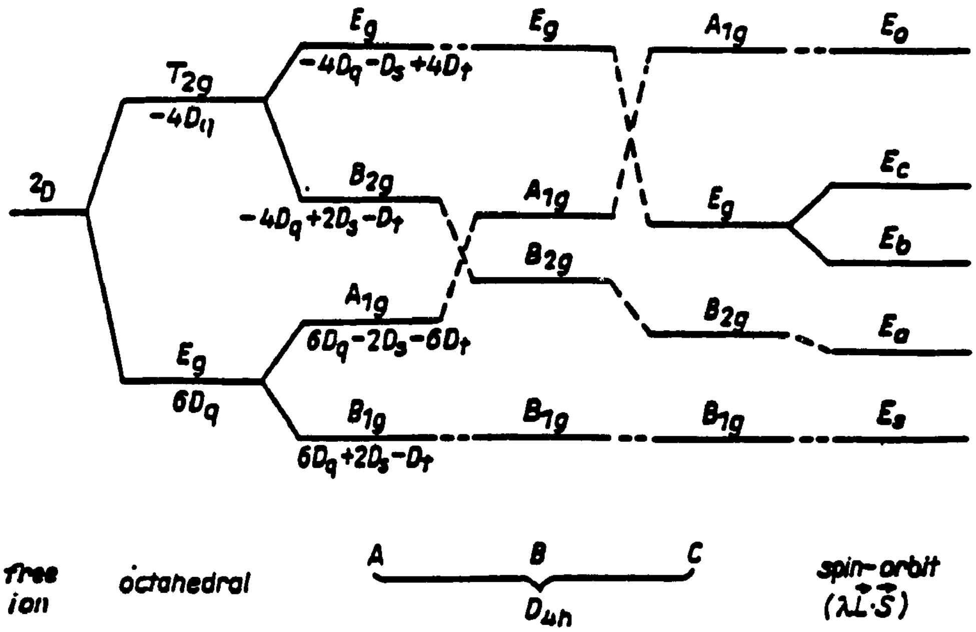

Figure VI.1. Energy-level diagram for the Cu^{2+} ion in a tetragonally-distorted octahedral crystal field, with increasing tetragonal distortions A, B and C; the limits of applicability are $|D_q| > \frac{7}{10}|D_s| > \frac{7}{6}|D_t|$, $\frac{7}{10}|D_s| > |D_q| > \frac{7}{6}|D_t|$, and $\frac{7}{10}|D_s| > \frac{7}{6}|D_t| > |D_q|$ for the tetragonal distortions A, B, and C, respectively.

in Figure VI.1 [23]. There are three qualitatively different energy level schemes, indicated as A, B, and C in Figure VI.1, corresponding to an initially pure octahedral field with increasing tetragonal distortions. The limits of applicability are $|D_q| > \frac{7}{10}|D_s| > \frac{7}{6}|D_t|$, $\frac{7}{10}|D_s| > |D_q| > \frac{7}{6}|D_t|$ and $\frac{7}{10}|D_s| > \frac{7}{6}|D_t| > |D_q|$ for the tetragonal distortions A, B, and C, respectively. Since the spin-orbit coupling constant, λ, of the Cu^{2+} ion is rather large, a significant effect of the spin-orbit coupling upon the spectrum of the Cu^{2+} complex is expected [19]. To first order in perturbation, splitting into five energy levels (Figure VI.1) of the Cu^{2+} ion (^2D configuration) is caused by the tetragonally-distorted octahedral field along with the spin-orbit coupling [47]. These five energy levels can be expressed as follows:

$$E_0 = 6D_q - 2D_s - 6D_t \quad (\text{orbital } d_{3z^2-r^2})\ ;$$

$$E_c = -4D_q - D_s + 4D_t - \lambda/2$$

(overlap of orbitals d_{xz} and d_{yz});

$$E_b = 1/2(-8D_q + D_s + 3D_t) + \lambda/4 +$$

$$\frac{1}{2}\sqrt{(-3D_s + 5D_t)^2 + \lambda(-3D_s + 5D_t) + 9\lambda^2/4}$$

(overlap of orbitals d_{xz} and d_{yz});

$$E_a = 1/2(-8D_q + D_s + 3D_t) + \lambda/4 -$$

$$\frac{1}{2}\sqrt{(-3D_s+5D_t)^2+\lambda(-3D_s+5D_t)+9\lambda^2/4} \quad (\text{orbital } d_{xy}) \;;$$

and

$$E_s = 6D_q + 2D_s - D_t \quad (\text{orbital } d_{x^2-y^2}) \;. \qquad (\text{VI.3})$$

In eqs. VI.3 $E_o > E_c > E_b > E_a > E_s$ for a large tetragonal distortion (scheme C), where E_s is the ground state. Using these, the energies of the d-d transfer bands can be derived by calculating the energy differences between the excited states (E_o, E_c, E_b, E_a) and the ground state (E_s).

VI.3. Optical-absorption spectrum of Cu^{2+} in MAT

The room-temperature optical-absorption spectrum of Cu^{2+}-doped MAT single crystal, in the wavelength range 190-820 nm [36], is exhibited in Figure VI.2. There are four bands in the visible range, occurring at ν_1 = 15,243 cm^{-1}, ν_2 = 16,611 cm^{-1}, ν_3 = 17,182 cm^{-1}, and ν_4 = 20,661 cm^{-1}, and two bands in the ultraviolet (UV) range, which are weak in intensity and are poorly resolved, occurring at about ν_5 = 36,500 cm^{-1} and ν_6 = 43,100 cm^{-1}.

From the profile of the absorption spectrum in the visible region, the observed bands at ν_2 and ν_3 can be regarded, respectively, as the d-d transfer bands between the ground-state E_s ($d_{x^2-y^2}$) and the excited states E_b and E_c, into which the two-fold degenerate level $d_{xz,yz}$ is split by the spin-orbit coupling. Thus, the band at 16,897 cm^{-1}, which is equal to the average value of the main band ν_3 and

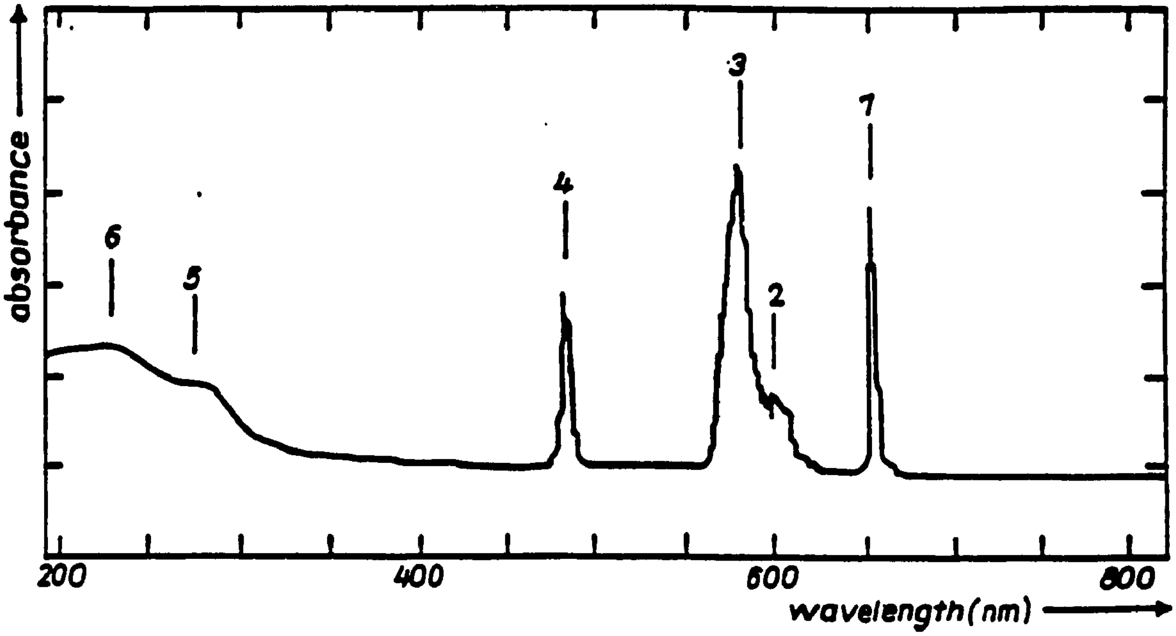

Figure VI.2. Room-temperature optical-absorption spectrum in the wavelength range 190 - 820 nm.

the shoulder on the longer-wavelength side, band ν_2, can be assigned as the d-d transfer band $d_{xz,yz} \longleftrightarrow d_{x^2-y^2}$, being usually the most intense band [54]. The other two bands, observed at ν_1 and ν_4, are assigned as $d_{xy} \longleftrightarrow d_{x^2-y^2}$ and $d_{3z^2-r^2} \longleftrightarrow d_{x^2-y^2}$ transfer bands, respectively, as can be seen from eqs. VI.3. The assignment of d-d transition bands shows that the local symmetry of Cu^{2+} ion in MAT belongs to the energy level scheme C in Figure VI.1, which corresponds to a big tetragonal distortion.

The crystal-field parameters D_s and D_t can be estimated from the optical-absorption energies ν_1, ν_2, ν_3, and ν_4, from eqs. VI.3, as follows:

$$\nu_4 = -4D_s - 5D_t ,$$

and

$$(\nu_2 + \nu_3)/2 - \nu_1 = -3D_s + 5D_t . \qquad \text{(VI.4)}$$

This yields $D_s = -3,188\ cm^{-1}$ and $D_t = -1,582\ cm^{-1}$. The four d-d transfer bands can now be calculated as functions of the parameter D_q with the assumption that $\lambda = -830\ cm^{-1}$, the value for free Cu^{2+} ion [1]. Then, the present optical data is found to fit well to $D_q = -1,525\ cm^{-1}$. This value is close to $-\nu_1/10$, as it should be, since $\nu_1 = -10D_q$, which is equal to $(E_a - E_s)$ in the limit $\lambda \to 0$, as seen from eqs. VI.3. Both the experimental energies and the energies calculated, using the presently-estimated values of D_q, D_s, and D_t of the d-d transfer bands, are listed in Table VI.1.

Table VI.1. Observed and calculated energies, and the assigned bands for Cu^{2+}-doped MAT with $D_q = -1{,}525$ cm^{-1}, $D_s = -3{,}188$ cm^{-1}, $D_t = -1{,}582$ cm^{-1}, and $\lambda = -830$ cm^{-1}. ν_1, ν_2, ν_3, and ν_4 correspond to the energies $(E_a - E_s)$, $(E_b - E_s)$, $(E_c - E_s)$, and $(E_0 - E_s)$, respectively, as shown in figure (VI.1).

transition	band position (cm^{-1}) observed	calculated
$d_{xy} \longleftrightarrow d_{x^2-y^2}$	ν_1 = 15,243	15,016
$d_{xz,yz} \longleftrightarrow d_{x^2-y^2}$	ν_2 = 16,611	16,723
	ν_3 = 17,182	17,319
$d_{3z^2} \longleftrightarrow d_{x^2-y^2}$	ν_4 = 20,661	20,662

The signs of D_q, D_s, and D_t are expected to be negative from the point-charge model, eqs. VI.2; these are in accordance with those estimated above using the energy levels given by the crystal-field theory, described by eqs. VI.3. However, the ratio D_t/D_q of the estimated values is close to unity; this should be less than 2/7 according to the point-charge model, described by eqs. VI.2. This is obviously due to the deficiency of the crystal-field theory. In practice, *ab initio* calculations are used to determine the energies and wave functions of the many-electron states, which characterize the bonding in molecules. Several semi-empirical molecular-orbital (MO) procedures have been proposed [21]. Smith [54] employed a semi-empirical MO method to explain the optical spectrum of tetragonal copper (II)-oxygen system. His method combined the point-charge and the angular-overlap models; the latter is based on the assumption that the amount by which the energy of the metal orbital is raised as a result of covalent bonding, is directly proportional to the square of the diatomic-overlap integral. About one quarter of the final energies, calculated by Smith, were accounted for by the electrostatic terms in the point-charge model, while the remaining, about three-quarter of the final energies, were accounted for by the angular-overlap terms.

For comparision, the results of the optical-absorption on Cu^{2+} ion in $BaCuSi_4O_{10}$ single crystal [14] are summerized as: (i) The three observed d-d transition bands, occurring at 12900, 15800 and 18800 cm^{-1}, have been assigned to be $d_{xy} \longleftrightarrow d_{x^2-y^2}$, $d_{xz,yz} \longleftrightarrow d_{x^2-y^2}$ and $d_{3z^2-r^2} \longleftrightarrow d_{x^2-y^2}$, respectively. (ii) The $d_{xz,yz} \longleftrightarrow d_{x^2-y^2}$ transfer band, has the maximum intensity, but the two lines of this band are not resolved. (iii) The Cu^{2+} ion in the crystal lattice is in a square-planar coordination with the oxygen ligands.

From the aasingnments of the d-d transition bands of the Cu^{2+} ion in MAT and a comparison with the study of Cu^{2+} ion in $BaCuSi_4O_{10}$, it appears that the Cu^{2+} ion in MAT single crystal sees a square-planar, D_{4h}, symmetry. It is due to the fact that when a Cu^{2+} ion substitutes for a Mg^{2+} ion in MAT, the two oxygen ligands of the Mg^{2+} ion along the axis, belonging to two different acetate groups, move rather far away from the centre of the Cu^{2+}-complex. This can be attributed to the JT effect [19]. The original complex, with an approximately tetragonally-distorted octahedral symmetry, now possesses only a square-planar symmetry.

The two presently-observed absorption bands in the UV range, occurring at frequencies ν_5 = 36,500 cm^{-1} and ν_6 = 43,100cm^{-1} are, probably, charge-transfer-transition bands, because they arise from the higher-lying energy levels, not shown in Figure VI.1. The present results can be compared with those for the $CuCl_4^{2-}$ complex, which possesses square-planar symmetry [16], for which three charge-transfer transitions have been observed in the UV range; they have been assigned as $1a_{2g} \longleftrightarrow 3b_{1g}$, $4e_u \longleftrightarrow 3b_{1g}$ and $3e_u \longleftrightarrow 3b_{1g}$

transitions, in order of decreasing wavelengths. For $CuCl_4^{2-}$, the intensities of the transitions $1a_{2g} \longleftrightarrow 3b_{1g}$ and $4e_u \longleftrightarrow 3b_{1g}$, are very weak; as well, these two transitions are close to each other in energy [16]. Using these results for $CuCl_4^{2-}$, combined with the poor resolution of the spectrometer used presently in the UV range, the transitions $1a_{2g} \longleftrightarrow 3b_{1g}$ and $4e_u \longleftrightarrow 3b_{1g}$ for Cu^{2+} in MAT can be considered to have the same energy $\nu_5 = 36{,}500\ cm^{-1}$. Finally, the remaining charge-transfer transition $3e_u \longleftrightarrow 3b_{1g}$ corresponds to the observed frequency $\nu_6 = 43{,}100\ cm^{-1}$.

CHAPTER VII

JAHN-TELLER EFFECT

The EPR technique has been extensively employed to study the Jahn-Teller effect (JTE) [1, 7, 22]. Many observations of the JTE have been reported on Cu^{2+}-doped single crystals, characterized by a high-symmetry host site for the Cu^{2+} ion [39].

Most cases of JTE for Cu^{2+} have been experimentally found to occur in diamagnetic host lattices. A model has been proposed to interpret the JTE in Cu^{2+}-doped diamagnetic host lattices. In this model, when the paramagnetic Cu^{2+} ion substitutes for an ion of a diamagnetic host lattice, local distortions are introduced because of the difference in size of the impurity ion from that of the host ion, as well as due to its paramagnetic nature. This fulfills the two conditions necessary for the occurrence of JTE [13]; namely, that the Cu^{2+} ion be in a degenerate electronic state, and that it occupy a minimum-energy non-degenerate state consequent to the small local distortion of the lattice that it produces.

JTE deals with complicated systems, which involve phonons and degenerate electronic ground states, as well as internal strains of variable strength and distortion in real crystals. When the kinetic energy of the ligand nuclei can be neglected, a static JTE is observed, otherwise a dynamic JTE manifests itself. The internal strain affects mainly the anisotropy of the EPR line positions and its shape. When the zero-order electronic states are non-degenerate, and they are insufficiently separated in energy compared to $\hbar\omega$ where ω is the frequency of the lattice phonons, a significant dynamic effect may be expected, which is the so-called pseudo JTE.

VII.1. Observation of static JTE of Cu^{2+} in PZST

The principal values of the $\tilde{g}$ and $\tilde{A}$ matrices, over the temperature range 4.2-295 K, as given in Table V.1.1, indicate a low symmetry of the Cu^{2+} complex in PZST, i.e. orthorhombically- distorted octahedral symmetry, since the three principal values, for each of the $\tilde{g}$ or $\tilde{A}$ matrices, are all different from each other. The independence of the EPR spectra, as well as that of the EPR line width, on the temperature below 295 K supports the occurrence of a static JTE.

The orthorhombic g-values due to the static JTE, as observed presently in PZST, can be analytically expressed as follows [1]:

$$g_1 = g_e - \frac{2\lambda}{\Delta} \left(\cos\frac{\phi}{2} + \sqrt{3}\,\sin\frac{\phi}{2} \right)^2;$$

$$g_2 = g_e - \frac{2\lambda}{\Delta} \left(\cos\frac{\phi}{2} - \sqrt{3}\,\sin\frac{\phi}{2} \right)^2;$$

$$g_3 = g_e - \frac{8\lambda}{\Delta} \cos^2\frac{\phi}{2} . \qquad \text{(VII.1)}$$

In eqs. VII.1 Δ (= $10D_q$, D_q has been defined in chapter VI) is the octahedral crystal-field-splitting constant for Cu^{2+} ion, ϕ is the vectorial angle of a polar coordinate system (ρ,ϕ) which describes the distortions Q_ε (= $\rho \sin\phi$) and Q_θ (= $\rho \cos\phi$) of the ML_6 complex, where M is Cu^{2+} and L are surrounding ligands, which are not, as yet, well identified for PZST.

For an arbitrary value of ϕ (except for $\phi = n\pi/3$, where n is an integer), the g values expressed by eqs. VII.1 correspond to an orthorhombic distortion of the octahedral symmetry (i.e., $g_1 \neq g_2 \neq g_3$); the directions of the principal values g_1, g_2, g_3 being along the three mutually perpendicular four-fold (tetragonal) axes of the ML_6 complex. The substitutions of the values of $\phi = \phi + 2\pi/3$, and $\phi = \phi + 4\pi/3$ in eqs. VII.1 interchange g_1, g_2, g_3 amongst themselves, i.e., they correspond to orthorhombic distortions about the two other tetragonal axes. The potential-energy surfaces, which are associated with the coupling between the magnetic electrons and the ligand nuclei, are referred to as the JT valleys. If ϕ_0 is the particular value that corresponds to the minimum, i.e., the bottom of the JT valley of one potential- energy surface, the ϕ values corresponding to the minima of the other two potential-energy surfaces are located at $\phi_0 + 2\pi/3$ and $\phi_0 + 4\pi/3$. In general, the energies of these three minima are different. In the case of Cu^{2+}-doped PZST, using the typical value of $\lambda/\Delta = -0.05$ [1] in eq. VII.1, and the measured values of g_1, g_2, g_3, ϕ_0 has been estimated to be approximately 30°.

There is only one substitutional site in the PZST single crystal lattice. In order to explain the superposition of the three sets of Cu^{2+} EPR spectra in the temperature range 4.2-295 K, Krishnan [25] proposed the existence of three domains in the crystal lattice. It is entirely possible to account for the present results by supposing that the different JT distortions of the Cu^{2+} complexes are randomly distributed with equal probabilities throughout the PZST crystal, rather than grouped into domains. This is further supported by examining the PZST crystal through a polarizing microscope, which does not reveal the existence of domains. That such a model naturally leads to a satisfactory explanation of the dynamic JTE observed at high-temperatures is explained in Sec. VII.2.

VII.2. Observation of dynamic JTE of Cu^{2+} in PZST

As the temperature was raised above 295 K, the h.f. lines of Cu^{2+} in PZST became broader due to relaxation effects. At T > 327 K the h.f. components became so broad that they were no longer resolved, only a single isotropic line was observed above 334 K. This is characteristic of the dynamic JTE. It occurs when the rate of tunneling through the barrier from one distorted configuration of the Cu^{2+} complex to the other exceeds the frequency difference between the corresponding EPR resonance lines for the different distorted configurations, i.e. that between the anisotropic spectra [22]. The present observation of static JTE upto 334 K is unusual; usually it occurs at low temperatures.

When the dynamic JTE occurs, only the time-average values of eqs. VII.1 are observed, since the vibrational frequency ($\approx 10^{13}$ Hz) is large compared to the frequency at which spin resonance is observed ($\approx 10^{10}$ Hz). This is the so-called time-averaging effect. Equations VII.1 yield the time-average values:

$$g_1 = g_2 = g_3 = g_e - 4\lambda/\Delta \quad ,$$

since

$$\langle \cos^2\phi/2 \rangle = \langle \sin^2\phi/2 \rangle = 1/2$$

and

$$\langle \cos(\phi/2)\sin(\phi/2) \rangle = 0 \ .$$

From the typical value of $\lambda/\Delta = -0.05$ for Cu^{2+} ion [1], $g_e - 4\lambda/\Delta$ is calculated to be 2.2; this value is very close to the presently observed g-value (2.191) at $T \geq 334$ K. The observation of only one isotropic line at $T \geq 334$ K can be explained to be due to motional averaging, caused by the rapid hopping between the three equivalent JT distorted sites, randomly distributed in the crystal with equal probabilities. Thus, at sufficiently high-temperatures the g value $(g_1 + g_2 + g_3)/3$ is expected, where g_1, g_2, and g_3 are the three principal values of the g matrix at lower temperatures. Using the g_1, g_2, g_3 values from Table V.1.1 at 295, 77, and 4.2 K, one finds the same average, i.e. $(g_1 + g_2 + g_3)/3 = 2.200$, within experimental error, at any temperature. The observed g value 2.191 from the broad EPR line at 334 K is, indeed, very close to this average g value.

Since the EPR spectrum for Cu^{2+} in PZST, above 334 K, is isotropic as revealed by both the position of the centre of the EPR line and the EPR linewidth, the oriented and random strains of the crystal are expected to be very small compared to kT (k is the Boltzmann constant), as deduced using the fact that the centre of the EPR line is influenced by oriented strains, while the EPR line-width is influenced by random strains [22]. The transition from static JTE at low temperatures to dynamic JTE at high temperatures has been experimentally determined presently to occur at 334 ± 1 K.

VII. 3. Observation of the pseudo JTE of Cu^{2+} in CASH and MASH

The principal values of the $\tilde{g}$ matrix, being all different from each other, over the temperature range 4.2 - 354 K for CASH, and 4.2-361 K for MASH, as plotted in Figures V.2.4 and V.3.3, indicate a low symmetry seen by the Cu^{2+} complexes in the CASH and MASH lattices, namely, orthorhombically-distorted octahedral symmetry. According to the crystal-field theory, the orbital doublet E_g of the

Cu^{2+} ion is split in a field of orthorhombic symmetry. This splitting is sufficiently small to allow the mixing of the two substates of E_g by coupling with the lattice vibrations. The vibronic mixing of the close-lying (pseudo-degenerate) levels due to the interaction of the Cu^{2+} ion with its ligands manifests itself in the pseudo JTE [6].

The molecular and electronic structure of the Cu^{2+} ion, surrounded by six identical ligands, is conventionally described in terms of JT coupling between the doubly degenerate electronic (E_g) and vibrational ($\mathcal{E}_g$) functions of the octahedral complex [6]. In a crystal lattice of octahedral symmetry, the first order $E_g \otimes \mathcal{E}_g$ vibronic coupling causes the potential surface of a Cu^{2+} complex to take the form of a "Mexican hat". The nuclear geometry fluctuates between the various configurations of D_{4h} and D_{2h} symmetries, which are generated by linear combinations of Q_θ and Q_ε, the components of the $\mathcal{E}_g$ vibrational mode. When higher-order coupling terms are included, the perimeter of the Mexican hat becomes warped, giving rise to three equivalent minima, whose projections correspond to different symmetries, which are generated by linear combinations of Q_θ and Q_ε. (Q_θ and Q_ε are conventionally expressed as $Q_\theta = \rho \cos\phi$ and $Q_\varepsilon = \rho \sin\phi$ in terms of a polar coordinate system (ρ, ϕ).) The projections of the three minima correspond to different ϕ values in the $(Q_\theta, Q_\varepsilon)$ space. Equivalently, the Mexican-hat potential results in three equivalent potential valleys. Ham [22] pointed out that a strain, having a tetragonal component, displaces the energy of the three configurations with respect to each other, thereby destroying their equivalence.

Comparing the Cu^{2+} principal g-values at 295 K in the CASH and MASH lattices with those in the pure $Cu(NH_4)_2(SO_4)_2.6H_2O$ lattice at 300 K ($g_z = 2.36$, $g_y = 2.209$, $g_x = 2.06$ [46]), it is found that these g-values are very close to each other. This indicates that the local symmetry of the Cu^{2+} ion either in the CASH lattice, or in MASH lattice, is close to that of the Cu^{2+} ion in the pure $Cu(NH_4)_2(SO_4)_2.6H_2O$ lattice, rather than that of the Cd^{2+} or Mg^{2+} ion, which the Cu^{2+} ion replaces, in the pure CASH or MASH lattice. Thus, a large orthorhombic distortion of the lattice occurs when the impurity ion Cu^{2+} enters the CASH lattice substituting for a Cd^{2+} or Mg^{2+} ion, due to (i) difference in the ionic radii of the Cu^{2+} and Cd^{2+}, or Mg^{2+}, ions and (ii) the paramagnetic nature of the Cu^{2+} ion. This orthorhombic distortion can be seen to be due to the three mutually perpendicular tetragonal components of the crystal field, which perturb the three equivalent potential valleys, resulting in three inequivalent potential valleys with different energy levels.

Silver and Getz [53] studied Cu^{2+}-doped Zn Tutton salts, and proposed that when the JT effect is strong with appreciable warping, and the overlap between the wave functions describing the potential valleys in the three different minima is rather small, the temperature dependent principal g- and A-values could be expressed as statistical averages, using the occupation probabilities of the three minima which possess different energies, under the assumption of short reorientation times which ensures Boltzmann population distributions. Petrashen et al. [46] expressed the expressions of the temperature-dependent principal g-values as follows:

$$g_z(T) = \frac{N_1}{N} g_{z1} + \frac{N_2}{N} g_{y2} + \frac{N_3}{N} g_{x3} ;$$

$$g_y(T) = \frac{N_1}{N} g_{y1} + \frac{N_2}{N} g_{z2} + \frac{N_3}{N} g_{y3} ;$$

and

$$g_x(T) = \frac{N_1}{N} g_{x1} + \frac{N_2}{N} g_{x2} + \frac{N_3}{N} g_{z3} ; \qquad \text{(VII.2)}$$

where g_z, g_y and g_x correspond to the Cd-$O_7(H_2O)$, Cd-$O_8(H_2O)$, and the Cd-$O_9(H_2O)$ directions in the $Cd(H_2O)_6^{2+}$ complex, respectively, or to the Mg-$O_7(H_2O)$, Mg-$O_8(H_2O)$, and the Mg-$O_9(H_2O)$ directions in the $Mg(H_2O)_6^{2+}$ complex. (The presently estimated principal values of the $\tilde{g}$ matrix are related to $g_{\alpha k}$ as follows: $g_{z1} = g_{z'}$, $g_{y1} = g_{y'}$, $g_{x1} = g_{x'}$.) N_1, N_2 and N_3 are the populations of the first, second and third potential valleys, so that the total population $N = N_1 + N_2 + N_3$; $g_{\alpha k}$ (α = x, y, z; k = 1, 2, 3) are the principal values of the $\tilde{g}$ matrix of the $Cu(H_2O)_6^{2+}$ complex in the k-th valley; the $g_{\alpha k}$ sets in eqs. VII.2 are expressed according to the identification of the JT configurations with the minima of the adiabatic potential in the (Q_θ, Q_ε) space. (The subscript k indicates the relative order of the energies of the three minima of the potential valleys, k = 1 indicates the lowest energy while k = 3 indicates the highest energy of these minima.) It is necessary to know $g_{\alpha k}$ in order to estimate $g_\alpha(T)$, $\alpha = x, y, z$. Generally speaking, g_k values are different in different valleys. However, $g_{\alpha 1}$ values may be used in place of all the $g_{\alpha k}$ (k = 1, 2, 3) for the case of small deformation of the octahedron at 4.2 K for the $Cu(H_2O)_6^{2+}$ complex, since the complex is fully localized in the valley possessing the lowest minimum energy (k = 1) at and below 4.2 K.

$\delta_{1,2}$, the energy splitting between the potential valleys 1 and 2, has been calculated [46,53] for Zn-Tutton salt under the assumption that $N_3 = 0$ at temperatures below 300 K, using the first two of eqs. VII.2. This is because the third of eqs. VII.2 yields $g_x(T) \approx g_{x1} \approx g_{x2}$ for this case. Thus, one has to use only the first two of eqs. VII.2, putting $N_3 = 0$, to estimate N_1 and N_2 which yield $\delta_{1,2}$, using Boltzman population distribution, i.e.,

$$N_1/N_i = \exp(\delta_{1,i}/kT) \qquad (i = 2,\ 3). \qquad \text{(VII.3)}$$

Equation VII.3 also yields the estimation of $\delta_{1,3}$, when N_3 is not equal to zero. As for estimating the value of $\delta_{1,3}$, the energy splitting between the potential valleys 1 and 3, Silver and Getz [53] took into account the increase in g_x at high temperatures, while Petrashen et al. [46] estimated the value of $\delta_{1,3}/\delta_{1,2}$, using the bond-lengths between the central diamagnetic ion and its ligands, as determined from X-ray data; they estimated the value of $\delta_{1,3}$ in terms of the value of $\delta_{1,2}$ using eqs. VII.2.

In the case of CASH, the symmetry of the $Cd(H_2O)_6^{2+}$ complex is a distorted tetragonally-compressed octahedron, since the bond-length difference between $Cd-O_7(H_2O)$ and $Cd-O_8(H_2O)$ is very small (0.001 Å) [42]. These two bond lengths can, thus, be assumed to be the same within experimental error (0.007 Å). According to Petrashen et al. [46] the value of $\delta_{1,3}/\delta_{1,2}$ could not be estimated from X-ray data in the present case. However, the same procedure can, here, be followed as that for Zn-Tutton salt except that the g_x value does not, here, change below 77 K, as compared to the case of Zn-Tutton salt for which it does not change below 300 K. It implies that the potential valley 3 must lie considerably higher in energy than the valley 2 in the present case, and that the value of $\delta_{1,3}$ in the present case, i.e., for Cu^{2+} in CASH, must be less than that for Cu^{2+} in the Zn-Tutton salt.

In order to calculate the ratio of the populations, N_1/N_2 for CASH, in the temperature range 4.2 - 77 K, only the first two equations in eqs. VII.2 have been used, because the value of g_x does not change in this temperature range. At temperatures above 77 K, all three of eqs. VII.2 are taken into account, since, here, g_x is temperature dependent. Finally, N_1/N_2 and N_1/N_3 ratios, as estimated from eqs. VII.2, at 295 K are 3.6 and 5.0, respectively, which yield, using Boltzmann-population distribution eq. VII.3, the values of $\delta_{1,2}$ and $\delta_{1,3}$ to be 260 cm^{-1} and 330 cm^{-1}, respectively, at 295 K.

Figure VII.1 exhibits the dependence of $\delta_{1,2}$ upon temperature in the range 4.2 - 295 K; it shows that $\delta_{1,2}$ increases, in general, with temperature, this increase being quite enhanced at lower temperatures, while it is rather small at intermediate temperatures, acquiring ultimately a steady value (around 260 cm^{-1}) at temperatures between 212 and 295 K. The temperature dependence of the energy $\delta_{1,2}$ is due to the deformation of the crystal lattice with changing temperature,[14] as revealed by the change of g_x, since N_3 is no longer zero, in the present case, at T > 77 K.

In the case of MASH, the symmetry of the $Mg(H_2O)_6^{2+}$ complex is a distorted tetragonally-compressed octahedral, since the bond length difference between $Mg\text{-}O_7(H_2O)$ and $Mg\text{-}O_8(H_2O)$ is 0.01 Å [28]. The host-metal ion, Mg^{2+}, is diamagnetic, the same effect, i.e. JTE, can be expected when Cu^{2+} ion enters into MASH lattice. The experimental results (Sec. V.3) confirm this prediction.

In order to calculated the ratio of the populations, N_1/N_2, for MASH in the temperature range 4.2-240 K, only the first two of the eqs. VII.2 have been used, because the g_x component of $\tilde{g}$ matrix does not change in this temperature range. The estimation of $\delta_{1,2}$ values, was then made, by the

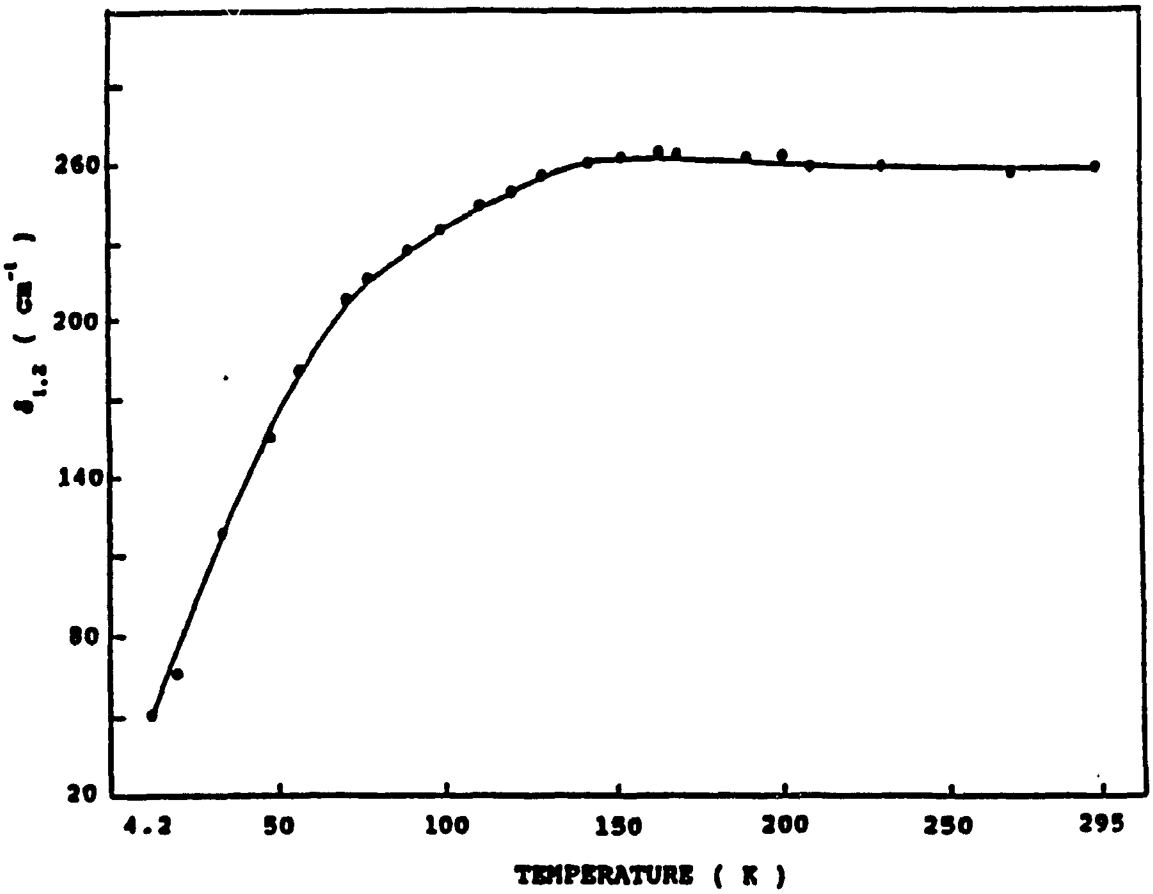

Figure VII.1. Temperature dependence of the energy splitting between the lowest and the intermediate potential valleys ($\delta_{1,2}$) for the $Cu(H_2O)_6^{2+}$ complex in $Cd(NH_4)_2(SO_4).6H_2O$ (CASH).

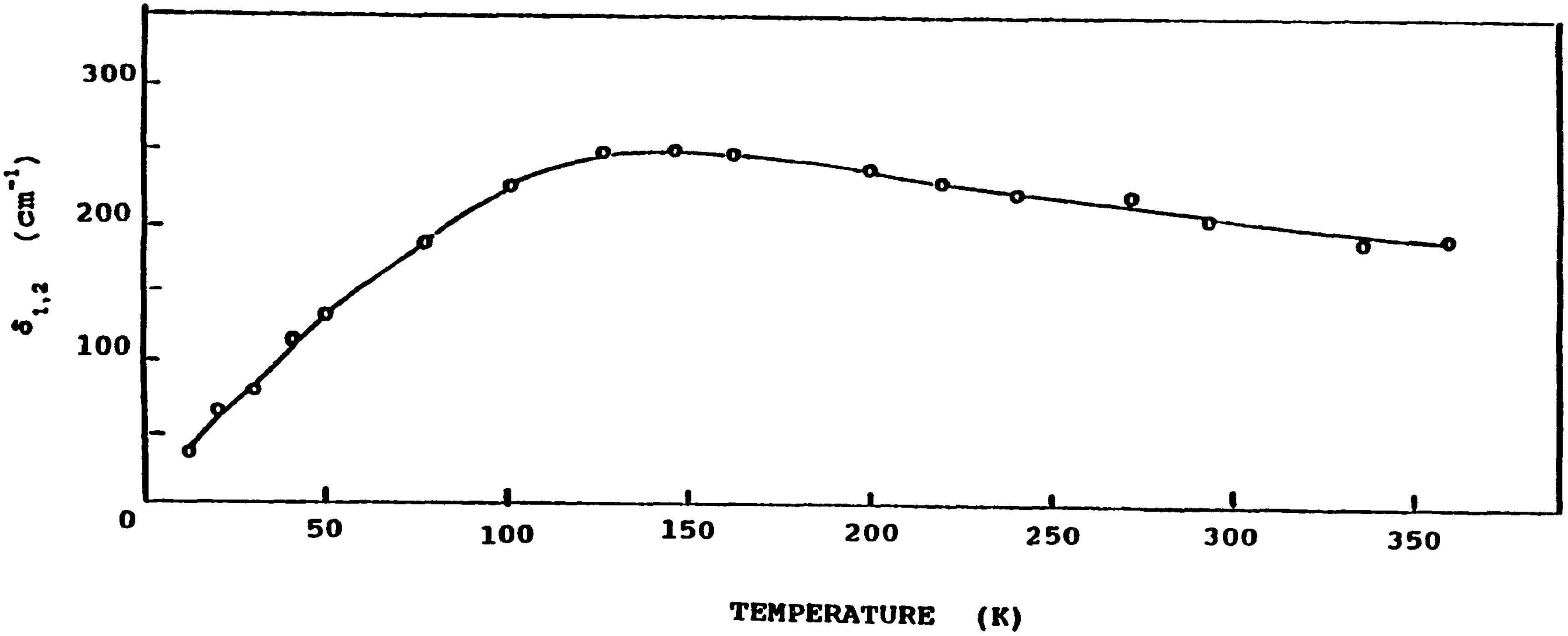

Figure VII.2. Temperature dependence of the energy splitting between the lowest and the intermediate potential valleys ($\delta_{1,2}$) for the $Cu(H_2O)_6^{2+}$ complex in $Mg(NH_4)_2(SO_4).6H_2O$ (MASH).

use of eq. VII.3, using these values of N_1/N_2. The values of $\delta_{1,2}$ estimated at $T \leq 240$ K are plotted in Figure VII.2. At $T > 240$ K, all three of eqs. VII.2 were taken into account, since g_x is here temperature dependent. Finally, N_1/N_2 and N_1/N_3 for MASH, as estimated from eqs. VII.2 and the values of $\delta_{1,3}/\delta_{1,2}$ estimated from eq. VII.3 at $T > 240$ K are as follows:

	272 K	295 K	336K	361 K
N_1/N_2	3.1	2.8	2.3	2.2
N_1/N_3	33	13	12	9.3
$\delta_{1,3}/\delta_{1,2}$	3.0	2.5	3.0	2.9

The value of $\delta_{1,3}/\delta_{1,2}$ at 295 K is close to that was predicted to be 3.2 at 300 K from X-ray data by Petrashen et al. [46].

These values of $\delta_{1,3}/\delta_{1,2}$ are easily understood if one examines the behavior of g_x value in the temperature range from 4.2 - 300 K. In the cases of Zn Tutton salts, $\delta_{1,3}/\delta_{1,2}$ was estimated to be 4.5 at 300 K [46], with the g_x value remaining unchanged in the temperature range 4.2-300 K [53]. For the case of CASH, $\delta_{1,3}/\delta_{1,2}$ at 295 K was estimated to be 1.3 presently, with the g_x component remaining unchanged over the temperature range 4.2-77 K, while in MASH, $\delta_{1,3}/\delta_{1,2}$ at 295 K was estimated to be 2.5 presently, with the g_x value remaining unchanged in the temperature range 4.2 - 240 K. Obviously, the temperature range, in which the g_x value does not change appreciably, is related to the value of $\delta_{1,3}/\delta_{1,2}$.

VII.4. Local symmetries of the Cu^{2+} complex

When Cu^{2+} impurity ions enter crystal lattices, the local symmetry of the host suffers a distortion due to JTE.

VII.4.1. Local symmetry of the Cu^{2+} in PZST

The present EPR studies of Cu^{2+} in PZST provided the details of the local symmetry at the Zn^{2+} site in PZST lattice, which were previously not available (details in Sec. V.1). In the case of Cu^{2+}-doped PZST, the principal values of the $\tilde{g}$ and $\tilde{A}$ tensors are found to be independent of temperature in the temperature range 4.2 - 295 K. This indicates that the populations N_1, N_2, and N_3 in the respective JT valleys are constant, and equal to each other, in this temperature range, according to eqs. VII.2. This is only possible when the energies of the three JT valleys are equal to each other, since the populations in the corresponding JT valleys are governed by Boltzmann distribution.

Petrashen et al. [46] have studied the dynamic JTE nature of $Cu(H_2O)_6^{2+}$ complexes in the zinc and copper Tutton salts, using EPR and X-ray data. They found that the ratio of the energy splittings between the three JT configurations of $Cu(H_2O)_6^{2+}$ complex (δ_{13}/δ_{12}), as estimated from the temperature-dependent principal values of the $\tilde{g}$ matrix, is close to that, which is estimated taking into account the symmetry of the $Zn(H_2O)_6^{2+}$ complex and the variation of the energy of the JT-ion due to the distortions. Thus, the symmetry of the host complex can be deduced from the energy splittings between the three JT valleys of the complex $Cu(H_2O)_6^{2+}$, as determined from EPR data. Proceeding in an analogous manner, it is concluded that since the energies of the three JT valleys of the Cu^{2+} complex are identical in PZST, the local symmetry of the Zn^{2+} ion in PZST is, either, regular octahedral, or, mostly likely, octahedral with a small trigonal distortion. When a Cu^{2+} ion substitutes for a Zn^{2+} ion in PZST, it changes the trigonally-distorted octahedral symmetry to orthorhombically- distorted octahedral symmetry, because of its different size, and different interaction with ligands. This manifests itself as the static JTE.

VII.4.2. Local symmetry of the Cu^{2+} in CASH

The local symmetry of the Cd^{2+} site in CASH is approximately a compressed tetragonally-distorted octahedron (details in Sec. V.2), because the bond length difference between Cd-O_7 (H_2O) and Cd-O_8 (H_2O) is very small (0 001Å) [42]. These two bond lengths can, thus, be assumed to be the same within experimental error (0.007Å).

The principal g-values, as estimated from the present EPR measurements, are orthorhombic, indicating that the local symmetry of Cu^{2+} in CASH crystal lattice is orthorhombic. Comparing the principal g values of Cu^{2+} in the pure $Cu(NH_4)_2(SO_4)_2.6H_2O$ [46], listed in Table VII.4.1, in which those of Cu^{2+} in CASH are also listed for convenience, it is found that the principal values of Cu^{2+} in the two crystal lattices at room and liquid-helium temperatures are quite close. Thus, the local symmetry cf Cu^{2+} in CASH at room and liquid-helium temperatures is very close to that of Cu^{2+} in the $Cu(NH_4)_2(SO_4)_2.6H_2O$ lattice. The bond lengths of Cu^{2+} in $Cu(NH_4)_2(SO_4)_2.6H_2O$ (orthorhombic symmetry) with its ligands are 2.230 Å, 2.072 Å, and 1.966 Å for Cu-O(7), Cu-O(8) and Cu-O(9), respectively; while the bond angles are 88.90° for O(7)-Cu-O(8), 90.65° for O(7)-Cu-O(9), and 88.9° for O(8)-Cu-O(9) [12] (Figure V.2.1). The conclusion is that the local symmetry of Cu^{2+} in CASH crystal lattice must be orthorhombically-distorted octahedral rather than approximately tetragonally-distorted octahedral.

VII.4.3. Local symmetry of Cu^{2+} in MASH

The local symmetry of Mg^{2+} ion in MASH is approximately a compressed tetragonally-distorted octahedral (details in Sec. V.3), for the bond length difference between $Mg\text{-}O_7(H_2O)$ and $Mg\text{-}O_8(H_2O)$ is only 0.01 Å [28]. When an impurity Cu^{2+} ion enters into the MASH lattice, the same consequence as that for the case of CASH can be expected. That is the local symmetry of Cu^{2+} in MASH is the same as that of Cu^{2+}

Table VII.4.1 The principal g-values of Cu^{2+} in $M(NH_4)_2(SO_4)_2.6H_2O$ (M = Cu, Cd and Mg) single crystals

HOST COMPOUND	TEMPERATURE (K)	g_z	g_y	g_x	Ref.
$Cu(NH_4)_2(SO_4)_2.6H_2O$	300	2.36	2.209	2.06	b
	77	2.424	2.11	2.067	b
	4.2	2.427	2.11	2.065	b
$Cd(NH_4)_2(SO_4)_2.6H_2O$	295	2.3373	2.2111	2.0712	a
	77	2.3613	2.1721	2.0522	a
	4.2	2.4290	2.1594	2.0513	a
$Mg(NH_4)_2(SO_4)_2.6H_2O$	295	2.324	2.220	2.209	a
	77	2.418	2.122	2.072	a
	4.2	2.426	2.144	2.068	a

a Present work.

b Data from Ref. [46]

ion in CASH.

The principal g values estimated from the present work are orthorhombic at 295, 77, and 4.2 K. Comparing with those of Cu^{2+} ion in pure $Cu(NH_4)_2(SO_4)_2.6H_2O$ single crystal, for convenience all these data are presented in Table VII.4.1, they are quite close to each other. The local symmetry of Cu^{2+} in MASH is orthorhombic, rather than compressed tetragonally-distorted octahedral, which is the local symmetry of Mg^{2+} ion in MASH lattice. This has to be attributed to JTE.

VII.4.4. Local symmetry of Cu^{2+} in MAT

In the case of Cu^{2+} in MAT crystal lattice the local symmetry changed somewhat due to JT distortion, when a Cu^{2+} ion substituted for a Mg^{2+} ion. The symmetry of the Cu^{2+}-complex in MAT can be considered to be square planar, rather than an elongated tetragonal. For details, see chapter VI.

CHAPTER VIII

ESTIMATION OF MOLECULAR-ORBITAL COEFFICIENTS OF Cu^{2+} IN MAT

Using the energy-level splittings of the Cu^{2+} ion in the lattice of MAT, it is possible to estimate the molecular-orbital (MO) coefficients for Cu^{2+} in MAT. The splitting of the d, or f orbitals of transition-metal ions in molecular complexes is usually described by crystal-field theory. However, it does not take into account the effect of interaction with the ligand electrons adequately. In fact, the crystal-field theory is not fully applicable to those complexes, which are characterized by strong interactions between the electron orbitals of the central atom and ligands, responsible for the formation of molecular orbitals.

The spin-Hamiltonian parameters (S.H.P.) of the transition-metal ions can be expressed in terms of (i) the coefficients of the MO; (ii) the energy separations between the excited states and the ground state of the ion; and (iii) the energies of the charge-transfer transition bands, which can be determined from optical spectrum. EPR, thus, becomes an integral tool for the estimation of the MO coefficients of transition-metal complexes, since S.H.P. are determined from EPR measurements. The optical-absorption data for Cu^{2+}-doped MAT indicates that the Cu^{2+} complex in MAT single crystal sees a local D_{4h} square-planar symmetry. For the Cu^{2+} complex in MAT the equatorial Cu-O (H_2O) bond

Table VIII.1. Molecular orbitals characteristics of the antibonding $3b_{1g}$, $2b_{2g}$, $2e_g$ levels and the bonding $1b_{2g}$, $1e_g$ levels

---

$$|3b_{1g}\rangle = \alpha_0|d_{x^2-y^2}\rangle - \beta_0\{\mu|\kappa_{\rho\sigma}(b_{1g})\rangle + (1-\mu^2)^{1/2}|\kappa_s(b_{1g})\rangle\},$$

$$|2b_{2g}\rangle = \alpha_1|d_{xy}\rangle - \beta_1|\kappa_{\rho\pi}(b_{2g})\rangle,$$

$$|2e_{g1}\rangle = \alpha_2|d_{xz}\rangle - \beta_2|\kappa_{\rho\pi}(e_{g1})\rangle,$$

$$|2e_{g2}\rangle = \alpha_2|d_{yz}\rangle - \beta_2|\kappa_{\rho\pi}(e_{g2})\rangle,$$

$$|1b_{2g}\rangle = \alpha_1'|d_{xy}\rangle + \beta_1'|\kappa_{\rho\pi}(b_{2g})\rangle,$$

$$|1e_{g1}\rangle = \alpha_2'|d_{xz}\rangle + \beta_2'|\kappa_{\rho\pi}(e_{g1})\rangle,$$

$$|1e_{g2}\rangle = \alpha_2'|d_{yz}\rangle - \beta_2'|\kappa_{\rho\pi}(e_{g2})\rangle,$$

$$|\kappa_{\rho\sigma}(b_{1g})\rangle = \frac{1}{2}\{-p_x(1) + p_y(2) + p_x(3) - p_y(4)\},$$

$$|\kappa_s\ (b_{1g})\rangle = \frac{1}{2}\{s(1) - s(2) + s(3) - s(4)\},$$

$$|\kappa_{\rho\pi}(b_{2g})\rangle = \frac{1}{2}\{p_y(1) + p_x(2) - p_y(3) - p_x(4)\},$$

$$|\kappa_{\rho\pi}(e_{g1})\rangle = \frac{1}{\sqrt{2}}\{p_z(1) - p_z(3)\},$$

$$|\kappa_{\rho\pi}(e_{g2})\rangle = \frac{1}{\sqrt{2}}\{p_z(2) - p_z(4)\},$$

---

length is 2.075 Å, being the average distance of Mg-H_2O (1) and Mg-H_2O (2) in the MAT host lattice [51].

Maki and McGarvey [26] were the first to apply the MO theory to the Cu^{2+} complex with tetragonally-distorted octahedral symmetry in order to derive theoretical expressions for the $\tilde{g}$ and $\tilde{A}$ matrices. The overlaps of the p orbitals of the four ligand oxygens in the equatorial plane, as well as those of the two oxygen ligands on the axis perpendicular to the equatorial plane, were subsequently taken into account by Smith [56], who derived theoretical expressions for the $\tilde{g}$ matrix, to second-order in perturbation; these were later extended to third-order in perturbation by Moreno [43]. Finally, Aramburu and Moreno [2] deduced the theoretical expressions for all three $\tilde{g}$, $\tilde{A}$ and the superhyperfine (s.h.f.) matrices of the Cu^{2+} square-planar complex, using the MO theory, to third-order in perturbation, taking into account the contributions from the bonding MO.

If one neglects, in a first step, the spin-orbit coupling, the MO characteristics of the antibonding levels $3b_{1g}$, $2b_{2g}$, $2e_g$ and those of the bonding levels $1b_{2g}$ and $1e_g$, corresponding to the ground state $^2B_{1g}$ of the complex, are as summarized in Table VIII.1 [8].

Explicitly, the S.H.P. can be formally expressed as functions of K_o, the core polarization contribution, and the eleven coefficients of MO α_i, β_i (i = 0, 1, 2), and α'_i, β'_i (i = 1, 2), and μ as follows [2]:

$$g_{\parallel} = g_e + ak_1 + a'k_1' \ ;$$

$$g_{\perp} = g_e + bk_2 + b'k_2' \ ;$$

$$A_{\parallel} = -K_{\circ} + 2A_0 + P(a + a' + \frac{3}{7}b + \frac{3}{7}b') \ ;$$

and

$$A_{\perp} = -K_{\circ} - A_0 + \frac{11P}{14}(b + b') \ . \qquad \text{(VIII.1)}$$

In eqs. VIII.1 g_e (=2.0023) is the free electron g value, P $= 2g_N\mu_B\mu_N\langle r^{-3}\rangle_M = 0.036\ \text{cm}^{-1}$ [24], where g_N, μ_N, and $\langle r^{-3}\rangle_M$ are, respectively, the nuclear g factor, the nuclear magneton and the average of the inverse-cube radius of the Cu^{2+} ion.

The various quantities appearing on the right-hand sides of eqs. VIII.1 are defined as follows:

$$A_0 = -\frac{2}{7}\alpha_0^2 P \ ;$$

$$k_1 = 1 - \frac{\beta_0}{\alpha_0} S - \frac{\beta_1}{2\alpha_1}\left(2S_1 + \frac{\beta_0}{\alpha_0}\Gamma(\mu)\right) \ ;$$

$$k_1' = 1 - \frac{\beta_0}{\alpha_0} S_0 + \frac{\beta_1'}{2\alpha_1'}\left(2S_1 + \frac{\beta_0}{\alpha_0}\Gamma(\mu)\right) \ ;$$

$$k_2 = 1 - \frac{\beta_0}{\alpha_0} S_0 - \frac{\beta_2}{\sqrt{2}\alpha_2}\left(\sqrt{2}S_2 + \frac{\beta_0}{\alpha_0}\Gamma(\mu)\right) \ ;$$

$$k_2' = 1 - \frac{\beta_0}{\alpha_0} S_0 + \frac{\beta_2'}{\sqrt{2}\alpha_2'}\left(\sqrt{2}S_2 + \frac{\beta_0}{\alpha_0}\Gamma(\mu)\right) \ ;$$

$$a = 8\alpha_0\alpha_1 \left(1 - \frac{\beta_0\beta_1\mu|\xi_L|}{2\alpha_0\alpha_1|\xi_M|}\right)|\xi_M|/\Delta_1 \;;$$

$$a' = 8\alpha_0^2\alpha_2'^2 \left(1 + \frac{\beta_0\beta_1'\mu|\xi_L|}{2\alpha_0\alpha_1'|\xi_M|}\right)|\xi_M|/\Delta_1' \;;$$

$$b = 2\alpha_0^2\alpha_2^2\left(1 - \frac{\beta_0\beta_2\mu|\xi_L|}{\sqrt{2}\alpha_0\alpha_2|\xi_M|}\right)|\xi_M|/\Delta_2 \;;$$

and

$$b' = 2\alpha_0^2\alpha_2'^2 \left(1 + \frac{\beta_0\beta_2'\mu|\xi_L|}{\sqrt{2}\alpha_0\alpha_2'|\xi_M|}\right)|\xi_M|/\Delta_2' \;. \qquad \text{(VIII.2)}$$

In eqs. VIII.2 Δ_1 and Δ_2 are the d-d transfer energies of the $d_{xy} \longleftrightarrow d_{x^2-y^2}$ and $d_{xz,yz} \longleftrightarrow d_{x^2-y^2}$ transitions, determined presently from the optical-absorption spectrum to be $\Delta_1 = 15{,}243$ cm^{-1} and $\Delta_2 = (\nu_2 + \nu_3)/2 = 16{,}897$ cm^{-1}, while Δ_1' and Δ_2' are the charge-transfer transition energies corresponding to the charge transitions $1b_{2g} \longleftrightarrow 3b_{1g}$ and $1e_g \longleftrightarrow 3b_{1g}$, respectively (determined presently from the optical-absorption spectrum to be 43,100 cm^{-1}, each). For comparision, it is noted that for the $CuCl_4^{2-}$ complex, which possesses a D_{4h} symmetry [16], the calculated values of Δ_1' and Δ_2' are found to be, respectively, higher and lower, in energy, than that of the observed charge-transfer transition band $3e_u \longleftrightarrow 3b_{1g}$. In eqs. VIII.2 ξ_M, ξ_L are, respectively, the spin-orbit coupling constants of the central metal ion (Cu^{2+}) and the ligand ions (O^{2-}) of the complex. (The values of $|\xi_M|$ and $|\xi_L/\xi_M|$ are assumed to be 830 cm^{-1} and 0.18 [56].) Further, in eqs. VIII.2 S_o, S_1 and S_2, in the expressions for k_1, k_1', k_2, and k_2', are the group-overlap integrals:

$$S_o = \mu S_{p\sigma} + \sqrt{(1 - \mu^2)}\, S_s \,,$$

$$S_1 = \langle d_{xy}|\chi_{p\pi}(b_{2g})\rangle \,,$$

and

$$S_2 = \langle d_{xz}|\chi_{p\pi}(e_g)\rangle \,; \qquad \text{(VIII.3)}$$

where

$$S_{p\sigma} = \langle d_{x^2-y^2}|\kappa_{p\sigma}(b_{1g})\rangle$$

and

$$S_s = \langle d_{x^2-y^2}|\kappa_s(b_{1g})\rangle \,. \qquad \text{(VIII.4)}$$

The group-overlap integrals $S_{p\sigma}$, S_s, S_1 and S_2 can be estimated in terms of S_e, the diatomic-overlap integrals between the 3d orbital of the Cu^{2+} ion and the 2s and 2p orbitals of the oxygen ligands. For a square-planar configuration, in which the contribution from the orbitals of axial atoms can be neglected, these group-overlap integrals are expressed as [55]:

$$S_{p\sigma} = \sqrt{3}S_e(2p\sigma, 3d\sigma),$$

$$S_s = \sqrt{3}S_e(2s\sigma, 3d\sigma),$$

$$S_1 = 2S_e(2p\pi, 3d\pi),$$

and

$$S_2 = \sqrt{2}S_e(2p\pi, 3d\pi).$$

Here the σ and π in parentheses after S_e indicate σ- and π-bonding, respectively. These diatomic-overlap integrals are calculated from the approximate formulae for the 3d-, 2s-, and 2p-orbitals in σ- or π-bonding [17, 18], using the double-ζ radial functions of the copper 3d-orbital [49]

$$\phi(3d) = 0.5933N_1'r^2e^{-5.95} + 0.5744N_2'r^2e^{-2.30},$$

and the oxygen 2s- and 2p- orbitals [15]

$$\phi(2s) = 0.70761N_1re^{-2.6880} + 0.37450N_2re^{-1.67543},$$
$$\phi(2p) = 0.33221N_3re-3.69445 + 0.74483N_4re^{-1.65864}.$$

By assuming the Cu-O bond length (R_e) in the equatorial plane to be 2.075 Å the values of the group-overlap integrals are here estimated to be $S_{p\sigma} = 0.132$, $S_s = 0.107$, $S_1 = 0.0730$ and $S_2 = 0.0516$.

$\Gamma(\mu)$, appearing in eqs. VIII.2, is given by

$$\Gamma(\mu) = \mu - (1 - \mu)^{1/2}R_e\langle s(1)|\frac{\partial}{\partial y(1)}|p_y(1)\rangle, \qquad \text{(VIII.5)}$$

where (1) refers to ligand 1, representive of the four equivalent (1, 2, 3, 4) oxygen ligands, while s and p_y denote the corresponding orbitals.

The value of the integral $\langle s(1)|\frac{\partial}{\partial y(1)}|p_y(1)\rangle$ in the expression for $\Gamma(\mu)$ in eqs. VIII.5 is 0.57, whose magnitude was estimated by Smith [56], while the sign was determined by Aramburu and Moreno [2], in accordance with the fact that the most-covalent systems experience positive g shifts, whereas the most-ionic ones negative g shifts.

The eleven MO coefficients (α_i, β_i; $i = 0, 1, 2$ and α'_i, β'_i; $i = 1, 2$, and μ), appearing in eqs. VIII.2 - VIII.5 have been defined in Table VIII.1. Specifically, α_i and β_i for $i = 0, 1, 2$, respectively, are the MO coefficients of the antibonding levels $3b_{1g}$, $2b_{2g}$, $2e_g$, while α'_i and β'_i for $i = 1, 2$ are, respectively, the MO coefficients of the bonding levels $2b_{2g}$, $2e_g$; here α refers to the coefficients of the central Cu^{2+} ion of the complex, while β to those for the ligands. μ and $(1-\mu^2)^{1/2}$ are, respectively, the coefficients of the p and s orbitals of the oxygen ligands in the $3b_{1g}$ configuration, which depend on the hybridization of the oxygen ion of the water molecule.

There exists a relationship between the antibonding and bonding MO coefficients of $2b_{2g}$ and $2e_g$ levels [4]:

$$\alpha_i\alpha'_i - \beta_i\beta'_i + \alpha_i\beta'_iS_i - \alpha'_i\beta_iS_i = 0 \; ; \quad i = 1, 2 \qquad \text{(VIII.6)}$$

Finally, the normalizations of the MO coefficients are [19]:

$$\alpha_i^2 + \beta_i^2 - 2\alpha_i\beta_iS_i = 1 \; ; \quad i = 0, 1, 2 \qquad \text{(VIII.7)}$$

and

$$\alpha_i'^2 + \beta_i'^2 + 2\alpha_i'^2 \beta_i'^2 S_i = 1 \;; \quad i = 1, 2. \qquad \text{(VIII.8)}$$

In the present case (Cu^{2+}-doped MAT) there are twelve unknown coefficients; these are the eleven MO coefficients and the core-polarization contribution (K_o). However, there are available only eleven equations: four expressions for the S.H.P., eqs. VIII.1, five normalization conditions between α_i and β_i ($i = 0, 1, 2$), and α_i' and β_i' ($i = 1, 2$), eqs. VIII.7 and VIII.8, and two equations between the coefficients of the antibonding and the bonding orbitals, eqs. VIII.6. In order to reduce the number of unknowns to be determined to eleven the value of the coefficient μ has here been assumed to be $\sqrt{3}/2$, corresponding to sp^3 hybridization of oxygen (water) ligand [58]. It is difficult to obtain well-defined solutions for the MO coefficients, because the equations relating the MO coefficients are non-linear. On the other hand, in order to estimate their values one can always fit the MO coefficients by a least-squares technique to $M = \sum_{i=1}^{4} (SHP^i_{cal.}/SHP^i_{obs.} - 1)^2$, with the condition that the best-fit MO coefficients minimize the value of M. Here SHP^i ($i = 1$-4) refer to the four principal values of the $\tilde{g}$ and $\tilde{A}$ matrices ($g_\parallel$, $g_\perp$, $A_\parallel$, and $A_\perp$), while obs. and cal. indicate their observed and calculated values, respectively.

The MO coefficients and K_o, so determined, using the program EUREKA on an IBM-PC XT, equipped with a MATH coprocessor chip 8087-2, are listed as follows:

$K_o(cm^{-1})$	α_0	β_0	α_1	β_1	α_2	β_2	α'_1	β'_1	α'_2	β'_2
125×10^{-4}	.88	.65	1.0	.01	.98	.26	.02	1.0	.21	.97

These coefficients are characterized by the value of M = 0.54. The presently-determined value of K_o = 125×10^{-4} cm^{-1} is very close to K_o = 130×10^{-4} cm^{-1}, which has been calculated theoretically for the free Cu^{2+} ion by Watson and Freeman [59]. The present values of the coefficients α_0, α_1, and α_2 imply that the nature of the bonding of the Cu^{2+} ion in MAT crystal lattice is not purely ionic. This is because $\alpha_0^2 = 0.77$ indicates that there is an appreciable in-plane covalent σ-bonding of Cu^{2+} ion with the oxygen ligands in the equatorial plane. (If $\alpha_0^2 = 1$, there would have been no covalent bonding.) On the other hand, there is no in-plane covalent π-bonding in the complex since $\alpha_1^2 = 1.0$. Although the axial ligands are not taken into account in the D_{4h} square-planar configuration, the present value of α_2^2, being very close to unity (= 0.96), indicates that the out-of-plane covalent π-bonding is quite small. Thus, the nature of bonding with the oxygen ligands along the axis, belonging to the two carboxyl groups, is expected to be mostly ionic.

The presently-determined values of K_o and the MO coefficients can be compared with those estimated by

Manakkil [27], using a rather simple model [26]. He only estimated the values of α_0, α_1, α_2 and K_o. His values for α_0 (=.86), α_1 (=.98) and α_2 (=.99) are very close to the present values, while $K_o = 115\times10^{-4}$ cm^{-1} is somewhat different from the present value.

CHAPTER IX

CONCLUSIONS

The research described in the present thesis can be summarized as follows:

Cu^{2+} doped $Zn(C_4H_4N_2)SO_4.3H_2O$ (PZST)

(i) The interpretation of the observed EPR spectra of Cu^{2+}-doped PZST over the temperature range 4.2-375 K has been provided in detail in the present thesis. Owing to the extended temperature range (4.2-375 K) over which the EPR measurements were carried out in the present work on a single crystal of PZST, it has been possible to study not only the nature of the EPR spectra at various temperatures, but also to confirm the occurrence of static and dynamic JTE in Cu^{2+}-doped PZST; the transition from static JTE to dynamic JTE occurs at 334 ± 1 K. It has been estimated that the heights of the three JT barriers are the same, equal to 230 cm^{-1} , over the range 4.2-295 K.

(ii) The present studies lead to the conclusion that the local symmetry of Zn^{2+} site in PZST lattice is most probably octahedral, or octahedral with a small trigonal distortion. This is in contradiction with the suggestion that the coordination around the zinc ion in PZST lattice is tetrahedral [57].

Additional, detailed, research on the crystal structure of PZST is required before its domain structure can be understood.

Cu^{2+} doped $Cd(NH_4)_2(SO_4).6H_2O$ (CASH) and $Mg(NH_4)_2(SO_4).6H_2O$ (MASH)

(i) The orthorhombic Cu^{2+} principal values of the $\tilde{g}^2$ and $\tilde{A}^2$ tensors in the temperature range 4.2 - 354 K for CASH, while in the temperature range 4.2-361 K for MASH, indicate that the local symmetry at a Cd^{2+} site, i.e., tetragonally-compressed octahedral symmetry, in the undoped CASH or MASH lattice, undergoes an orthorhombic distortion when the Cu^{2+} ion enters the CASH or MASH lattice and substitutes for a Cd^{2+} ion of MASH.

(ii) Forbidden h.f. transitions were observed in the Cu^{2+} EPR spectrum in the single-crystal specimen at 4.2 K for CASH, while at 77 K (poorly resolved), and 4.2 K for MASH. The quadrupole interaction matrix $\tilde{Q}$ for both CASH and MASH was estimated at 4.2 K from their line positions.

(iii) The present study of both the single-crystal and polycrystalline specimens, over the temperature range 4.2 - 354 K for CASH and over 4.2-361 K for MASH, provided the temperature dependence of the principal values of the $\tilde{g}$ matrix. The variation of their values was interpreted to be due to the pseudo JT effect, experienced by the $Cu(H_2O)_6^{2+}$ complex, in the CASH or MASH single-crystal lattice. The ratios of the energy splittings between the three adiabatic potential valleys ($\delta_{1,2}$ and $\delta_{1,3}$) have been estimated from the temperature dependence of the principal values of the $\tilde{g}$ matrix.

Cu^{2+} doped $Ni(NH_4)_2(SO_4).6H_2O$ (NASH)

EPR measurements of Cu^{2+}-doped NASH were made at 295, 77, and 4.2 K. The orthorhombic principal g values at 295, 77, and 4.2 K show that the Cu^{2+} ion is in an orthorhombically-distorted octahedral symmetry. Only the Cu^{2+} EPR line due to the Zeeman splittings was observed at 295 and 77 K. At 4.2 K, the Cu^{2+} h.f. structure was also observed, only for the spectrum located at lower magnetic-field values. The non observation of h.f. structure can be attributed to dipole-dipole and exchange interactions between the paramagnetic host Ni^{2+} ion and impurity Cu^{2+} ion, which broaden the EPR lines.

Cu^{2+} doped $Mg(CH_3COO)_2.4H_2O$ (MAT)

(i) The present EPR and optical-absorption studies have enabled the determination of the spin-Hamiltonian parameters $g_{\parallel}$, $g_{\perp}$, $A_{\parallel}$ and $A_{\perp}$, as well as the crystal-field parameters D_q, D_s, and D_t. They have been used to estimate the core polarization, K_o, and the MO coefficients for Cu^{2+} in MAT lattice.

(ii) The values of $g_{\parallel}$ and $A_{\perp}$, determined presently, are significantly larger than, while those of $g_{\perp}$ and $A_{\parallel}$ are very close to, those reported by Manakkil [27]. Further, the presently-determined principal values of the $\tilde{g}$- and $\tilde{A}$-tensors at liquid-helium temperature are the same as those determined at liquid-nitrogen temperature, within experimental error. Manakkil [27] did not carry out any EPR measurements at liquid-helium temperature.

(iii) The optical-absorption spectrum has been explained well in terms of a D_{4h} square-planar configuration of the O^{2-} ligands in the Cu^{2+} complex taking into account the spin-orbit coupling. The presently-determined MO coefficients indicate that, for the Cu^{2+} complex in MAT lattice, the bonding between the Cu^{2+} ion and the oxygen ligands in the square-planar configuration is partly covalent, while the bonding between the Cu^{2+} ion and its axial oxygen ligands is mostly ionic.

REFERENCES

1. A. Abragam and B. Bleaney, *Electron Paramagnetic Resonance of Transition Ions,* Clarendon Press, Oxford (1970).

2. J.A. Aramburu and M. Moreno, J.Chem. Phys. 83, 6071 (1985).

3. C.J. Ballhausen, *Introduction to Ligand Field Theory,* McGraw-Hill Publ. Co., New York (1962).

4. C.J. Ballhausen and H.B. Gray, Inorg. Chem. 1, 111 (1962).

5. C.J. Ballhausen and H.B. Gray, *Molecular Orbital Theory,* W.A. Benjamin, Inc.,. New York (1965).

6. I.B. Bersuker and V.Z. Polinger, *Theoretical Background of the Jahn-Teller Effect,* in the *Dynamical Jahn-Teller Effect in Localized Systems* , Ed. by Yu.E. Perlin, and M. Wagner, Elsevier Science Publisher B.V., North-Holland, Amsterdam (1984).

7. H. Bill, *Observation of the Jahn-Teller Effect,* in *Dynamical Jahn-Teller Effect in Localized Systems* Ed. by Yu.E. Perlin, and M. Wagner, Elsevier Science Publisher B.V., North-Holland, Amsterdam (1984).

8. B. Bleaney, R.P. Penrose and B.J. Plumption, Proc. R. Soc. A198, 406 (1949).

9. B. Bleaney, K.D. Bowers, and D.J.E. Ingram, Proc. Phys. Soc. A64, 758 (1951).

10. B. Bleaney, K.D. Bowers, and D.J.E. Inagram, Proc.

Phys. Soc. A228, 147 (1955).

11. B. Bleaney, K.D. Bowers, and M.H.L. Pryce, Proc. Phys. Soc. A228, 166 (1955).

12. G.M. Brown and R. Chidambaram, Acta Cryst. B25, 676 (1969).

13. J. Callaway, *Quantum Theory of the Solid State,* Academic, New York (1976).

14. M.G. Clark and R.G. Burns, J. Chem. Soc. A, 1034 (1967).

15. E. Clement and C. Roetti, *Atomic Data, Nuclear Data Tables* 14, 177 (1974).

16. S.D. Dejardins, K.W. Penfield, S.L. Cohen, R.L. Musselman, and E.I. Solomon, J. Am. Chem. Soc. 105, 4590 (1983).

17. H.H. Faffé and G.O. Doak, J. Chem. Phys. 21, 196 (1953).

18. H.H. Faffé, J. Chem. Phys. 21, 258 (1953).

19. J. Ferguson, Progr. Inorg. Chem. 12, 159 (1970).

20. J. Fujita, K. Nakamoto, and M. Kobayashi, J. Am. Chem. Soc. 78, 3963 (1956).

21. M. Gerloch and R.C. Slade, *Ligand-field parameters,* Cambridge University Press (1973).

22. F.S. Ham, *Electron Paramagnetic Resonance* Ed. by S. Geschwind, Plenum New York (1972).

23. N.S. Hush and R.J.M. Hobbs, Progr. Inorg. Chem. 10, 357 (1968).

24. A. Kawamori and I. Miyagawa, J. Chem. Phys. 55, 1335

(1971).

25. V.G. Krishnan, J. Phys. C: Sol. Stat. Phys. 11, 3493 (1978).

26. A.H. Maki and B.R. McGarvey, J. Chem. Phys. 29, 31 (1958).

27. T.J. Manakkil, Ph.D. Thesis, New Mexico State University (1967).

28. T.N. Margulis and D.H. Templeton, Z. Krist. 117, 344 (1962).

29. B.R. McGarvey, *Electron Paramagnetic Resonance of Transition-metal Complexes*, in *Transition Metal Chemistry* edited by R.L. Carlin, Vol. 3, Marcel Dekker, Inc. New York (1966).

30. S.K. Misra and S. Subramanian, J. Phys. C: Sol. Stat. Phys. 15, 7199 (1982).

31. S.K. Misra, Magn. Reson. Rev. 10, 285 (1986).

32. S.K. Misra, Arab. J. Sci. & Eng. 13, 255 (1988).

33. S.K. Misra, Physica B151, 433 (1988).

34. S.K. Misra and C. Wang, Phys. Rev. B39, 8832 (1989).

35. S.K. Misra and U. Orhun, Phys. Rev. B39, 2856 (1989).

36. S.K. Misra and C. Wang, Phys. Stat. Sol. B154, 259 (1989).

37. S.K. Misra and C. Wang, J. Phys.: Condes. Matter 1, 771 (1989).

38. S.K. Misra and C. Wang, Phys. Rev. B41, 1 (1990).

39. S.K. Misra and C. Wang, *EPR of Cu^{2+} in Single and Poly crystals*, Magn. Reson. Rev. (in press).

40. H. Montgomery and E.C. Lingafelter, Acta Cryst. 17, 747 (1964).

41. H. Montgomery and E.C. Lingafelter, Acta Cryst. 17, 1478 (1964).

42. H. Montgomery and F.C. Lingafelter, Acta Cryst. 20, 728 (1966).

43. M. Moreno, J. Phys. C9, 3277 (1976).

44. F. Panlik and L. Erdey, Acta Chim. Acad. Sci. 13, 117 (1957).

45. R.P. Penrose, Nature, Lond. 163, 992 (1949).

46. V.E. Petrashen. Yu.V. Yablokov, and R.L. Davidovich, Phys. Stat. Sol B101, 117 (1980).

47. C.P. Poole, Jr., and H.A. Farach, *The Theory of Magnetic Resonance*, John Wiley & Sons, New York (1972).

48. C.P. Poole, Jr., *Electron Spin Resonance* 2nd Ed., John Wiley & Sons, Inc. New York (1983).

49. J.W. Richardson, W.C. Nieuwpoort, R.R. Powell, and W.E. Edgell, J. Chem. Phys. 36, 1057 (1962).

50. N. Satyanarayana, Mol. Phys. 55, 111 (1985).

51. J. Shankar, P.G. Khubchandani, and V.M. Padmanabhan, Proc. Indian Acad. Sci. A45, 117 (1957).

52. G.R. Sharp, M.Sc. Thesis, Concordia University, (1972).

53. B.L. Silver and D. Getz, J. Chem. Phys. 61, 638 (1974).

54. D.W. Smith, J. Chem. Soc. A, 176 (1970).

55. D.W. Smith, J. Chem. Soc. A, 1498 (1970).

56. D.W. Smith, J. Chem. Soc. A, 3108 (1970).

57. A. Tenhunen, Acta Chim. Scand. 22, 1827 (1972).

58. J.G. Verkade, *A Pictorial Approach to Molecular Bonding,* Springer Verlag, New York (1986).

59. R.E. Watson and A.J. Freeman, *Hyperfine Interactions,* Academic Press, Inc., New York (1967).

APPENDIX I

PUBLISHED PAPERS

This appendix contains the copies of the following papers published on the material related to this thesis:

(i) S. K. Misra and C. Wang, *Low and high-temperature electron paramagnetic resonance studies on* Cu^{2+}*-doped monopyrazine zinc sulphate trihydrate single crystal: observation of the Jahn-Teller effect.*

(ii) S. K. Misra and C. Wang, *EPR and optical-absorption studies of* Cu^{2+}*-doped* $Mg(CH_3COO)_2.4H_2O$ *single crystal.*

(iii) S. K. Misra and C. Wang, *EPR of* Cu^{2+}*-doped cadmium ammonium sulphate: Pseudo-Jahn-Teller effect.*

J. Phys.: Condens. Matter 1 (1989) 771–781. Printed in the UK

Low- and high-temperature electron paramagnetic resonance studies on Cu^{2+}-doped monopyrazine zinc sulphate trihydrate single crystal: observation of the Jahn–Teller effect

Sushil K Misra and Chunzheng Wang
Physics Department, Concordia University, 1455 de Maisonneuve Boulevard West, Montreal, Quebec, Canada H3G 1M8

Received 15 June 1988, in final form 17 August 1988

Abstract. Electron paramagnetic resonance studies on a single crystal of Cu^{2+}-doped monopyrazine zinc sulphate trihydrate (PZST) have been made over an extended temperature range (4.2–375 K). Three physically equivalent, but magnetically inequivalent, Cu^{2+} complexes have been observed. The spin-Hamiltonian parameters are rigorously evaluated at 334, 295, 77 and 4.2 K, by the method of least-squares fitting, utilising numerical diagonalisation of the spin-Hamiltonian matrix on a digital computer. The principal values of the $\tilde{g}$- and $\tilde{A}$-tensors indicate that, in PZST, the Cu^{2+} ion experiences an octahedral symmetry with orthorhombic distortion. The data are interpreted to conclude the occurrence of both static and dynamic Jahn–Teller effects over the temperature range of investigation, the transition from static to dynamic Jahn–Teller effect occurring at 334 ± 1 K.

1. Introduction

The understanding of the ground states of the Cu^{2+} ion (3d^9 electron configuration) in different symmetries of crystal fields is an important topic in electron paramagnetic resonance (EPR). Many studies have been particularly devoted to crystal fields characterised by octahedral symmetry, or octahedral symmetry with a small trigonal distortion, for which the Cu^{2+} ion possesses the twofold-degenerate ground state E_g. Many occurrences of the Jahn–Teller effect (JTE) have been reported in these situations. JTE has been observed by means of EPR in many zinc salts doped by Cu^{2+} ions, e.g. in zinc Tutton salts (Silver *et al* 1974, Petrashen *et al* 1980), zinc fluorosilicate hexahydrate (Bleaney and Ingram 1950), zinc fluorotitanante hexahydrate (De *et al* 1984), zinc bromate hexahydrate (Jesion *et al* 1976, 1977), hexaimidazole zinc dichloride tetrahydrate (Keijzers *et al* 1983) and $K_2Zn(ZrF_6)_2\cdot 6H_2O$ (Petrashen *et al* 1978). The occurrence of JTE in such cases can be explained as follows. Most cases of JTE for Cu^{2+} are found to occur in diamagnetic host lattices. The diamagnetic ions possess a closed outer electronic shell, thereby causing the local symmetry of the host lattice to be high. When the paramagnetic Cu^{2+} ion is introduced into the diamagnetic host lattice, substituting for the diamagnetic ions, some local distortions are introduced because its size is different from that of the host ions, as well as being paramagnetic. This fulfils the two conditions necessary for the occurrence of JTE (Callaway 1976); namely, that the Cu^{2+} ion be in a degenerate electronic state, and that it occupy a minimum-energy non-degenerate state consequent to the small local distortion of the lattice that it produces.

EPR study of Cu^{2+}-doped monopyrazine zinc sulphate trihydrate, $Zn(C_4H_4N_2)SO_4 \cdot 3H_2O$ (hereafter PZST), has been previously reported by Krishnan (1978), at 295 K on a single-crystal specimen and at 77 K on a polycrystalline specimen. His EPR spectra revealed the existence of three magnetically different sites for Cu^{2+}, although there is only one substitutional position available for Cu^{2+} in the unit cell of PZST. Krishnan explained this to be due to the presence of three domains. He suggested the occurrence of a static JTE in Cu^{2+}-doped PZST from the features of the EPR spectra; the orthorhombic g-values revealed that the admixture of the $|3Z^2 - r^2\rangle$ orbital into the $|X^2 - Y^2\rangle$ orbital was less than 5%.

It is the purpose of this paper to present more detailed EPR studies on Cu^{2+}-doped PZST single crystal. The occurrence of JTE in this low-symmetry crystal is deduced by studying the features of the temperature-dependent EPR spectra. The measurements are carried out over an extended temperature range (4.2–375 K), making it possible to observe a dynamic JTE at high temperatures and a static JTE at lower temperatures. The Cu^{2+} spin-Hamiltonian parameters are evaluated using a rigorous least-squares fitting procedure (Misra 1986, 1988a, b).

2. Sample preparation and crystal structure

Cu^{2+}-doped single crystals were grown by slow evaporation of an aqueous solution, consisting of stoichiometric amounts of pyrazine ($C_4H_4N_2$) and $ZnSO_4 \cdot 7H_2O$, to which was added a sufficient quantity of $CuSO_4 \cdot 5H_2O$ so that there is one Cu^{2+} ion for every 100 Zn ions. The grown crystal possessed the same form as that of the crystal that was used for EPR measurements by Krishnan (1978). It looks like a parallelepiped. The crystal structure of PZST has been reported by Tenhunen (1972) to be triclinic (space group P1); the unit-cell dimensions are $a = 10.734$ Å, $b = 4.427$ Å, $c = 6.927$ Å, $\alpha = 121.15°$, $\beta = 82.57°$, $\gamma = 104.02°$. There is one formula per unit cell ($Z = 1$).

So far, no structure-analysis data have provided the exact positions of Zn^{2+} ions in the lattice of PZST crystal. That the water molecules are not structural water can be concluded from experimental data: the infrared spectrum of PZST reveals that there is no band that confirms water coordination in PZST (Fujita *et al* 1956). In addition, the thermogravimetric curve (Panlik and Erdey 1957) indicates that the three water molecules of PZST are rapidly removed at 115 °C.

3. Experimental arrangement and EPR data

The EPR spectra were recorded on a homodyne X-band Varian V4502 spectrometer, using a 100 kHz field modulation for room- and higher-temperature measurements, and 400 Hz field modulation for measurements at liquid-nitrogen and liquid-helium temperatures. The magnetic-field measurements were made with a Bruker (B-NM20) gaussmeter. The temperature was varied by the use of a heater resistor inside the liquid-helium cryostat for low-temperature measurements. For high-temperature measurements, a Varian variable-temperature controller (model No E4540), attached to a microprocessor digital thermometer, manufactured by Omega (model No 870), was employed.

The angular variation of the data was observed for the Zeeman field (H) orientation in three mutually perpendicular planes at every temperature of measurement. The spectra were recorded for the orientation of H at every 4° interval at room and higher temperatures, and at every 5° interval at liquid-nitrogen and liquid-helium temperatures. The most even face of the single-crystal specimen was chosen to define the ZX plane, the plane that contains the crystallographic c axis. The orientation of g_3, the largest g-value (the direction of H for which the positions of the lines are at the minimum) in this plane, was chosen to be the Z axis. For EPR measurements in the ZY and XY planes the specimen was set so that it could be rotated about the X and Z axes, keeping the external magnetic field direction fixed.

3.1. EPR spectra at room, liquid-nitrogen and liquid-helium temperatures

The EPR spectra for Cu^{2+}-doped PZST at liquid-nitrogen and liquid-helium temperatures are not much different from that at room temperature. This can be seen from figure 1,

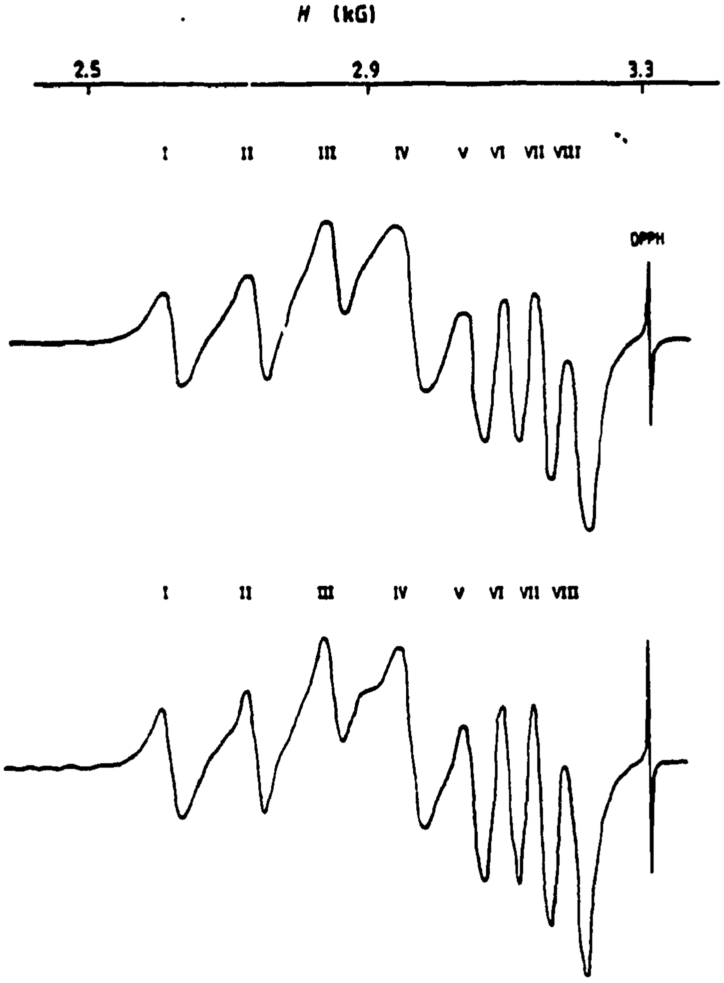

Figure 1. EPR spectra of Cu^{2+}-doped PZST at low temperatures. The upper spectrum is recorded at liquid-nitrogen temperature and the lower one at liquid-helium temperature for H at 75° from the Z axis in the ZY plane.

which exhibits the EPR spectra for the magnetic field orientation at 75° from the *Z* axis in the *ZY* plane, at liquid-nitrogen and liquid-helium temperatures. It consists of three sets of four hyperfine (HF) lines, typical of the Cu^{2+} ion; the lines corresponding to the less-abundant isotope of Cu^{2+} (^{65}Cu, 30.91% abundance) could not be clearly seen. The three sets of spectra belong to three physically equivalent, but magnetically inequivalent, Cu^{2+} complexes; thus their angular variations are different, as can be seen from figure 2, exhibiting the angular variations of spectra in the *ZY* plane at liquid-helium temperature. The line widths do not change significantly, as one lowers the temperature from room to liquid-helium temperature; they are 25, 22, 22, 34, 26, 25, 26 and 21 G, respectively, for the eight clearly resolved EPR lines in increasing order of magnetic field. As can be seen from figure 1, one actually sees only eight clearly resolved lines (indicated as I, II, III; IV, V, VI, VII and VIII). The four lowest-field lines belong to Cu^{2+} ion occupying

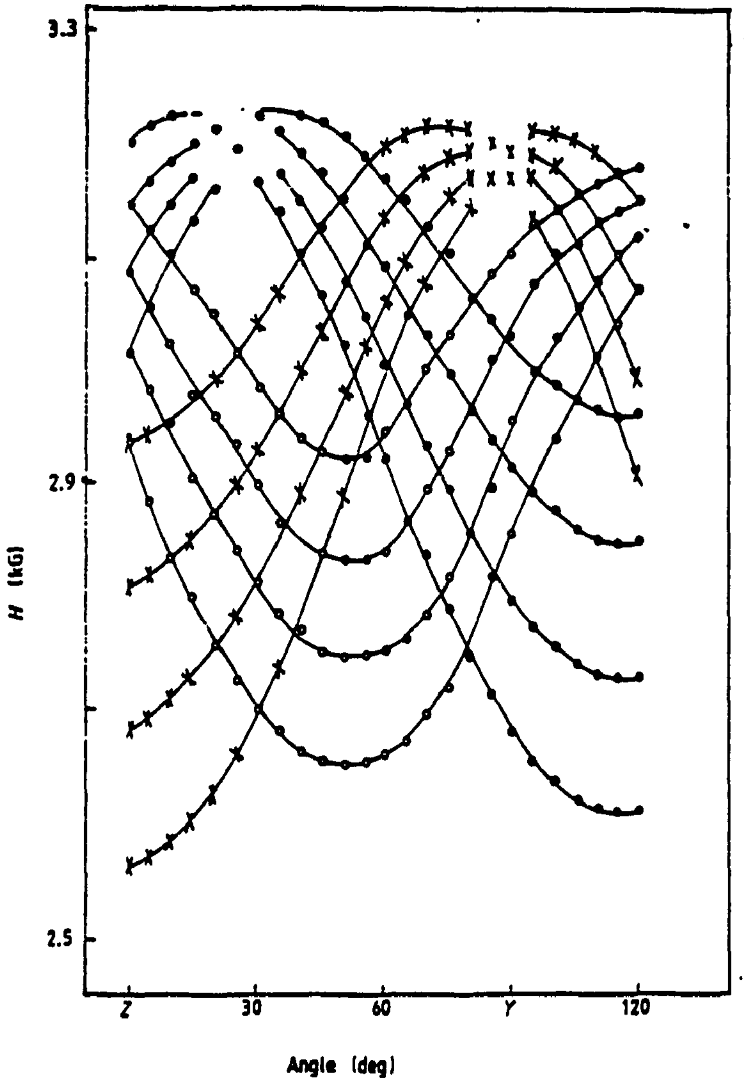

Figure 2. Angular variation of Cu^{2+} EPR spectra in PZST at 4.2 K for the orientation of *H* in the *ZY* plane. The full curves connect data points, observed for the same transition. Open circles, full circles and crosses represent three differentsets of spectra.

Table 1. The principal values of the $\tilde{g}$- and $\tilde{A}$-tensors (square roots of the principal values of the $\tilde{g}^2$- and $\tilde{A}^2$-tensors, respectively) for Cu^{2+} in PZST at different temperatures. The principal $\tilde{g}$-values are dimensionless, while the principal $\tilde{A}$-values (A_1, A_2, A_3) are in gigahertz. The labelling is such that $g_3 > g_1 > g_2$.

Temperature (K)	g_3	g_1	g_2	A_3	A_1	A_2	Ref.
295	2.3875	2.1924	2.0205	0.324	0.181	0.104	a
295	2.414	2.216	2.109	0.357	0.201	0.132	b
77	2.3876	2.1923	2.0200	0.326	0.182	0.105	a
77	2.42			0.362			c
4.2	2.3868	2.1929	2.0190	0.328	0.185	0.105	a
334	2.191	2.191	2.191				a

[a] Present work.

[b] Krishnan (1978), for a single-crystal specimen.

[c] Krishnan (1978), for a polycrystalline specimen.

site I, the four highest-field lines belong to Cu^{2+} ion occupying site II, while the four lines belonging to Cu^{2+} ion occupying site III overlap the highest-field line of site I and the three lowest-field lines of site II, i.e. overlapping lines IV, V, VI and VII.

The EPR spectra of Cu^{2+} ion in PZST are fitted to the following spin Hamiltonian:

$$\mathcal{H} = \mu_B H \cdot \tilde{g} \cdot S + S \cdot \tilde{A} \cdot I \tag{1}$$

where μ_B is the Bohr magneton, S ($=\frac{1}{2}$) is the electronic spin and I ($=\frac{3}{2}$) is the nuclear spin of Cu^{2+}.

The principal values of the $\tilde{g}^2$- and $\tilde{A}^2$-tensors and their direction cosines were evaluated by the use of a procedure previously described (Misra 1986, 1988a, b). The principal values of the $\tilde{g}$- and $\tilde{A}$-tensors so evaluated, at various temperatures, are listed in table 1, which also includes the principal values reported by Krishnan (1978). It is

Table 2. Direction cosines of the principal axes of the $\tilde{g}$- and $\tilde{A}$-tensors of Cu^{2+} in PZST. (The same as those of the $\tilde{g}^2$- and $\tilde{A}^2$-tensors respectively.) The direction cosines of the $\tilde{g}^2$-tensor are given with respect to the laboratory axes (X, Y, Z) (as defined in § 3), while those of the $\tilde{A}$-tensor are expressed relative to (X', Y', Z'), the principal axes of the $\tilde{g}^2$-tensor. The values are those found at 295 K.

	Direction cosines of the $\tilde{g}^2$-tensor		
	Z	X	Y
Z'	0.4510	0.2010	0.8696
X'	−0.6486	0.7431	0.1647
Y'	−0.6131	−0.6383	0.4655
	Direction cosines of the $\tilde{A}^2$-tensor		
	Z'	X'	Y'
Z''	0.9999	0.0062	0.0140
X''	−0.0064	0.9998	0.0191
Y''	−0.0103	−0.0192	0.9998

Table 3. Same details as in the caption of table 2. The values are those found at 77 K.

	Direction cosines of the $\bar{g}^2$-tensor		
	Z	X	Y
Z'	0.4192	0.2720	0.8662
X'	−0.6498	0.7562	0.0770
Y'	−0.6341	−0.5952	0.4937

	Direction cosines of the $\bar{A}^2$-tensor		
	Z'	X'	Y'
Z''	0.9999	0.0062	0.0100
X''	−0.0064	0.9999	0.0156
Y''	−0.0099	−0.0158	0.9998

noted here that the principal values of the $\bar{g}$- and $\bar{A}$-tensors are the same, within experimental error, for the three magnetically inequivalent Cu^{2+} complexes. The direction cosines of the principal axes of the $\bar{g}$- and $\bar{A}$-tensors are listed in tables 2–4 at 295, 77 and 4.2 K respectively. (It should be pointed out that the principal values of the $\bar{g}$- and $\bar{A}$-tensors are the square roots of the principal values of the $\bar{g}^2$- and $\bar{A}^2$-tensors respectively, while the direction cosines of the principal axes of the $\bar{g}$- and $\bar{A}$-tensors are the same as those of the $\bar{g}^2$- and $\bar{A}^2$-tensors, respectively.)

It is seen from table 1 that the principal values of the $\bar{g}$- and $\bar{A}$-tensors remain the same, within experimental error, over the temperature range 77–295 K, while tables 2 and 3 reveal that the principal axes of the $\bar{g}^2$- and $\bar{A}^2$-tensors are found to remain coincident over this temperature range. Although the principal values of the $\bar{g}$- and $\bar{A}$-tensors at 4.2 K (table 1) are found to be the same as those at room and liquid-nitrogen temperatures, within experimental error, the principal axes of the $\bar{A}^2$-tensor are no longer coincident with those of the $\bar{g}^2$-tensor (table 4).

Table 4. Same details as in the caption of table 2. The values are those found at 4.2 K.

	Direction cosines of the $\bar{g}^2$-tensor		
	Z	X	Y
Z'	0.3649	0.2468	0.8978
X'	−0.6372	0.7692	0.0476
Y'	−0.6788	−0.5895	0.4379

	Direction cosines of the $\bar{A}^2$-tensor		
	Z'	X'	Y'
Z''	0.9969	0.0788	0.0058
X''	−0.0698	0.9126	−0.4028
Y''	−0.3700	0.4011	0.9153

3.2. *EPR spectra above room temperature*

Above room temperature, the EPR spectra of Cu^{2+}-doped single crystal of PZST are significantly different from those at room and lower temperatures; the HF lines of Cu^{2+} become broader and weaker. Finally, at 334 ± 1 K, only one single, broad, isotropic line is observed; both the position of the line centre and the line width are independent of the orientation of the external magnetic field. There is no significant change in the line width as the temperature is raised to 375 K, the temperature at which dehydration of the crystal begins to take place. As listed in table 1, this single isotropic line corresponds to $g = 2.191 = (g_1 + g_2 + g_3)/3$, where g_1, g_2 and g_3 are the principal values of the $\tilde{g}$-tensor at room temperature (these values are the same as those below room temperature).

Upon lowering the temperature again below 334 K, after having raised the temperature above 334 K, the features of the EPR spectra return, as observed before. This observation was repeated three times, and each time the features of the EPR spectra were recaptured exactly the same as before recycling through temperatures higher than 334 K. Figure 3 shows the temperature variation of EPR spectra of Cu^{2+}-doped PZST over the range 295–374 K for the external magnetic field orientation at 75° from the Z axis in the ZY plane.

4. Discussion

4.1. *Temperatures below 295 K (static JTE)*

The principal values of the $\tilde{g}$- and $\tilde{A}$-tensors, over the temperature range 4.2–295 K, as given in table 1, indicate a low symmetry of Cu^{2+} complex in PZST, i.e. orthorhombically distorted octahedral symmetry, since the three principal values, for each of the $\tilde{g}$- or $\tilde{A}$-tensors, are all different from each other. The independence of the EPR spectra, as well as that of the EPR line width, on the temperature below 295 K supports the occurrence of a static JTE, as proposed previously by Krishnan (1978).

The orthorhombic principal g-values due to the static JTE, for any magnetically inequivalent Cu^{2+} complex, as observed presently in PZST, can be analytically expressed as follows (Abragam and Bleaney 1970):

$$\begin{aligned} g_1 &= g_e - (2\lambda/\Delta)[\cos(\varphi/2) + \sqrt{3}\sin(\varphi/2)]^2 \\ g_2 &= g_e - (2\lambda/\Delta)[\cos(\varphi/2) - \sqrt{3}\sin(\varphi/2)]^2 \\ g_3 &= g_e - (8\lambda/\Delta)\cos^2(\varphi/2). \end{aligned} \tag{2}$$

In equations (2) g_e is the g-value of the free electron (=2.0023); λ is the spin–orbit coupling constant for the free Cu^{2+} ion (= $-830\ \mathrm{cm^{-1}}$); Δ (=$120B_4^0$) is the octahedral crystal-field splitting constant for Cu^{2+} ion; φ is the vectorial angle of a polar coordinate system (ρ, φ) which describes the distortions Q_ϵ (=$\rho \sin\varphi$) and Q_θ (=$\rho\cos\varphi$) of the ML_6 complex, where M is Cu^{2+} and L are surrounding ligands, which are not as yet well identified for PZST.

For an arbitrary value of φ (except for $\varphi = n\pi/3$, where n is an integer), the g-values of equations (2) correspond to an orthorhombic distortion of octahedral symmetry (i.e. $g_1 \neq g_2 \neq g_3$), the directions of the principal values g_1, g_2 and g_3 being along the three mutually perpendicular fourfold (tetragonal) axes of the ML_6 complex. The substitutions of the values of $\varphi = \varphi + 2\pi/3$ and $\varphi = \varphi + 4\pi/3$ in equations (2) interchange g_1, g_2 and g_3 amongst themselves, i.e. they correspond to orthorhombic distortions about the

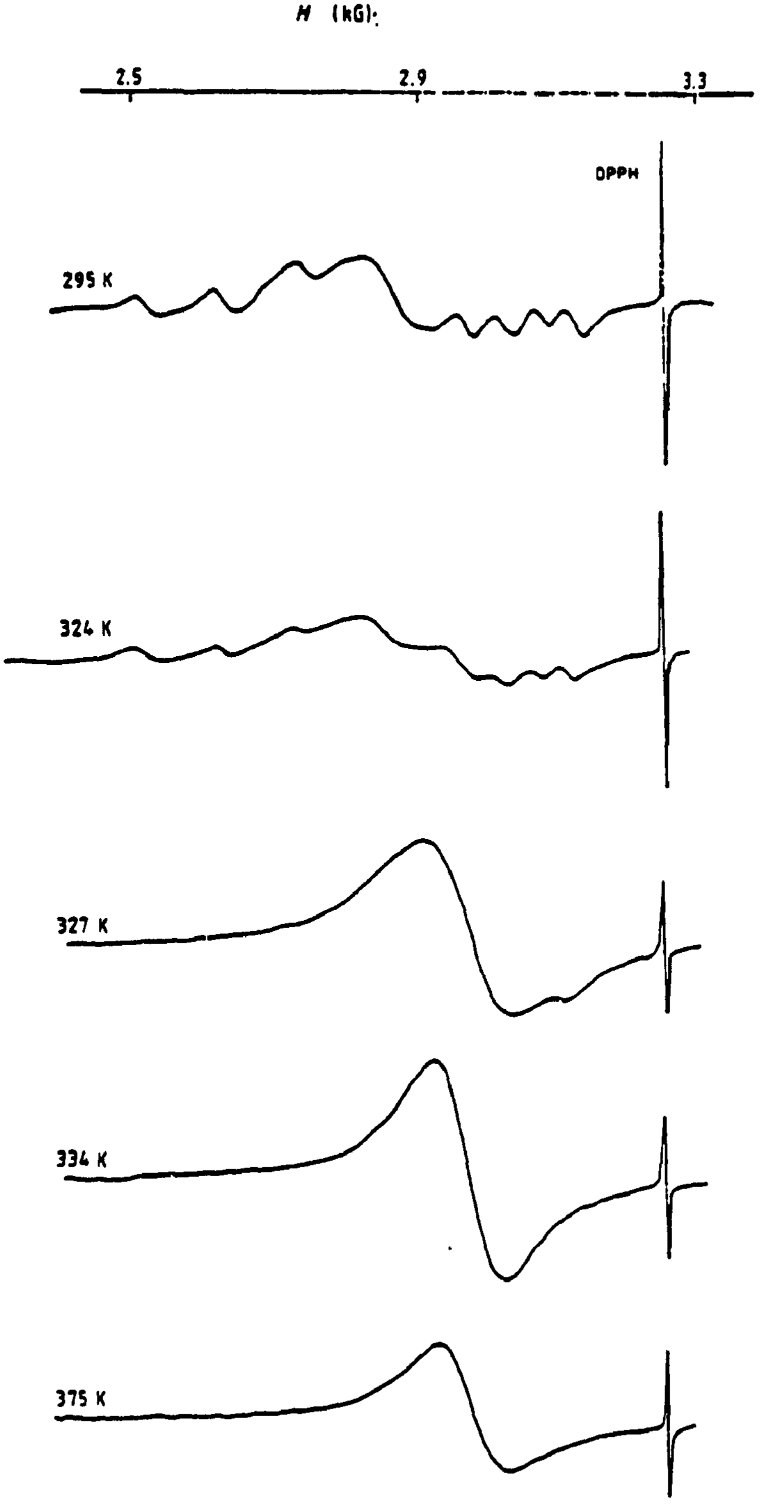

Figure 3. EPR spectra of Cu^{2+}-doped PZST for H at 75° from the Z axis in the ZY plane at 295, 324, 327, 334 and 375 K.

two other tetragonal axes. The potential-energy surfaces, which are associated with the coupling between the magnetic electrons and the ligand nuclei, are referred to as the JT valleys. If φ_0 is the particular value that corresponds to the minimum (i.e. the bottom of the JT valley) of one potential-energy surface, the φ-values corresponding to the minima of the other two potential-energy surfaces are located at $\varphi_0 + 2\pi/3$ and $\varphi_0 + 4\pi/3$. In general, the energies of these three minima are different. In the case of Cu^{2+}-doped PZST, using the typical value of $\lambda/\Delta = -0.05$ (Abragam and Bleaney 1970) in equation (2), and the measured values of g_1, g_2 and g_3, φ_0 has been estimated to be approximately 30°.

Although Krishnan (1978) has ascribed the presence of three sets of EPR spectra at 295 K to the existence of three domains in the crystal, it is entirely possible to account for the present results by supposing that the different JT distortions of the Cu^{2+} complexes (ML_6 type) are randomly distributed with equal probabilities throughout the crystal, rather than grouped into domains. This is further supported by examining the PZST crystal through a polarising microscope, which does not reveal the existence of domains. That such a view naturally leads to a satisfactory explanation of the high-temperature spectrum is presented in § 4.2.

The temperature-dependent principal values $g_i(T)$ and $A_i(T)$ ($i = 1, 2, 3$) can be expressed, in general, as the averages over the three JT potential valleys, with the corresponding weight factors being in proportion to the populations N_1, N_2 and N_3 in the respective JT valleys (Petrashen *et al* 1978). In the case of Cu^{2+}-doped PZST, the principal values of the $\tilde{g}$- and $\tilde{A}$-tensors are found to be independent of temperature in the range 4.2–295 K: this indicates that N_1, N_2 and N_3 are constant, and equal to each other, over the range 4.2–295 K. This is only possible when the energies of the three JT valleys are equal to each other, since the populations in the corresponding JT valleys are governed by a Boltzmann distribution.

Petrashen *et al* (1980) have studied the dynamic JTE nature of $Cu(H_2O)_6^{2+}$ complexes in the zinc and copper Tutton salts, using the EPR and x-ray data. They found that the ratio of the energy splittings between the three JT configurations of the $Cu(H_2O)_6^{2+}$ complex (δ_{13}/δ_{12}), estimated from the temperature-dependent principal values of the $\tilde{g}$-tensor, is close to that estimated taking into account the symmetry of the $Zn(H_2O)_6^{2+}$ complex and the variation of the energy of the JT ion due to the distortions. Thus, the symmetry of the host complex can be deduced from the energy splittings between the three JT valleys of the complex $Cu(H_2O)_6^{2+}$, as determined from EPR data. Proceeding in analogous manner, it is concluded that the energies of the three JT valleys of the Cu^{2+} complex are identical in PZST: the local symmetry of the Zn^{2+} ion in PZST is either regular octahedral or most likely octahedral with a small trigonal distortion. When a Cu^{2+} ion substitutes for a Zn^{2+} ion in PZST, it changes the trigonally distorted octahedral symmetry to orthorhombically distorted octahedral symmetry, because of its different size, and different interaction with ligands. This manifests as static JTE.

The ground state of the Cu^{2+} ion, experiencing an orthorhombic distortion in an octahedral crystal field, is an admixture of $|X^2 - Y^2\rangle$ and $|3Z^2 - r^2\rangle$ orbitals: which one of these two is predominant can be determined from the R-value (Budley and Hathaway 1970), defined to be $R = (g_1 - g_2)/(g_3 - g_1)$, where $g_3 > g_1 > g_2$. When the R-value is greater than unity, a predominantly $|3Z^2 - r^2\rangle$ ground state is expected, while a predominantly $|X^2 - Y^2\rangle$ ground state is expected when it is less than unity. Since the calculated R-value for the present case is less than unity at room temperature and below, the predominant ground state of Cu^{2+} ion, in PZST single crystal, is the $|X^2 - Y^2\rangle$. Further, the admixture of the excited state $|3Z^2 - r^2\rangle$ is given by $\sin^2(\varphi_0/2)$, because the ground state for Cu^{2+} can be expressed as $\cos(\varphi_0/2)|X^2 - Y^2\rangle + \sin(\varphi_0/2)|3Z^2 - r^2\rangle$ (Abragam and Bleaney 1970). This admixture is less than 7% since $\varphi_0 = 30°$ in the present case, as determined above.

4.2. *Temperatures greater than 295 K (dynamic JTE)*

As the temperature is raised above 295 K, the HF lines of Cu^{2+} become broader through relaxation effects. At $T > 327$ K the HF components become so broad that they are no longer resolved, and only a single isotropic line is observed above 334 K. This is characteristic of a dynamic JTE. This occurs when the rate of tunnelling through the barrier from one distorted configuration of the Cu^{2+} complex (ML_6 type) to the other exceeds the frequency difference between the corresponding EPR resonance lines for the different distorted configurations, i.e. that between the anisotropic spectra (Ham 1972). From the time-averaging effect, when the dynamic JTE occurs, equations (2) yield $g_1 = g_2 = g_3 = g_e - 4\lambda/\Delta$, since the averages $\langle\cos^2(\varphi/2)\rangle = \langle\sin^2(\varphi/2)\rangle = \frac{1}{2}$ and $\langle\cos(\varphi/2)\sin(\varphi/2)\rangle = 0$. From the typical value of $\lambda/\Delta = -0.05$ for Cu^{2+} ion (Abragam and Bleaney 1970), $g_e - 4\lambda/\Delta$ is calculated to be 2.2, very close to the observed g-value (2.191) at $T \geqslant 334$ K. This is characteristic of the type I dynamic JTE (Ham 1972).

Since the EPR spectrum for Cu^{2+} in PZST above 334 K is isotropic as revealed by both the position of the centre of the EPR line and the EPR linewidth, the oriented and random strains are expected to be very small compared to kT, as deduced using the fact that the centre of the EPR line is influenced by the oriented strains, while the EPR line width is influenced by the random strains (Ham 1972).

The observation of only one isotropic line at $T \geqslant 334$ K can be explained to be due to motional averaging, because of rapid hopping between the three equivalent JT-distorted sites, randomly distributed in the crystal with equal probabilities. One then expects a high-temperature 'g'-value of $g = (g_1 + g_2 + g_3)/3 = 2.2$. The observed '$g$'-value of 2.191 is almost equal to 2.2.

5. Concluding remarks

The interpretation of the observed EPR spectra of Cu^{2+}-doped PZST over the temperature range 4.2–375 K has been provided in detail in the present paper. Owing to the extended temperature range (4.2–375 K) over which the EPR measurements were carried out in the present work on a single crystal of PZST, it has been possible not only to study the nature of the EPR spectra at various temperatures but also to confirm the observation of both static and dynamic JTE in Cu^{2+}-doped PZST: the transition between them occurs at 334 ± 1 K. It has been estimated that the heights of the three JT barriers are the same over the range 4.2–295 K.

The present studies lead to the conclusion that the local symmetry of Zn^{2+} site in PZST lattice is most probably octahedral, or octahedral with a small trigonal distortion. This is in contradiction with the suggestion that the coordination around the zinc ion in PZST lattice is tetrahedral (Tenhunen 1972).

The high-temperature EPR spectra are found to be well explained by supposing that the different JT distortions of the Cu^{2+} complex in PZST are randomly distributed with equal probabilities throughout the crystal, rather than being due to the existence of three domains as suggested by Krishnan (1978). This is further supported by the fact that no domains were indeed found upon examination through a polarising microscope.

Acknowledgments

The authors are grateful to the Natural Sciences and Engineering Research Council of Canada for financial support (Grant No A4485), and to the Concordia University Computer Centre for providing their facilities to analyse the data.

References

Abragam A and Bleaney B 1970 *Electron Paramagnetic Resonance of Transition Ions* (Oxford: Clarendon)
Bleaney B and Ingram D J E 1950 *Proc. Phys. Soc.* A **63** 408
Budley R J and Hathaway B J 1970 *J. Chem. Soc.* A 2799
Callaway J 1976 *Quantum Theory of the Solid State* (New York: Academic)
De D K, Rubins R S and Black T D 1984 *Phys. Rev.* B **29** 71
Fujita J, Nakamoto K and Kobayashi M 1956 *J. Am. Chem. Soc.* **78** 3963
Ham F S 1972 *Electron Paramagnetic Resonance* ed. S Geschwind (New York: Plenum) p 54
Jesion A, Shing Y H and Walsh D 1977 *Phys. Rev.* B **16** 3012
Jesion A, Shing Y H, Walsh D and Donnay J D H 1976 *J. Phys. C: Solid State Phys.* **9** L219
Keijzers C P, Jansen T, de Boer E and Van Kalkeren G 1983 *J. Magn. Reson.* **52** 211
Krishnan V G 1978 *J. Phys. C: Solid State Phys.* **11** 3493
Misra S K 1986 *Magn. Reson. Rev.* **10** 285
—— 1988a *Arab. J. Sci. Eng.* **13** 255
—— 1988b *Physica B* **151** 433
Panlik F and Erdey L 1957 *Acta Chim. Acad. Sci.* **13** 117
Petrashen V E, Yablokov Yu V and Davidovich R L 1978 *Phys. Status Solidi* b **88** 439
—— 1980 *Phys. Status Solidi* b **101** 117
Silver B L and Getz D 1974 *J. Chem. Phys.* **61** 638
Tenhunen A 1972 *Acta Chim. Scand.* **22** 1827

phys. stat. sol. (b) 154, 259 (1989)

Subject classification: 71.70; 76.30; 78.50; S12

Department of Physics, Concordia University, S. G. Williams Campus, Montreal[1])

EPR and Optical-Absorption Studies of Cu^{2+}-Doped $Mg(CH_3COO)_2 \cdot 4H_2O$ Single Crystal

Core Polarization and Molecular-Orbital Coefficients

By

Sushil K. Misra and Chunzheng Wang

X-band EPR measurements on a single crystal of Cu^{2+}-doped magnesium acetate tetrahydrate, $Mg(CH_3COO)_2 \cdot 4H_2O$, are made at 295, 77, and 4.2 K. The Cu^{2+} spin-Hamiltonian parameters are evaluated, at all these temperatures, from the EPR line positions by means of a rigorous least-squares fitting method. The principal values of the g^2 and A^2 tensors indicate that the local symmetry of the Cu^{2+} ion, in the host lattice of $Mg(CH_3COO)_2 \cdot 4H_2O$ crystal, is tetragonal. The room-temperature optical-absorption spectrum, recorded in the 190 to 820 nm wavelength range, is exploited to study the crystal-field and charge-transfer transitions of the Cu^{2+} ion. On the other hand, both the room-temperature optical-absorption and EPR data are used to estimate the core polarization contribution (K) and the molecular-orbital coefficients for the Cu^{2+} ion doping $Mg(CH_3COO)_2 \cdot 4H_2O$.

On a mesuré le RPE à bande-X sur un monocristal de $Mg(CH_3COO)_2 \cdot 4H_2O$, dopé par l'ion Cu^{2+} à 295, à 77 et à 4.2 K. Les paramètres du spin hamiltonian du Cu^{2+} ont été évalués, à toutes ces températures, par une méthode rigoureuse d'adaptation aux moindres carrés, utilisant les positions des raies RPE. Les valeurs principales des tenseurs g^2 et A^2 indiquent que la symétrie locale de l'ion Cu^{2+}, dans le réseau-hôte du cristal de $Mg(CH_3COO)_2 \cdot 4H_2O$, est tétragonal. Le spectre d'absorption optique, à la température ambiante, enregistré dans l'intervalle de longueur d'onde 190 à 820 nm, a été exploité afin d'étudier les transitions du champ cristallin, ainsi que celles du transfert de charge. D'un autre coté, à la fois les donées d'absorption optique et les données de RPE, à la température ambiante, ont été utilisées, afin d'estimer la contribution de la polarisation du core et des coefficients de l'orbite moléculaire pour l'ion Cu^{2+} dopant $Mg(CH_3COO)_2 \cdot 4H_2O$.

1. Introduction

Some EPR studies of Mn^{2+}- and Cu^{2+}-doped magnesium acetate tetrahydrate, $Mg(CH_3COO)_2 \cdot 4H_2O$ (hereafter MAT), single crystal at 295 and 77 K have been reported by Manakkil [1], indicating that these paramagnetic ions substitute for the magnesium ions in the MAT lattice, forming tetragonal (i.e., elongated octahedron) complexes. The spin-Hamiltonian parameters for these ions were evaluated from the EPR line positions, observed for the magnetic field orientations along three mutually orthogonal magnetic axes, using perturbation expressions. Further, using the theoretical expressions for the tensors g and A, as developed by Maki and McGarvey [2], Manakkil [1] evaluated the molecular-orbital (MO) coefficients. However, to this end, he used the optical-absorption data of Cu^{2+} in $Cu(CH_3COO)_2 \cdot H_2O$ aqueous solution, rather than those in Cu^{2+}-doped MAT crystal, to determine the energy separations between the excited states and the ground state of the Cu^{2+}-complex in MAT. This

---

[1]) 1455 de Maisonneuve Boulevard West, Montreal, Quebec, Canada H3G 1M8.

assumption is far-fatched, because the environment of Cu^{2+} ion in the $Cu(CH_3COO)_2 \cdot H_2O$ solution is much different from that in the MAT crystal. No optical-absorption studies of the impurity Cu^{2+} ion in the MAT single crystal have so far been reported.

The purpose of the present paper is to report detailed X-band EPR studies, not only at room temperature and 77 K, but also at 4.2 K, as well as optical-absorption studies of Cu^{2+}-doped MAT single crystal in the wavelength range 190 to 820 nm at 295 K. The EPR data will be used to estimate the principal values and orientations of the principal axes of the tensors g^2 and A^2, while both the EPR and optical data will be used to estimate the MO coefficients of the Cu^{2+}-complex in Cu^{2+}-doped MAT single crystal.

2. Sample Preparation and Crystal Structure

Cu^{2+}-doped single crystals of MAT were grown by slow evaporation of an aqueous solution of $Mg(CH_3COO)_2 \cdot 4H_2O$, to which was added a sufficient quantity of $Cu_2(CH_3COO)_4 \cdot 4H_2O$, so that there was one Cu^{2+} ion for every 100 Mg^{2+} ions.

The crystal structure of MAT, as determined from X-ray data, has been reported by Shankar et al. [3]. It is monoclinic (space group C_{2h}^5-$P_{2_1/c}$); the unit cell dimensions are: $a = 0.475$ nm, $b = 1.179$ nm, $c = 0.852$ nm, and $\beta = 94° 54'$. There are two formula units per unit cell ($Z = 2$); each Mg^{2+} ion is surrounded by four water molecules, two H_2O (1) and two H_2O (2), in the equatorial plane, and by two oxygen ions belonging to the two acetate groups situated on the axis perpendicular to the equatorial plane. The distances between the Mg^{2+} ion and the oxygen ions of the H_2O (1) and H_2O (2) molecules are 0.207 and 0.208 nm, respectively, and those between the Mg^{2+} ion and the two oxygen ions, which belong to the two acetate groups, are 0.211 nm each. The local site symmetry of the Mg^{2+} ion is, thus, approximately tetragonal (elongated octahedron).

3. Experimental Arrangement and Spectra

3.1 *Experimental arrangement*

3.1.1 EPR

The EPR spectra were recorded on a X-band Varian V4502 spectrometer, equipped with a 100 kHz field modulation for room-temperature measurement, and a 400 Hz field modulation for liquid-nitrogen and liquid-helium temperature measurements. The magnetic field was measured with a Burker (B-NM20) gaussmeter. For low-temperature measurements, the temperature was varied by a heater resistor inside the liquid-helium cryostat. Temperatures in the liquid-nitrogen and liquid-helium temperature ranges were determined by measuring the resistances of the platinum and germanium resistors, respectively, using appropriate calibration charts.

The angular variation of EPR spectra was recorded, at any temperature, for the Zeeman field (***B***) orientation in three mutually perpendicular planes. This was done for the orientation of ***B*** at every 4° interval at room temperature, and at every 5° interval at liquid-nitrogen and liquid-helium temperatures. The largest flat plane, which contains the *c*-axis of the single-crystal specimen, which grows into monoclinic form, was chosen to define the *zx* plane. The direction of ***B***, in this plane, for which the positions of the hyperfine (h.f.) lines are at the minimum values of ***B***, was chosen to be the *z*-axis.

3.1.2 Optical

Optical-absorption spectrum was recorded on a Hewlett-Packard spectrometer (model 8452A) in the wavelength range 190 to 820 nm. The absorption spectrum, and the wavelengths of the absorbed peaks, were recorded directly via a microcomputer.

3.2 EPR spectra and spin-Hamiltonian parameters

The EPR spectrum for Cu^{2+}-doped MAT single crystal at room temperature consists of two sets of four hyperfine (h.f.) lines each. This indicates that there exist two magnetically inequivalent, but physically equivalent, Cu^{2+} centres in the unit cell of MAT, as expected from the crystal structure of MAT. Each Cu^{2+} centre is characterized by four hyperfine lines, since its electron spin $S = 1/2$ and nuclear spin $I = 3/2$ for the two stable isotopies of copper, Cu^{63} (69.05% abundant) and Cu^{65} (30.95% abundant), with non-zero nuclear magnetic moments. The EPR spectra at both the liquid-nitrogen and liquid-helium temperatures are different from those at room temperature, insofar as the h.f. linewidth and the splitting of EPR lines due to the Cu^{63} and Cu^{65} isotopes are concerned. The h.f. lines corresponding to Cu^{63} and Cu^{65} split clearly from each other at liquid-helium temperature, as can be seen from the spectrum, recorded for the orientation of $\boldsymbol{B}$ at 28° from the z-axis in the zx plane, displayed in Fig. 1. Two sets of h.f. lines corresponding to the two impurity sites for Cu^{2+} ions in the unit cell of MAT are exhibited in Fig. 1: the set occurring at lower magnetic field is designated as that belonging to site I, while the other one belonging to site II. For site I, only the outer h.f. lines for Cu^{65} and Cu^{63}, i.e., those corresponding to the allowed transitions $M = 1/2,\ m = \pm 3/2 \leftrightarrow M = -1/2,\ m = \pm 3/2$ split completely from each other (Fig. 1). (Here M and m refer to the electronic and nuclear magnetic quantum numbers,

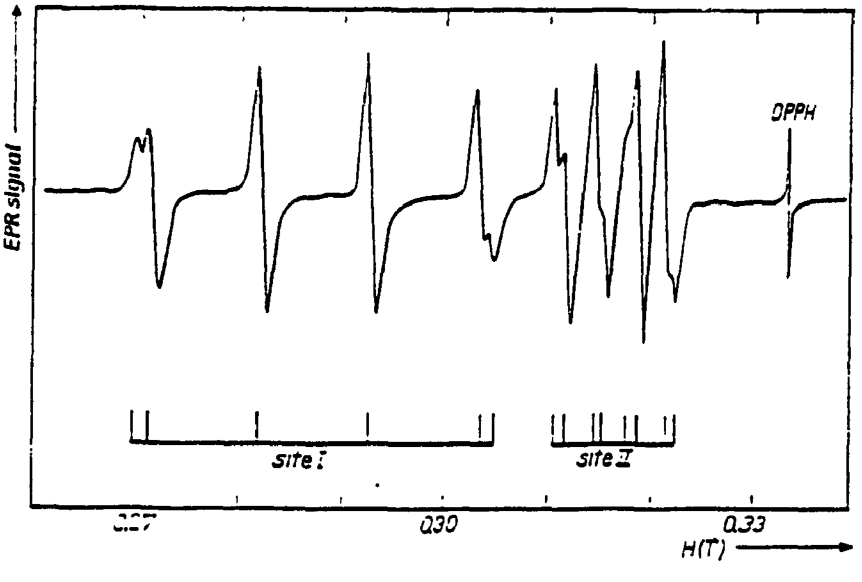

Fig. 1. First-derivative X-band EPR spectrum of Cu^{2+}-doped MAT at liquid-helium temperature for the orientation of $\boldsymbol{B}$ at 28° from the z-axis in the zx plane. The h.f. lines corresponding to the magnetic isotopes Cu^{63} and Cu^{65}, as well as the two spectra corresponding to the two sites (I and II) for Cu^{2+}, have been indicated. The two central h.f. lines for site I due to the two isotopes overlap each other

Table 1

The principal values of the tensors g and A (square roots of the principal values of the tensors g^2 and A^2 respectively) for Cu^{2+} in MAT at different temperatures. The g principal values are dimensionless, while the A principal values are in cm^{-1}. The labelling is such that $g_{\parallel} > g_{\perp}$. The errors of the presently estimated g principal values are ± 0.0018 and those for A principal values are ± 0.0002 cm^{-1}

temperature (K)	isotope	$g_{\parallel}$	$g_{\perp}$	$A_{\parallel}$	$A_{\perp}$	ref.
295	$Cu^{63,65}$	2.3738	2.0960	0.0108	0.0027	*)
300	$Cu^{63,65}$	2.347	2.095	0.0108	0.0026	[1]
77	Cu^{63}	2.3882	2.0962	0.0121	0.0031	*)
	Cu^{65}	2.3882	2.0962	0.0130	0.0034	*)
77	Cu^{63}	2.347	2.095	0.0121	0.0031	[1]
	Cu^{65}	2.347	2.095	0.0130	0.0034	[1]
4.2	Cu^{63}	2.3884	2.0963	0.0121	0.0031	*)
	Cu^{65}	2.3884	2.0963	0.0130	0.0034	*)

*) Present work.

respectively.) On the other hand, for site II all the four h.f. lines, i.e., those corresponding to the transitions $1/2, m \to -1/2; m$; $m = 3/2, 1/2, -1/2, -3/2$ for the two isotopes split completely (Fig. 1). The EPR h.f. linewidth at both the liquid-nitrogen and liquid-helium temperatures is $(13 \pm 1) \times 10^{-4}$ T, while at room temperature it is $(34 \pm 1) \times 10^{-4}$ T; these linewidths are independent of the orientation and magnitude of $\boldsymbol{B}$.

The observed EPR line positions of Cu^{2+} in MAT, for each of the Cu^{63} and Cu^{65} isotopes, were fitted to the following spin Hamiltonian:

$$\mathcal{H} = \mu_B \boldsymbol{B} \cdot g \cdot \boldsymbol{S} + \boldsymbol{S} \cdot A \cdot \boldsymbol{I}, \tag{1}$$

where μ_B is the Bohr magneton.

The principal values of the tensors g^2 and A^2, and their direction cosines, were evaluated by the use of a rigorous least-squares fitting procedure [4 to 6]. The direction cosines of the tensor g^2 were calculated with respect to the laboratory axes (x, y, z), while those of the tensor A^2 were calculated with respect to the principal axes of the tensor g^2. (The principal values of the matrices g and A are the square roots of the principal values of the tensors g^2 and A^2, respectively, while the direction cosines of the principal axes of the matrices g and A are the same as those of the tensors g^2 and A^2, respectively.) The principal values of the tensors g and A at 295, 77, and 4.2 K are listed in Table 1, which also includes the values estimated by Manakkil [1].

It is seen from Table 1 that two principal values of the tensor g are the same ($g_1 = g_2 = g_{\perp}$), being smaller than the third principal value of the tensor g ($g_3 = g_{\parallel}$). This suggests that the local symmetry of the Cu^{2+} ion in MAT is tetragonal (elongated octahedron); this is compatible with the X-ray results [3].

3.3 Optical spectrum

The room-temperature optical-absorption spectrum of Cu^{2+}-doped MAT single crystal, in the wavelength range 190 to 820 nm, is exhibited in Fig. 2. There are four bands in the visible range, occurring at $\nu_1 = 15243$ cm^{-1}, $\nu_2 = 16611$ cm^{-1}, $\nu_3 = 17182$ cm^{-1}, and $\nu_4 = 20661$ cm^{-1}, and two bands in the ultraviolet (UV) range,

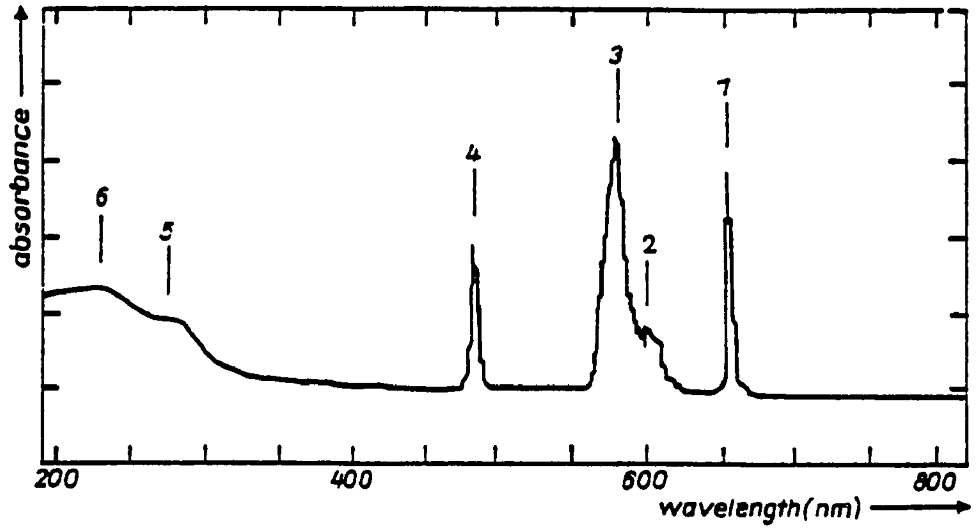

Fig. 2. Room-temperature optical-absorption spectrum in the wavelength range 190 to 820 nm. The lines indicated by 1 to 6 correspond to the energies ν_1 to ν_6, respectively, as cited in the text

which are weak in intensity and are poorly resolved, occurring at about $\nu_5 = 36\,500\ \text{cm}^{-1}$ and $\nu_6 = 43\,100\ \text{cm}^{-1}$.

The energy levels of the Cu^{2+} ion in a tetragonally-distorted octahedral symmetry (D_{4h}), as calculated using the crystal-field theory, are shown in Fig. 3. They are determined from the crystal-field Hamiltonian $\mathcal{H}_{cf}$, given as [7]:

$$\mathcal{H}_{cf} = D_q\left[\tfrac{35}{12}\hat{L}_z^4 - \tfrac{155}{12}\hat{L}_z^2 + 6 + \tfrac{5}{24}(\hat{L}_+^4 + \hat{L}_-^4)\right] + D_s(\hat{L}_z^2 - 2) - \\ - D_t\left[\tfrac{35}{12}\hat{L}_z^4 - \tfrac{155}{12}\hat{L}_z^2 + 6\right]. \qquad (2)$$

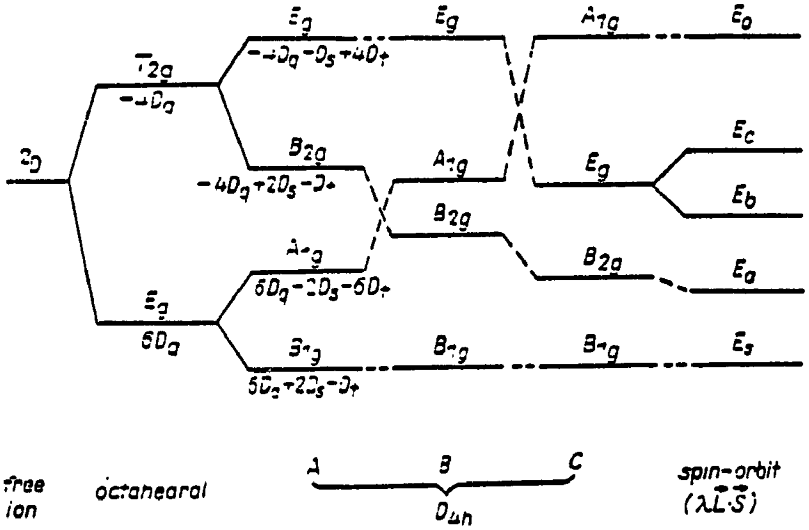

Fig. 3. Energy-level diagram for the Cu^{2+} ion in a tetragonally-distorted octahedral crystal field, with increasing tetragonal distortions A, B, and C; the limits of applicability are $|D_q| > \frac{7}{10}|D_s| > \frac{7}{5}|D_t|$, $\frac{7}{10}|D_s| > |D_q| > \frac{7}{5}|D_t|$ and $\frac{7}{10}|D_s| > \frac{7}{5}|D_t| > |D_q|$ for the tetragonal distortions A, B, and C, respectively

In (2), the first term represents the Hamiltonian for the purely-octahedral field, while the second and third terms represent the Hamiltonians for the tetragonally-distorted field. The parameters D_q, D_s, and D_t in (2) are referred to as the octahedral, and the second- and fourth-order tetragonal field parameters, respectively. They are expressed, using the point-charge model, as [8]

$$D_q = -\frac{1}{6} Ze^2 \frac{\langle r^4 \rangle}{R_e^5},$$

$$D_s = -\frac{2}{7} Ze^2 \frac{\langle r^2 \rangle}{R_e^3}\left(1 - \frac{R_e^3}{R_a^3}\right),$$

and

$$D_t = -\frac{2}{7} Ze^2 \frac{\langle r^4 \rangle}{R_e^5}\left(1 - \frac{R_e^5}{R_a^5}\right). \tag{3}$$

where Ze, $\langle r^2 \rangle$, $\langle r^4 \rangle$, R_e, and R_a are, respectively, the charge of the ligands, the mean-square and mean-fourth-power radii of the Cu^{2+} ion orbitals, and the distances of the ligands in the equatorial plane and those situated upon the axis perpendicular to the equatorial plane and the Cu^{2+} ion. The crystal-field parameters D_q, D_s, and D_t are usually determined from optical spectrum. There are three qualitatively different energy-level schemes [9], indicated as A, B, and C in Fig. 3, corresponding to an initially pure octahedral field with increasing tetragonal distortions corresponding to (2). Since the spin–orbit coupling constant, λ, of the Cu^{2+} ion is rather large, a significant effect of the spin–orbit coupling upon the spectrum of Cu^{2+} complex is expected [10]. To first order in perturbation, splitting into five energy levels (Fig. 3) of the Cu^{2+} ion (^2D configuration) is caused by the tetragonally distorted octahedral field along with the spin–orbit coupling [11]. These five energy levels can be expressed as follows:

$$E_0 = 6D_q - 2D_s - 6D_t \qquad (\text{orbital } d_{3z^2-r^2}),$$

$$E_c = -4D_q - D_s - 4D_t - \frac{\lambda}{2} \qquad (\text{overlap of orbitals } d_{xz} \text{ and } d_{yz}),$$

$$E_b = \frac{1}{2}(-8D_q + D_s + 3D_t) + \frac{\lambda}{4} + \frac{1}{2}\sqrt{(-3D_s + 5D_t)^2 + \lambda(-3D_s + 5D_t) + \frac{9\lambda^2}{4}}$$
$$(\text{overlap of orbitals } d_{xz} \text{ and } d_{yz}),$$

$$E_a = \frac{1}{2}(-8D_q + D_s + 3D_t) + \frac{\lambda}{4} - \frac{1}{2}\sqrt{(-3D_s + 5D_t)^2 - \lambda(-3D_s + 5D_t) + \frac{9\lambda^2}{4}} \qquad (\text{orbital } d_{xy}),$$

and

$$E_s = 6D_q + 2D_s - D_t \qquad (\text{orbital } d_{x^2-y^2}). \tag{4}$$

In (2) $E_0 > E_c > E_b > E_a > E_s$ for the large tetragonal distortions (scheme C); E_s is the ground state. Using these, the energies of the d–d transfer bands can be derived by calculating the energy differences between the excited states (E_0, E_c, E_b, E_a) and the ground state (E_s).

From the profile of the absorption spectrum in the visible region, the observed bands at ν_2 and ν_3 can be regarded, respectively, as the d–d transfer bands between the ground-state E_s ($d_{x^2-y^2}$) and the excited states E_b and E_c, into which the two-fold degenerate level $d_{xz,yz}$ is split by the spin–orbit coupling. Thus, the band at 16897 cm^{-1}, which is equal to the average value of the main band ν_3 and the shoulder on the longer-wavelength side, band ν_2, can be assigned as the d–d transfer band $d_{xz,yz} \leftrightarrow d_{x^2-y^2}$, being usually the most intense band [12]. The other two bands, observed at ν_1 and ν_4, are assigned as $d_{xy} \leftrightarrow d_{x^2-y^2}$ and $d_{3z^2-r^2} \leftrightarrow d_{x^2-y^2}$ transfer bands, respectively, as can be seen from (4).

The crystal-field parameters D_s and D_t can be estimated from the optical-absorption energies ν_1, ν_2, ν_3, and ν_4, from (4), as follows:

$$\nu_4 = -4D_s - 5D_t$$

and

$$\tfrac{1}{2}(\nu_2 + \nu_3) - \nu_1 = -3D_s - 5D_t \,. \tag{5}$$

This yields $D_s = -3188$ cm^{-1} and $D_t = -1582$ cm^{-1}. The four d–d transfer bands can now be calculated as functions of the parameter D_q with the assumption that $\lambda = -830$ cm^{-1}, the value for free Cu^{2+} ion [13]. Then the present optical data is found to fit well to $D_q = -1525$ cm^{-1}. This value is close to $-\nu_1/10$, as it should be, since $\nu_1 = -10D_q$, which is equal to $(E_a - E_s)$ in the limit $\lambda \to 0$, as seen from (4). Both the experimental energies and energies calculated, using the presently-estimated values of D_q, D_s, and D_t of the d–d transfer bands, are listed in Table 2.

The negative signs of D_q, D_s, and D_t are to be expected from the point-charge model, equations (3); these are in accordance with those estimated above using the energy levels given by the crystal-field theory, equations (4). However, the ratio D_t/D_q of the estimated values is close to unity; this should be less than 2/7 according to the point-charge model, equations (3). This is obviously a deficiency of the crystal-field theory. In practice, ab initio calculations are used to determine the energies and wave functions of the many-electron states, which characterize the bonding in molecules. Several semi-empirical molecular-orbital (MO) procedures have been proposed [8]. Smith [14] employed a semi-empirical MO method to explain the optical spectrum of tetragonal copper (II)–oxygen system. His method combined the point-charge and angular-overlap models; the latter is based on the assumption that the amount by which the energy of the metal orbital is raised, as a result of covalent bonding, is

Table 2

Observed and calculated energies, and assignments of the bands for Cu^{2+}-doped MAT with $D_q = -1525$ cm^{-1}, $D_s = -3188$ cm^{-1}, $D_t = -1582$ cm^{-1}, and $\lambda = -830$ cm^{-1}. ν_1, ν_2, ν_3, and ν_4 correspond to the energies $(E_a - E_s)$, $(E_b - E_s)$, $(E_c - E_s)$, and $(E_0 - E_s)$, respectively, as shown in Fig. 3

transition	band position (cm^{-1})	
	observed	calculated
$d_{xy} \leftrightarrow d_{x^2-y^2}$	$\nu_1 = 15243$	15016
	$\nu_2 = 16611$	16723
$d_{xz,yz} \leftrightarrow d_{x^2-y^2}$	$\nu_3 = 17182$	17319
$d_{3z^2} \leftrightarrow d_{x^2-y^2}$	$\nu_4 = 20661$	20662

directly proportional to the square of the diatomic-overlap integral. About one quarter of the final energies. calculated by Smith. were accounted for by the electrostatic terms in the point-charge model. while the remaining. about three-quarter of the final energies. were accounted for by the angular-overlap terms.

From the assignments of the d–d transfer bands. it appears that the Cu^{2+} ion in MAT single crystal experiences a square planar, D_{4h}. symmetry. It is due to the fact that when Cu^{2+} ion substitutes for a Mg^{2+} ion in MAT crystal. the two oxygen ligands of Mg^{2+} along the axis. belonging to two different acetate groups. move rather far from the centre of the Cu^{2+} complex. due to the Jahn-Teller effect [15]. The original complex. with an approximately tetragonally-distorted octahedral symmetry. now possesses only a square-planar symmetry.

The optical-absorption spectrum of Cu^{2+}-doped MAT in the visible region is similar to that of Cu^{2+}-doped $BaCuSi_4O_{10}$ single crystal [16], in which Cu^{2+} ion is also in a square-planar coordination with the oxygen ligands. for which the three observed d–d transfer bands. occurring at 12900. 15800. and 18800 cm^{-1}. have been assigned as $d_{xy} \leftarrow d_{x^2-y^2}$. $d_{xz,yz} \leftarrow d_{x^2-y^2}$. and $d_{3z^2-r^2} \leftarrow d_{x^2-y^2}$, respectively. The $d_{xz,yz} \leftarrow d_{x^2-y^2}$ transfer band. has the maximum intensity; the two lines of this band were not resolved [16]. perhaps due to inferior sensitivity of the spectrometer used.

The two presently-observed absorption bands in the UV range. occurring at frequencies $\nu_5 = 36500\ cm^{-1}$ and $\nu_6 = 43100\ cm^{-1}$ are. probably. charge-transfer-transition bands. because they arise from the higher-lying energy levels. not shown in Fig. 3. The present results can be compared with those for $CuCl_4^{2-}$ complex. which possesses square-planar symmetry [17]. for which there have been observed three charge-transfer transitions in the UV range: they have been assigned as $1a_{2g} \leftarrow 3b_{1g}$, $4e_u \leftarrow 3b_{1g}$. and $3e_u \leftarrow 3b_{1g}$ transitions. in order of decreasing wavelengths. For $CuCl_4^{2-}$, the intensities of the transitions $1a_{2g} \leftarrow 3b_{1g}$ and $4e_u \leftarrow 3b_{1g}$, are very weak; as well. these two transitions are close in energy [17]. Using these results for $CuCl_4^{2-}$. combined with the poor resolution of the spectrometer. used presently, in the UV range. the transitions $1a_{2g} \leftarrow 3b_{1g}$ and $4e_u \leftarrow 3b_{1g}$ for Cu^{2+} in MAT can be considered to have the same observed energy $\nu_5 = 36500\ cm^{-1}$. Finally. the remaining charge-transfer transition $3e_u \leftarrow 3b_{1g}$ corresponds to the observed frequency $\nu_6 = 43100\ cm^{-1}$.

4. Molecular Orbitals of Cu^{2+} in MAT Lattice

Using the energy-level splitting of the Cu^{2+} ion in the lattice of MAT single crystal, it is possible to evaluate the coefficients of the MO for Cu^{2+}-doped MAT. The splitting of d, or f, orbitals of transition-metal ions in molecular complexes is usually described by crystal-field theory. However. it does not take into account the effect of interaction with the ligand electrons adequately. In fact. the crystal-field theory is not fully applicable to those complexes. which are characterized by strong interactions between the electronic orbitals of the central atom and ligands. responsible for the formation of molecular orbitals.

The spin-Hamiltonian parameters (S.H.P.) of the transition-metal ions can be expressed in terms of (i) the coefficients of the MOs: (ii) the energy separations between the excited states and the ground state of the ion: and (iii) the energies of the charge-transfer transition bands. which can be determined from the optical spectrum. EPR. thus. becomes an integral tool for the estimation of the MO coefficients of transition-metal complexes. since S.H.P. are determined from EPR measurements. The optical-absorption data for Cu^{2+}-doped MAT indicates that the Cu^{2+} complex in MAT single crystal sees a local D_{4h} square-planar symmetry. For the Cu^{2+} complex in MAT the equatorial Cu–O (H_2O) bond length is 0.2075 nm, being the average distance of Mg–H_2O (1) and Mg–H_2O (2) in the MAT host lattice [3].

Maki and McGarvey [2] were the first to apply the MO theory to the Cu^{2+} complex with tetragonally-distorted octahedral symmetry in order to derive theoretical expressions for the tensors g and A. The overlaps of the p-orbitals of the four ligand oxygens in the equatorial plane, as well as those of the two oxygen ligands on the axis perpendicular to the equatorial plane, were subsequently taken into account by Smith [18], who derived theoretical expressions for the tensor g, to second-order in perturbation; these were later extended to third-order in perturbation by Moreno [19]. Finally, Aramburu and Moreno [20] deduced the theoretical expressions for all three, g, A and the superhyperfine (s.h.f.) tensors of the Cu^{2+} square-planar complex, using the MO theory, to third-order in perturbation, taking into account the contributions from the bonding MOs.

Explicitly, the S.H.P. can be formally expressed as functions of K, the core polarization contribution, and the eleven coefficients of MO α_i, β_i ($i = 0, 1, 2$), and α_i', β_i' ($i = 1, 2$), and μ as follows [20]:

$$g_{\parallel} = g_e + ak_1 + a'k_1',$$

$$g_{\perp} = g_e + bk_2 + b'k_2',$$

$$A_{\parallel} = -K + 2A_0 + P(a + a' + \tfrac{3}{7} b + \tfrac{3}{7} b').$$

and

$$A_{\perp} = -K - A_0 + \frac{11P}{14}(b + b'). \tag{6}$$

In (6) g_e (= 2.0023) is the free electron g value. $P = 2g_N\mu_B\mu_N\langle r^{-3}\rangle_M = 0.036\ \text{cm}^{-1}$ [21], where g_N, μ_N, and $\langle r^{-3}\rangle_M$ are, respectively, the nuclear g factor, the nuclear magneton and the average of the inverse-cube radius of the Cu^{2+} ion.

The various quantities appearing on the right-hand sides of (6) are defined as follows:

$$A_0 = -\tfrac{2}{7}\alpha_0^2 P,$$

$$k_1 = 1 - \frac{\beta_0}{\alpha_0} S - \frac{\beta_1}{2\alpha_1}\left(2S_1 + \frac{\beta_0}{\alpha_0}\Gamma(\mu)\right),$$

$$k_1' = 1 - \frac{\beta_0}{\alpha_0} S_0 + \frac{\beta_1'}{2\alpha_1'}\left(2S_1 + \frac{\beta_0}{\alpha_0}\Gamma(\mu)\right),$$

$$k_2 = 1 - \frac{\beta_0}{\alpha_0} S_0 - \frac{\beta_2}{\sqrt{2}\,\alpha_2}\left(\sqrt{2}\,S_2 + \frac{\beta_0}{\alpha_0}\Gamma(\mu)\right),$$

$$k_2' = 1 - \frac{\beta_0}{\alpha_0} S_0 + \frac{\beta_2'}{\sqrt{2}\,\alpha_2'}\left(\sqrt{2}\,S_2 + \frac{\beta_0}{\alpha_0}\Gamma(\mu)\right),$$

$$a = 8\alpha_0\alpha_1\left(1 - \frac{\beta_0\beta_1\mu\,|\xi_L|}{2\alpha_0\alpha_1\,|\xi_M|}\right)\frac{|\xi_M|}{\Delta_1},$$

$$a' = 8\alpha_0^2\alpha_2'^2\left(1 + \frac{\beta_0\beta_1'\mu\,|\xi_L|}{2\alpha_0\alpha_1'\,|\xi_M|}\right)\frac{|\xi_M|}{\Delta_1'},$$

$$b = 2\alpha_0^2\alpha_2^2\left(1 - \frac{\beta_0\beta_2\mu\,|\xi_L|}{\sqrt{2}\,\alpha_0\alpha_2\,|\xi_M|}\right)\frac{|\xi_M|}{\Delta_2},$$

and

$$b' = 2\lambda_0^2\alpha_2^2\left(1 + \frac{\beta_0\beta_2'\mu\,|\xi_L|}{\sqrt{2}\,\alpha_0\alpha_2'\,|\xi_M|}\right)\frac{|\xi_M|}{\Delta_2'}. \tag{7}$$

In equations (7) Δ_1 and Δ_2 are the d–d transfer energies of the $d_{xy} \leftrightarrow d_{x^2-y^2}$ and $d_{xz,yz} \leftrightarrow d_{x^2-y^2}$ transitions, determined presently from the optical-absorption spectrum to be $\Delta_1 = 15243$ cm^{-1} and $\Delta_2 = (\nu_2 + \nu_3)/2 = 16897$ cm^{-1}, while Δ_1' and Δ_2' are the charge-transfer transition energies corresponding to the charge transitions $1b_{2g} \leftrightarrow 3b_{1g}$ and $1e_g \leftrightarrow 3b_{1g}$, respectively (determined presently from the optical-absorption spectrum to be 43100 cm^{-1}, each). For comparison, it is noted that for the $CuCl_4^{2-}$ complex, which possesses a D_{4h} symmetry [17], the calculated values of Δ_1' and Δ_2' are found to be, respectively, higher, and lower, in energy, than that of the observed charge-transfer transition band $3e_u \leftrightarrow 3b_{1g}$. In equations (7) ξ_M, ξ_L are, respectively, the spin–orbit coupling constants of the central metal ion (Cu^{2+}) and the ligand ions (O^{2-}) of the complex. (The values of $|\xi_M|$ and $|\xi_L/\xi_M|$ are assumed to be 830 cm^{-1} and 0.18 [18].) Further, in (7) S_0, S_1 and S_2, in the expressions for k_1, k_1', k_2, and k_2', are the group-overlap integrals,

$$S_0 = \mu S_{p\sigma} + \sqrt{(1-\mu^2)}\,S_s\,,$$

$$S_1 = \langle d_{xy}\,|\chi_{p\pi}\,(b_{2g})\rangle\,,$$

and

$$S_2 = \langle d_{xz}\,|\chi_{p\pi}\,(e_g)\rangle\,, \tag{8}$$

where

$$S_{p\sigma} = \langle d_{x^2-y^2}\,|\chi_{p\sigma}\,(b_{1g})\rangle$$

and

$$S_s = \langle d_{x^2-y^2}\,|\chi_s\,(b_{1g})\rangle\,. \tag{9}$$

The group-overlap integrals $S_{p\sigma}$, S_s, S_1, and S_2 can be estimated in terms of S_e, the diatomic-overlap integrals between the 3d orbital of the Cu^{2+} ion and the 2s and 2p orbitals of the oxygen ligands. For a square-planar configuration, in which the contribution from the orbitals of axial atoms can be neglected, these group-overlap integrals are expressed as [22]

$$S_{p\sigma} = \sqrt{3}\,S_e(2p\sigma,\,3d\sigma)\,,$$

$$S_s\ = \sqrt{3}\,S_e(2s\sigma,\,3d\sigma)\,,$$

$$S_1\ = 2\ S_e(2p\pi,\,3d\pi)\,,$$

and

$$S_2\ = \sqrt{2}\,S_e(2p\pi,\,3d\pi)\,.$$

Here the σ and π in the parentheses after S_e indicate σ- and π-bonding, respectively. These diatomic-overlap integrals are calculated from the approximate formulae for the 3d-, 2s-, and 2p-orbitals in σ- or π-bonding [23, 24], using the double-ζ radial functions of the copper 3d-orbital [25], and the oxygen 2s- and 2p-orbitals [26]. By assuming the Cu–O bond length (R_e) in the equatorial plane to be 0.2075 nm the values of the group-overlap integrals are here estimated to be $S_{p\sigma} = 0.132$, $S_s = 0.107$, $S_1 = 0.0730$ and $S_2 = 0.0516$.

$\Gamma(\mu)$, appearing in (7), is given by

$$\Gamma(\mu) = \mu - (1-\mu)^{1/2}\,R_e\left\langle s(1)\left|\frac{\partial}{\partial y(1)}\right|p_y(1)\right\rangle, \tag{10}$$

where (1) refers to the ligand 1, representive of the four equivalent (1, 2, 3, 4) oxygen ligands, while s and p_yd enote the corresponding orbitals.

The value of the integral $\langle s(1)|\partial/\partial y(1)|p_y(1)\rangle$ in the expression for $\Gamma(\mu)$ in (10) is 0.57, whose magnitude was estimated by Smith [18], while the sign was determined by Aramburu and Moreno [20], in accordance with the fact that the most-covalent systems experience positive g shifts, whereas the most-ionic ones negative g shifts.

The eleven MO coefficients (α_i, β_i; $i = 0, 1, 2$ and α'_i, β'_i; $i = 1, 2$, and μ), appearing in (7) to (10) have the same definitions as those given by Aramburu and Moreno [20]. Specifically, α_i and β_i for $i = 0, 1, 2$, respectively, are the MO coefficients of the antibonding levels $3b_{1g}$, $2b_{2g}$, $2e_g$, while α'_i and β'_i for $i = 1, 2$ are, respectively, the MO coefficients of the bonding levels $2b_{2g}$, $2e_g$; here α refers to the coefficients of the central Cu^{2+} ion of the complex, while β to those for the ligands. μ and $(1 - \mu^2)^{1/2}$ are, respectively, the coefficients of the p and s orbitals of the oxygen ligands in the $3b_{1g}$ configuration, which depend on the hybridization of the oxygen ion of the water molecule.

There exists a relationship between the antibonding and bonding MO coefficients of $2b_{2g}$ and $2e_g$ levels [27],

$$\alpha_i\alpha'_i - \beta_i\beta'_i + \alpha_i\beta'_iS_i - \alpha'_i\beta_iS_i = 0; \qquad i = 1, 2\,. \tag{11}$$

Finally, the normalizations of the MO coefficients are [28]

$$\alpha_i^2 - \beta_i^2 - 2\alpha_i\beta_iS_i = 1; \qquad i = 0, 1, 2 \tag{12}$$

and

$$\alpha_i'^2 + \beta_i'^2 + 2\alpha'_i\beta'_iS_i = 1; \qquad i = 1, 2\,. \tag{13}$$

In the present case (Cu^{2+}-doped MAT) there are twelve unknown coefficients; these are the eleven MO coefficients and the core-polarization contribution (K). However, there are available only eleven equations: four expressions for the S.H.P., equations (6), five normalization conditions between α_i and β_i ($i = 0, 1, 2$), and α'_i and β'_i ($i = 1, 2$), equations (12) and (13), and two equations between the coefficients of the antibonding and the bonding orbitals, equations (11). In order to reduce the number of unknowns to be determined to eleven the value of the coefficient μ has here been assumed to be $\sqrt{3}/2$, corresponding to sp^3 hybridization of oxygen (water) ligand [29]. It is difficult to obtain well-defined solutions for the MO coefficients, because the equations relating the MO coefficients are non-linear. On the other hand, in order to estimate their values one can always fit the MO coefficients by a least-squares technique to $M = \sum_{i=1}^{4} (\mathrm{SHP}^i_{\mathrm{cal.}}/\mathrm{SHP}^i_{\mathrm{obs.}} - 1)^2$, with the condition that the best-fit MO coefficients minimize the value of M. Here SHP^i ($i = 1$ to 4) refer to the four principal values of the tensors g and A ($g_\parallel$, $g_\perp$, $A_\parallel$, and $A_\perp$), while obs. and cal. indicate their observed and calculated values, respectively.

The MO coefficients and K, so determined, using the program EUREKA on an IBM-PC XT, equipped with a MATH Coprocessor chip 8087-2, are listed as follows:

K (cm^{-1})	α_0	β_0	α_1	β_1	α_2	β_2	α'_1	β'_1	α'_2	β'_2
125×10^{-4}	0.88	0.65	1.0	0.01	0.98	0.26	0.02	1.0	0.21	0.97

These coefficients are characterized by the value of $M = 0.54$. The presently-determined value of $K = 125 \times 10^{-4}\ \mathrm{cm}^{-1}$ is very close to $K = 130 \times 10^{-4}\ \mathrm{cm}^{-1}$, which has been calculated theoretically for the free Cu^{2+} ion by Watson and Freeman [30]. The present values of the coefficients α_0, α_1, and α_2 imply that the nature of the bonding of the Cu^{2+} ion in MAT crystal lattice is not purely ionic. This is because $\alpha_0^2 = 0.77$ indicates that there is an appreciable in-plane covalent σ-bonding of Cu^{2+} ion with the oxygen ligands in the equatorial plane. (If $\alpha_0^2 = 1$. there would have been no covalent bonding.) On the other hand, there is no in-plane covalent π-bonding in the complex since $\alpha_1^2 = 1.0$. Although the axial ligands are not taken into account in the D_{4h} square-planar configuration. the present value of α_2^2. being very close to unity ($= 0.96$). indicates that the out-of-plane covalent π-bonding is quite small. Thus. the nature of bonding with the oxygen ligands along the axis, belonging to the two carboxyl groups. is expected to be mostly ionic.

The presently-determined values of K and the MO coefficients can be compared with those estimated by Manakkil [1] using a rather simple model [2]. He only estimated the values of α_0. α_1. α_2. and K. His values for α_0 ($= 0.86$). α_1 ($= 0.98$). and α_2 ($= 0.99$) are very close to the present values. while $K = 115 \times 10^{-4}$ cm^{-1} is somewhat different from the present value.

5. Concluding Remarks

The present EPR and optical absorption studies have enabled the determination of the spin-Hamiltonian parameters $g_{\|}$, $g_{\perp}$. $A_{\|}$ and $A_{\perp}$, as well as the crystal-field parameters D_q. D_s. and D_t. These have been used to estimate the core polarization K and the coefficients of MO and K for Cu^{2+} in MAT lattice.

The values of $g_{\|}$ and $A_{\perp}$, determined presently, are significantly larger than. while those of $g_{\perp}$ and $A_{\|}$ are very close to. those reported by Manakkil [1]. Further. the presently-determined principal values of the tensors g and A at liquid-helium temperature are the same as those determined at liquid nitrogen temperature. within experimental error. Manakkil [1] did not carry out any EPR measurements at liquid-helium temperature.

The optical-absorption spectrum has been explained well in terms of a D_{4h} square-planar configuration of the O^{2-} ligands in the Cu^{2+} complex taking into account the spin–orbit coupling. The presently-determined MO coefficients indicate that for the Cu^{2+} complex in MAT lattice. the bonding between the Cu^{2+} ion and the oxygen ligands in the square-planar configuration is partly covalent, while the bonding between the Cu^{2+} ion and its axial oxygen ligands is mostly ionic.

Acknowledgements

The authors are grateful to the Natural Sciences and Engineering Research Council of Canada for financial support (grant number A4485), and to the Concordia University Computer center for providing their facilities to analyze the data. We are thankful to the Chemistry Department for allowing us to record the optical-absorption spectrum on their spectrometer.

References

[1] T. J. Manakkil, Ph.D. Thesis, New Mexico State Univ., 1967 (unpublished).
[2] A. H. Maki and B. R. McGarvey, J. chem. Phys. 29, 31 (1958).
[3] J. Shankar, P. G. Khubchandani, and V. M. Padmanabhan, Proc. Indian Acad. Sci. A45, 117 (1957).
[4] S. K. Misra, Mag. Res. Rev. 10, 286 (1986).
[5] S. K. Misra, Arabian J. Sci. Engng. 13, 255 (1988).
[6] S. K. Misra, Physica (Utrecht) B151, 433 (1988).
[7] C. J. Ballhausen, Introduction to Ligand Field Theory, McGraw-Hill Publ. Co., New York 1962 (p. 100).
[8] M. Gerloch and R. C. Slade, Ligand-field Parameters, Cambridge University Press, 1973 (p. 92).
[9] N. S. Hush and R. J. M. Hobbs, Progr. inorg. Chem. 10, 357 (1968).

[10] J. Ferguson, Progr. inorg. Chem. 12, 159 (1970).

[11] C. P. Poole, Jr. and H. A. Farach, The Theory of Magnetic Resonance, John Wiley & Sons, New York 1972 (p. 359).

[12] D. W. Smith, J. Chem. Soc. A, 176 (1970).

[13] A. Abragam and B. Bleaney, Electron Paramagnetic Resonance of Transition Ions, Clarendon Press, Oxford 1970 (p. 399).

[14] D. W. Smith, J. Chem. Soc. A, 176 (1970).

[15] B. R. McGarvey, Electron Spin Resonance of Transition-metal Complexes, in: Transition Metal Chemistry Vol. 3, Ed. by R. L. Carlin, Marcel Dekker, Inc., New York 1966 (p. 89).

[16] M. G. Clark and R. G. Burns, J. Chem. Soc. A, 1034 (1967).

[17] S. D. Desjardins, K. W. Penfield, S. L. Cohen, R. L. Musselman, and E. I. Solomon, J. Amer. Chem. Soc. 105, 4590 (1983).

[18] D. W. Smith, J. Chem. Soc. A, 3108 (1970).

[19] M. Moreno, J. Phys. C 9, 3277 (1976).

[20] J. A. Aramburu and M. Moreno, J. chem. Phys. 83, 6071 (1985).

[21] A. Kawamori and I. Miyagawa, J. chem. Phys. 55, 1336 (1971).

[22] D. W. Smith, J. Chem. Soc. A, 1498 (1970).

[23] H. H. Jaffé and G. O. Doak, J. chem. Phys. 21, 196 (1953).

[24] H. H. Jaffé, J. chem. Phys. 21, 258 (1953).

[25] J. W. Richardson, W. C. Nieuwpoort, R. R. Powell, and W. E. Edgell, J. chem. Phys. 36, 1057 (1962).

[26] E. Clementi and C. Roetti, Atomic Data, Nuclear Data Tables 14, 177 (1974).

[27] C. J. Ballhausen and H. B. Gray, Inorg. Chem. 1, 111 (1962).

[28] C. J. Ballhausen and H. B. Gray, Molecular Orbital Theory, W. A. Benjamin, Inc., New York 1965 (p. 92).

[29] J. G. Verkade, A Pictorial Approach to Molecular Bonding, Springer-Verlag, New York 1986 (p. 45).

[30] R. E. Watson and A. J. Freeman, Hyperfine Interactions, Academic Press, Inc. New York 1967.

(Received February 8, 1989)

PHYSICAL REVIEW B
CONDENSED MATTER

THIRD SERIES, VOLUME 41, NUMBER 1 1 JANUARY 1990

EPR of Cu^{2+}-doped cadmium ammonium sulfate: Pseudo-Jahn-Teller effect

Sushil K. Misra and Chunzheng Wang
Physics Department, Concordia University, 1455 de Maisonneuve Boulevard West, Montreal, Quebec, Canada H3G 1M8

(Received 9 June 1989)

X-band EPR measurements on both single-crystal and polycrystalline specimens of Cu^{2+}-doped cadmium ammonium sulfate, $Cd(NH_4)_2(SO_4)_2 \cdot 6H_2O$, have been made over the temperature range 4.2–354 K. Hyperfine Cu^{2+} forbidden transitions were observed at 4.2 K. The spin-Hamiltonian parameters, including the quadrupole-interaction tensor $\tilde{Q}$ (at 4.2 K only), are estimated by the use of a rigorous least-squares fitting procedure from EPR line positions recorded at 295, 77, and 4.2 K for the single-crystal specimen. The temperature dependence of the g values are explained by taking into account the pseudo-Jahn-Teller effect experienced by the $Cu(H_2O)_6{}^{2+}$ complex. The differences in the energies of the three Jahn-Teller configurations of the $Cu(H_2O)_6{}^{2+}$ complex have been estimated.

I. INTRODUCTION

An EPR study of the Cu^{2+} ion in a cadmium ammonium sulfate, $Cd(NH_4)_2(SO_4)_2 \cdot 6H_2O$ (hereafter CAS) single crystal at 300 and 77 K has been reported by Satyanarayana,[1] indicating that the impurity ion substituted for a Cd^{2+} ion in the CAS host lattice. The ground state of the Cu^{2+} ion was determined, from the observed orthorhombic spin-Hamiltonian parameters (SHP), to be predominantly the $|X^2-Y^2\rangle$ orbital, with an admixture of the $|3Z^2-R^2\rangle$ orbital.

Silver and Getz[2,3] examined in detail the temperature dependence of the EPR spectra of Cu^{2+} introduced in the Zn Tutton salt $K_2Zn(SO_4)_2 \cdot 6D_2O$. They related the temperature-dependent principal g values, and the differences in the energy splittings between the three Jahn-Teller (JT) configurations to the unpaired electron (Boltzmann) populations in the three potential valleys. Petrashen *et al.*[4] studied the pseudo JT nature of $Cu(H_2O)_6{}^{2+}$ complexes in zinc Tutton salts, and estimated the differences in the energy splittings between three JT potential valleys from the EPR and x-ray data. They established a relation between the ratios of the energy splittings ($\delta_{1,3}/\delta_{1,2}$) of the three JT configurations of the $Cu(H_2O)_6{}^{2+}$ complex and the symmetry of the host complex.

Misra and Wang[5] proposed a model to interpret the JT effect in Cu^{2+}-doped diamagnetic host lattices. Specifically, in this model, the diamagnetic ions, due to their closed outer electronic shells, cause the local symmetry of the host lattice to be high. When the paramagnetic Cu^{2+} ion substitutes for a diamagnetic ion in this lattice, local distortions are introduced because of the difference in size from that of the host ion, as well as due to its paramagnetic nature. In the case of Cu^{2+}-doped CAS lattice, the pseudo JT effect, similar to that which occurs in the lattice of Zn Tutton salts, might be expected, because the Cd^{2+} ion is diamagnetic.

It is the purpose of this paper to present more detailed EPR studies on Cu^{2+}-doped CAS single-crystal and powder specimens. The measurements are carried out over an extended temperature range, 4.2–354 K, making it possible to observe the pseudo JT effect. At 4.2 K the forbidden hyperfine (hf) transitions are observed unlike that at higher temperatures. The Cu^{2+} SHP, including the quadrupole interaction tensor, are presently evaluated using a rigorous least-square fitting (LSF) procedure, fitting simultaneously a large number of line positions observed for several orientations of the Zeeman field (**B**). The powder data are used to study detailed temperature variations of the g values required to estimate the energy splittings between the potential valleys of the $Cu(H_2O)_6{}^{2+}$ complex.

II. SAMPLE PREPARATION AND CRYSTAL STRUCTURE

Cu^{2+}-doped CAS single crystals were grown by slow evaporation of an aqueous solution, consisting of stoichiometric amounts of $3CdSO_4 \cdot 8H_2O$ and $(NH_4)_2SO_4$, to which was added a sufficient quantity of $CuSO_4 \cdot 5H_2O$, so that there was one Cu^{2+} ion for every 100 Cd^{2+} ions.

The crystal structure of CAS has been reported by Montgomery and Lingafelter[6] to be monoclinic (space group $P_{2_1/a}$); the unit-cell dimensions are $a = 9.43$ Å, $b = 12.82$ Å, $c = 6.29$ Å, $\beta = 106°52'$. There are two formula units per unit cell ($Z = 2$); each Cd^{2+} ion is surrounded by six water molecules. The bond lengths between the central ion Cd^{2+} and the ligand atoms are 2.298 Å, 2.297 Å, and 2.241 Å for Cd—O(7) (H_2O), Cd—O(8) (H_2O), and Cd—O(9) (H_2O), respectively; while the bond angles are 89.1° for O(7)—Cd—O(8), 92.6° for O(7)—Cd—O(9), and 91.3° for O(8)—Cd—O(9).[6] [The positions of Cd, O(7), O(8), and O(9) are defined in Ref. 6.] These data indicate that the Cd^{2+} ion in CAS is approximately in a compressed tetragonally distorted octahedral crystal field.

III. EXPERIMENTAL ARRANGEMENT AND EPR DATA

The EPR spectra were recorded on a *X*-band Varian V4502 spectrometer using a 100-kHz field modulation for measurements of room (RT) and high temperatures and 400 Hz field modulation for measurements at liquid-nitrogen (LNT) and liquid-helium (LHT) temperatures. The magnetic field was measured with a Bruker (B-NM20) gaussmeter. For low-temperature EPR experiments, the temperature was varied by a heater resister inside the liquid-helium cryostat. Temperatures in the liquid-nitrogen and liquid-helium ranges were determined by measuring the resistances of the platinum and germanium resistors, respectively, using appropriate calibration charts. For high-temperature spectra, a Varian Associates variable-temperature controller (model No. E4540) attached to a microprocessor digital thermometer manufactured by Omega (model No. 870) was employed.

The angular variations of the EPR line positions were recorded for the orientation of **B** in three mutually perpendicular planes at all temperatures of measurement for the single-crystal specimen. The spectra were recorded for the orientation of **B** at every 4° interval at room and high temperatures, and at every 5° interval at LNT and LHT. The largest flat plane, which contains the crystallographic *c* axis of the single-crystal specimen, was chosen to define the *zx* plane. The direction of **B**, in this plane, for which the positions of the hf lines were at the minimum values of **B**, was chosen to be the *z* axis, while the direction at 90° to this defined the *x* axis. (The *y* axis is, of course, perpendicular to the *zx* plane.) For EPR measurements in the *zy* and *xy* planes at RT the single-crystal specimen was rotated about the *x* and *z* axes, respectively, keeping the direction of **B** fixed. At LNT and LHT, **B** was rotated about the *x* and *z* axes keeping the single-crystal specimen fixed.

The EPR spectra of the powder specimen were recorded at various temperatures in the temperature range 4.2–354 K in order to study the temperature dependence of the *g* values.

A. Single-crystal EPR spectra at 295, 77, and 4.2 K

The single-crystal EPR spectra of Cu^{2+}-doped CAS at 295, 77, and 4.2 K were found to be quite different from each other in their profiles as seen from Fig. 1, which exhibits EPR spectra for the orientation of **B** at 10° from the *z* axis in the *zx* plane. The spectrum at 295 K consists of two broad lines, which indicate the presence of two physically equivalent, but magnetically inequivalent, Cu^{2+} complexes in the unit cell of the CAS lattice. At 77 K these two broad lines split, due to the Cu^{2+} hf interaction, into two sets of tetrads due to the more abundant isotope ^{63}Cu (69.09% abundance); the lines corresponding to the less-abundant isotope of Cu^{2+} (^{65}Cu, 30.91% abundance) could not be clearly seen. At 4.2 K, some satellite lines, corresponding to the hf forbidden transitions, were observed.

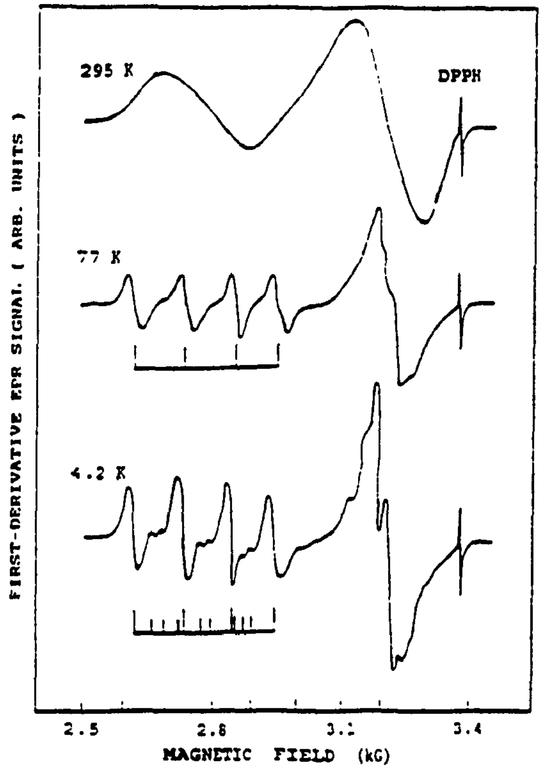

FIG. 1. Single-crystal EPR spectra of Cu^{2+}-doped CAS for **B** at 10° from the *z* axis in the *zx* plane at various temperatures: the allowed hf lines at 77 and 4.2 K are indicated by longer bars, the eight short bars indicate the forbidden-transition line positions corresponding to the transitions $\Delta m = -1, +1, -2, +2, +2, -2, +1, -1$, respectively, as expressed in order from low to high magnetic field values.

TABLE I. Principal values of the $\tilde{g}$ and $\tilde{A}$ matrices (square roots of the principal values of the $\tilde{g}^2$ and $\tilde{A}^2$ tensors, respectively), and the $\tilde{Q}$ tensor for Cu^{2+} in the CAS single-crystal specimen at different temperatures. The principal g values are dimensionless, while the principal values of the $\tilde{A}$ matrix and the $\tilde{Q}$ tensor are in GHz.

Temperature (K)	$g_{z'}$	$g_{y'}$	$g_{x'}$	$A_{z'}$	$A_{y'}$	$A_{x'}$	$Q_{z'}$	$Q_{y'}$	$Q_{x'}$	Ref.
295	2.3373	2.2111	2.0712							a
295	2.331	2.202	2.073							b
77	2.3613	2.1721	2.0522	0.333	0.074	0.151				a
77	2.355	2.172	2.054	0.333	0.078	0.157				b
4.2	2.4290	2.1594	2.0513	0.335	0.077	0.156	0.013	−0.012	−0.001	a

[a] Present work.

[b] Data from Ref. 1.

The EPR spectra of Cu^{2+} ion in CAS is described by the following spin Hamiltonian:

$$\mathcal{H}=\mu_B \mathbf{S}\cdot\tilde{g}\cdot\mathbf{B}+\mathbf{S}\cdot\tilde{A}\cdot\mathbf{I}+\mathbf{I}\cdot\tilde{Q}\cdot\mathbf{I}-\mu_N\mathbf{I}\cdot\tilde{g}_N\cdot\mathbf{B}\ . \tag{1}$$

In Eq. (1), μ_B and μ_N are, respectively, the Bohr and nuclear magnetons, while $\tilde{A}$ and $\tilde{Q}$ are, respectively, the hf-interaction matrix and the quadrupole-coupling tensor. S $(=\frac{1}{2})$ is the electronic spin and I $(=\frac{3}{2})$ is the nuclear spin of the Cu^{2+} ion.

The principal values of the $\tilde{g}^2$ ($\tilde{g}^T\cdot\tilde{g}$; superscript T denotes transposition of a matrix) and $\tilde{A}^2$($\tilde{A}^T\cdot\tilde{A}$) tensors, as well as their direction cosines, were evaluated by the use of a least-squares fitting procedure previously described.[7-9] The direction cosines of the $\tilde{g}^2$ tensor were calculated with respect to the laboratory axes (x,y,z), while those of the $\tilde{A}^2$ tensor were calculated with respect to the principal axes of the $\tilde{g}^2$ tensor. The directions of the principal axes of the $\tilde{g}^2$ tensor did not change with temperature; the principal axes of the $\tilde{A}^2$ tensor were coincident with those of the $\tilde{g}^2$ tensor at LNT and LHT, within experimental errors. The principal values of the $\tilde{g}$ and $\tilde{A}$ matrices at various temperatures are listed in Table I, which also includes the values estimated by Satyanarayana.[1] Table II gives the direction cosines of the principal axes of the $\tilde{g}$ and $\tilde{A}$ matrices.

The elements of the $\tilde{Q}$ tensor were evaluated from the forbidden hf line positions employing another LSF procedure: using the computer program which was used to calculate the $\tilde{Q}$ tensor in the case of VO^{2+}-doped $K_2C_2O_4\cdot H_2O$ (Ref. 10) modified to take into account the different nuclear spin of Cu^{2+} and the forbidden hf transitions, $\Delta m=\pm1$, ±2. In this program, the previously determined values of $\tilde{g}^2$ and $\tilde{A}^2$ tensors were used as constants; only the components of the $\tilde{Q}$ matrix were varied. A total of 258 forbidden hf line positions which included six forbidden hf lines for each orientation of the external magnetic field in the three mutually perpendicular planes zx, zy, and xy were simultaneously fitted in the LSF procedure. The matrix of the $\tilde{Q}$, so determined, was diagonalized to obtain the principal values of the $\tilde{Q}$ tensor as well as its direction cosines with respect to the principal axes of the $\tilde{g}^2$ tensor. There are eight forbidden hf transitions for $\Delta M=\pm1$; $\Delta m=\pm1,\pm2$, which are expected theoretically (here M and m are, respectively, the electronic and nuclear magnetic quantum numbers); however, only six forbidden transition lines are observed in the best-resolved EPR spectrum. At LHT, the allowed- and forbidden-line positions for any orientation of $\mathbf{B}$ were calculated using the SHP evaluated previously, so that the observed hf forbidden transition lines could be identified. The results indicate that the two remaining forbidden-transition lines, not clearly resolved, lie extremely close to the allowed hf lines as shown in Fig. 1. The principal values of the $\tilde{Q}$ tensor are included in Table I, while the direction cosines of its principal axes are included in Table II.

B. Powder EPR spectrum (4.2–354 K)

In order to study the temperature dependence of the g values the EPR spectra of the CAS polycrystalline specimen were recorded in the temperature range 4.2–354 K.

TABLE II. Direction cosines of the $\tilde{g}$, $\tilde{A}$ matrices (same as those the $\tilde{g}^2$ and $\tilde{A}^2$ tensors) and those of the $\tilde{Q}$ tensor for Cu^{2+} in the CAS single-crystal specimen at 4.2 K. The principal axes of the $\tilde{g}$ matrix are expressed with respect to the laboratory axes (x,y,z), defined in Sec. III A. The principal axes of the $\tilde{A}$ matrix are coincident with those of the $\tilde{g}$ matrix, and the principal axes of the $\tilde{Q}$ tensor are expressed relative to (x',y',z'), the principal axes of the $\tilde{g}$ matrix.

	z	x	y		z'	x'	y'
$g_{z'}, A_{z'}$	0.996	0.091	−0.022	$Q_{z'}$	0.970	0.242	0.032
$g_{x'}, A_{x'}$	−0.042	0.227	−0.973	$Q_{x'}$	−0.195	0.848	−0.493
$g_{y'}, A_{y'}$	−0.084	0.970	0.230	$Q_{y'}$	−0.147	0.472	0.869

Some of these are plotted in Fig. 2. As can be seen from Fig. 2, a single broad EPR line is observed at high temperatures which consists of three components, corresponding to the three principal values g_{zz}, g_{yy}, and g_{xx}, whereas at low temperatures, the components (corresponding to g_{zz}) lying at the highest values of the magnetic field exhibits the hf structure, while the hf structure corresponding to the other two components (g_{xx} and g_{yy}) is not resolved, even at 4.2 K. This is in accordance with the previously reported[1] spectrum of CAS, and different from the cases of Cu^{2+}-doped Zn Tutton salts where the three components of hf coupling were well resolved, even at temperatures slightly above 77 K.[2] This indicates that the Cu^{2+} spins have a rather strong interaction with the CAS lattice compared to that with the lattices of Zn Tutton salts.[1] The principal g values, as estimated for the polycrystalline CAS specimen at various temperatures, are plotted in Fig. 3.

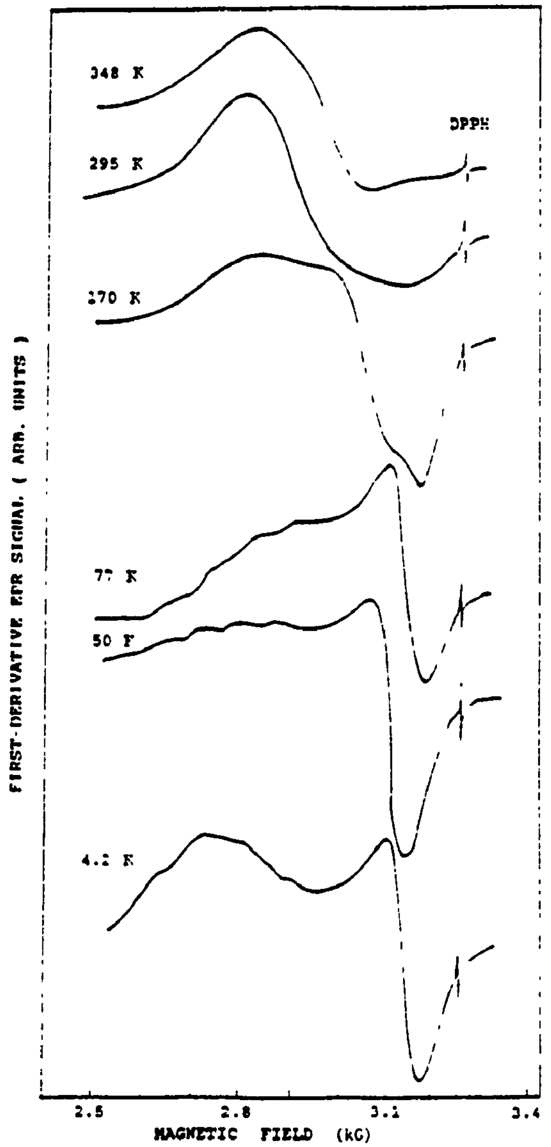

FIG. 2. Polycrystalline EPR spectra of Cu^{2+}-doped CAS at various temperatures.

The experimental data described above for either the single-crystal or polycrystalline specimen reveal the following features: (i) All the principal values of the Cu^{2+} $\tilde{g}$ and $\tilde{A}$ matrices ($g_{\alpha\alpha}$, $A_{\alpha\alpha}$; $\alpha=x, y, z$) are temperature dependent, except that g_{xx} does not change appreciably in the temperature range 4.2–77 K. The directions of the principal axes of the $\tilde{g}$ and $\tilde{A}$ matrices are coincident at all temperatures within the experimental error. (ii) The average of the principal values of the $\tilde{g}$ matrix at various temperatures is close to 2.2 which is equal to $(g_e - 4\lambda/\Delta)$, where g_e is the g value of the free electron $(=2.0023)$, λ $(=-830\ cm^{-1})$ (Ref. 11) is the spin-orbit coupling constant for the free Cu^{2+} ion, and Δ is the octahedral crystal-field-splitting constant for the Cu^{2+} ion $(\lambda/\Delta = -0.05)$.[11] (iii) The widths of EPR lines are temperature dependent.

IV. JAHN-TELLER EFFECT

The principal values of the $\tilde{g}$ matrix, being all different from each other over the temperature range 4.2–354 K as plotted in Fig. 3, indicate a low symmetry of the Cu^{2+} complex in the CAS lattice, namely, orthorhombically distorted octahedral symmetry. According to the crystal-field theory, the orbital doublet E_g of the Cu^{2+} ion is split in a field of orthorhombic symmetry. This splitting is sufficiently small to allow the mixing of the two substates of E_g by coupling with the lattice vibrations. The vibronic mixing of the close-lying (pseudodegenerate) levels due to the interaction of the Cu^{2+} ion with its lagands manifests itself in the pseudo Jahn-Teller (JT) effect.[12]

The molecular and electronic structure of the Cu^{2+} ion, surrounded by six identical ligands, is conventionally described in terms of JT coupling between the doubly degenerate electronic (E_g) and vibrational (ε_g) functions of the octahedral complex.[12] Assuming a harmonic-vibrational potential and taking into consideration only the linear coupling terms gives rise to the well-known Mexican-hat potential surface. The nuclear geometry fluctuates between the various conformations of D_{4h} and D_{2h} symmetries, which are generated by linear combinations of Q_θ and Q_ε, the components of the ε_g vibrational mode. Q_θ and Q_ε are conventionally expressed as $Q_\theta = \rho\cos\phi$ and $Q_\varepsilon = \rho\sin\phi$ in terms of a polar coordinate system (ρ,ϕ). When higher-order coupling terms are included, the perimeter of the Mexican-hat becomes warped giving rise to three equivalent minima whose projections correspond to different ϕ values in the $(Q_\theta, Q_\varepsilon)$ space. Equivalently, the Mexican-hat potential results in three equivalent potential valleys. Ham[13] pointed out that a strain, having a tetragonal component, displaces the energy of the three configurations with respect to each other, thereby destroying their equivalence. Comparing the Cu^{2+} principal g values at 295 K in the CAS lattice with those in the pure $Cu(NH_4)_2(SO_4)_2 \cdot 6H_2O$ lat-

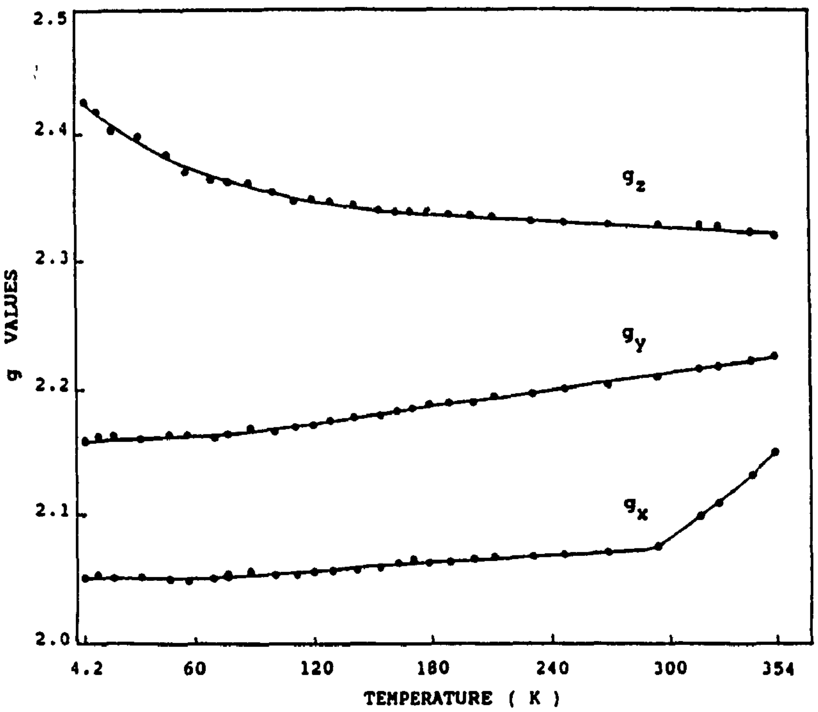

FIG. 3. Temperature variation of the principal g values of the Cu^{2+} in CAS. The values at 4.2, 77, and 295 K are those estimated from a single-crystal EPR lines, while those at other temperatures are estimated from line positions of a polycrystalline specimen.

tice at 300 K,[4] it is found that the two sets of g values are very close to each other. This indicates that the local symmetry of the Cu^{2+} ion in the CAS lattice is close to that of the Cu^{2+} ion in the pure $Cu(NH_4)_2(SO_4)_2 \cdot 6H_2O$ lattice rather than that of the Cd^{2+} ion, which the Cu^{2+} ion replaces in the pure CAS lattice. Thus, a large orthorhombic distortion of the lattice occurs when the impurity ion Cu^{2+} enters the CAS lattice substituting for a Cd^{2+} ion due to the difference in the ionic radii of the Cu^{2+} and Cd^{2+} ions and the paramagnetic nature of the Cu^{2+} ion. This orthorhombic distortion can be seen to be due to the three mutually perpendicular tetragonal components of the crystal field which perturb the three equivalent potential valleys resulting in three inequivalent potential valleys with different energy levels.

Silver and Getz[2] studied Cu^{2+}-doped Zn Tutton salts and proposed that when the JT effect is strong with appreciable warping and the overlap between the wave functions describing the potential valleys in the three different minima is rather small, the temperature dependent principal g and A values could be expressed as statistical averages using the occupation probabilities of the three minima which possess different energies under the assumption of short reorientation times which ensures Boltzmann population distributions. Petrashen *et al.*[4] expressed the expressions of the temperature-dependent principal g values as follows:

$$g_z(T)=\frac{N_1}{N}g_{z1}+\frac{N_2}{N}g_{y2}+\frac{N_3}{N}g_{x3}\,,$$

$$g_y(T)=\frac{N_1}{N}g_{y1}+\frac{N_2}{N}g_{z2}+\frac{N_3}{N}g_{y3}\,, \tag{2}$$

and

$$g_x(T)=\frac{N_1}{N}g_{x1}+\frac{N_2}{N}g_{x2}+\frac{N_3}{N}g_{z3}\,,$$

where the g_z, g_y, and g_x correspond to the Cd—O(7) (H_2O), Cd—O(8) (H_2O), and the Cd—O(9) (H_2O) directions, respectively, in the $Cd(H_2O)_6{}^{2+}$ complex. (The presently estimated principal values of the g matrix are related to $g_{\alpha k}$ as follows: $g_{z1}=g_{z'}$, $g_{y1}=g_{y'}$, $g_{x1}=g_{x'}$.) N_1, N_2, and N_3 are the populations of the first, second, and third potential valleys so that the total population $N=N_1+N_2+N_3$; $g_{\alpha k}$ ($\alpha=x, y, z$; $k=1, 2, 3$) are the principal values of the g matrix of the $Cu(H_2O)_6{}^{2+}$ complex in the kth valley; the $g_{\alpha k}$ sets in (2) are expressed according to the identification of the JT configurations with the minima of the adiabatic potential in the (Q_θ, Q_ϵ) space. (The subscript k indicates the relative order of the energies of the three minima of the potential valleys. $k=1$ indicates the lowest energy while $k=3$ indicates the highest energy of these minima.) It is necessary to know $g_{\alpha k}$ in order to estimate $g_\alpha(T)(\alpha=x, y, z)$. Generally speaking, $g_{\alpha k}$ values are different in different valleys. However, $g_{\alpha 1}$ values may be used in place of all the $g_{\alpha k}$, $(k=1, 2, 3)$ for the case of small deformations of the octahedron at 4.2 K for the $Cu(H_2O)_6^{2+}$ complex, since the complex is fully localized in the valley possessing the lowest minimum energy $(k=1)$ at and below 4.2 K.

$\delta_{1,2}$, the energy splitting between the potential valleys 1 and 2, has been calculated[2,4] for Zn-Tutton salt under the assumption that $N_3=0$ at temperatures below 300 K using the first two equations of (2). This is because the third equation of (2) yields $g_x(T)\approx g_{x1}\approx g_{x2}$ for this case. Thus, one has to use only the first two equations of (2), putting $N_3=0$ to estimate N_1 and N_2 which yield $\delta_{1,2}$, using a Boltzmann population distribution. As for estimating the value of $\delta_{1,3}$, the energy splitting between the potential valleys 1 and 3, Silver and Getz[2] took into account the increase in g_x at high temperatures while Petrashen *et al.*[4] estimated the value of $\delta_{1,3}/\delta_{1,2}$, using the bond lengths between the central diamagnetic ion and its ligands as determined from the x-ray data; they estimated the value of $\delta_{1,3}$ in terms of the value of $\delta_{1,2}$ using (2). The symmetry of the $Cd(H_2O)_6^{2+}$ complex in the CAS lattice is a distorted tetragonally compressed octahedron since the bond-length difference between Cd—O(7)(H_2O) and Cd—O(8)(H_2O) is very small (0.001 Å).[6] Thus, these two bond lengths can be assumed to be the same within experimental error (0.007 Å). According to Petrashen *et al.*[4] the value of $\delta_{1,3}/\delta_{1,2}$ could not be estimated from x-ray data in the present case. As for the present case, the same procedure can be followed as that for Zn-Tutton salt except that the g_x value does not here change below 77 K, as compared to the case of Zn-Tutton salt for which it does not change below 300 K. It implies that the potential valley 3 must lie considerably higher in energy than the valley 2 in the present case, and that the value of $\delta_{1,3}$ in the present case, i.e., for Cu^{2+} in CAS, must be less than that for Cu^{2+} in the Zn-Tutton salt.

In order to calculate the ratio of the populations, N_1/N_2, in the temperature range 4.2–77 K, only the first two equations in (2) have been used because the value of g_x does not change in this temperature range. At temperatures above 77 K, the three equations of (2) are taken into account since g_x is temperature dependent in this range. Finally, the N_1/N_2 and N_1/N_3 ratios, as estimated from (2), at 295 K are 3.6 and 5.0, respectively, which yield, using Boltzmann population distribution, i.e., $N_1/N_i=\exp(\delta_{1,i}/kT)$, the values of $\delta_{1,2}$ and $\delta_{1,3}$ to be 260 and 330 cm^{-1}, respectively, at 295 K.

Figure 4 exhibits the dependence of $\delta_{1,2}$ upon temperature in the range 4.2–295 K; it shows that $\delta_{1,2}$ increases, in general, with temperature, this increase being quite enhanced at lower temperatures while slow at intermediate temperatures, acquiring ultimately a steady value (around 260 cm^{-1}) at temperatures between about 212 and 295 K. The temperature dependence of the energy $\delta_{1,2}$ is due to the deformation of the crystal lattice with changing temperature,[14] as revealed by the change of g_x since N_3 is no longer zero in the present case at $T>77$ K.

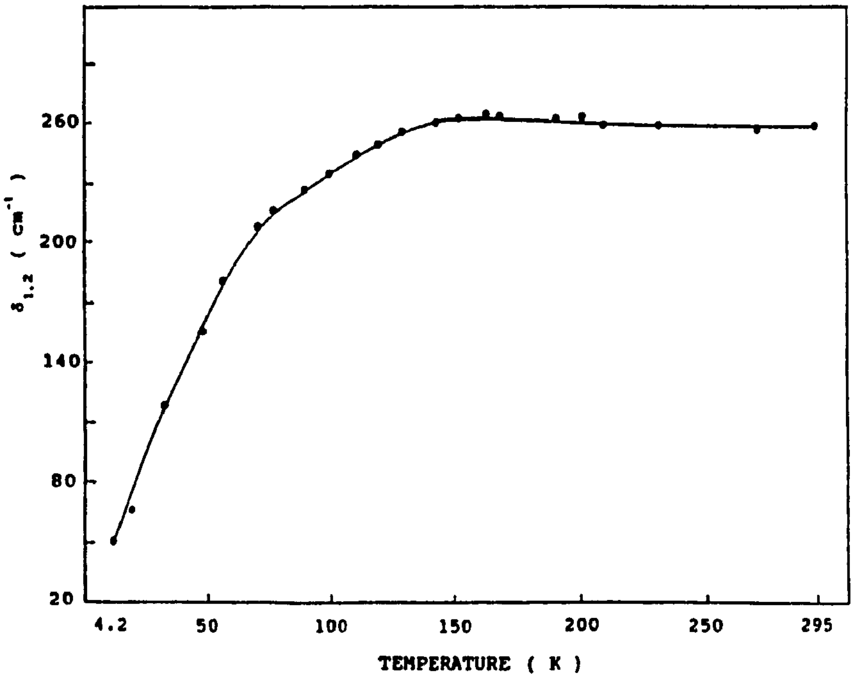

FIG. 4. Temperature dependence of the energy splitting between the lowest and the intermediate potential valleys ($\delta_{1,2}$) for the $Cu(H_2O)_6^{2+}$ complex in CAS.

V. CONCLUDING REMARKS

The main results of the present EPR study can be summarized as follows:

(i) The orthorhombic Cu^{2+} principal values of the $\tilde{g}^2$ and $\tilde{A}^2$ tensors in the temperature range 4.2–354 K indicate that the local symmetry at a Cd^{2+} site, i.e., tetragonal-compressed octahedral symmetry, in the undoped CAS lattice suffers an orthorhombic distortion when the Cu^{2+} ion enters the CAS lattice.

(ii) Forbidden hf transitions were observed in the Cu^{2+} EPR spectrum in the single-crystal CAS specimen at 4.2 K. The quadrupole interaction matrix $\tilde{Q}$ was estimated from their line positions.

(iii) The present study of both the single-crystal and polycrystalline specimens over the temperature range 4.2–354 K provided the temperature dependence of the principal components of the $\tilde{g}$ matrix. The variation of their values was interpreted to be due to the pseudo JT effect experienced by the $Cu(H_2O)_6^{2+}$ complex in the CAS single-crystal lattice. The ratio of the energy splittings between the three adiabatic potential valleys ($\delta_{1,2}$ and $\delta_{1,3}$) have been estimated from the temperature dependence of the principal values of the $\tilde{g}$ matrix.

ACKNOWLEDGMENTS

The authors are grateful to the Natural Sciences and Engineering Research Council of Canada for financial support (Grant No. A4485), and to the Concordia University Computer Centre for providing their facilities to analyze the data.

---

[1] N. Satyanarayana, Mol. Phys. **55**, 111 (1985).
[2] B. L. Silver and D. Getz, J. Chem. Phys. **61**, 638 (1974).
[3] D. Getz and B. L. Silver, J. Chem. Phys. **61**, 630 (1974).
[4] V. E. Petrashen, Yu. V. Yablokov, and R. L. Davidovich, Phys. Status Solidi B **101**, 117 (1980).
[5] S. K. Misra and C. Wang, J. Phys.: Condens. Matter **1**, 771 (1989).
[6] H. Montgomery and E. C. Lingafelter, Acta. Crystallogr. **20**, 728 (1966).
[7] S. K. Misra, Magn. Reson. Rev. **10**, 289 (1986).
[8] S. K. Misra, Arab. J. Sci. & Eng. **13**, 255 (1988).
[9] S. K. Misra, Physica B **151**, 433 (1988).
[10] S. K. Misra and Changlu Wang, Phys. Rev. B **39**, 8832 (1989).
[11] A. Abragam and B. Bleaney, *Electron Paramagnetic Resonance of Transition Ions* (Oxford, Clarendon, 1970).
[12] I. B. Bersuker and V. Z. Polinger, in *The Dynamical Jahn-Teller Effect in Localized Systems*, (North-Holland, Amsterdam, 1984).
[13] F. S. Ham, in *Electron Paramagnetic Resonance*, edited by S. Geschwind (Plenum, New York, 1972), p. 27.
[14] V. E. Petrashen, Yu. V. Yablokov, and R. L. Davidovich, Phys. Status Solidi B **78**, K69 (1976).

APPENDIX II

COMPUTER PROGRAMS

This appendix contains the computer programs for estimation of (i) the six independent of the $\tilde{g}^2$ tensor from the fine-structure line positions, (ii) the six independent components of $\tilde{A}^2$ tensor from the h.f. line positions, using the $\tilde{g}^2$ components as initial values as obtained from (i), (iii) the twelve independent components of the $\tilde{g}^2$ and $\tilde{A}^2$ tensors from the h.f. line positions, and (iv) the five independen components of the $\tilde{Q}$ tensor.

```
      PROGRAM CUG (INPUT,OUTPUT,TAPE5=INPUT,TAPE6=OUTPUT)
C     NO =THE NO. OF FIRST MAG FIELD
C         IN DATA INCLUDED IN FITTING
C     M  =NO. OF PARAMETERS
C     L4 =NO. OF ITERATIONS ALLOWED
C     LL5=PARAMETER WHICH TELLS
C         COMPUTATIONS OF SMD OF INDIVIDUAL LINES
C               :WTIH L4 ITERATIONS IF LL5=0
C               :WITHOUT ANY ITERATIONS IF LL5=1
C     Q1 =MIN. VALUE OF SUM OF SQUARES FOR FITS
C         (CHI-SQUARE TOLERANCE)
C     Z(I)=MAGNETIC FIELD VALUES FOR FITS
C     B  =PARAMETER MATRIX
C     N  =NO. OF DATA POINTS USED IN LEAST-SQARES FITTING
C     Q1 =N/10
C     Q2 =TOLERANCE ON GRAD(CHI**2) =APPROX .01
C     FM(I) = MEASURED VALUES
C     FC(I) = CALCULATED VALUES
C     ERR(I)= STANDARD DEVIATION ON FM(I) = SQRT(FM(I))
C
C      DIMENSIONS OF A,B IN EXAM AND MATINV SUBROUTINES
C     SHOULD BE THE SAME AS THOSE OF B2,B1 RESPECTIVELY IN
C     THE MAIN PROOGRAM AND IN CURFIT
C
C      DIMENSIONS OF Q,V IN JACOBI1 SHOULD BE THE SAME AS
C     THOSE OF B3,B2 RESPECTIVELY IN CURFIT
C
C     NUMBER=INDEX THAT CHANGES WITH EACH NEW CASE
C     NCASES=NO. OF CASES CONSIDERED.
C            ITS VALUE SHOULD BE ENTERED.
C
C     KILL=0 THE SAME CASE IS COMPUTED COMPLETELY
C         =1 THE CASE IS DROPPED AND MOVED TO NEXT ONE
C            (NEGATIVE SQUARE ROOT ENCOUNTERED)
C
C
```

```
C      THIS PROGRAM ANALYSES KRAMER*S DOUBLETS DATA,
C                   SPECIAL FOR CU2+
C      B(1)-B(6)=G-SQUARE COMPONENTS-(ZZ,ZX,XX,ZY,YY,XY)
C        B(7),B(8),B(9) ARE MISORIENTATION ANGLES IN
C        ZX,ZY,XY PLANES, ENTERED IN DEGREES.
C
       DIMENSION Z(200),FM(200),FC(200),DF(200),ERR(200),
      1B(13),B1(13),B2(13,13),DC(3500),ABC(2),Y(4),
      2THETA(200),HN(200),ZZ(200,20), HHDPPH(200,20),NN(25),
      3GG(13,20),SMD(20),IBB(200,2),SSMD(200),TEETA(200,20),
      4G(13,20),GSQRT(3),DELHH(200,20),DELH(200)
       DIMENSION AG(3,3),AAG(6),E(40),VR(3,3),VI(3,3),
      1FREQ(20),FACTOR(20),ADD(20),NZERO(1),NCASES(1),
      2LZX(1),LZY(1),LXY(1)
       DIMENSION FFREQ(200,20),AADD(200,20),
      1FFACTR(200,20),BG(9)
       DIMENSION VG2(3),VB(3,3),VG(3),VG2R2(3),
      1VGR2(3),D(3),WK(50)
       COMMON/DATA1/ABC,Y
       COMMON/DATA2/DC
       COMMON/DATA3/DELH
       EQUIVALENCE(Z,DC),(FM,DC(201)),(DF,DC(401)),
      1(FC,DC(601)),(ERR,DC(801)),(THETA,DC(1001)),
      2(HN,DC(1201)),(B,DC(2500)),(B2,DC(2600)),
      3(N,DC(1575)),(L4,DC(1576)),(Q1,DC(1577)),
      4(Q2,DC(1578)),(M,DC(1579)),(I,DC(1580)),
      5(L,DC(1581)),(B1,DC(2550)),(IBB,DC(2000)),
      6(SMD,DC(1989)),(NUMBER,DC(1988))
C
C*****  ANGLES IN ZX PLANE ARE ENTERED TO BE BETWEEN 0 AND
C     360 (2.*PI), THOSE IN THE ZY PLANE ARE ENTERED TO BE
C     NEGATIVE,I.E. BETWEEN LESS THAN 0 AND -360 (2.*PI),
C     THOSE IN THE XY PLANE ARE ENTERED BY FIRST CONVERTING
C     TO BE BETWEEN 0 AND 360 (2.*PI) AND THEN ADDING 9000
C     TO THEM (EXAMPLE: IN THE XY PLANE THE ANGLE -5 DEG
C     FROM X IN XY PLAN IS FIRST CONVERTED TO 355 DEG AND
```

```
C    THEN ENTERED AS 9355.)
C
      READ(5,*) NZERO,NCASES,LZX,LZY,LXY
      WRITE(6,5123) NZERO,NCASES,LZX,LZY,LXY
 5123 FORMAT(1X, 6HNZERO=,I8, 7NCASES=,I8,
     14HLZX=,I8, 4HLZY=,I8, 4HLXY=,I8)
      READ(5,*)(ZZ(J,NCASES),J=1,LZX)
      READ(5,*)(TEETA(J,NCASES),J=1,LZX)
      II=LZX+1
      NII=LZX+LZY
      READ(5,*)(ZZ(J,NCASES),J=II,NII)
      READ(5,*)(TEETA(J,NCASES),J=II,NII)
      II=II+LZY
      NII=NII+LXY
      READ(5,*)(ZZ(J,NCASES),J=II,NII)
      READ(5,*)(TEETA(J,NCASES),J=II,NII)
      NN(NCASES)=NII
      READ(5,*)(FFREQ(J,NCASES),J=1,NII)
      READ(5,*)(DELHH(J,NCASES),J=1,NII)
      READ(5,*)(AADD(J,NCASES),J=1,NII)
      READ(5,*)(FFACTR(J,NCASES),J=1,NII)
      READ(5,*)(G(J,NCASES),J=1,6)
  188 FORMAT(1H1)
    8 FORMAT(1X,4HQ1 = ,E13.5,5X,4HQ2 = ,E13.5)
  137 FORMAT(3X,I2,5X,E16.6/)
  136 FORMAT(10X,* INITIAL PARAME
     1TERS*,//3X,*J*,10X,*B(J)*//)
  135 FORMAT(1X,11H PARAME
     1TERS,//3X,1HJ,10X,4HB(J),27X,6HERRORS//)
    9 FORMAT(2X,*HN=*,10(F9.4,4X))
  140 FORMAT(3X,I2,5X,E16.6,15X,E16.6/)
  138 FORMAT(5X,14H CASE NUMBER =,I2//)
  141 FORMAT(10X,6H SMD =,E13.5//)
  235 FORMAT (15X,5(E13.5,8X)/)
C
  144 FORMAT(5X,*LINE NUMBER*,5X,*LINE POSI
```

```
    1TION*,7X,*ANGLE*,/)
145 FORMAT(6X,I3,9X,F10.1,11X,F8.2)
    RD=3.1415926/180.
    NUMBER=1
    NCASES=1
    NUMBII=NUMBER
    Q1 =1.E-8
    Q2 =1.E-20
    WRITE (6,188)
  1 CONTINUE
    M=6
    MM=M
    L4=5
    N=NN(NUMBER)
    DO 209 LL=1,9
209 B(LL)=0.
    DO 210 LL=1,MM
210 B(LL)=G(LL,NUMBER)
    WRITE (6,138) NUMBER
    WRITE (6,136)
    WRITE (6,137) (J,B(J),J=1,M)
    N1=N
    DO 3 IJK = 1,N1
    HN(IJK)=FFREQ(IJK,NUMBER)
    THETA(IJK)=TEETA(IJK,NUMBER)
    Z(IJK)=ZZ(IJK,NUMBER)*FFACTR(IJK,NUMBER)+
   1 AADD(IJK,NUMBER)
    DELH(IJK)=DELHH(IJK,NUMBER)
  3 CONTINUE
    WRITE(6,144)
    DO 146 IJK=1,N1
146 WRITE(6,145) IJK,Z(IJK),THETA(IJK)
    WRITE(6,8)Q1,Q2
    WRITE(6,9)  (HN(J),J=1,N1)
    DO 201 J = 1,N1
201 FM(J)=HN(J)
```

```
      CALL CURFIT
      WRITE(6,188)
      WRITE(6,135)
      DO 220 LL=1,M
  220 GG(LL,NUMBER) = B(LL)
      WRITE(6,140)(J,B(J),B1(J),J=1,M)
      SSS=0.
C     SSS1 IS SMD(1),THAT IS WHEN ALL (LINES) SIGMA=1
      SSS1=0
      WRITE(6,11140) N1,N
11140 FORMAT(*N1=*,I3,*N=*,I3)
      DO 555 ID=1,N1
      SSS=DF(ID)**2
      SSS2=DF(ID)**2/(ERR(ID)**2)
      SSS1=SSS1+SSS
      WRITE(6,656) ID,SSS,Z(ID),SSS2
 555  CONTINUE
      WRITE(6,657)SSS1
  657 FORMAT(10X,*SMD(1)*,E13.5,//)
  656 FORMAT(10X,*LINE NUMBER = *,I2,5X,*SMD(1) = *,
     1E13.5,*     MAG. FIELD VALUE = *,E13.5,*SMD=*,E13.5)
  301 FORMAT(10X,*FREQUENCY NO. = *,I3,5X,*EIGEN
     1VALUE1 =*,I3,5X,* EIGENVALUE 2 =*,I3)
      WRITE(6,188)
      AG(1,1)=B(1)
      AG(1,2)=B(2)
      AG(1,3)=B(4)
      AG(2,2)=B(3)
      AG(2,3)=B(6)
      AG(3,3)=B(5)
      AG(2,1)=AG(1,2)
      AG(3,1)=AG(1,3)
      AG(3,2)=AG(2,3)
C      CALL SVLVC1(AG,50,50,E,40,VR,30,40,3,ITER)
      CALL JACOBI (3,AG,1,NR,VR)
  995 FORMAT (5X,I4)
```

```
  996 CONTINUE
      WRITE(6,998)
  998 FORMAT(5X,*EIGENVALUES OF G-SQUARE -TENSOR ARE:*,/)
      WRITE(6,888) (AG(II,II),II=1,3)
      DO 23 J6=1,3
      IF(AG(J6,J6).LT.(0.)) GO TO 24
      GSQRT(J6)=SQRT(AG(J6,J6))
      WRITE(6,26) J6,GSQRT(J6)
      GO TO 23
   24 WRITE(6,25) NUMBER,J6
   23 CONTINUE
   25 FORMAT(5X,*CASE NO.=*,I3,* EIGEN
     1VALUE *,I2,* OF G-SQUARE TENSOR IS NEGATIVE*)
   26 FORMAT(5X,*EIGENVALUE *,I2,* OF G-TENSOR IS =*,E16.6)
      WRITE(6,887)
  887 FORMAT(5X,*EIGENVECTORS OF G-SQUARE -TENSOR ARE:*,/)
  888 FORMAT(5X,3(E16.6,5X),/)
      DO 885 II=1,3
  885 WRITE(6,888)(VR(JJ,II),JJ=1,3)
      VB(1,1)=B1(1)
      VB(1,2)=B1(2)
      VB(1,3)=B1(4)
      VB(2,2)=B1(3)
      VB(3,3)=B1(5)
      VB(2,3)=B1(6)
      VB(3,2)=VB(2,3)
      VB(2,1)=VB(1,2)
      VB(3,1)=VB(1,3)
C     FOLLOWING CALCULATES VARIANCES
C     VARIANCE OF G-SQUARE COMPONENTS
      WRITE(6,38)
   38 FORMAT(5X,*VARIANCES OF G-SQUARE COMPONENTSARE=*,//)
      DO 31 K=1,3
      VG2(K)=0.
      DO 31 II=1,3
      DO 31 JJ=1,3
```

```
      VG2(K)=VG2(K)+(VB(II,JJ)*VR(II,K)*VR(JJ,K))**2
      VG2R2(K)=SQRT(VG2(K))
   31 CONTINUE
      WRITE(6,32)VG2
   32 FORMAT(5X,*VG2(1)=*,E16.6,2X,*VG2(2)=*,E16.6,2X,
     1*VG2(3)=*,E16.6,//)
      WRITE(6,39)
   39 FORMAT(5X,*STANDARD DEVIATIONS OF G-SQUARE
     1TENSOR COMPONENTS ARE=*,//)
      WRITE(6,40)VG2R2
   40 FORMAT(5X,*VG2R2(1)=*,E16.6,2X,
     1*VG2R2(2)=*,E16.6,2X,
     2*VG2R2(3)=*,E16.6,//)
C     VARIANCE OF G-TENSOR COMPONENTS
      DO 33 K=1,3
      VG(K)=VG2(K)/(4.*AG(K,K))
      VGR2(K)=SQRT(VG(K))
   33 CONTINUE
      WRITE(6,35)
   35 FORMAT(5X,*VARIANCES OF G-TENSOR
     1COMPONENTS ARE=*,//)
      WRITE (6,34)VG
   34 FORMAT(5X,*VG(1)=*,E16.6,2X,*VG(2)=*,
     1E16.6,2X,*VG(3)=*,E16.6,//)
      WRITE(6,36)
   36 FORMAT(5X,*STANDARD DEVIATIONS OF
     1G-TENSOR COMPONENTS ARE=*,//)
      WRITE(6,37)VGR2
   37 FORMAT(5X,*VGR2(1)=*,E16.6,2X,*VGR2(2)=*,
     1E16.6,2X,*VGR2(3)=*,E16.6,//)
      WRITE(6,188)
      NUMBER=NUMBER+1
      IF ( NUMBER - NCASES) 1,1,2
    2 CONTINUE
      WRITE(6,188)
      DO 230 LL=NUMBII,NCASES
```

```
      WRITE (6,138) LL
      WRITE (6,141) SMD(LL)
  230 WRITE (6,235) (GG(LM,LL),LM=1,M)
      STOP
      END

      SUBROUTINE CURFIT
C
C     EXAM  HANDLES ALL MATRICES OF DIMENSIONS UPTO THE
C     DIMS.MM OF A,B,C THAT IS M IS LESS THAN OR EQUAL TO MM
C     (SAME IS TRUE OF MATINV AND JACOBI)
C
C
C         F O R T R A N  4
      DIMENSION Z(200),FM(200),FC(200),DF(200),ERR(200),
     1B(13),B1(13),DC(3500),ABC(2),Y(4),X(200),GRAD(13),
     2D1(13),D2(13,13),SMD(10),B3(50,50),B2(13,13)
      DIMENSION AI(13,13),W(40),ZR(13,13),ZI(13,13),FV1(13),
     1FM1(2,13),FV2(13)
      COMMON/DATA1/ABC,Y
      COMMON/DATA2/DC
      EQUIVALENCE (Z,DC),(FM,DC(201)),(DF,DC(401)),
     1(FC,DC(601)),(ERR,DC(801)),(B,DC(2500)),
     2(GRAD,DC(2513)),(B2,DC(2600)),(N,DC(1575)),
     3(L4,DC(1576)),(Q1,DC(1577)),(Q2,DC(1578)),
     4(M,DC(1579)),(I,DC(1580)),(L,DC(1581)),
     5(D1,DC(2800)),(D2,DC(2900)),
     6(SMD,DC(1989)),(NUMBER,DC(1988))
      EQUIVALENCE(B1,DC(2550)),(NZ,DC(2490))
      DATA(ABC=2HNO,3HYES),(Y=1H ,1HC,1H*,1HM)
C
      L1 = 0
      SA = 0.0
      MM = M
      DO 1000 J =1,MM
      B1(J)=0.0
```

```
     DO 1000 K = 1,MM
1000 B2(J,K)=0.0
     WRITE(6,901)
     NN = N
     DO 100 II = 1,NN
     I=II
     L=1
     CALL FUNC(2)
     X(II)=ERR(II)**2
901  FORMAT(5X,10H FUNC2,210   )
     DF(II) =FM(II) - FC(II)
     DO 101 J=1,MM
     B1(J)=B1(J)-(2.0*DF(II)*D1(J))/X(II)
     DO 101 K=1,MM
 101 B2(J,K)=B2(J,K)-(2.0*(DF(II)*D2(J,K)-
    1 D1(J)*D1(K)))/X(II)
     SA = SA + DF(II)**2/X(II)
 100 CONTINUE
     WRITE(6,901)
     GMOD=0.0
     DO 102 J=1,MM
 102 GMOD=GMOD+B1(J)**2
     WRITE(6,243)SA,GMOD
 243 FORMAT (1X,26H*INITIAL VALUE SUM OF SQ.=,E13.5,20X,
    117H*SQ MOD OF GRAD =,E13.5)
     WRITE(6,1751)
1751 FORMAT(14H0 DERIVATIVES-)
     WRITE(6,240)(B1(J),J=1,MM)
 240 FORMAT (15X,5(E13.5,8X)/)
     IF (SA - Q1) 110, 110, 200
 110 LE = 1
     GO TO 600
 200 S = 0.0
     GMOD = 0.0
     BMOD = 0.0
     PROD = 0.0
```

```
      A2=ABC(1)
      DO 210 J =1,MM
      B1(J) = 0.0
      DO 210 K=1,MM
  210 B2(J,K) = 0.0
      WRITE(6,902)
      DO 220 II=1,NN
      I=II
      L=1
      CALL FUNC(2)
      X(II)=ERR(II)**2
 902  FORMAT(5X,10H FUNC2,210  )
      DF(II) = FM(II) - FC(II)
      DO 221 J=1,MM
      B1(J) = B1(J) - (2.0*DF(II)*D1(J))/X(II)
      DO 221 K =1,MM
  221 B2(J,K) = B2(J,K) - (2.0*(DF(II)*D2(J,K) -
     1 D1(J)*D1(K)))/X(II)
  220 CONTINUE
      WRITE(6,902)
      DO 230 J=1,MM
  230 GRAD(J) = B1(J)
      L1 = L1 + 1
      WRITE(6,903)
      CALL EXAM (B2,B1,MM,LF)
      WRITE(6,903)
 903  FORMAT(5X,9H EXAM,230  )
      IF (LF)  250, 250, 305
  250 DO 231 II=1,MM
      DO 231 JJ=1,MM
      AI(II,JJ)=0.
  231 B3(II,JJ)=B2(II,JJ)
      WRITE(6,904)
C      CALL SVLVC1(B3,50,50,W,40,ZR,30,40,13,ITER)
      CALL JACOBI1(13,B3,1,NR,ZR)
      DO 5005 IR=1,MM
```

```
      DO 5005 JR=1,MM
 5005 B2(IR,JR)=ZR(JR,JR)
      WRITE(6,904)
 904  FORMAT(5X,12H JACOBI1,231  )
      DO 235 K =1,MM
  235 B1(K)=B3(K,K)
      A2=ABC(2)
      DO 260 J=1,MM
  260 D1(J) = 0.0
      DO 270 J=1,MM
      DO 270 K=1,MM
  270 D1(K) = D1(K) + B2(J,K) *GRAD(J)
      DO 275 J = 1, MM
      IF (B1(J))  280, 290, 285
  280 B1(J) = - B1(J)
  285 D1(J) = D1(J)/B1(J)
      GO TO 275
  290 D1(J) = 0.0
  275 CONTINUE
      DO 295 J=1,MM
  295 B1(J) = 0.0
      DO 300 J=1,MM
      DO 300 K=1,MM
  300 B1(J) = B1(J) + B2(J,K)*D1(K)
  305 DO 310 J=1,MM
      GMOD = GMOD + GRAD(J)**2
      BMOD = BMOD + B1(J)**2
  310 PROD = PROD + GRAD(J)*B1(J)
      IF (GMOD - Q2)  315, 315, 320
  315 LE = 2
      WRITE(6,1761) GMOD
 1761 FORMAT(5X,7H GMOD =,E13.5//)
      GO TO 600
  320 C=PROD/SQRT(BMOD*GMOD)
      IF (C) 335, 335, 400
  335 LE = 4
```

```
      GO TO 600
  400 LD = 0
      L3 = 0
      DO 410 J=1,MM
  410 GRAD(J) = B(J) - B1(J)
      WRITE(6,905)
  450 DO 420 II=1,NN
      I=II
      L=2
      CALL FUNC (1)
      X(II)=ERR(II)**2
 905  FORMAT(5X,10H FUNC1,450   )
      DF(II) = FM(II) - FC(II)
      S = S + DF(II)**2/X(II)
  420 CONTINUE
      IF (SA - S) 435, 500, 500
  435 LD = LD + 1
  430 DO 440 J=1,MM
      B1(J) = B1(J)/2.0
 906  FORMAT(5X,16H BINARY CHOP,430   )
  440 GRAD(J) = B(J) - B1(J)
      S = 0.0
      L3 = L3 + 1
      IF (L3-150)450,460,460
  460 LE = 5
      GO TO 600
  500 IF (LD) 505, 505, 506
  506 LD = 0
      GO TO 430
  505 DO 510 J=1,MM
  510 B(J) = GRAD(J)
      SA = S
      IF (SA - Q1) 507, 507, 530
  507 LE = 1
      GO TO 600
  530 IF (L4) 200, 200, 900
```

```
 900 WRITE(6,920)L1,IA2,L3,S,GMOD,(B(J),J=1,MM)
 920 FORMAT(//,15H ITERATION NO.=,I5,10X,*   TRANSFORMA
    1TION MADE TO PRINCIPAL AXES = *,A4,10X,   18H BI
    2NARY CHOP USED=,I3,6H TIMES/1X,* WEIGHTED SUM OF SQ
    3UARES = *,E14.7,25X,*   SQUARE MODULUS OF GRADIEN
    4T = *,E14.7,/20H   PARAMETERS B(J)  ,/(6E17.8)/)
     IF (L1 - L4) 200, 910, 910
 910 LE = 6
     GO TO 600
 600 DO 710 J=1,MM
     B1(J) = 0.0
     DO 710 K=1,MM
 710 B2(J,K) = 0.0
     L=1
     DO 721 II=1,NN
     I=II
     CALL FUNC(2)
     X(II)=ERR(II)**2
     DF(II) = FM(II) - FC(II)
     DO 720 J=1,MM
     B1(J) = B1(J) - (2.0*DF(II)*D1(J))/X(II)
     DO 720 K=1,MM
 720 B2(J,K) = B2(J,K) - ((DF(II)*D2(J,K) -
    1 D1(J)*D1(K)))/X(II)
 721 CONTINUE
     CALL MATINV(B2,MM,B1,1,DETERM)
     DO 730 J=1,MM
     IF (B2(J,J)) 2001,2001,2002
2001 B1(J) = -SQRT(-B2(J,J))
     GO TO 730
2002 B1(J) = SQRT(B2(J,J))
 730 CONTINUE
     DO 740 J=1,MM
     DO 740 K=1,MM
 740 B2(J,K)=B2(J,K)/(B1(J)*B1(K))
     WRITE(6,551)LE,SA
```

```
  551 FORMAT(//,* EXIT NUMBER=*,I3,20X,* WEIGHT
     1ED SUM OF SQUARES=*,E15.8//)
      SMD(NUMBER)=SA
      GO TO 105
  103 CONTINUE
      SMD(NUMBER)=SA
      WRITE(6,104)
  104 FORMAT(/,5X,*LL5=1,SO NO ITERATIONS DONE*,/)
  105 CONTINUE
      RETURN
      END
      SUBROUTINE FUNC(LX)
C     SUBROUTINE FUNC
      DIMENSION DC(3500),B(13,2),D1(13),FC(200),Z(200),
     1HN(200),S(2,2),R(2,2),SIGN(200),THETA(200),
     2IBB(200,2),D2(13,13),ERR(200)
      DIMENSION AR(2,2),AI(2,2),W(2),ZR(2,2),ZI(2,2),FV1(2),
     1FM1(2,2),SZ(2,2),SX(2,2),SY(2,2),
     2SR(2,2),SI(2,2),FV2(2),BG(9)
      DIMENSION DELH(200)
      COMMON/DATA2/DC
      COMMON/DATA3/DELH
      EQUIVALENCE (Z,DC),(FC,DC(601)),(THETA,DC(1001)),
     1(B,DC(2500)),(D1,DC(2800)),(D2,DC(2900)),
     2(M,DC(1579)),(I,DC(1580)),(L,DC(1581)),(HN,DC(1201)),
     3(IBB,DC(2000)),(N,DC(1575)),(NZ,DC(2490)),
     4(NUMBER ,DC(1988)),(ERR,DC(801))
      FACTOR=92.732/66252.
      RD=3.1415926/180.
      PI2=2.*3.1415926
      B(7,L)=0.
      B(8,L)=0.
      B(9,L)=0.
  130 CONTINUE
  131 CONTINUE
      IF(THETA(I).GT.720.) GO TO 10
```

```
      IF(THETA(I).LT.(0.)) GO TO 13
      ALZ=COS((THETA(I)+B(7,L))*RD)
      ALX=SIN((THETA(I)+B(7,L))*RD)
      ALY=0.
      GO TO 14
   13 CONTINUE
      ALZ=COS((-THETA(I)+B(8,L))*RD)
      ALX=0.
      ALY=SIN((-THETA(I)+B(8,L))*RD)
   14 CONTINUE
      GO TO 15
   10 CONTINUE
      ALZ=0.
      ALX=COS((THETA(I)+B(9,L))*RD)
      ALY=SIN((THETA(I)+B(9,L))*RD)
   15 CONTINUE
  132 CONTINUE
  139 FORMAT(5X,3(E16.6,5X),/)
      IF(Z(I).NE.(0.)) GO TO 135
      FC(I)=HN(I)
      GO TO 134
  135 CONTINUE
      FCI=(B(1,L)*ALZ*ALZ+
     1 2.*B(2,L)*ALZ*ALX+B(3,L)*ALX*ALX+2.*B(4,L)*ALZ*ALY+
     2 B(5,L)*ALY*ALY+2.*B(6,L)*ALX*ALY)
C     FOLLOWING FOR NEGATIVE FCI
      IF(FCI.GT.(0.).OR.FCI.EQ.(0.)) GO TO 192
      DO 193 JJ=1,9
  193 BC(JJ)=B(JJ,L)
      KILL=1
      WRITE(6,190) I
      WRITE(6,191) (B(JJ,L),JJ=1,9)
      LL6=I
      GO TO 110
  190 FORMAT(/,5X,*NEGATIVE FCI FOR LINE NO. =*,I3,/)
  191 FORMAT(5X,6E12.6,/)
```

```
 192 CONTINUE
     FC(I)=Z(I)*FACTOR*SQRT(FCI)
     ERR(I)=SQRT(FCI)*DELH(I)*FACTOR
 134 CONTINUE
     IF(LX-1) 110,110,121
 121 CONTINUE
     IF(Z(I).EQ.(0.)) GO TO 915
     DO 235 IZ=1,13
     D1(IZ) = 0.0
     DO 235 JZ=1,13
 235 D2(IZ,JZ) =0.0
 133 CONTINUE
     F=2.*FC(I)/((Z(I)*FACTOR)**2)
     FF=2.*RD/F
     D1(1)=ALZ**2/F
     D1(2)=2.*ALZ*ALX/F
     D1(3)=ALX**2/F
     D1(4)=2.*ALZ*ALY/F
     D1(5)=ALY**2/F
     D1(6)=2.*ALX*ALY/F
     D1(7)=0.
     D1(8)=0.
     D1(9)=0.
     IF(THETA(I).GT.(720.)) GO TO 910
     IF(THETA(I).LT.(0.)) GO TO 913
     ANG7=(THETA(I)+B(7,L))*RD
     D1(7)=FF*(B(1,L)*ALZ*(-SIN(ANG7))+B(2,L)*(ALX*
    1 (-SIN(ANG7))+ALZ*COS(ANG7))+B(3,L)*ALX*COS(ANG7))
     GO TO 914
 913 CONTINUE
     ANG8=(-THETA(I)+B(8,L))*RD
     D1(8)=FF*(B(1,L)*ALZ*(-SIN(ANG8))+B(4,L)*(ALY*
    1 (-SIN(ANG8))+ALZ*COS(ANG8))+B(5,L)*ALY*COS(ANG8))
 914 CONTINUE
     GO TO 915
 910 CONTINUE
```

```
      ANG9=(THETA(I)+B(9,L))*RD
      D1(9)=FF*(B(3,L)*ALX*(-SIN(ANG9))+B(6,L)*(ALY*
     1 (-SIN(ANG9))+ALX*COS(ANG9))+B(5,L)*ALY*COS(ANG9))
  915 CONTINUE
  110 CONTINUE
      RETURN
      END
      SUBROUTINE EXAM(A,B,M,LF)
C     SUBROUTINE EXAM
C       F O R T R A N  4
      DIMENSION A(13,13),B(13),C(13)
      DO 80 J=1,M
   80 C(J)=A(J,J)
      IF(A(1,1)) 60,200,70
   60 A(1,1) =-SQRT(-A(1,1))
      GO TO 300
   70 A(1,1) =SQRT(A(1,1))
      GO TO 100
  100 IF(M-1)400,400,110
  110 DO 115 K=2,M
  115 A(1,K)=A(1,K)/(A(1,1)        )
      DO 120 J=2,M
      J1=J-1
      S=A(J,J)
      DO 125 L=1,J1
  125 S=S-A(L,J)**2
      IF (S) 50,200,40
   50 A(J,J) =-SQRT(-S)
      GO TO 300
   40 A(J,J) =SQRT(S)
      GO TO 130
  130 IF(J-M)135,400,400
  135 J2=J+1
      DO 120 K=J2,M
      S=A(J,K)
      DO 145 L=1,J1
```

```
  145 S=S-A(L,J)*A(L,K)
  120 A(J,K)=S/A(J,J)
  400 B(1)=B(1)/A(1,1)
      IF(M-1)420,420,405
  405 DO 410 J=2,M
      S=B(J)
      J1=J-1
      DO 415 L=1,J1
  415 S=S-A(L,J)*B(L)
  410 B(J)=S/A(J,J)
  420 B(M)=B(M)/A(M,M)
      J=M-1
  435 IF(J)450,450,425
  425 S=B(J)
      J2=J+1
      DO 430 L=J2,M
  430 S=S-A(J,L)*B(L)
      B(J)=S/A(J,J)
      J=J-1
      GO TO 435
  450 LF=1
      GO TO 460
  200 LF=0
      GO TO 460
  300 LF=-1
  460 DO 465 J=1,M
      A(J,J)=C(J)
      IF(J-M)470,475,475
  470 J2=J+1
      DO 465 K=J2,M
  465 A(J,K)=A(K,J)
  475 RETURN
      END
      SUBROUTINE MATINV(A,N,B,M,DETERM)
C     SUBROUTINE MATINV
C       F O R T R A N  4
```

```
C     MATRIX INVERSION WITH ACCOMPANYING
C            SOLUTION OF LINEAR EQUATIONS
      DIMENSION IPIVOT(13),A(13,13),B(13,1),
     1 INDEX(13,2),PIVOT(13)
      EQUIVALENCE (IROW,JROW),(ICOLUM,JCOLUM),
     1 (AMAX,T,SWAP)
      DETERM=1.0
      DO 20 J=1,N
   20 IPIVOT(J)=0
      DO 550 I=1,N
      AMAX=0.0
      DO 105 J=1,N
      IF(IPIVOT(J)-1)60,105,60
   60 DO 100 K=1,N
      IF(IPIVOT(K)-1)80,100,740
   80 IF(ABS(AMAX)-ABS(A(J,K)))85,100,100
   85 IROW=J
      ICOLUM=K
      AMAX=A(J,K)
  100 CONTINUE
  105 CONTINUE
      IPIVOT(ICOLUM)=IPIVOT(ICOLUM)+1
      IF (IROW-ICOLUM)140,260,140
  140 DETERM=-DETERM
      DO 200 L=1,N
      SWAP=A(IROW,L)
      A(IROW,L)=A(ICOLUM,L)
  200 A(ICOLUM,L)=SWAP
      IF(M)260,260,210
  210 DO 250 L=1,M
      SWAP=B(IROW,L)
      B(IROW,L)=B(ICOLUM,L)
  250 B(ICOLUM,L)=SWAP
  260 INDEX(I,1)=IROW
      INDEX(I,2)=ICOLUM
      PIVOT(I)=A(ICOLUM,ICOLUM)
```

```
      DETERM=DETERM*PIVOT(I)
      A(ICOLUM,ICOLUM)=1.0
      DO 350 L=1,N
  350 A(ICOLUM,L)=A(ICOLUM,L)/PIVOT(I)
      IF(M)380,380,360
  360 DO 370 L=1,M
  370 B(ICOLUM,L)=B(ICOLUM,L)/PIVOT(I)
  380 DO 550 L1=1,N
      IF (L1-ICOLUM)400,550,400
  400 T=A(L1,ICOLUM)
      A(L1,ICOLUM)=0.0
      DO 450 L=1,N
  450 A(L1,L)=A(L1,L)-A(ICOLUM,L)*T
      IF(M)550,550,460
  460 DO 500 L=1,M
  500 B(L1,L)=B(L1,L)-B(ICOLUM,L)*T
  550 CONTINUE
      DO 710 I=1,N
      L=N+1-I
      IF(INDEX(L,1)-INDEX(L,2))630,710,630
  630 JROW=INDEX(L,1)
      JCOLUM=INDEX(L,2)
      DO 705 K=1,N
      SWAP=A(K,JROW)
      A(K,JROW)=A(K,JCOLUM)
      A(K,JCOLUM)=SWAP
  705 CONTINUE
  710 CONTINUE
  740 RETURN
      END
      SUBROUTINE JACOBI1(N,Q,JVEC,M,V)
C     SUBPROGRAM FOR DIAGONALIZATION OF
C                MATRIX Q BY SUCCESSIVE ROTATIONS
      DIMENSION Q(13,13),V(13,13),X(13),IH(13)
C
C     NEXT 8 STATEMENTS FOR SETTING
```

```
C           INITIAL VALUES OF MATRIX V
C
      IF(JVEC) 10,15,10
   10 DO 14 I=1,N
      DO 14 J=1,N
      IF(I-J) 12,11,12
   11 V(I,J)=1.0
      GO TO 14
   12 V(I,J)=0.
   14 CONTINUE
C
   15 M=0
C     NEXT 8 STATEMENTS SCAN FOR
C            LARGEST OFF DIAG. ELEM. IN EACH ROW
C     X(I) CONTAINS LARGEST ELEMENT IN ITH ROW
C     IH(I) HOLDS SECOND SUBSCRIPT
C           DEFINING POSITION OF ELEMENT
C
      MI=N-1
      DO 30 I=1,MI
      X(I)=0.
      MJ=I+1
      DO 30 J=MJ,N
      IF (X(I)-ABS (Q(I,J))) 20,20,30
   20 X(I)=ABS (Q(I,J))
      IH(I)=J
   30 CONTINUE
C
C     NEXT 7 STATEMENTS FIND FOR
C            MAXIMUM OF X(I)S FOR PIVOT ELEMENT
   40 DO 70 I=1,MI
      IF(I-1) 60,60,45
   45 IF (XMAX-X(I)) 60,70,70
   60 XMAX=X(I)
      IP=I
      JP=IH(I)
```

```
   70 CONTINUE
C
C     NEXT 2 STATEMENTS TEST FOR XMAX,
C              IF LESS THAN 10**-8,GO TO 1000
C
      EPSI=1.E-12
      IF (XMAX-EPSI) 1000,1000,148
C
  148 M=M+1
C
C     NEXT 11 STATEMENTS FOR
C              COMPUTING TANG,SINE,COSN,Q(I,I),Q(J,J)
C
      IF (Q(IP,IP)-Q(JP,JP)) 150,151,151
  150 TANG =-2.*Q(IP,JP)/(ABS(Q(IP,IP)-Q(JP,JP))+
     1 SQRT((Q(IP,IP)-Q(JP,JP))**2+4.*Q(IP,JP)**2))
      GO TO 160
  151 TANG =+2.*Q(IP,JP)/(ABS(Q(IP,IP)-Q(JP,JP))+
     1 SQRT((Q(IP,IP)-Q(JP,JP))**2+4.*Q(IP,JP)**2))
  160 COSN=1.0/SQRT(1.0+TANG**2)
      SINE=TANG*COSN
      QII= Q(IP,IP)
      Q(IP,IP)= COSN**2*(QII+TANG*(2.*Q(IP,JP)+
     1 TANG*Q(JP,JP)))
      Q(JP,JP)= COSN**2*(Q(JP,JP)-TANG*(2.*Q(IP,JP)-
     1 TANG*QII))
C
      Q(IP,JP)=0.
C
C     NEXT 4 STATEMENTS FOR PSEUDO
C              RANK OF THE E1GENVALUES
      IF (Q(IP,IP)-Q(JP,JP)) 152,153,153
  152 TEMP=Q(IP,IP)
      Q(IP,IP)=Q(JP,JP)
      Q(JP,JP)=TEMP
C
```

```
C     NEXT 6 STATEMENTS ADJUST
C            SIN, COS FOR COMPUTATION OF Q(I,K),V(I,K)
C
      IF(SINE) 154,155,155
  154 TEMP=+COSN
      GO TO 170
  155 TEMP=-COSN
  170 COSN=ABS(SINE)
      SINE=TEMP
C
C     NEXT 10 STATEMENTS FOR INSPECTING  THE I"S BETWEEN
C     I+1 AND N-1 TO DETERMINE WHETHER A NEW MAXIMUM VALUE
C     SHOULD BE COMPUTED SINCE THE PRESENT MAXIMUM IS IN
C     THE I OR J ROW
C
  153 DO 350 I=1,MI
      IF (I-IP) 210,350,200
  200 IF (I-JP) 210,350,210
  210 IF (IH(I)-IP) 230,240,230
  230 IF (IH(I)-JP) 350,240,350
  240 K= IH(I)
      TEMP=Q(I,K)
      Q(I,K)=0.
      MJ=I+1
      X(I)=0.
C
C     NEXT 5 STATEMENTS SEARCH
C            IN DEPLETED ROW FOR NEW MAXIMUM
C
      DO 320  J=MJ,N
      IF (X(I)-ABS(Q(I,J))) 300,300,320
  300 X(I)=ABS(Q(I,J))
      IH(I)=J
  320 CONTINUE
      Q(I,K)=TEMP
  350 CONTINUE
```

```
C
      X(IP)=0.
      X(JP)=0.
C
C     NEXT 30 STATEMENTS FOR
C             CHANGING THE OTHER ELEMENTS OF Q
C
      DO 530 I=1,N
C
      IF (I-IP) 370,530,420
  370 TEMP=Q(I,IP)
      Q(I,IP)=COSN*TEMP+SINE*Q(I,JP)
      IF (X(I)-ABS(Q(I,IP))) 380,390,390
  380 X(I)=ABS(Q(I,IP))
      IH(I)=IP
  390 Q(I,JP)=-SINE*TEMP+COSN*Q(I,JP)
      IF (X(I)-ABS(Q(I,JP))) 400,530,530
  400 X(I)=ABS(Q(I,JP))
      IH(I)=JP
      GO TO 530
C
  420 IF (I-JP) 430,530,480
  430 TEMP =Q(IP,I)
      Q(IP,I)=COSN*TEMP+SINE*Q(I,JP)
      IF (X(IP)-ABS(Q(IP,I))) 440,450,450
  440 X(IP)=ABS(Q(IP,I))
      IH(IP)=I
  450 Q(I,JP)=-SINE*TEMP+COSN*Q(I,JP)
      IF (X(I)-ABS(Q(I,JP))) 400,530,530
C
  480 TEMP=Q(IP,I)
      Q(IP,I)=COSN*TEMP+SINE*Q(JP,I)
      IF(X(IP)-ABS(Q(IP,I))) 490,500,500
  490 X(IP)=ABS(Q(IP,I))
      IH(IP)=I
  500 Q(JP,I)=-SINE*TEMP+COSN*Q(JP,I)
```

```
      IF (X(JP)-ABS(Q(JP,I))) 510,530,530
  510 X(JP)=ABS(Q(JP,I))
      IH(JP)=I
  530 CONTINUE
C
C     NEXT 6 STATEMENTS TEST FOR
C             COMPUTATION OF EIGENVECTORS
C
      IF (JVEC) 540,40,540
  540 DO 550 I=1,N
      TEMP=V(I,IP)
      V(I,IP)= COSN*TEMP+SINE*V(I,JP)
  550 V(I,JP)=-SINE*TEMP+COSN*V(I,JP)
      GO TO 40
 1000 RETURN
      END
      SUBROUTINE JACOBI(N,Q,JVEC,M,V)
C     SUBPROGRAM FOR DIAGONALIZATION OF
C               MATRIX Q BY SUCCESSIVE ROTATIONS
       DIMENSION Q(3,3),V(3,3),X(3),IH(3)
   13 FORMAT (2E15.5)
C
C     NEXT 8 STATEMENTS FOR SETTING
C             INITIAL VALUES OF MATRIX V
C
      IF(JVEC) 10,15,10
   10 DO 14 I=1,N
      DO 14 J=1,N
      IF(I-J) 12,11,12
   11 V(I,J)=1.0
      GO TO 14
   12 V(I,J)=0.
   14 CONTINUE
C
   15 M=0
C     NEXT 8 STATEMENTS SCAN FOR LARGEST OFF DIAG. ELEM.
```

```
C     IN EACH ROW X(I) CONTAINS LARGEST ELEMENT IN ITH
C     ROW IH(I) HOLDS SECOND SUBSCRIPT DEFINING
C     POSITION OF ELEMENT
C
      MI=N-1
      DO 30 I=1,MI
      X(I)=0.
      MJ=I+1
      DO 30 J=MJ,N
      IF (X(I)-ABS (Q(I,J))) 20,20,30
   20 X(I)=ABS (Q(I,J))
      IH(I)=J
   30 CONTINUE
C
C     NEXT 7 STATEMENTS FIND FOR
C              MAXIMUM OF X(I)S FOR PIVOT ELEMENT
   40 DO 70 I=1,MI
      IF(I-1) 60,60,45
   45 IF (XMAX-X(I)) 60,70,70
   60 XMAX=X(I)
      IP=I
      JP=IH(I)
   70 CONTINUE
C
C     NEXT 2 STATEMENTS TEST FOR XMAX,
C              IF LESS THAN 10**-8,GO TO 1000
C
      EPSI=1.E-12
      IF (XMAX-EPSI) 1000,1000,148
C
  148 M=M+1
C
C     NEXT 11 STATEMENTS FOR COMPUTING
C              TANG,SINE,COSN,Q(I,I),Q(J,J)
C
      IF (Q(IP,IP)-Q(JP,JP)) 150,151,151
```

```
  150 TANG =-2.*Q(IP,JP)/(ABS(Q(IP,IP)-Q(JP,JP))+
     1 SQRT((Q(IP,IP)-Q(JP,JP))**2+4.*Q(IP,JP)**2))
      GO TO 160
  151 TANG =+2.*Q(IP,JP)/(ABS(Q(IP,IP)-Q(JP,JP))+
     1 SQRT((Q(IP,IP)-Q(JP,JP))**2+4.*Q(IP,JP)**2))
  160 COSN=1.0/SQRT(1.0+TANG**2)
      SINE=TANG*COSN
      QII= Q(IP,IP)
      Q(IP,IP)= COSN**2*(QII+TANG*(2.*Q(IP,JP)+
     1 TANG*Q(JP,JP)))
      Q(JP,JP)= COSN**2*(Q(JP,JP)-TANG*(2.*Q(IP,JP)-
     1 TANG*QII))
C
      Q(IP,JP)=0.
C
C     NEXT 4 STATEMENTS FOR PSEUDO
C            RANK OF THE E1GENVALUES
      IF (Q(IP,IP)-Q(JP,JP)) 152,153,153
  152 TEMP=Q(IP,IP)
      Q(IP,IP)=Q(JP,JP)
      Q(JP,JP)=TEMP
C     NEXT 6 STATEMENTS ADJUST
C            SIN, COS FOR COMPUTATION OF Q(I,K),V(I,K)
C
      IF(SINE) 154,155,155
  154 TEMP=+COSN
      GO TO 170
  155 TEMP=-COSN
  170 COSN=ABS(SINE)
      SINE=TEMP
C
C     NEXT 10 STATEMENTS FOR INSPECTING  T8E IHS BETWEEN
C     I+1 AND N-1 TO DETERMINE WHETHER A NEW MAXIMUM VALUE
C     SHOULD BE COMPUTED SINCE THE PRESENT MAXIMUM IS IN
C     THE I OR J ROW
C
```

```
  153 DO 350 I=1,MI
      IF (I-IP) 210,350,200
  200 IF (I-JP) 210,350,210
  210 IF (IH(I)-IP) 230,240,230
  230 IF (IH(I)-JP) 350,240,350
  240 K= IH(I)
      TEMP=Q(I,K)
      Q(I,K)=0.
      MJ=I+1
      X(I)=0.
C
C     NEXT 5 STATEMENTS SEARCH
C             IN DEPLETED ROW FOR NEW MAXIMUM
C
      DO 320  J=MJ,N
      IF (X(I)-ABS(Q(I,J))) 300,300,320
  300 X(I)=ABS(Q(I,J))
      IH(I)=J
  320 CONTINUE
      Q(I,K)=TEMP
  350 CONTINUE
C
      X(IP)=0.
      X(JP)=0.
C
C     NEXT 30 STATEMENTS FOR
C              CHANGING THE OTHER ELEMENTS OF Q
C
      DO 530 I=1,N
C
      IF (I-IP) 370,530,420
  370 TEMP=Q(I,IP)
      Q(I,IP)=COSN*TEMP+SINE*Q(I,JP)
      IF (X(I)-ABS(Q(I,IP))) 380,390,390
  380 X(I)=ABS(Q(I,IP))
      IH(I)=IP
```

```
   390 Q(I,JP)=-SINE*TEMP+COSN*Q(I,JP)
       IF (X(I)-ABS(Q(I,JP))) 400,530,530
   400 X(I)=ABS(Q(I,JP))
       IH(I)=JP
       GO TO 530
C
   420 IF (I-JP) 430,530,480
   430 TEMP=Q(IP,I)
       Q(IP,I)=COSN*TEMP+SINE*Q(I,JP)
       IF (X(IP)-ABS(Q(IP,I))) 440,450,450
   440 X(IP)=ABS(Q(IP,I))
       IH(IP)=I
   450 Q(I,JP)=-SINE*TEMP+COSN*Q(I,JP)
       IF (X(I)-ABS(Q(I,JP))) 400,530,530
C
   480 TEMP=Q(IP,I)
       Q(IP,I)=COSN*TEMP+SINE*Q(JP,I)
       IF(X(IP)-ABS(Q(IP,I))) 490,500,500
   490 X(IP)=ABS(Q(IP,I))
       IH(IP)=I
   500 Q(JP,I)=-SINE*TEMP+COSN*Q(JP,I)
       IF (X(JP)-ABS(Q(JP,I))) 510,530,530
   510 X(JP)=ABS(Q(JP,I))
       IH(JP)=I
   530 CONTINUE
C
C      NEXT 6 STATEMENTS TEST FOR
C             COMPUTATION OF E1GENVECTORS
C
       IF (JVEC) 540,40,540
   540 DO 550 I=1,N
       TEMP=V(I,IP)
       V(I,IP)= COSN*TEMP+SINE*V(I,JP)
   550 V(I,JP)=-SINE*TEMP+COSN*V(I,JP)
       GO TO 40
  1000 AAM=FLOAT(M)
```

```
WRITE (6,13) EPSI,AAM
RETURN
END
```

```
      PROGRAM CUA (INPUT,OUTPUT,TAPE7=INPUT,TAPE58=OUTPUT)
C     THIS PROGRAM ANALYSES EPR DATA WITH NUCLEAR HYPERFINE
C     LINES WITH ELECTRON SPIN S=1/2 AND NUCLEAR SPIN I=3/2
C     FOR HOST/CU2+ USING FIRST-ORDER PERTUBATION THEORY
C
C     M  =NO. OF PARAMETERS
C     L4 =NO. OF ITERATIONS ALLOWED
C     Q1 =MIN. VALUE OF SUM OF SQUARES FOR FITS
C         (CHI-SQUARE TOLERANCE)
C     Z(I)=MAGNETIC FIELD VALUES FOR FITS
C     B  =PARAMETER MATRIX
C     N  =NO. OF  DATA POINTS USED IN LEAST-SQARES FITTING
C     Q1 =N/10
C     Q2 =TOLERANCE ON GRAD(CHI**2) =APPROX .01
C     FM(I) = MEASURED VALUES
C     FC(I) = CALCULATED VALUES
C     ERR(I)= STANDARD DEVIATION ON FM(I) = SQRT(FM(I))
C
C      DIMENSIONS OF A,B IN EXAM AND MATINV SUBROUTINES
C     SHOULD BE THE SAME AS THOSE OF B2,B1 RESPECTIVELY IN
C     THE MAIN PROOGRAM AND IN CURFIT
C
C     ENTER TEETA IN DEGREES
C     DIMENSIONS OF Q,V IN JACOBI1 SHOULD BE THE SAME AS
C     THOSE OF B3,B2 RESPECTIVELY IN CURFIT
C
C     PARAMETERS=I.GT IS G**2-TENSOR
C            (G**2ZZ,G**2ZX,G**2XX,G**2ZY,G**2YY,G**2XY)
C            GGT(J,NUMBER) REPRESENTS G-SQUARE TENSOR.
C                II. (B(I),I=1,6)=AZZ,AZX,AXX,AZY,AYY,AXY
C     A=A-SQUARE TENSOR ABOVE
C                ENTER A WITH POSITIVE SIGN
C
C     DELANG(I,J),J=1,2,3 ARE ANGLE CORRECTIONS FOR ZX,ZY,XY
C     PLANES AS DETERMINED BY "KRDBLT" FOR VARIOUS CASES.
C
```

```
C     NUMBER=INDEX THAT CHANGES WITH EACH NEW CASE ITS
C       VALUE SHOULD BE THAT OF THE FIRST CASE CONSIDERED.
C     NCASES=NO. OF LAST CASE CONSIDERED.
C       ITS VALUE SHOULD BE ENTERED.
C
C     N1(J1,NUMBER)=NO.OF LINES(FOR VARIOUS ORIENTATIONS)
C     FOR J1 HYPERFINE LINE OF CASE NO.=NUMBER
C
C     DATA FILE SHOULD BE USED LZX,LZY,LXY ARE THE NUMBER OF
C   THE ANGLES ON THE ZX,ZY,XY PLANES WHICH ARE CONSIDERED.
C
C     ZZ(J,K,L)=LINE POSITIONS,J=WHICH ONE OF K=HYPERFINE
C   LINE OF CASE NO.=L
C
      DIMENSION Z(400),FM(400),FC(400),DF(400),ERR(400),
     1B(12),B1(12),B2(12,12),DC(5000),ABC(2),Y(4),HN(400),
     2G(6,8),GG(6,8),SMD(9), AAA(3,3),QQQ(3,3),AAV(3,3),
     3QQV(3,3),IBB(400,2),THETA(400),D1(12),D2(12,12),
     4HHN(3,8),AADD(3,8),FFACTR(3,8),TEETA(100,4,8),
     5ZZ(100,4,8),NN(8),N1(4,8),GGT(6,9),GT(6),ACOSZ(400),
     6ACOSX(400),ACOSY(400),DELANG(8,3),AJ1(400),GGTL(8,3),
     7GGTM(8,3),GGTLL(8,3),GGTMM(8,3),GGTNN(8,3),GGTN(8,3),
     8DELHH(400,8),DELH(400),A4(3),LZX(1),LZY(1),LXY(1),
     9NZERO(1),NCASES(1)
      COMMON/DATA1/ABC,Y
      COMMON/DATA2/DC,ACOSZ,ACOSX,ACOSY,AJ1,GGTL,GGTM,GGTN
      COMMON/DATA3/DELH
      EQUIVALENCE (Z,DC),(FM,DC(401)),(FC,DC(801)),
C    1(DF,DC(1201)), (ERR,DC(1601)),(HN,DC(2001)),
     2(THETA,DC(2401)),(IBB,DC(2801)),(B,DC(4101)),
     3(B1,DC(4125)),(B2,DC(4137)),(N,DC(4301)),
     4(L4,DC(4302)),(Q1,DC(4303)),(Q2,DC(4304)),
     5(M,DC(4305)),(I,DC(4306)),(L,DC(4307)),(BO,DC(4308)),
     6(SMD,DC(4309)),(SSMD,DC(4320)),(D1,DC(4321)),
     7(D2,DC(4333)),(NUMBER,DC(4100)),(GT,DC(4093))
C
```

```
      READ(7,*) NZERO,NCASES,LZX,LZY,LXY
      WRITE(58,5123) NZERO,NCASES,LZX,LZY,LXY
5123  FORMAT(1X, 6HNZERO=,I8, 7HNCASES=,I8,
     14HLZX=,I8, 4HLZY=,I8, 4HLXY=,I8)
      READ(7,*)(HHN(J,NCASES),J=1,3)
      READ(7,*)(FFACTR(J,NCASES),J=1,3)
      READ(7,*)(AADD(J,NCASES),J=1,3)
      READ(7,*)(GGT(J,NCASES),J=1,6)
      READ(7,*)(G(J,NCASES),J=1,6)
      READ(7,*)(DELANG(NCASES,J),J=1,3)
      READ(7,*)(GGTLL(NCASES,J),J=1,3)
      READ(7,*)(GGTMM(NCASES,J),J=1,3)
      READ(7,*)(GGTNN(NCASES,J),J=1,3)
      READ(7,*)(N1(J,NCASES),J=1,4)
      NSUM=LZX+LZY+LXY
      NSUM=4*NSUM
      READ(7,*)(DELHH(J,NCASES),J=1,NSUM)
      READ(7,*)(TEETA(J,1,NCASES),J=1,LZX)
      READ(7,*)(ZZ(J,1,NCASES),J=1,LZX)
      READ(7,*)(ZZ(J,2,NCASES),J=1,LZX)
      READ(7,*)(ZZ(J,3,NCASES),J=1,LZX)
      READ(7,*)(ZZ(J,4,NCASES),J=1,LZX)
      II=LZX+1
      NXY=LZX+LZY
      READ(7,*)(TEETA(J,1,NCASES),J=II,NXY)
      READ(7,*)(ZZ(J,1,NCASES),J=II,NXY)
      READ(7,*)(ZZ(J,2,NCASES),J=II,NXY)
      READ(7,*)(ZZ(J,3,NCASES),J=II,NXY)
      READ(7,*)(ZZ(J,4,NCASES),J=II,NXY)
      II=NXY+1
      NXY=NXY+LXY
      READ(7,*)(TEETA(J,1,NCASES),J=II,NXY)
      READ(7,*)(ZZ(J,1,NCASES),J=II,NXY)
      READ(7,*)(ZZ(J,2,NCASES),J=II,NXY)
      READ(7,*)(ZZ(J,3,NCASES),J=II,NXY)
      READ(7,*)(ZZ(J,4,NCASES),J=II,NXY)
```

```
C
  188 FORMAT(1H1)
    8 FORMAT(1X,4HQ1 = ,E13.5,5X,4HQ2 = ,E13.5)
  137 FORMAT (3X,I2,5X,E16.6/)
  136 FORMAT(10X,19H INITIAL PARAMETERS//
     13X,1HJ,10X,4HB(J)//)
  135 FORMAT(1X,11H PARAMETERS//
     13X,1HJ,10X,4HB(J),27X,6HERRORS//)
    9 FORMAT(2X,4H HN= ,F9.4)
  140 FORMAT(3X,I2,5X,E16.6,15X,E16.6/)
  138 FORMAT(5X,14H CASE NUMBER =,I2//)
  141 FORMAT(10X,6H SMD =,E13.5//)
  235 FORMAT (15X,5(E13.5,8X)/)
  236 FORMAT(15X,3(E13.5,8X)///)
  237 FORMAT(15X,*DIAGONAL ELEMENTS OF A-
     1SQUARE TENSOR ARE=*,///)
  238 FORMAT(15X,*"A" DIR. COS.(ROWS) ACC. TO E.
     1VALS. ABOVE=  *,///)
      PI2=2.*3.1415926
      RD=PI2/360.
      NZERO=1
      NUMBER=NZERO
      NCASES=1
      M=6
      L4=7
      Q1=1.E-8
      Q2=1.E-20
      MM=M
      WRITE(58,188)
    1 CONTINUE
       N11=N1(1,NUMBER)
       DO 1188 J=1,4
       DO 1188 J1=1,N11
 1188 TEETA(J1,J,NUMBER)=TEETA(J1,1,NUMBER)
       DO 9242 J1=1,3
       GGTL(NUMBER,J1)=GGTLL(NUMBER,J1)
```

```
       GGTM(NUMBER,J1)=GGTMM(NUMBER,J1)
 9242  GGTN(NUMBER,J1)=GGTNN(NUMBER,J1)
       LINE=0
      DO 150 J1=1,4
      NN1=N1(J1,NUMBER)
      DO 150 I1=1,NN1
      LINE=LINE+1
      AJ1(LINE)=J1
      THETA(LINE)=TEETA(I1,J1,NUMBER)
      IF(THETA(LINE).GT.8000.) GO TO 155
      IF(THETA(LINE).LT.0.) GO TO 160
      TH=THETA(LINE)*RD+DELANG(NUMBER,1)*RD
      ACOSZ(LINE)=COS(TH)
      ACOSX(LINE)=SIN(TH)
      ACOSY(LINE)=0.
      HN(LINE)=HHN(1,NUMBER)
C     Z(LINE)=(ZZ(I1,J1,NUMBER)+
     1AADD(1,NUMBER))*FFACTR(1,NUMBER)
       Z(LINE)=(ZZ(I1,J1,NUMBER)*
     1FFACTR(1,NUMBER)+AADD(1,NUMBER))
      IF(ZZ(I1,J1,NUMBER).EQ.0.) Z(LINE)=0.
 9160 FORMAT(5X,*ACOSZ ETC=*,3E12.5)
      GO TO 165
  160 TH=-THETA(LINE)*RD + DELANG(NUMBER,2)*RD
      ACOSZ(LINE)=COS(TH)
      ACOSY(LINE)=SIN(TH)
      ACOSX(LINE)=0.
      HN(LINE)=HHN(2,NUMBER)
C     Z(LINE)=(ZZ(I1,J1,NUMBER)+
     1AADD(2,NUMBER))*FFACTR(2,NUMBER)
      Z(LINE)=(ZZ(I1,J1,NUMBER)*
     1FFACTR(2,NUMBER)+AADD(2,NUMBER))
      IF(ZZ(I1,J1,NUMBER).EQ.0.) Z(LINE)=0.
      GO TO 165
  155 TH=THETA(LINE)*RD+DELANG(NUMBER,3)*RD
      ACOSZ(LINE)=0.
```

```
      ACOSX(LINE)=COS(TH)
      ACOSY(LINE)=SIN(TH)
      HN(LINE)=HHN(3,NUMBER)
C     Z(LINE)=(ZZ(I1,J1,NUMBER)+
     1AADD(3,NUMBER))*FFACTR(3,NUMBER)
      Z(LINE)=(ZZ(I1,J1,NUMBER)*
     1FFACTR(3,NUMBER)+AADD(3,NUMBER))
      IF(ZZ(I1,J1,NUMBER).EQ.0.) Z(LINE)=0.
  165 CONTINUE
  150 CONTINUE
      NN(NUMBER)=LINE
      N=NN(NUMBER)
      N9=N
      DO 181 LL=1,12
  181 B(LL)=0.
      DO 210 LL=1,MM
  210 B(LL)=G(LL,NUMBER)
      WRITE(58,138) NUMBER
      WRITE(58,136)
      WRITE(58,137) (J,B(J),J=1,M)
      WRITE(58,6659)
      WRITE(58,6657) (Z(J),J=1,N)
      WRITE(58,6660)
      WRITE(58,6657) (HN(J),J=1,N)
 6660 FORMAT(5X,*FREQUENCY-KLYSTRON ARE=*,/)
 6659 FORMAT(5X,*MAG. FIELD VALUES ARE=*,/)
 6657 FORMAT(5X,8(E12.5,2X))
      DO 180 J1=1,6
  180 GT(J1)=GGT(J1,NUMBER)
      DO 201 II=1,N9
      DELH(II)=DELHH(II,NUMBER)
  201 FM(II) = HN(II)
      CALL CURFIT
      SMD(NUMBER) = SSMD
      WRITE(58,188)
      WRITE(58,135)
```

```
      DO 220 LL=1,M
  220 GG(LL,NUMBER) = B(LL)
      WRITE(58,140)(J,B(J),B1(J),J=1,M)
      WRITE(58,188)
    3 CONTINUE
      SSS=0.
      SSS1=0.
      DO 555 ID=1,N
      SSS=DF(ID)**2
      SSS1=SSS1+SSS
      WRITE(58,656) ID,SSS
555   CONTINUE
      WRITE(58,6656) SSS1
6656  FORMAT(/,10X,*CHI-SQUARE=*,E13.5,/)
 656  FORMAT(10X,*LINE NUMBER = *,I3,5X,*SMD = *,E13.5)
      AAA(1,1) = B(1)
      AAA(1,2) = B(2)
      AAA(2,2) = B(3)
      AAA(1,3) = B(4)
      AAA(3,3) = B(5)
      AAA(2,3) = B(6)
      DO 20 J1 = 1,2
      J4 = J1 + 1
      DO 20 J2 = J4,3
      AAA(J2,J1) = AAA(J1,J2)
   20 CONTINUE
      CALL JACOBI3(3,AAA,1,NR,AAV)
      WRITE (58,237)
      WRITE(58,236) (AAA(J1,J1),J1 = 1,3)
      WRITE (58,238)
      DO 25 J1 = 1,3
      WRITE (58,236) (AAV(J2,J1),J2 = 1,3)
   25 CONTINUE
      DO 245 J=1,3
       IF (AAA(J,J) .LT. 1.0E-4) AAA(J,J)=0
  245 A4(J)=SQRT(AAA(J,J))
```

```
      WRITE (58,246)
      WRITE(58,236)(A4(J),J=1,3)
  246 FORMAT(5X,*PRINCIPAL VALUES OF A-TENSOR ARE=*,/)
      NUMBER=NUMBER+1
      IF(NUMBER-NCASES) 1,1,2
    2 CONTINUE
      DO 230 LL=NZERO,NCASES
      WRITE(58,138) LL
      WRITE(58,141) SMD(LL)
  230 WRITE (58,235) (GG(LM,LL),LM=1,MM)
      STOP
      END
      SUBROUTINE CURFIT
C
C     EXAM HANDLES ALL MATRICES OF DIMENSIONS UPTO THE
C     DIMS.MM OF A,B,C THAT IS M IS LESS THAN OR EQUAL TO MM
C     (SAME IS TRUE OF MATINV AND JACOBI)
C
C     EQUIVALENCE OF GRAD BEGINS AT
C     DIMENSION OF B AFTER THE EQUIV. OF B
C
C         F O R T R A N  4
      DIMENSION Z(400),FM(400),FC(400),DF(400),ERR(400),
     1B(12),B1(12),B2(12,12),DC(5000),ABC(2),Y(4),
     2X(400),GRAD(12),D1(12),D2(12,12),B3(12,12),SMD(9),
     3HN(400),ACOSZ(400),ACOSX(400),ACOSY(400)
      DIMENSION IBB(400,2),THETA(400),GT(6)
      DIMENSION AJ1(400),GGTL(8,3),GGTM(8,3),GGTN(8,3)
      COMMON/DATA1/ABC,Y
      COMMON/DATA2/DC,ACOSZ,ACOSX,ACOSY,AJ1,GGTL,GGTM,GGTN
      EQUIVALENCE (Z,DC),(FM,DC(401)),(FC,DC(801)),
     1(DF,DC(1201)),(ERR,DC(1601)),(HN,DC(2001)),
     2(THETA,DC(2401)),(IBB,DC(2801)),(B,DC(4101)),
     3(B1,DC(4125)),(B2,DC(4137)),(N,DC(4301)),
     4(L4,DC(4302)),(Q1,DC(4303)),(Q2,DC(4304)),
     5(M,DC(4305)),(I,DC(4306)),(L,DC(4307)),(BO,DC(4308)),
```

```
     5(SMD,DC(4309)),(SSMD,DC(4320)),(D1,DC(4321)),
     6(D2,DC(4333)),(GRAD,DC(4113)),(NUMBER,DC(4100)),
     7(GT,DC(4093))
C
      ABC(1)="NO"
      ABC(2)="YES"
      L1 = 0
      SA = 0.0
      MM=M
      I6=I
      NN=N
      DO 1000 J=1,MM
      B1(J)=0.0
      DO 1000 K=1,MM
 1000 B2(J,K)=0.0
      DO 100 I6 = 1, NN
      L=1
      I=I6
      CALL FUNC(2)
      X(I6)=ERR(I6)**2
 901  FORMAT(5X,10H FUNC2,210  )
      DF(I6) =FM(I6) - FC(I6)
      DO 101 J=1,MM
      B1(J)=B1(J)-(2.0*DF(I6)*D1(J))/X(I6)
      DO 101 K=1,MM
  101 B2(J,K)=B2(J,K)-(2.0*(DF(I6)*D2(J,K)-
     1D1(J)*D1(K)))/X(I6)
  100 SA = SA + DF(I6)**2/X(I6)
      GMOD=0.0
      DO 102 J=1,M
  102 GMOD=GMOD+B1(J)**2
      WRITE(58,243)SA,GMOD
  243 FORMAT (1X,26H*INITIAL VALUE SUM OF SQ.=
     1E13.5,20X,17H*SQ MOD OF GRAD =E13.5)
      WRITE(58,1751)
 1751 FORMAT(14H0 DERIVATIVES-)
```

```
      WRITE(58,240)(B1(J),J=1,M)
  240 FORMAT (15X,5(E13.5,8X)/)
      IF (SA - Q1) 110, 110, 200
  110 LE = 1
      GO TO 600
  200 S = 0.0
      GMOD = 0.0
      BMOD = 0.0
      PROD = 0.0
      A2=ABC(1)
      DO 210 J = 1, MM
      B1(J) = 0.0
      DO 210 K = 1, MM
  210 B2(J,K) = 0.0
      WRITE(58,902)
      DO 220 I6 = 1, NN
      L=1
      I=I6
      CALL FUNC(2)
      X(I6)=ERR(I6)**2
 902  FORMAT(5X,10H FUNC2,210  )
      DF(I6) = FM(I6) - FC(I6)
      DO 220 J = 1, MM
      B1(J) = B1(J) - (2.0*DF(I6)*D1(J))/X(I6)
      DO 220 K = 1, MM
  220 B2(J,K) = B2(J,K) - (2.0*(DF(I6)*D2(J,K) -
     1D1(J)*D1(K)))/X(I6)
       DO 230 J = 1, MM
  230 GRAD(J) = B1(J)
      L1 = L1 + 1
      CALL EXAM (B2,B1,M,LF)
      WRITE(58,903)
 903  FORMAT(5X,9H EXAM,230  )
      WRITE (58,914) LF
  914 FORMAT (5X,I3)
      IF (LF)  250, 250, 305
```

```
 250 DO 231 II=1,M
     DO 231 JJ=1,M
 231 B3(II,JJ)=B2(II,JJ)
     WRITE (58,904)
     CALL JACOBI4(M,B3,4,NR,B2)
904  FORMAT(5X,12H JACOBI1,231   )
     WRITE(58,904)
     DO 235 I6=1,MM
 235 B1(I6)=B3(I6,I6)
     A2=ABC(2)
     DO 260 J = 1, MM
 260 D1(J) = 0.0
     DO 270 J = 1, MM
     DO 270 K = 1, MM
 270 D1(K) = D1(K) + B2(J,K) *GRAD(J)
     DO 275 J = 1, MM
     IF (B1(J))  280, 290, 285
 280 B1(J) = - B1(J)
 285 D1(J) = D1(J)/B1(J)
     GO TO 275
 290 D1(J) = 0.0
 275 CONTINUE
     DO 295 J = 1, MM
 295 B1(J) = 0.0
     DO 300 J = 1, MM
     DO 300 K = 1, MM
 300 B1(J) = B1(J) + B2(J,K)*D1(K)
 305 DO 310 J=1,MM
     GMOD = GMOD + GRAD(J)**2
     BMOD = BMOD + B1(J)**2
 310 PROD = PROD + GRAD(J)*B1(J)
     IF (GMOD - Q2)  315, 315, 320
 315 LE = 2
     WRITE(58,1761) GMOD
1761 FORMAT(5X,7H GMOD =,E13.5//)
     GO TO 600
```

```
 320 C=PROD/SQRT(BMOD*GMOD)
     IF (C) 335, 335, 400
 335 LE = 4
     GO TO 600
 400 LD = 0
     L3 = 0
     DO 410 J = 1, MM
 410 GRAD(J) = B(J) - B1(J)
 450 DO 420 I6 = 1, NN
     L=2
     I=I6
     CALL FUNC (1)
     X(I6)=ERR(I6)**2
905  FORMAT(5X,10H FUNC1,450  )
     DF(I6) = FM(I6) - FC(I6)
 420 S = S + DF(I6)**2/X(I6)
     WRITE(58,905)
     IF (SA - S) 435, 500, 500
 435 LD = LD + 1
 430 DO440 J = 1, MM
     B1(J) = B1(J)/2.0
906  FORMAT(5X,16H BINARY CHOP,430  )
 440 GRAD(J) = B(J) - B1(J)
     WRITE(58,906)
     S = 0.0
     L3 = L3 + 1
     IF(L3-5)450,460,460
 460 LE = 5
     GO TO 600
 500 IF (LD) 505, 505, 506
 506 LD = 0
     GO TO 430
 505 DO 510 J = 1, MM
 510 B(J) = GRAD(J)
     SA = S
     IF (SA - Q1) 507, 507, 530
```

```
 507 LE = 1
     GO TO 600
 530 IF (L4) 200, 200, 900
 900 WRITE(58,920)L1,A2,L3,S,GMOD,(B(J),J=1,M)
 920 FORMAT(//,15H ITERATION NO.=I5,10X,
    143H   TRANSFORMATION MADE TO PRINCIPAL AXES = A4,
    210X,   18H BINARY CHOP USED=I3,6H TIMES/1X,27H W
    3EIGHTED SUM OF SQUARES = E14.7,25X,32H   SQUARE MO
    4DULUS OF GRADIENT = E14.7/20H   PARAME
    5TERS B(J) -/(6E17.8)/)
     IF (L1 - L4) 200, 910, 910
 910 LE = 6
     GO TO 600
 600 DO 710 J=1,MM
     B1(J) = 0.0
     DO 710 K=1,MM
 710 B2(J,K) = 0.0
     L=1
     WRITE(58,907)
 907 FORMAT(5X,* FUNC(2),720 *)
     DO 720 I6 = 1, NN
     I=I6
     CALL FUNC(2)
     X(I6)=ERR(I6)**2
     DF(I6) = FM(I6) - FC(I6)
     DO 720 J = 1, MM
     B1(J) = B1(J) - (2.0*DF(I6)*D1(J))/X(I6)
     DO 720 K = 1, MM
 720 B2(J,K) = B2(J,K) - ((DF(I6)*D2(J,K) -
    1D1(J)*D1(K)))/X(I6)
     WRITE (58,3029)
3029 FORMAT(* I AM LOST IN MANTINV*)
     CALL MATINV(B2,M,B1,1,DETERM)
     WRITE (58,3029)
     DO 730 J=1,MM
     IF (B2(J,J)) 2001,2001,2002
```

```
2001  B1(J)  = -SQRT(-B2(J,J))
      GO TO  730
2002  B1(J)= SQRT(B2(J,J))
  730 CONTINUE
      DO 740 J=1,MM
      DO 740 K=1,MM
  740 B2(J,K)=B2(J,K)/(B1(J)*B1(K))
      WRITE(58,551)LE,SA
  551 FORMAT(//,13H EXIT NUMBER=I3,20X,25H WEIGH
     1TED SUM OF SQUARES=E15.8//)
      SSMD = SA
9999  CONTINUE
      RETURN
      END

      SUBROUTINE FUNC(LX)
C     SUBROUTINE FUNC
C
C
      DIMENSION DC(5000),B(12,2),D1(12),D2(12,12),FC(400),
     1Z(400),S(4,4),SIGN(400),HN(400),ST(4,4,16),FM(400),
     2DF(400),DELH(400),ERR(400),B1(12),B2(12,12),SMD(9),
     3ACOSZ(400),ACOSX(400),ACOSY(400),IBB(400,2),
     4THETA(400),DD(16),GT(6),AJ1(400),AL(400),AM(400),
     5AN(400),GGTL(8,3),GGTM(8,3),GGTN(8,3)
      COMMON/DATA2/DC,ACOSZ,ACOSX,ACOSY,AJ1,GGTL,GGTM,GGTN
      COMMON/DATA3/DELH
      EQUIVALENCE (Z,DC),(FM,DC(401)),(FC,DC(801)),
     1(DF,DC(1201)), (ERR,DC(1601)),(HN,DC(2001)),
     2(THETA,DC(2401)),(IBB,DC(2801)),(B,DC(4101)),
     3(B1,DC(4125)),(B2,DC(4137)),(N,DC(4301)),
     4(L4,DC(4302)),(Q1,DC(4303)),(Q2,DC(4304)),
     5(M,DC(4305)),(I,DC(4306)),(L,DC(4307)),(BO,DC(4308)),
     6(SMD,DC(4309)),(SSMD,DC(4320)),(D1,DC(4321)),
     7(D2,DC(4333)),(NUMBER,DC(4100)),(GT,DC(4093))
      IF(Z(I).EQ.0.) GO TO 135
```

```
      BETA=92.732/66252.
      BETAN=.00054464*BETA
      RD=3.1415926/180.
      R2=SQRT(2.0)
      R3=SQRT(3.0)
      R5=SQRT(5.0)
      R7=SQRT(7.0)
      FACTOR=92.732/66252.
      AL(I)=ACOSZ(I)*GGTL(NUMBER,1)+ACOSX(I)*
     1GGTL(NUMBER,2)+ACOSY(I)*GGTL(NUMBER,3)
      AM(I)=ACOSZ(I)*GGTM(NUMBER,1)+ACOSX(I)*
     2GGTM(NUMBER,2)+ACOSY(I)*GGTM(NUMBER,3)
      AN(I)=ACOSZ(I)*GGTN(NUMBER,1)+ACOSX(I)*
     3GGTN(NUMBER,2)+ACOSY(I)*GGTN(NUMBER,3)
      FCI=GT(1)*AL(I)**2+GT(3)*AM(I)**2+GT(5)*AN(I)**2
      ENELSP=Z(I)*BETA*SQRT(FCI)
      BB1=GT(1)*AL(I)**2
      BB3=GT(3)*AM(I)**2
      BB5=GT(5)*AN(I)**2
      BB2=2.*SQRT(GT(1)*GT(3))*AL(I)*AM(I)
      BB4=2.*SQRT(GT(1)*GT(5))*AL(I)*AN(I)
      BB6=2.*SQRT(GT(3)*GT(5))*AM(I)*AN(I)
      AEFF2=B(1,L)*BB1+B(3,L)*BB3+B(5,L)*BB5+
     1 B(2,L)*BB2+B(4,L)*BB4+B(6,L)*BB6
      AMI=2.5-AJ1(I)
      IF(AEFF2.LT.(0.)) GO TO 109
      AEFF=SQRT(AEFF2/FCI)
      HYPFEN=AEFF*AMI
      FC(I)=ENELSP+HYPFEN
      ERR(I)=SQRT(FCI)*DELH(I)*FACTOR
      ERR(I)=1.
      GO TO 136
  135 CONTINUE
      FC(I)=HN(I)
      ERR(I)=1.
  136 CONTINUE
```

```
      IF(LX-1)110,110,120
  120 CONTINUE
      DO  235 IZ = 1,12
      D1(IZ) = 0.0
      DO  235 JZ = 1,12
  235 D2(IZ,JZ) =0.0
      IF(Z(I).EQ.0.) GO TO 110
      DDD=.5*AMI/(FCI*AEFF)
      D1(1)=DDD*BB1
      D1(2)=DDD*BB2
      D1(3)=DDD*BB3
      D1(4)=DDD*BB4
      D1(5)=DDD*BB5
      D1(6)=DDD*BB6
      GO TO 110
  109 WRITE(58,108) I
  108 FORMAT(5X,*NEG AEFF2 FOR I=*,I3)
      FC(I)=FM(I)
      DO 197 JJ=1,6
  197 D1(JJ)=0.
  110 CONTINUE
      RETURN
      END
      SUBROUTINE EXAM(A,B,M,LF)
C     SUBROUTINE EXAM
C       F O R T R A N  4
      DIMENSION A(12,12),B(12),C(12)
      DO 80 J=1,M
   80 C(J)=A(J,J)
      IF(A(1,1)) 60,200,70
   60 A(1,1) =-SQRT(-A(1,1))
      GO TO 300
   70 A(1,1) =SQRT(A(1,1))
      GO TO 100
  100 IF(M-1)400,400,110
  110 DO 115 K=2,M
```

```
115 A(1,K)=A(1,K)/(A(1,1)           )
    DO 120 J=2,M
    J1=J-1
    S=A(J,J)
    DO 125 L=1,J1
125 S=S-A(L,J)**2
    IF (S) 50,200,40
 50 A(J,J) =-SQRT(-S)
    GO TO 300
 40 A(J,J) =SQRT(S)
    GO TO 130
130 IF(J-M)135,400,400
135 J2=J+1
    DO 120 K=J2,M
    S=A(J,K)
    DO 145 L=1,J1
145 S=S-A(L,J)*A(L,K)
120 A(J,K)=S/A(J,J)
400 B(1)=B(1)/A(1,1)
    IF(M-1)420,420,405
405 DO 410 J=2,M
    S=B(J)
    J1=J-1
    DO 415 L=1,J1
415 S=S-A(L,J)*B(L)
410 B(J)=S/A(J,J)
420 B(M)=B(M)/A(M,M)
    J=M-1
435 IF(J)450,450,425
425 S=B(J)
    J2=J+1
    DO 430 L=J2,M
430 S=S-A(J,L)*B(L)
    B(J)=S/A(J,J)
    J=J-1
    GO TO 435
```

```
  450 LF=1
      GO TO 460
  200 LF=0
      GO TO 460
  300 LF=-1
  460 DO 465 J=1,M
      A(J,J)=C(J)
      IF(J-M)470,475,475
  470 J2=J+1
      DO 465 K=J2,M
  465 A(J,K)=A(K,J)
  475 RETURN
      END

      SUBROUTINE MATINV(A,N,B,M,DETERM)
C       F O R T R A N  4
C     MATRIX INVERSION WITH ACCOMPANYING SOLUTION
C            OF LINEAR EQUATIONS
      DIMENSION IPIVOT(12),A(12,12),B(12,1),
     1INDEX(12,2),PIVOT(12)
      EQUIVALENCE (IROW,JROW),(ICOLUM,JCOLUM),(AMAX,T,SWAP)
      DETERM=1.0
      DO 20 J=1,N
   20 IPIVOT(J)=0
      DO 550 I=1,N
      AMAX=0.0
      DO 105 J=1,N
      IF(IPIVOT(J)-1)60,105,60
   60 DO 100 K=1,N
      IF(IPIVOT(K)-1)80,100,740
   80 IF(ABS(AMAX)-ABS(A(J,K)))85,100,100
   85 IROW=J
      ICOLUM=K
      AMAX=A(J,K)
  100 CONTINUE
  105 CONTINUE
```

```
    IPIVOT(ICOLUM)=IPIVOT(ICOLUM)+1
    IF (IROW-ICOLUM)140,260,140
140 DETERM=-DETERM
    DO 200 L=1,N
    SWAP=A(IROW,L)
    A(IROW,L)=A(ICOLUM,L)
200 A(ICOLUM,L)=SWAP
    IF(M)260,260,210
210 DO 250 L=1,M
    SWAP=B(IROW,L)
    B(IROW,L)=B(ICOLUM,L)
250 B(ICOLUM,L)=SWAP
260 INDEX(I,1)=IROW
    INDEX(I,2)=ICOLUM
    PIVOT(I)=A(ICOLUM,ICOLUM)
    DETERM=DETERM*PIVOT(I)
    A(ICOLUM,ICOLUM)=1.0
    DO 350 L=1,N
350 A(ICOLUM,L)=A(ICOLUM,L)/PIVOT(I)
    IF(M)380,380,360
360 DO 370 L=1,M
370 B(ICOLUM,L)=B(ICOLUM,L)/PIVOT(I)
380 DO 550 L1=1,N
    IF (L1-ICOLUM)400,550,400
400 T=A(L1,ICOLUM)
    A(L1,ICOLUM)=0.0
    DO 450 L=1,N
450 A(L1,L)=A(L1,L)-A(ICOLUM,L)*T
    IF(M)550,550,460
460 DO 500 L=1,M
500 B(L1,L)=B(L1,L)-B(ICOLUM,L)*T
550 CONTINUE
    DO 710 I=1,N
    L=N+1-I
    IF(INDEX(L,1)-INDEX(L,2))630,710,630
630 JROW=INDEX(L,1)
```

```
      JCOLUM=INDEX(L,2)
      DO 705 K=1,N
      SWAP=A(K,JROW)
      A(K,JROW)=A(K,JCOLUM)
      A(K,JCOLUM)=SWAP
  705 CONTINUE
  710 CONTINUE
  740 RETURN
      END

      SUBROUTINE JACOBI2(N,Q,JVEC,M,V)
C     SUBPROGRAM FOR DIAGONALIZATION OF MATRIX Q
C     BY SUCCESSIVE ROTATIONS
      DIMENSION Q(6,6),V(6,6),X(6),IH(6)
C
C     NEXT 8 STATEMENTS FOR SETTING
C             INITIAL VALUES OF MATRIX V
C
      IF(JVEC) 10,15,10
   10 DO 14 I=1,N
      DO 14 J=1,N
      IF(I-J) 12,11,12
   11 V(I,J)=1.0
      GO TO 14
   12 V(I,J)=0.
   14 CONTINUE
C
   15 M=0
C     NEXT 8 STATEMENTS SCAN FOR
C             LARGEST OFF DIAG. ELEM. IN EACH ROW
C     X(I) CONTAINS LARGEST ELEMENT IN ITH ROW
C     IH(I) HOLDS SECOND SUBSCRIPT
C             DEFINING POSITION OF ELEMENT
C
      MI=N-1
      DO 30 I=1,MI
```

```
      X(I)=0.
      MJ=I+1
      DO 30 J=MJ,N
      IF (X(I)-ABS (Q(I,J))) 20,20,30
   20 X(I)=ABS (Q(I,J))
      IH(I)=J
   30 CONTINUE
C
C     NEXT 7 STATEMENTS FIND FOR MAXIMUM OF
C              X(I)S FOR PIVOT ELEMENT
   40 DO 70 I=1,MI
      IF(I-1) 60,60,45
   45 IF (XMAX-X(I)) 60,70,70
   60 XMAX=X(I)
      IP=I
      JP=IH(I)
   70 CONTINUE
C
C     NEXT 2 STATEMENTS TEST FOR XMAX,
C              IF LESS THAN 10**-8,GO TO 1000
C
      EPSI=1.E-12
      IF (XMAX-EPSI) 1000,1000,148
C
  148 M=M+1
C
C     NEXT 11 STATEMENTS FOR COMPUTING
C               TANG,SINE,COSN,Q(I,I),Q(J,J)
C
      IF (Q(IP,IP)-Q(JP,JP)) 150,151,151
  150 TANG =-2.*Q(IP,JP)/(ABS(Q(IP,IP)-Q(JP,JP))+
     1SQRT((Q(IP,IP)-Q(JP,JP))**2+4.*Q(IP,JP)**2))
      GO TO 160
  151 TANG =+2.*Q(IP,JP)/(ABS(Q(IP,IP)-Q(JP,JP))+
     1SQRT((Q(IP,IP)-Q(JP,JP))**2+4.*Q(IP,JP)**2))
  160 COSN=1.0/SQRT(1.0+TANG**2)
```

```
      SINE=TANG*COSN
      QII= Q(IP,IP)
      Q(IP,IP)= COSN**2*(QII+
     1 TANG*(2.*Q(IP,JP)+TANG*Q(JP,JP)))
      Q(JP,JP)= COSN**2*(Q(JP,JP)-
     1 TANG*(2.*Q(IP,JP)-TANG*QII))
C
      Q(IP,JP)=0.
C
C     NEXT 4 STATEMENTS FOR PSEUDO
C            RANK OF THE E1GENVALUES
      IF (Q(IP,IP)-Q(JP,JP)) 152,153,153
  152 TEMP=Q(IP,IP)
      Q(IP,IP)=Q(JP,JP)
      Q(JP,JP)=TEMP
C
C     NEXT 6 STATEMENTS ADJUST SIN, COS
C            FOR COMPUTATION OF Q(I,K),V(I,K)
C
      IF(SINE) 154,155,155
  154 TEMP=+COSN
      GO TO 170
  155 TEMP=-COSN
  170 COSN=ABS(SINE)
      SINE=TEMP
C
C     NEXT 10 STATEMENTS FOR INSPECTING  THE I"S BETWEEN
C     I+1 AND N-1 TO DETERMINE WHETHER A NEW MAXIMUM VALUE
C     SHOULD BE COMPUTED SINCE THE PRESENT MAXIMUM IS IN THE
C     I OR J ROW
C
  153 DO 350 I=1,MI
      IF (I-IP) 210,350,200
  200 IF (I-JP) 210,350,210
  210 IF (IH(I)-IP) 230,240,230
  230 IF (IH(I)-JP) 350,240,350
```

```
  240 K= IH(I)
      TEMP=Q(I,K)
      Q(I,K)=0.
      MJ=I+1
      X(I)=0.
C
C     NEXT 5 STATEMENTS SEARCH
C            IN DEPLETED ROW FOR NEW MAXIMUM
C
      DO 320  J=MJ,N
      IF (X(I)-ABS(Q(I,J))) 300,300,320
  300 X(I)=ABS(Q(I,J))
      IH(I)=J
  320 CONTINUE
      Q(I,K)=TEMP
  350 CONTINUE
C
      X(IP)=0.
      X(JP)=0.
C
C     NEXT 30 STATEMENTS FOR
C             CHANGING THE OTHER ELEMENTS OF Q
C
      DO 530 I=1,N
C
      IF (I-IP) 370,530,420
  370 TEMP=Q(I,IP)
      Q(I,IP)=COSN*TEMP+SINE*Q(I,JP)
      IF (X(I)-ABS(Q(I,IP))) 380,390,390
  380 X(I)=ABS(Q(I,IP))
      IH(I)=IP
  390 Q(I,JP)=-SINE*TEMP+COSN*Q(I,JP)
      IF (X(I)-ABS(Q(I,JP))) 400,530,530
  400 X(I)=ABS(Q(I,JP))
      IH(I)=JP
      GO TO 530
```

```
C
  420 IF (I-JP) 430,530,480
  430 TEMP =Q(IP,I)
      Q(IP,I)=COSN*TEMP+SINE*Q(I,JP)
      IF (X(IP)-ABS(Q(IP,I))) 440,450,450
  440 X(IP)=ABS(Q(IP,I))
      IH(IP)=I
  450 Q(I,JP)=-SINE*TEMP+COSN*Q(I,JP)
      IF (X(I)-ABS(Q(I,JP))) 400,530,530
C
  480 TEMP=Q(IP,I)
      Q(IP,I)=COSN*TEMP+SINE*Q(JP,I)
      IF(X(IP)-ABS(Q(IP,I))) 490,500,500
  490 X(IP)=ABS(Q(IP,I))
      IH(IP)=I
  500 Q(JP,I)=-SINE*TEMP+COSN*Q(JP,I)
      IF (X(JP)-ABS(Q(JP,I))) 510,530,530
  510 X(JP)=ABS(Q(JP,I))
      IH(JP)=I
  530 CONTINUE
C
C     NEXT 6 STATEMENTS TEST FOR
C            COMPUTATION OF EIGENVECTORS
C
      IF (JVEC) 540,40,540
  540 DO 550 I=1,N
      TEMP=V(I,IP)
      V(I,IP)= COSN*TEMP+SINE*V(I,JP)
  550 V(I,JP)=-SINE*TEMP+COSN*V(I,JP)
      GO TO 40
 1000 RETURN
      END
      SUBROUTINE JACOBI4(N,Q,JVEC,M,V)
C     SUBPROGRAM FOR DIAGONALIZATION OF
C                MATRIX Q BY SUCCESSIVE ROTATIONS
      DIMENSION Q(12,12),V(12,12),X(12),IH(12)
```

```
   13 FORMAT (2E15.5)
C
C        NEXT 8 STATEMENTS FOR SETTING
C               INITIAL VALUES OF MATRIX V
C
         IF(JVEC) 10,15,10
   10 DO 14 I=1,N
         DO 14 J=1,N
         IF(I-J) 12,11,12
   11 V(I,J)=1.0
         GO TO 14
   12 V(I,J)=0.
   14 CONTINUE
C
   15 M=0
C        NEXT 8 STATEMENTS SCAN FOR LARGEST OFF DIAG. ELEM.
C        IN EACH ROW X(I) CONTAINS LARGEST ELEMENT IN ITH ROW
C        IH(I) HOLDS SECOND SUBSCRIPT DEFINING POSITION OF ELEMENT
C
         MI=N-1
         DO 30 I=1,MI
         X(I)=0.
         MJ=I+1
         DO 30 J=MJ,N
         IF (X(I)-ABS (Q(I,J))) 20,20,30
   20 X(I)=ABS (Q(I,J))
         IH(I)=J
   30 CONTINUE
C
C        NEXT 7 STATEMENTS FIND FOR
C               MAXIMUM OF X(I)S FOR PIVOT ELEMENT
   40 DO 70 I=1,MI
         IF(I-1) 60,60,45
   45 IF (XMAX-X(I)) 60,70,70
   60 XMAX=X(I)
         IP=I
```

```
      JP=IH(I)
   70 CONTINUE
C
C     NEXT 2 STATEMENTS TEST FOR XMAX,
C            IF LESS THAN 10**-8,GO TO 1000
C
      EPSI=1.E-12
      IF (XMAX-EPSI) 1000,1000,148
C
  148 M=M+1
C
C     NEXT 11 STATEMENTS FOR COMPUTING
C             TANG,SINE,COSN,Q(I,I),Q(J,J)
C
      IF (Q(IP,IP)-Q(JP,JP)) 150,151,151
  150 TANG =-2.*Q(IP,JP)/(ABS(Q(IP,IP)-Q(JP,JP))+
     1SQRT((Q(IP,IP)-Q(JP,JP))**2+4.*Q(IP,JP)**2))
      GO TO 160
  151 TANG =+2.*Q(IP,JP)/(ABS(Q(IP,IP)-Q(JP,JP))+
     1SQRT((Q(IP,IP)-Q(JP,JP))**2+4.*Q(IP,JP)**2))
  160 COSN=1.0/SQRT(1.0+TANG**2)
      SINE=TANG*COSN
      QII= Q(IP,IP)
      Q(IP,IP)= COSN**2*(QII+
     1 TANG*(2.*Q(IP,JP)+TANG*Q(JP,JP)))
      Q(JP,JP)= COSN**2*(Q(JP,JP)-
     1 TANG*(2.*Q(IP,JP)-TANG*QII))
C
      Q(IP,JP)=0.
C
C     NEXT 4 STATEMENTS FOR PSEUDO RANK OF THE E1GENVALUES
      IF (Q(IP,IP)-Q(JP,JP)) 152,153,153
  152 TEMP=Q(IP,IP)
      Q(IP,IP)=Q(JP,JP)
      Q(JP,JP)=TEMP
C     NEXT 6 STATEMENTS ADJUST
```

```
C             SIN, COS FOR COMPUTATION OF Q(I,K),V(I,K)
C
      IF(SINE) 154,155,155
  154 TEMP=+COSN
      GO TO 170
  155 TEMP=-COSN
  170 COSN=ABS(SINE)
      SINE=TEMP
C
C     NEXT 10 STATEMENTS FOR INSPECTING  T8E IHS BETWEEN
C     I+1 AND N-1 TO DETERMINE WHETHER A NEW MAXIMUM VALUE
C     SHOULD BE COMPUTED SINCE THE PRESENT MAXIMUM IS IN THE
C     I OR J ROW
C
  153 DO 350 I=1,MI
      IF (I-IP) 210,350,200
  200 IF (I-JP) 210,350,210
  210 IF (IH(I)-IP) 230,240,230
  230 IF (IH(I)-JP) 350,240,350
  240 K= IH(I)
      TEMP=Q(I,K)
      Q(I,K)=0.
      MJ=I+1
      X(I)=0.
C
C     NEXT 5 STATEMENTS SEARCH
C             IN DEPLETED ROW FOR NEW MAXIMUM
C
      DO 320  J=MJ,N
      IF (X(I)-ABS(Q(I,J))) 300,300,320
  300 X(I)=ABS(Q(I,J))
      IH(I)=J
  320 CONTINUE
      Q(I,K)=TEMP
  350 CONTINUE
C
```

```
      X(IP)=0.
      X(JP)=0.
C
C     NEXT 30 STATEMENTS FOR
C             CHANGING THE OTHER ELEMENTS OF Q
C
      DO 530 I=1,N
C
      IF (I-IP) 370,530,420
  370 TEMP=Q(I,IP)
      Q(I,IP)=COSN*TEMP+SINE*Q(I,JP)
      IF (X(I)-ABS(Q(I,IP))) 380,390,390
  380 X(I)=ABS(Q(I,IP))
      IH(I)=IP
  390 Q(I,JP)=-SINE*TEMP+COSN*Q(I,JP)
      IF (X(I)-ABS(Q(I,JP))) 400,530,530
  400 X(I)=ABS(Q(I,JP))
      IH(I)=JP
      GO TO 530
C
  420 IF (I-JP) 430,530,480
  430 TEMP=Q(IP,I)
      Q(IP,I)=COSN*TEMP+SINE*Q(I,JP)
      IF (X(IP)-ABS(Q(IP,I))) 440,450,450
  440 X(IP)=ABS(Q(IP,I))
      IH(IP)=I
  450 Q(I,JP)=-SINE*TEMP+COSN*Q(I,JP)
      IF (X(I)-ABS(Q(I,JP))) 400,530,530
C
  480 TEMP=Q(IP,I)
      Q(IP,I)=COSN*TEMP+SINE*Q(JP,I)
      IF(X(IP)-ABS(Q(IP,I))) 490,500,500
  490 X(IP)=ABS(Q(IP,I))
      IH(IP)=I
  500 Q(JP,I)=-SINE*TEMP+COSN*Q(JP,I)
      IF (X(JP)-ABS(Q(JP,I))) 510,530,530
```

```
  510 X(JP)=ABS(Q(JP,I))
      IH(JP)=I
  530 CONTINUE
C
C     NEXT 6 STATEMENTS TEST FOR
C             COMPUTATION OF E1GENVECTORS
C
      IF (JVEC) 540,40,540
  540 DO 550 I=1,N
      TEMP=V(I,IP)
      V(I,IP)= COSN*TEMP+SINE*V(I,JP)
  550 V(I,JP)=-SINE*TEMP+COSN*V(I,JP)
      GO TO 40
 1000 AAM=FLOAT(M)
      WRITE (58,13) EPSI,AAM
      RETURN
      END
      SUBROUTINE JACOBI3(N,Q,JVEC,M,V)
C     SUBPROGRAM FOR DIAGONALIZATION OF
C                MATRIX Q BY SUCCESSIVE ROTATIONS
       DIMENSION Q(3,3),V(3,3),X(3),IH(3)
   13 FORMAT (2E15.5)
C
C     NEXT 8 STATEMENTS FOR SETTING
C             INITIAL VALUES OF MATRIX V
C
      IF(JVEC) 10,15,10
   10 DO 14 I=1,N
      DO 14 J=1,N
      IF(I-J) 12,11,12
   11 V(I,J)=1.0
      GO TO 14
   12 V(I,J)=0.
   14 CONTINUE
C
   15 M=0
```

```
C     NEXT 8 STATEMENTS SCAN FOR LARGEST OFF DIAG. ELEM.
C     IN EACH ROW X(I) CONTAINS LARGEST ELEMENT IN ITH ROW
C     IH(I) HOLDS SECOND SUBSCRIPT DEFINING POSITION
C     OF ELEMENT
C
      MI=N-1
      DO 30 I=1,MI
      X(I)=0.
      MJ=I+1
      DO 30 J=MJ,N
      IF (X(I)-ABS (Q(I,J))) 20,20,30
   20 X(I)=ABS (Q(I,J))
      IH(I)=J
   30 CONTINUE
C
C     NEXT 7 STATEMENTS FIND FOR
C            MAXIMUM OF X(I)S FOR PIVOT ELEMENT
   40 DO 70 I=1,MI
      IF(I-1) 60,60,45
   45 IF (XMAX-X(I)) 60,70,70
   60 XMAX=X(I)
      IP=I
      JP=IH(I)
   70 CONTINUE
C
C     NEXT 2 STATEMENTS TEST FOR XMAX,
C            IF LESS THAN 10**-8,GO TO 1000
C
      EPSI=1.E-12
      IF (XMAX-EPSI) 1000,1000,148
C
  148 M=M+1
C
C     NEXT 11 STATEMENTS FOR COMPUTING
C             TANG,SINE,COSN,Q(I,I),Q(J,J)
C
```

```
      IF (Q(IP,IP)-Q(JP,JP)) 150,151,151
  150 TANG =-2.*Q(IP,JP)/(ABS(Q(IP,IP)-Q(JP,JP))+
     1SQRT((Q(IP,IP)-Q(JP,JP))**2+4.*Q(IP,JP)**2))
      GO TO 160
  151 TANG =+2.*Q(IP,JP)/(ABS(Q(IP,IP)-Q(JP,JP))+
     1SQRT((Q(IP,IP)-Q(JP,JP))**2+4.*Q(IP,JP)**2))
  160 COSN=1.0/SQRT(1.0+TANG**2)
      SINE=TANG*COSN
      QII= Q(IP,IP)
      Q(IP,IP)= COSN**2*(QII+
     1 TANG*(2.*Q(IP,JP)+TANG*Q(JP,JP)))
      Q(JP,JP)= COSN**2*(Q(JP,JP)-
     1 TANG*(2.*Q(IP,JP)-TANG*QII))
C
      Q(IP,JP)=0.
C
C     NEXT 4 STATEMENTS FOR PSEUDO RANK OF THE E1GENVALUES
      IF (Q(IP,IP)-Q(JP,JP)) 152,153,153
  152 TEMP=Q(IP,IP)
      Q(IP,IP)=Q(JP,JP)
      Q(JP,JP)=TEMP
C     NEXT 6 STATEMENTS ADJUST
C            SIN,COS FOR COMPUTATION OF Q(I,K),V(I,K)
C
      IF(SINE) 154,155,155
  154 TEMP=+COSN
      GO TO 170
  155 TEMP=-COSN
  170 COSN=ABS(SINE)
      SINE=TEMP
C
C     NEXT 10 STATEMENTS FOR INSPECTING  T8E IHS BETWEEN
C     I+1 AND N-1 TO DETERMINE WHETHER A NEW MAXIMUM VALUE
C     SHOULD BE COMPUTED SINCE THE PRESENT MAXIMUM IS IN
C     THE I OR J ROW
C
```

```
  153 DO 350 I=1,MI
      IF (I-IP) 210,350,200
  200 IF (I-JP) 210,350,210
  210 IF (IH(I)-IP) 230,240,230
  230 IF (IH(I)-JP) 350,240,350
  240 K= IH(I)
      TEMP=Q(I,K)
      Q(I,K)=0.
      MJ=I+1
      X(I)=0.
C
C     NEXT 5 STATEMENTS SEARCH
C            IN DEPLETED ROW FOR NEW MAXIMUM
C
      DO 320  J=MJ,N
      IF (X(I)-ABS(Q(I,J))) 300,300,320
  300 X(I)=ABS(Q(I,J))
      IH(I)=J
  320 CONTINUE
      Q(I,K)=TEMP
  350 CONTINUE
C
      X(IP)=0.
      X(JP)=0.
C
C     NEXT 30 STATEMENTS FOR
C             CHANGING THE OTHER ELEMENTS OF Q
C
      DO 530 I=1,N
C
      IF (I-IP) 370,530,420
  370 TEMP=Q(I,IP)
      Q(I,IP)=COSN*TEMP+SINE*Q(I,JP)
      IF (X(I)-ABS(Q(I,IP))) 380,390,390
  380 X(I)=ABS(Q(I,IP))
      IH(I)=IP
```

```
  390 Q(I,JP)=-SINE*TEMP+COSN*Q(I,JP)
      IF (X(I)-ABS(Q(I,JP))) 400,530,530
  400 X(I)=ABS(Q(I,JP))
      IH(I)=JP
      GO TO 530
C
  420 IF (I-JP) 430,530,480
  430 TEMP=Q(IP,I)
      Q(IP,I)=COSN*TEMP+SINE*Q(I,JP)
      IF (X(IP)-ABS(Q(IP,I))) 440,450,450
  440 X(IP)=ABS(Q(IP,I))
      IH(IP)=I
  450 Q(I,JP)=-SINE*TEMP+COSN*Q(I,JP)
      IF (X(I)-ABS(Q(I,JP))) 400,530,530
C
  480 TEMP=Q(IP,I)
      Q(IP,I)=COSN*TEMP+SINE*Q(JP,I)
      IF(X(IP)-ABS(Q(IP,I))) 490,500,500
  490 X(IP)=ABS(Q(IP,I))
      IH(IP)=I
  500 Q(JP,I)=-SINE*TEMP+COSN*Q(JP,I)
      IF (X(JP)-ABS(Q(JP,I))) 510,530,530
  510 X(JP)=ABS(Q(JP,I))
      IH(JP)=I
  530 CONTINUE
C
C     NEXT 6 STATEMENTS TEST FOR
C            COMPUTATION OF E1GENVECTORS
C
      IF (JVEC) 540,40,540
  540 DO 550 I=1,N
      TEMP=V(I,IP)
      V(I,IP)= COSN*TEMP+SINE*V(I,JP)
  550 V(I,JP)=-SINE*TEMP+COSN*V(I,JP)
      GO TO 40
 1000 AAM=FLOAT(M)
```

```
WRITE (58,13) EPSI,AAM
RETURN
END
```

```
      PROGRAM CUGA (INPUT,OUTPUT,TAPE5=INPUT,TAPE58=OUTPUT)
C     THIS PROGRAM ANALYSES EPR DATA WITH NUCLEAR HYPERFINE
C     LINES WITH ELECTRON SPIN S=1/2 AND NUCLEAR SPIN I=3/2
C     FOR SIGLE CRYSTAL/CU2+. IT FITS BOTH G-SQUARE AND A-
C     SQUARE TENSOR ELEMENTS (12 PARAMETERS) ------SECOND
C     ORDER PERTURBATION.
C
C     M  =NO. OF PARAMETERS
C     L4 =NO. OF ITERATIONS ALLOWED
C     Q1 =MIN. VALUE OF SUM OF SQUARES FOR FITS( CHI-SQUARE
C         TOLERANCE)
C     Z(I)=MAGNETIC FIELD VALUES FOR FITS
C     B  =PARAMETER MATRIX
C     N  =NO. OF  DATA POINTS USED IN LEAST-SQARES FITTING
C     Q1 =N/10
C     Q2 =TOLERANCE ON GRAD(CHI**2) =APPROX .01
C     FM(I) = MEASURED VALUES
C     FC(I) = CALCULATED VALUES
C     ERR(I)= STANDARD DEVIATION ON FM(I) = SQRT(FM(I))
C
C      DIMENSIONS OF A,B IN EXAM AND MATINV SUBROUTINES
C     SHOULD BE THE SAME AS THOSE OF B2,B1 RESPECTIVELY IN
C     THE MAIN PROOGRAM AND IN CURFIT
C
C     ENTER TEETA IN DEGREES
C     DIMENSIONS OF Q,V IN JACOBI1 SHOULD BE THE SAME AS
C     THOSE OF B3,B2 RESPECTIVELY IN CURFIT
C
C     PARAMETERS=I. GT IS G**2-TENSOR
C             (G**2ZZ,G**2ZX,G**2XX,G**2ZY,G**2YY,G**2XY)
C             GGT(J,NUMBER) REPRESENTS G-SQUARE TENSOR.
C                II. (B(I),I=1,6)=AZZ,AZX,AXX,AZY,AYY,AXY
C     A=A-SQUARE TENSOR ABOVE
C                ENTER A WITH POSITIVE SIGN
C
C     DELANG(I,J),J=1,2,3 ARE ANGLE CORRECTIONS FOR ZX,ZY,
```

```
C         XY PLANES AS DETERMINED BY "KRDBLT" FOR VARIOUS
C         CASES.
C
C     NUMBER=INDEX THAT CHANGES WITH EACH NEW CASE ITS VALUE
C            SHOULD BE THAT OF THE FIRST CASE CONSIDERED.
C     NCASES=NO. OF LAST CASE CONSIDERED. ITS VALUE SHOULD
C            BE ENTERED.
C
C     N1(J1,NUMBER)=NO.OF LINES(FOR VARIOUS ORIENTATIONS)
C     FOR J1 HYPERFINE LINE OF CASE NO.=NUMBER
C
C     ZZ(J,K,L)=LINE POSITIONS,J=WHICH ONE OF
C               K=HYPERFINE LINE OF CASE NO.=L
C
C
      DIMENSION Z(400),FM(400),FC(400),DF(400),ERR(400),
     1B(12),B1(12),B2(12,12),DC(5000),ABC(2),Y(4),HN(400),
     2G(6,12),GG(6,8),SMD(9),AAA(3,3),QQQ(3,3),AAV(3,3),
     3QQV(3,3),IBB(400,2),THETA(400),D1(12),D2(12,12),
     4HHN(3,8),AADD(3,8),FFACTR(3,8),TEETA(100,4,8),
     5ZZ(100,4,8),NN(8),N1(4,8),ACOSZ(400),ACOSX(400),
     6ACOSY(400),DELANG(8,3),AJ1(400),GGT(3,3),GGTT(8,3,3),
     7DELHH(400,8),DELH(400),A4(3),LZX(1),LZY(1),LXY(1),
     8NZERO(1),NCASES(1)
C
      COMMON/DATA1/ABC,Y
      COMMON/DATA2/DC,ACOSZ,ACOSX,ACOSY,AJ1
      COMMON/DATA3/DELH
      EQUIVALENCE (Z,DC),(FM,DC(401)),(FC,DC(801)),
     1(DF,DC(1201)),(ERR,DC(1601)),(HN,DC(2001)),
     2(THETA,DC(2401)),(IBB,DC(2801)),(B,DC(4101)),
     3(B1,DC(4125)),(B2,DC(4137)),(N,DC(4301)),
     4(L4,DC(4302)),(Q1,DC(4303)),(Q2,DC(4304)),
     5(M,DC(4305)),(I,DC(4306)),(L,DC(4307)),(BO,DC(4308)),
     6(SMD,DC(4309)),(SSMD,DC(4320)),(D1,DC(4321)),
     7(D2,DC(4333)),(NUMBER,DC(4100)),(GT,DC(4093))
```

```
C
      READ(5,*) NZERO,NCASES,LZX,LZY,LXY
      WRITE(58,5123) NZERO,NCASES,LZX,LZY,LXY
 5123 FORMAT(1X, 6HNZERO=,I8, 7HNCASES=,I8,
     1 4HLZX=,I8, 4HLZY=,I8, 4HLXY=,I8)
      READ(5,*)(HHN(J,NCASES),J=1,3)
      READ(5,*)(FFACTR(J,NCASES),J=1,3)
      READ(5,*)(AADD(J,NCASES),J=1,3)
      READ(5,*)(G(NCASES,J),J=1,3)
      READ(5,*)(G(NCASES,J),J=7,12)
      READ(5,*)(DELANG(NCASES,J),J=1,3)
      READ(5,*)(GGTT(NCASES,1,J),J=1,3)
      READ(5,*)(GGTT(NCASES,2,J),J=1,3)
      READ(5,*)(GGTT(NCASES,3,J),J=1,3)
      READ(5,*)(N1(J,NCASES),J=1,4)
      NSUM=0
      II=0
      NXY=0
      NSUM=LZX+LZY+LXY
      NSUM=4*NSUM
      READ(5,*)(DELHH(J,NCASES),J=1,NSUM)
      READ(5,*)(TEETA(J,1,NCASES),J=1,LZX)
      READ(5,*)(ZZ(J,1,NCASES),J=1,LZX)
      READ(5,*)(ZZ(J,2,NCASES),J=1,LZX)
      READ(5,*)(ZZ(J,3,NCASES),J=1,LZX)
      READ(5,*)(ZZ(J,4,NCASES),J=1,LZX)
      II=LZX+1
      NXY=LZX+LZY
      READ(5,*)(TEETA(J,1,NCASES),J=II,NXY)
      READ(5,*)(ZZ(J,1,NCASES),J=II,NXY)
      READ(5,*)(ZZ(J,2,NCASES),J=II,NXY)
      READ(5,*)(ZZ(J,3,NCASES),J=II,NXY)
      READ(5,*)(ZZ(J,4,NCASES),J=II,NXY)
      II=NXY+1
      NXY=NXY+LXY
      READ(5,*)(TEETA(J,1,NCASES),J=II,NXY)
```

```
      READ(5,*)(ZZ(J,1,NCASES),J=II,NXY)
      READ(5,*)(ZZ(J,2,NCASES),J=II,NXY)
      READ(5,*)(ZZ(J,3,NCASES),J=II,NXY)
      READ(5,*)(ZZ(J,4,NCASES),J=II,NXY)
C
  188 FORMAT(1H1)
    8 FORMAT(1X,4HQ1 = ,E13.5,5X,4HQ2 = ,E13.5)
  137 FORMAT (3X,I2,5X,E16.6/)
  136 FORMAT(10X,19H INITIAL
     1PARAMETERS//3X,1HJ,10X,4HB(J)//)
  135 FORMAT(1X,11H PARAMETERS//3X,1HJ,
     110X,4HB(J),27X,6HERRORS//)
    9 FORMAT(2X,4H HN= ,F9.4)
  140 FORMAT(3X,I2,5X,E16.6,15X,E16.6/)
  138 FORMAT(5X,14H CASE NUMBER =,I2//)
  141 FORMAT(10X,6H SMD =,E13.5//)
  235 FORMAT (15X,5(E13.5,8X)/)
  236 FORMAT(15X,3(E13.5,8X)///)
 7237 FORMAT(15X,*DIAGONAL ELEMENTS
     1OF G-SQUARE TENSOR ARE=*,///)
  237 FORMAT(15X,*DIAGONAL ELEMENTS
     1OF A-SQUARE TENSOR ARE=*,///)
  238 FORMAT(15X,*"G" DIR. COS.(ROWS) ACC.
     1TO E.VALS. ABOVE=  *,///)
 7238 FORMAT(15X,*"A" DIR. COS.(ROWS) ACC.
     1TO E.VALS. ABOVE=  *,///)
      PI2=2.*3.1415926
      RD=PI2/360.
      NZERO=1
      NUMBER=NZERO
      NCASES=1
      M=12
      L4=7
      Q1=1.E-8
      Q2=1.E-20
      MM=M
```

```
      WRITE(58,188)
    1 CONTINUE
       N11=N1(1,NUMBER)
       DO 1188 J=1,4
       DO 1188 J1=1,N11
 1188 TEETA(J1,J,NUMBER)=TEETA(J1,1,NUMBER)
       DO 300 IA=1,3
       DO 300 JA=1,3
 300   GGT(IA,JA)=GGTT(NUMBER,IA,JA)
      WRITE(58,121)
      DO 122 IA=1,3
  122 WRITE(58,123) (GGT(IA,JA),JA=1,3)
  121 FORMAT(5X,*ELEMENTS OF INITIAL GGT MATRIX AS THE
     1MATRIX OF DIR. COSINES OF G-SQUARE TENSOR ARE=*,//)
  123 FORMAT(5X,3(F10.6,2X),/)
       CALL EULER(GGT,THITA,PHI,PSI)
       B(4)=THITA
       B(5)=PHI
       B(6)=PSI
       LINE=0
      DO 150 J1=1,8
      NN1=N1(J1,NUMBER)
      DO 150 I1=1,NN1
      LINE=LINE+1
      AJ1(LINE)=J1
      THETA(LINE)=TEETA(I1,J1,NUMBER)
      IF(THETA(LINE).GT.8000.) GO TO 155
      IF(THETA(LINE).LT.0.) GO TO 160
      TH=THETA(LINE)*RD+DELANG(NUMBER,1)*RD
      ACOSZ(LINE)=COS(TH)
      ACOSX(LINE)=SIN(TH)
      ACOSY(LINE)=0.
      HN(LINE)=HHN(1,NUMBER)
C     Z(LINE)=(ZZ(I1,J1,NUMBER)+
     1AADD(1,NUMBER))*FFACTR(1,NUMBER)
      Z(LINE)=(ZZ(I1,J1,NUMBER)*
```

```
     1FFACTR(1,NUMBER)+AADD(1,NUMBER))
      IF(ZZ(I1,J1,NUMBER).EQ.0.) Z(LINE)=0.
 9160 FORMAT(5X,*ACOSZ ETC=*,3E12.5)
      GO TO 165
  160 TH=-THETA(LINE)*RD + DELANG(NUMBER,2)*RD
      ACOSZ(LINE)=COS(TH)
      ACOSY(LINE)=SIN(TH)
      ACOSX(LINE)=0.
      HN(LINE)=HHN(2,NUMBER)
C     Z(LINE)=(ZZ(I1,J1,NUMBER)+
     1AADD(2,NUMBER))*FFACTR(2,NUMBER)
      Z(LINE)=(ZZ(I1,J1,NUMBER)*
     1FFACTR(2,NUMBER)+AADD(2,NUMBER))
      IF(ZZ(I1,J1,NUMBER).EQ.0.) Z(LINE)=0.
      GO TO 165
  155 TH=THETA(LINE)*RD+DELANG(NUMBER,3)*RD
      ACOSZ(LINE)=0.
      ACOSX(LINE)=COS(TH)
      ACOSY(LINE)=SIN(TH)
      HN(LINE)=HHN(3,NUMBER)
C     Z(LINE)=(ZZ(I1,J1,NUMBER)+
     1AADD(3,NUMBER))*FFACTR(3,NUMBER)
      Z(LINE)=(ZZ(I1,J1,NUMBER)*
     1FFACTR(3,NUMBER)+AADD(3,NUMBER))
      IF(ZZ(I1,J1,NUMBER).EQ.0.) Z(LINE)=0.
  165 CONTINUE
  150 CONTINUE
      NN(NUMBER)=LINE
      N=NN(NUMBER)
      N9=N
      DO 210 LL=1,MM
      IF (LL.GT.3.AND.LL.LT.7) GO TO 210
      B(LL)=G(NUMBER,LL)
  210 CONTINUE
      WRITE(58,138) NUMBER
      WRITE(58,136)
```

```
      WRITE(58,137) (J,B(J),J=1,M)
      WRITE(58,6659)
      WRITE(58,6657) (Z(J),J=1,N)
      WRITE(58,6660)
      WRITE(58,6657) (HN(J),J=1,N)
 6660 FORMAT(5X,*FREQUENCY-KLYSTRON ARE=*,/)
 6659 FORMAT(5X,*MAG. FIELD VALUES ARE=*,/)
 6657 FORMAT(5X,8(E12.5,2X))
      DO 201 II=1,N9
      DELH(II)=DELHH(II,NUMBER)
  201 FM(II) = HN(II)
      CALL CURFIT
      SMD(NUMBER) = SSMD
      WRITE(58,188)
      WRITE(58,135)
      DO 220 LL=1,M
  220 GG(LL,NUMBER) = B(LL)
      WRITE(58,140)(J,B(J),B1(J),J=1,M)
      WRITE(58,188)
    3 CONTINUE
      SSS=0.
      SSS1=0.
      DO 555 ID=1,N
      SSS=DF(ID)**2
      SSS1=SSS1+SSS
      WRITE(58,656) ID,SSS
 555  CONTINUE
      WRITE(58,6656) SSS1
 6656 FORMAT(/,10X,*CHI-SQUARE=*,E13.5,/)
  656 FORMAT(10X,*LINE NUMBER = *,I3,5X,*SMD = *,E13.5)
      WRITE (58,7237)
      WRITE(58,236) (B(J1),J1 = 1,3)
      WRITE (58,238)
      SB4L=SIN(B(4))
      CB4L=COS(B(4))
      SB5L=SIN(B(5))
```

```
      CB5L=COS(B(5))
      SB6L=SIN(B(6))
      CB6L=COS(B(6))
      GGT(1,1)=CB4L
      GGT(1,2)=SB4L*SB5L
      GGT(1,3)=-SB4L*CB5L
      GGT(2,1)=SB6L*SB4L
      GGT(2,2)=CB6L*CB5L-CB4L*SB5L*SB6L
      GGT(2,3)=CB6L*SB5L+CB4L*CB5L*SB6L
      GGT(3,1)=CB6L*SB4L
      GGT(3,2)=-SB6L*CB5L-CB4L*SB5L*CB6L
      GGT(3,3)=-SB6L*SB5L+CB4L*CB5L*CB6L
      DO 25 J1 = 1,3
      WRITE (58,236)  (GGT(J1,J2),J2 = 1,3)
   25 CONTINUE
      DO 245 J=1,3
  245 A4(J)=SQRT(B(J))
      WRITE (58,246)
      WRITE(58,236)(A4(J),J=1,3)
  246 FORMAT(5X,*PRINCIPAL VALUES OF G-TENSOR ARE=*,/)
      AAA(1,1)=B(7)
      AAA(1,2)=B(8)
      AAA(2,2)=B(9)
      AAA(1,3)=B(10)
      AAA(3,3)=B(11)
      AAA(2,3)=B(12)
      DO 720 J1=1,2
      J4=J1+1
      DO 720 J2=J4,3
      AAA(J2,J1)=AAA(J1,J2)
  720 CONTINUE
      CALL JACOBI3(3,AAA,1,NR,AAV)
      WRITE (58,237)
      WRITE (58,236)  (AAA(J1,J1),J1=1,3)
      WRITE (58,7238)
      DO 725 J1=1,3
```

```
      WRITE (58,236) (AAV(J2,J1),J2=1,3)
  725 CONTINUE
      DO 7245 J=1,3
       IF (AAA(J,J) .LT. 1.0E-4) AAA(J,J)=0
 7245 A4(J)=SQRT(AAA(J,J))
      WRITE (58,7246)
      WRITE (58,236) (A4(J),J=1,3)
 7246 FORMAT(5X,*PRINCIPAL VALUES OF A-TENSOR ARE=*,/)
      NUMBER=NUMBER+1
      IF(NUMBER-NCASES) 1,1,2
    2 CONTINUE
      DO 230 LL=NZERO,NCASES
      WRITE(58,138) LL
      WRITE(58,141) SMD(LL)
  230 WRITE (58,235) (GG(LM,LL),LM=1,MM)
      STOP
      END
      SUBROUTINE CURFIT
C
C     EXAM  HANDLES ALL MATRICES OF DIMENSIONS UPTO THE
C     DIMS.MM OF A,B,C THAT IS M IS LESS THAN OR EQUAL TO
C     MM (SAME IS TRUE OF MATINV AND JACOBI)
C
C     EQUIVALENCE OF GRAD BEGINS AT DIMENSION OF
C               B AFTER THE EQUIV. OF B
C
C        F O R T R A N  4
      DIMENSION Z(400),FM(400),FC(400),DF(400),ERR(400),
     1B(12),B1(12),B2(12,12),DC(5000),ABC(2),Y(4),X(400),
     2GRAD(12),D1(12),D2(12,12),B3(12,12),SMD(9),HN(400),
     3ACOSZ(400),ACOSX(400),ACOSY(400)
      DIMENSION IBB(400,2),THETA(400),GT(6)
      DIMENSION AJ1(400),GGTL(8,3),GGTM(8,3),GGTN(8,3)
      COMMON/DATA1/ABC,Y
      COMMON/DATA2/DC,ACOSZ,ACOSX,ACOSY,AJ1
      EQUIVALENCE (Z,DC),(FM,DC(401)),(FC,DC(801)),
```

```
     1(DF,DC(1201)),(ERR,DC(1601)),(HN,DC(2001)),
     2(THETA,DC(2401)),(IBB,DC(2801)),(B,DC(4101)),
     3(B1,DC(4125)),(B2,DC(4137)),(N,DC(4301)),
     4(L4,DC(4302)),(Q1,DC(4303)),(Q2,DC(4304)),
     5(M,DC(4305)),(I,DC(4306)),(L,DC(4307)),(BO,DC(4308)),
     6(SMD,DC(4309)),(SSMD,DC(4320)),(D1,DC(4321)),
     7(D2,DC(4333)),(GRAD,DC(4113)),
     6(NUMBER,DC(4100)),(GT,DC(4093))
C
      ABC(1)="NO"
      ABC(2)="YES"
      L1 = 0
      SA = 0.0
      MM=M
      I6=I
      NN=N
      DO 1000 J=1,MM
      B1(J)=0.0
      DO 1000 K=1,MM
 1000 B2(J,K)=0.0
      DO 100 I6 = 1, NN
      L=1
      I=I6
      CALL FUNC(2)
      X(I6)=ERR(I6)**2
 901  FORMAT(5X,10H FUNC2,2I0   )
      DF(I6) =FM(I6) - FC(I6)
      DO 101 J=1,MM
      B1(J)=B1(J)-(2.0*DF(I6)*D1(J))/X(I6)
      DO 101 K=1,MM
  101 B2(J,K)=B2(J,K)-(2.0*(DF(I6)*D2(J,K)-
     1D1(J)*D1(K)))/X(I6)
  100 SA = SA + DF(I6)**2/X(I6)
      GMOD=0.0
      DO 102 J=1,M
  102 GMOD=GMOD+B1(J)**2
```

```
      WRITE(58,243)SA,GMOD
  243 FORMAT (1X,26H*INITIAL VALUE SUM OF SQ.=E13.5,20X,
     117H*SQ MOD OF GRAD =E13.5)
      WRITE(58,1751)
 1751 FORMAT(14H0 DERIVATIVES-)
      WRITE(58,240)(B1(J),J=1,M)
  240 FORMAT (15X,5(E13.5,8X)/)
      IF (SA - Q1) 110, 110, 200
  110 LE = 1
      GO TO 600
  200 S = 0.0
      GMOD = 0.0
      BMOD = 0.0
      PROD = 0.0
      DO 210 K = 1, MM
  210 B2(J,K) = 0.0
      WRITE(58,902)
      DO 220 I6 = 1, NN
      L=1
      I=I6
      CALL FUNC(2)
      X(I6)=ERR(I6)**2
 902  FORMAT(5X,10H FUNC2,210   )
      DF(I6) = FM(I6) - FC(I6)
      DO 220 J = 1, MM
      B1(J) = B1(J) - (2.0*DF(I6)*D1
  200 S = 0.0
      GMOD = 0.0
      BMOD = 0.0
      PROD = 0.0
      DO 210 K = 1, MM
  210 B2(J,K) = 0.0
      WRITE(58,902)
      DO 220 I6 = 1, NN
      L=1
      I=I6
      CALL FUNC(2)
```

```
      X(I6)=ERR(I6)**2
902   FORMAT(5X,10H FUNC2,210  )
      DF(I6) = FM(I6) - FC(I6)
      DO 220 J = 1, MM
      B1(J) = B1(J) - (2.0*DF(I6)*D1     DO 231 JJ=1,M
 231  B3(II,JJ)=B2(II,JJ)
      WRITE (58,904)
      CALL JACOBI4(M,B3,4,NR,B2)
904   FORMAT(5X,12H JACOBI1,231  )
      WRITE(58,904)
      DO 235 I6=1,MM
 235  B1(I6)=B3(I6,I6)
      A2=ABC(2)
      DO 260 J = 1, MM
 260  D1(J) = 0.0
      DO 270 J = 1, MM
      DO 270 K = 1, MM
 270  D1(K) = D1(K) + B2(J,K) *GRAD(J)
      DO 275 J = 1, MM
      IF (B1(J))  280, 290, 285
 280  B1(J) = - B1(J)
 285  D1(J) = D1(J)/B1(J)
      GO TO 275
 290  D1(J) = 0.0
 275  CONTINUE
      DO 295 J = 1, MM
 295  B1(J) = 0.0
      DO 300 J = 1, MM
      DO 300 K = 1, MM
 300  B1(J) = B1(J) + B2(J,K)*D1(K)
 305  DO 310 J=1,MM
      GMOD = GMOD + GRAD(J)**2
      BMOD = BMOD + B1(J)**2
 310  PROD = PROD + GRAD(J)*B1(J)
      IF (GMOD - Q2)  315, 315, 320
 315  LE = 2
```

```
     WRITE(58,1761) GMOD
1761 FORMAT(5X,7H GMOD =,E13.5//)
     GO TO 600
 320 C=PROD/SQRT(BMOD*GMOD)
     IF (C) 335, 335, 400
 335 LE = 4
     GO TO 600
 400 LD = 0
     L3 = 0
     DO 410 J = 1, MM
 410 GRAD(J) = B(J) - B1(J)
 450 DO 420 I6 = 1, NN
     L=2
     I=I6
     CALL FUNC (1)
     X(I6)=ERR(I6)**2
905  FORMAT(5X,10H FUNC1,450  )
     DF(I6) = FM(I6) - FC(I6)
 420 S = S + DF(I6)**2/X(I6)
     WRITE(58,905)
     IF (SA - S) 435, 500, 500
 435 LD = LD + 1
 430 DO440 J = 1, MM
     B1(J) = B1(J)/2.0
906  FORMAT(5X,16H BINARY CHOP,430  )
 440 GRAD(J) = B(J) - B1(J)
     WRITE(58,906)
     S = 0.0
     L3 = L3 + 1
     IF(L3-5)450,460,460
 460 LE = 5
     GO TO 600
 500 IF (LD) 505, 505, 506
 506 LD = 0
     GO TO 430
 505 DO 510 J = 1, MM
```

```
 510 B(J) = GRAD(J)
     SA = S
     IF (SA - Q1) 507, 507, 530
 507 LE = 1
     GO TO 600
 530 IF (L4) 200, 200, 900
 900 WRITE(58,920)L1,A2,L3,S,GMOD,(B(J),J=1,M)
 920 FORMAT(//,15H ITERATION NO.=I5,10X,43H   TRANSFOR
    1MATION MADE TO PRINCIPAL AXES = A4,10X,   18H BINARY
    2CHOP USED=I3,6H TIMES/1X,27H WEIGHTED SUM OF SQUARES =
    3E14.7,25X,32H   SQUARE MODULUS OF GRADIENT = E14.7/
    420H   PARAMETERS B(J) -/(6E17.8)/)
     IF (L1 - L4) 200, 910, 910
 910 LE = 6
     GO TO 600
 600 DO 710 J=1,MM
     B1(J) = 0.0
     DO 710 K=1,MM
 710 B2(J,K) = 0.0
     L=1
     WRITE(58,907)
 907 FORMAT(5X,* FUNC(2),720 *)
     DO 720 I6 = 1, NN
     I=I6
     CALL FUNC(2)
     X(I6)=ERR(I6)**2
     DF(I6) = FM(I6) - FC(I6)
     DO 720 J = 1, MM
     B1(J) = B1(J) - (2.0*DF(I6)*D1(J))/X(I6)
     DO 720 K = 1, MM
 720 B2(J,K) = B2(J,K) - ((DF(I6)*D2(J,K) -
    1D1(J)*D1(K)))/X(I6)
     WRITE (58,3029)
3029 FORMAT(* I AM LOST IN MANTINV*)
     CALL MATINV(B2,M,B1,1,DETERM)
     WRITE (58,3029)
```

```
      DO 730 J=1,MM
      IF (B2(J,J)) 2001,2001,2002
2001  B1(J) = -SQRT(-B2(J,J))
      GO TO 730
2002  B1(J)= SQRT(B2(J,J))
  730 CONTINUE
      DO 740 J=1,MM
      DO 740 K=1,MM
  740 B2(J,K)=B2(J,K)/(B1(J)*B1(K))
      WRITE(58,551)LE,SA
  551 FORMAT(//,13H EXIT NUMBER=I3,20X,25H WEIGHTED SUM
     1OF SQUARES=E15.8//)
      SSMD = SA
9999  CONTINUE
      RETURN
      END

      SUBROUTINE FUNC(LX)
C     SUBROUTINE FUNC
C
C
      DIMENSION DC(5000),B(12,2),D1(12),D2(12,12),FC(400),
     1Z(400),S(4,4),SIGN(400),HN(400),ST(4,4,16),FM(400),
     2DF(400),DELH(400),ERR(400),B1(12),B2(12,12),SMD(9),
     3ACOSZ(400),ACOSX(400),ACOSY(400),IBB(400,2),
     4THETA(400),DD(16),GT(6),AJ1(400),AL(400),AM(400),
     5AN(400),GGT(3,3),C1(12),AZ(6),AX(6),AY(6),GB(6),
     6F2(6),C2(12),C3(12),CK(12),F4(12),CC(12),AK2(6),BB(6)
      COMMON/DATA2/DC,ACOSZ,ACOSX,ACOSY,AJ1
      COMMON/DATA3/DELH
      EQUIVALENCE (Z,DC),(FM,DC(401)),(FC,DC(801)),
     1(DF,DC(1201)),(ERR,DC(1601)),(HN,DC(2001)),
     2(THETA,DC(2401)),(IBB,DC(2801)),(B,DC(4101)),
     3(B1,DC(4125)),(B2,DC(4137)),(N,DC(4301)),
     4(L4,DC(4302)),(Q1,DC(4303)),(Q2,DC(4304)),
     5(M,DC(4305)),(I,DC(4306)),(L,DC(4307)),(BO,DC(4308)),
```

```
   6(SMD,DC(4309)),(SSMD,DC(4320)),(D1,DC(4321)),
   7(D2,DC(4333)),(NUMBER,DC(4100)),(GT,DC(4093))
    IF(Z(I).EQ.0.) GO TO 135
    BETA=92.732/66252.
    BETAN=.00054464*BETA
    RD=3.1415926/180.
    FACTOR=92.732/66252.
    SB4L=SIN(B(4,L))
    CB4L=COS(B(4,L))
    SB5L=SIN(B(5,L))
    CB5L=COS(B(5,L))
    SB6L=SIN(B(6,L))
    CB6L=COS(B(6,L))
    GGT(1,1)=CB4L
    GGT(1,2)=SB4L*SB5L
    GGT(1,3)=-SB4L*CB5L
    GGT(2,1)=SB6L*SB4L
    GGT(2,2)=CB6L*CB5L-CB4L*SB5L*SB6L
    GGT(2,3)=CB6L*SB5L+CB4L*CB5L*SB6L
    GGT(3,1)=CB6L*SB4L
    GGT(3,2)=-SB6L*CB5L-CB4L*SB5L*CB6L
    GGT(3,3)=-SB6L*SB5L+CB4L*CB5L*CB6L
    IF (I.GT.1) GO TO 119
    WRITE(58,118)
    DO 117 IA=1,3
117 WRITE(58,116) (GGT(IA,IB),IB=1,3)
116 FORMAT(5X,3(F10.6,3X),/)
118 FORMAT(5X,*ELEMENTS OF COMPUTED GGT MATRIX FROM
   1EULER ANGLES ARE=*, //)
119 CONTINUE
    AL(I)=ACOSZ(I)*GGT(1,1)+ACOSX(I)*GGT(1,2)+
   1 ACOSY(I)*GGT(1,3)
    AM(I)=ACOSZ(I)*GGT(2,1)+ACOSX(I)*GGT(2,2)+
   2 ACOSY(I)*GGT(2,3)
    AN(I)=ACOSZ(I)*GGT(3,1)+ACOSX(I)*GGT(3,2)+
   3 ACOSY(I)*GGT(3,3)
```

```
      FCI=B(1,L)*AL(I)**2+B(2,L)*AM(I)**2+B(3,L)*AN(I)**2
      ENELSP=Z(I)*BETA*SQRT(FCI)
      BB(1)=B(1,L)*AL(I)**2
      BB(3)=B(2,L)*AM(I)**2
      BB(5)=B(3,L)*AN(I)**2
      BB(2)=2.*SQRT(B(1,L)*B(2,L))*AL(I)*AM(I)
      BB(4)=2.*SQRT(B(1,L)*B(3,L))*AL(I)*AN(I)
      BB(6)=2.*SQRT(B(2,L)*B(3,L))*AM(I)*AN(I)
      AEFF2=B(7,L)*BB(1)+B(9,L)*BB(3)+B(11,L)*BB(5)+
     1 B(8,L)*BB(2)+B(10,L)*BB(4)+B(12,L)*BB(6)
      AMI=2.5-AJ1(I)
      IF(AEFF2.LT.(0.)) GO TO 109
      AEFF=SQRT(AEFF2/FCI)
      HYPFEN=AEFF*AMI
      CC(7)=B(7,L)**2+B(8,L)**2+B(10,L)**2
      CC(8)=B(7,L)*B(8,L)+B(8,L)*B(9,L)+B(10,L)*B(12,L)
      CC(9)=B(8,L)**2+B(9,L)**2+B(12,L)**2
      CC(10)=B(7,L)*B(10,L)+B(8,L)*B(12,L)+B(10,L)*B(11,L)
      CC(11)=B(10,L)**2+B(12,L)**2+B(11,L)**2
      CC(12)=B(8,L)*B(10,L)+B(9,L)*B(12,L)+B(11,L)*B(12,L)
      CKK=CC(7)*BB(1)+CC(9)*BB(3)+CC(11)*BB(5)+CC(8)*BB(2)+
     1    CC(10)*BB(4)+CC(12)*BB(6)
      AKK=SQRT(CKK/AEFF2)
      AI=3.5
      AI1=AI*(AI+1.)
      DELE3=(0.5*(B(7,L)+B(9,L)+B(11,L))*(AI1-AMI**2)-
     1 AKK**2*(AI1-3.*AMI**2)/2.-HYPFEN**2)/(2.*ENELSP)
      FC(I)=ENELSP+HYPFEN+DELE3
      ERR(I)=SQRT(FCI)*DELH(I)*FACTOR
      ERR(I)=1.
      GO TO 136
  135 CONTINUE
      FC(I)=HN(I)
      ERR(I)=1.
  136 CONTINUE
      IF(LX-1)110,110,120
```

```
  120 CONTINUE
      DO  235 IZ = 1,12
      D1(IZ) = 0.0
      DO  235 JZ = 1,12
  235 D2(IZ,JZ) =0.0
      IF(Z(I).EQ.0.) GO TO 110
      DDD=.5*AMI/(FCI*AEFF)
      C2(7)=DDD*BB(1)
      C2(8)=DDD*BB(2)
      C2(9)=DDD*BB(3)
      C2(10)=DDD*BB(4)
      C2(11)=DDD*BB(5)
      C2(12)=DDD*BB(6)
C
      BETAB=BETA*Z(I)
      GZ=SQRT(B(1,L))
      GX=SQRT(B(2,L))
      GY=SQRT(B(3,L))
      AZZ=SQRT(BB(1))
      AXX=SQRT(BB(3))
      AYY=SQRT(BB(5))
      AZ(1)=0.5*AL(I)/GZ
      AZ(2)=AZ(3)=0.
      AX(2)=0.5*AM(I)/GX
      AX(1)=AX(3)=0.
      AY(3)=0.5*AN(I)/GY
      AY(1)=AY(2)=0.
      ALL=ACOSX(I)
      AMM=ACOSY(I)
      ANN=ACOSZ(I)
      AZ(4)=GZ*(ALL*CB4L*SB5L-AMM*CB4L*CB5L-ANN*SB4L)
      AZ(5)=GZ*(ALL*SB4L*CB5L+AMM*SB4L*SB5L)
      AZ(6)=0.
      AX(4)=GX*(ALL*SB4L*SB5L*SB6L-AMM*SB4L*
     1CB5L*SB6L+ANN*CB4L*SB6L)
      AX(5)=GX*(ALL*(-CB6L*SB5L-CB4L*CB5L*SB6L)+
```

```
     1AMM*(CB6L*CB5L-CB4L*SB5L*SB6L))
      AX(6)=GX*(ALL*(-SB6L*CB5L-CB4L*SB5L*CB6L)+
     1AMM*(-SB6L*SB5L+CB4L*CB5L*CB6L)+ANN*CB6L*SB4L)
      AY(4)=GY*(ALL*SB4L*SB5L*CB6L-
     1AMM*SB4L*CB5L*CB6L+ANN*CB6L*CB5L)
      AY(5)=GY*(ALL*(SB6L*SB5L-CB4L*CB5L*CB6L)+
     1AMM*(-SB6L*CB5L-CB4L*SB5L*CB6L))
      AY(6)=GY*(ALL*(-CB6L*CB5L+CB4L*SB5L*SB6L)+
     1AMM*(-CB6L*SB5L-CB4L*CB5L*SB6L)-ANN*SB6L*SB4L)
      DO 910 IA=1,6
      GB(IA)=(AZZ*AZ(IA)+AXX*AX(IA)+
     1AYY*AY(IA))*BETAB/ENELSP
      IA1=IA+6
      C1(IA1)=0.
  910 C1(IA)=BETAB*GB(IA)
C     C1(IA) ARE DERIVATIVES OF ENELSP
      AXX=SQRT(BB(3))
      AYY=SQRT(BB(5))
      AZZ=SQRT(BB(1))
      F2(1)=2.*AZ(1)*(AZZ*B(7,L)+AXX*B(8,L)+AYY*B(10,L))
      F2(2)=2.*AX(2)*(AZZ*B(8,L)+AXX*B(9,L)+AYY*B(12,L))
      F2(3)=2.*AY(3)*(AZZ*B(10,L)+AXX*B(12,L)+AYY*B(11,L))
      DO 915 IA=4,6
      F2(IA)=2.*(AXX*AX(IA)*B(9,L)+AYY*AY(IA)*B(11,L)+
     1       AZZ*AZ(IA)*B(7,L)+(AXX*AY(IA)+AYY*AX(IA))*
     2       B(12,L)+(AXX*AZ(IA)+AZZ*AX(IA))*B(8,L)+
     3       (AYY*AZ(IA)+AZZ*AY(IA))*B(10,L))
  915 CONTINUE
      F4(1)=2.*AZ(1)*(AZZ*CC(7)+AXX*CC(8)+AYY*CC(10))
      F4(2)=2.*AX(2)*(AZZ*CC(8)+AXX*CC(9)+AYY*CC(12))
      F4(3)=2.*AY(3)*(AZZ*CC(10)+AXX*CC(12)+AYY*CC(11))
      DO 920 IA=4,6
      F4(IA)=2.*(AXX*AX(IA)*CC(9)+AYY*AY(IA)*CC(11)+
     1   AZZ*AZ(IA)*CC(7)+(AXX*AY(IA)+AYY*AX(IA))*CC(12)+
     2   (AXX*AZ(IA)+AZZ*AX(IA))*CC(8)+
     3   (AYY*AZ(IA)+AZZ*AY(IA))*CC(10))
```

```
  920 CONTINUE
      DO 925 IA=1,6
  925 C2(IA)=(-BETAB*HYPFEN*GB(IA)/ENELSP+
     1      (BETAB**2)*F2(IA)/(2.*(ENELSP**2)*HYPFEN))*AMI
C     C2(IA) ARE DERIVATIVES OF HYPFEN
      DO 927 IA=1,6
      IA1=IA+1
  927 C2(IA1)=(AMI**2)*BB(IA)/(0.5*FCI*HYPFEN)
      DO 930 IA=1,6
  930 AK2(IA)=((BETAB*AMI/(ENELSP*HYPFEN))**2)*(F4(IA)-
     1    (2.*CCK/(ENELSP*HYPFEN))*
     2    (C1(IA)*HYPFEN+ENELSP*C2(IA)))
      DO 935 IA=1,6
  935 C3(IA)=(ENELSP*(-0.5*(AI1-3.*(AMI**2))*AK2(IA)-2.*
     1HYPFEN*C2(IA))-(0.5*(B(7,L)+B(9,L)+B(11,L))*
     2(AI1-(AMI**2))-0.5*(AKK**2)*(AI1-3.*(AMI**2))-
     3HYPFEN**2)*C1(IA))/(2.*(ENELSP**2))
C     C3(IA) ARE DERIVATIVES OF DELE3
C
      F4(7)=2.*BB(1)*B(7,L)+BB(2)*B(8,L)+BB(4)*B(10,L)
      F4(8)=2.*(BB(1)+BB(3))*B(8,L)+BB(2)*(B(7,L)+B(9,L))+
     1 BB(4)*B(12,L)+BB(6)*B(10,L)
      F4(9)=2.*BB(3)*B(9,L)+BB(2)*B(8,L)+BB(6)*B(12,L)
      F4(10)=2.*(BB(1)+BB(5))*B(10,L)+BB(4)*(B(7,L)+
     2 B(11,L))+BB(2)*B(12,L)+BB(6)*B(8,L)
      F4(11)=2.*BB(5)*B(11,L)+BB(4)*B(10,L)+BB(6)*B(12,L)
      F4(12)=2.*(BB(3)+BB(5))*B(12,L)+BB(6)*(B(9,L)+
     3 B(11,L))+BB(2)*B(10,L)+BB(4)*B(8,L)
      DO 1237 IA=7,12
 1237 CK(IA)=-AKK*C2(IA)/(AEFF*AMI)+F4(IA)/
     1 (2.*FCI*(AEFF**2)*AKK)
      DO 1236 IA=7,12
      AIA=0.
      IF (IA.EQ.7.OR.IA.EQ.9.OR.IA.EQ.11) AIA=1.
 1236 C3(IA)=(AKK*CK(IA)*(3.*AMI**2-AI1)+0.5*
     1 (AI1-AMI**2)*AIA-2.*HYPFEN*C2(IA))/(2.*ENELSP)
```

```
      DO 1235 IA=1,12
 1235 D1(IA)=C1(IA)+C2(IA)+C3(IA)
      GO TO 110
  109 WRITE(58,108) I
  108 FORMAT(5X,*NEG AEFF2 FOR I=*,I3)
      FC(I)=FM(I)
      DO 197 JJ=1,12
  197 D1(JJ)=0.
  110 CONTINUE
      RETURN
      END
C
      SUBROUTINE EULER(GGT,THETA,PHI,PSI)
C     THIS PROGRAMME CALCULATES THE EULER ANGLES THETA,
C     PHI AND PSI FROM THE DIRECTION COSINES OF G-SQUARE
C     DIAGONAL MATRIX.
C
      DIMENSION GGT(3,3),TPS(4,4,4),AMTRX(9),BMTRX(64,9),
     1 A(64),B(64),C(64),IA(64),IB(64),IC(64),ABSMT(9)
      AMTRX(1)=GGT(1,1)
      AMTRX(2)=GGT(1,2)
      AMTRX(3)=GGT(1,3)
      AMTRX(4)=GGT(2,1)
      AMTRX(5)=GGT(2,2)
      AMTRX(6)=GGT(2,3)
      AMTRX(7)=GGT(3,1)
      AMTRX(8)=GGT(3,2)
      AMTRX(9)=GGT(3,3)
      DO 50 I=1,9
   50 ABSMT(I)=AMTRX(I)/ABS(AMTRX(I))
      ATHETA=ACOS(ABS(AMTRX(1)))
      APHI=ATAN(ABS(AMTRX(2)/AMTRX(3)))
      APSI=ATAN(ABS(AMTRX(4)/AMTRX(7)))
      API=3.141592654
      DO 5 I1=1,4
      DO 5 I2=1,4
```

```
      DO 5 I3=1,4
      IJK=I3+(I2-1)*4+(I1-1)*16
      IF (I1.EQ.1.) THETA=ATHETA
      IF (I2.EQ.1.) PHI=APHI
      IF (I3.EQ.1.) PSI=APSI
      IF (I1.EQ.2) THETA=API-ATHETA
      IF (I1.EQ.3) THETA=API+ATHETA
      IF (I1.EQ.4) THETA=2.*API-ATHETA
      IF (I2.EQ.2) PHI=API-APHI
      IF (I2.EQ.3) PHI=API+APHI
      IF (I2.EQ.4) PHI=2.*API-APHI
      IF (I3.EQ.2) PSI=API-APSI
      IF (I3.EQ.3) PSI=API+APSI
      IF (I3.EQ.4) PSI=2.*API-APSI
      BMTRX(IJK,1)=COS(THETA)
      BMTRX(IJK,2)=SIN(THETA)*SIN(PHI)
      BMTRX(IJK,3)=-SIN(THETA)*COS(PHI)
      BMTRX(IJK,4)=SIN(THETA)*SIN(PSI)
      BMTRX(IJK,5)=COS(PHI)*COS(PSI)-
     1 COS(THETA)*SIN(PHI)*SIN(PSI)
      BMTRX(IJK,6)=SIN(PHI)*COS(PSI)+
     1 COS(THETA)*COS(PHI)*SIN(PSI)
      BMTRX(IJK,7)=SIN(THETA)*COS(PSI)
      BMTRX(IJK,8)=-COS(PHI)*SIN(PSI)-
     1 COS(THETA)*SIN(PHI)*COS(PSI)
      BMTRX(IJK,9)=-SIN(PHI)*SIN(PSI)+
     1 COS(THETA)*COS(PHI)*COS(PSI)
      DO 100 I=1,9
  100 BMTRX(IJK,I)=BMTRX(IJK,I)/ABS(BMTRX(IJK,I))
      IA(IJK)=I1
      IB(IJK)=I2
      IC(IJK)=I3
      WRITE(58,60) IJK,IA(IJK),IB(IJK),IC(IJK),BMTRX(IJK,1),
     1  BMTRX(IJK,2),BMTRX(IJK,3),BMTRX(IJK,4),BMTRX(IJK,5),
     2  BMTRX(IJK,6),BMTRX(IJK,7),BMTRX(IJK,8),BMTRX(IJK,9)
   60 FORMAT(5X,4(I3,2X),9(F8.2,1X),/)
```

```
5  CONTINUE
   DO 25 IJK=1,64
   ACOS2=0.
   DO 10 II=1,9
10 ACOS2=ACOS2+(BMTRX(IJK,II)-ABSMT(II))**2
   WRITE(58,55) ACOS2,IA(IJK),IB(IJK),IC(IJK)
55 FORMAT(5X,*ACOS2=*,E10.4,3X,*IA=*,I2,
  13X,*IB=*,I2,3X,*IC=*,I2,/)
   IF (ACOS2.GT.(0.01)) GO TO 15
   WRITE(58,35) IJK, IA(IJK),IB(IJK),IC(IJK)
   I1=IA(IJK)
   I2=IB(IJK)
   I3=IC(IJK)
   I4=IJK
15 CONTINUE
25 CONTINUE
35 FORMAT(2X,*IJK=*,I4,2X,*IA=*,I4,
  12X,*IB=*,I4,2X,*IC=*,I4,/)
40 FORMAT(2X,*THETA=*,F10.4,2X,*PHI=*,
  1F10.4,2X,*PSI=*,F10.4,2X,       *DTAETA=*,F10.4,
  22X,*DPHI=*,F10.4,2X,*DPSI=*,F10.4)
   IF (I1.EQ.1) THETA=ATHETA
   IF (I2.EQ.1) PHI=APHI
   IF (I3.EQ.1) PSI=APSI
   IF (I1.EQ.2) THETA=API-ATHETA
   IF (I1.EQ.3) THETA=API+ATHETA
   IF (I1.EQ.4) THETA=2.*API-ATHETA
   IF (I2.EQ.2) PHI=API-APHI
   IF (I2.EQ.3) PHI=API+APHI
   IF (I2.EQ.4) PHI=2.*API-APHI
   IF (I3.EQ.2) PSI=API-APSI
   IF (I3.EQ.3) PSI=API+APSI
   IF (I3.EQ.4) PSI=2.*API-APSI
   DTHETA=180.*THETA/API
   DPHI=180.*PHI/API
   DPSI=180.*PSI/API
```

```
      WRITE(58,40) THETA,PHI,PSI,DTHETA,DPHI,DPSI
      RETURN
      END
C
      SUBROUTINE EXAM(A,B,M,LF)
C       F O R T R A N  4
      DIMENSION A(12,12),B(12),C(12)
      DO 80 J=1,M
   80 C(J)=A(J,J)
      IF(A(1,1)) 60,200,70
   60 A(1,1) =-SQRT(-A(1,1))
      GO TO 300
   70 A(1,1) =SQRT(A(1,1))
      GO TO 100
  100 IF(M-1)400,400,110
  110 DO 115 K=2,M
  115 A(1,K)=A(1,K)/(A(1,1)        )
      DO 120 J=2,M
      J1=J-1
      S=A(J,J)
      DO 125 L=1,J1
  125 S=S-A(L,J)**2
      IF (S) 50,200,40
   50 A(J,J) =-SQRT(-S)
      GO TO 300
   40 A(J,J) =SQRT(S)
      GO TO 130
  130 IF(J-M)135,400,400
  135 J2=J+1
      DO 120 K=J2,M
      S=A(J,K)
      DO 145 L=1,J1
  145 S=S-A(L,J)*A(L,K)
  120 A(J,K)=S/A(J,J)
  400 B(1)=B(1)/A(1,1)
      IF(M-1)420,420,405
```

```
  405 DO 410 J=2,M
      S=B(J)
      J1=J-1
      DO 415 L=1,J1
  415 S=S-A(L,J)*B(L)
  410 B(J)=S/A(J,J)
  420 B(M)=B(M)/A(M,M)
      J=M-1
  435 IF(J)450,450,425
  425 S=B(J)
      J2=J+1
      DO 430 L=J2,M
  430 S=S-A(J,L)*B(L)
      B(J)=S/A(J,J)
      J=J-1
      GO TO 435
  450 LF=1
      GO TO 460
  200 LF=0
      GO TO 460
  300 LF=-1
  460 DO 465 J=1,M
      A(J,J)=C(J)
      IF(J-M)470,475,475
  470 J2=J+1
      DO 465 K=J2,M
  465 A(J,K)=A(K,J)
  475 RETURN
      END

      SUBROUTINE MATINV(A,N,B,M,DETERM)
C       F O R T R A N  4
C     MATRIX INVERSION WITH ACCOMPANYING SOLUTION
C     OF LINEAR EQUATIONS
      DIMENSION IPIVOT(12),A(12,12),B(12,1),
     1 INDEX(12,2),PIVOT(12)
```

```
      EQUIVALENCE (IROW,JROW),(ICOLUM,JCOLUM),(AMAX,T,SWAP)
      DETERM=1.0
      DO 20 J=1,N
   20 IPIVOT(J)=0
      DO 550 I=1,N
      AMAX=0.0
      DO 105 J=1,N
      IF(IPIVOT(J)-1)60,105,60
   60 DO 100 K=1,N
      IF(IPIVOT(K)-1)80,100,740
   80 IF(ABS(AMAX)-ABS(A(J,K)))85,100,100
   85 IROW=J
      ICOLUM=K
      AMAX=A(J,K)
  100 CONTINUE
  105 CONTINUE
      IPIVOT(ICOLUM)=IPIVOT(ICOLUM)+1
      IF (IROW-ICOLUM)140,260,140
  140 DETERM=-DETERM
      DO 200 L=1,N
      SWAP=A(IROW,L)
      A(IROW,L)=A(ICOLUM,L)
  200 A(ICOLUM,L)=SWAP
      IF(M)260,260,210
  210 DO 250 L=1,M
      SWAP=B(IROW,L)
      B(IROW,L)=B(ICOLUM,L)
  250 B(ICOLUM,L)=SWAP
  260 INDEX(I,1)=IROW
      INDEX(I,2)=ICOLUM
      PIVOT(I)=A(ICOLUM,ICOLUM)
      DETERM=DETERM*PIVOT(I)
      A(ICOLUM,ICOLUM)=1.0
      DO 350 L=1,N
  350 A(ICOLUM,L)=A(ICOLUM,L)/PIVOT(I)
      IF(M)380,380,360
```

```
  360 DO 370 L=1,M
  370 B(ICOLUM,L)=B(ICOLUM,L)/PIVOT(I)
  380 DO 550 L1=1,N
      IF (L1-ICOLUM)400,550,400
  400 T=A(L1,ICOLUM)
      A(L1,ICOLUM)=0.0
      DO 450 L=1,N
  450 A(L1,L)=A(L1,L)-A(ICOLUM,L)*T
      IF(M)550,550,460
  460 DO 500 L=1,M
  500 B(L1,L)=B(L1,L)-B(ICOLUM,L)*T
  550 CONTINUE
      DO 710 I=1,N
      L=N+1-I
      IF(INDEX(L,1)-INDEX(L,2))630,710,630
  630 JROW=INDEX(L,1)
      JCOLUM=INDEX(L,2)
      DO 705 K=1,N
      SWAP=A(K,JROW)
      A(K,JROW)=A(K,JCOLUM)
      A(K,JCOLUM)=SWAP
  705 CONTINUE
  710 CONTINUE
  740 RETURN
      END

      SUBROUTINE JACOBI2(N,Q,JVEC,M,V)
C     SUBPROGRAM FOR DIAGONALIZATION OF MATRIX Q
C                BY SUCCESSIVE ROTATIONS
      DIMENSION Q(6,6),V(6,6),X(6),IH(6)
C
C     NEXT 8 STATEMENTS FOR SETTING
C            INITIAL VALUES OF MATRIX V
C
      IF(JVEC) 10,15,10
   10 DO 14 I=1,N
```

```
      DO 14 J=1,N
      IF(I-J) 12,11,12
   11 V(I,J)=1.0
      GO TO 14
   12 V(I,J)=0.
   14 CONTINUE
C
   15 M=0
C     NEXT 8 STATEMENTS SCAN FOR LARGEST OFF DIAG. ELEM.
C     IN EACH ROW X(I) CONTAINS LARGEST ELEMENT IN ITH ROW
C     IH(I) HOLDS SECOND SUBSCRIPT DEFINING POSITION
C     OF ELEMENT
C
      MI=N-1
      DO 30 I=1,MI
      X(I)=0.
      MJ=I+1
      DO 30 J=MJ,N
      IF (X(I)-ABS (Q(I,J))) 20,20,30
   20 X(I)=ABS (Q(I,J))
      IH(I)=J
   30 CONTINUE
C
C     NEXT 7 STATEMENTS FIND FOR MAXIMUM
C             OF X(I)S FOR PIVOT ELEMENT
   40 DO 70 I=1,MI
      IF(I-1) 60,60,45
   45 IF (XMAX-X(I)) 60,70,70
   60 XMAX=X(I)
      IP=I
      JP=IH(I)
   70 CONTINUE
C
C     NEXT 2 STATEMENTS TEST FOR XMAX,
C             IF LESS THAN 10**-8,GO TO 1000
C
```

```
      EPSI=1.E-12
      IF (XMAX-EPSI) 1000,1000,148
C
  148 M=M+1
C
C     NEXT 11 STATEMENTS FOR COMPUTING
C             TANG,SINE,COSN,Q(I,I),Q(J,J)
C
      IF (Q(IP,IP)-Q(JP,JP)) 150,151,151
  150 TANG =-2.*Q(IP,JP)/(ABS(Q(IP,IP)-Q(JP,JP))+
     1SQRT((Q(IP,IP)-Q(JP,JP))**2+4.*Q(IP,JP)**2))
      GO TO 160
  151 TANG =+2.*Q(IP,JP)/(ABS(Q(IP,IP)-Q(JP,JP))+
     1SQRT((Q(IP,IP)-Q(JP,JP))**2+4.*Q(IP,JP)**2))
  160 COSN=1.0/SQRT(1.0+TANG**2)
      SINE=TANG*COSN
      QII= Q(IP,IP)
      Q(IP,IP)= COSN**2*(QII+TANG*(2.*Q(IP,JP)+
     1TANG*Q(JP,JP)))
      Q(JP,JP)= COSN**2*(Q(JP,JP)-
     1TANG*(2.*Q(IP,JP)-TANG*QII))
C
      Q(IP,JP)=0.
C
C     NEXT 4 STATEMENTS FOR PSEUDO
C            RANK OF THE E1GENVALUES
      IF (Q(IP,IP)-Q(JP,JP)) 152,153,153
  152 TEMP=Q(IP,IP)
      Q(IP,IP)=Q(JP,JP)
      Q(JP,JP)=TEMP
C
C     NEXT 6 STATEMENTS ADJUST SIN,COS
C            FOR COMPUTATION OF Q(I,K),V(I,K)
C
      IF(SINE) 154,155,155
  154 TEMP=+COSN
```

```
      GO TO 170
  155 TEMP=-COSN
  170 COSN=ABS(SINE)
      SINE=TEMP
C
C     NEXT 10 STATEMENTS FOR INSPECTING  THE I"S BETWEEN
C             I+1 AND N-1 TO DETERMINE WHETHER A NEW MAXIMUM
C             VALUE SHOULD BE COMPUTED SINCETHE PRESENT
C             MAXIMUM IS IN THE I OR J ROW
C
  153 DO 350 I=1,MI
      IF (I-IP) 210,350,200
  200 IF (I-JP) 210,350,210
  210 IF (IH(I)-IP) 230,240,230
  230 IF (IH(I)-JP) 350,240,350
  240 K= IH(I)
      TEMP=Q(I,K)
      Q(I,K)=0.
      MJ=I+1
      X(I)=0.
C
C     NEXT 5 STATEMENTS SEARCH IN DEPLETED ROW
C            FOR NEW MAXIMUM
C
      DO 320  J=MJ,N
      IF (X(I)-ABS(Q(I,J))) 300,300,320
  300 X(I)=ABS(Q(I,J))
      IH(I)=J
  320 CONTINUE
      Q(I,K)=TEMP
  350 CONTINUE
C
      X(IP)=0.
      X(JP)=0.
C
C     NEXT 30 STATEMENTS FOR CHANGING
```

```
C              THE OTHER ELEMENTS OF Q
C
      DO 530 I=1,N
C
      IF (I-IP) 370,530,420
  370 TEMP=Q(I,IP)
      Q(I,IP)=COSN*TEMP+SINE*Q(I,JP)
      IF (X(I)-ABS(Q(I,IP))) 380,390,390
  380 X(I)=ABS(Q(I,IP))
      IH(I)=IP
  390 Q(I,JP)=-SINE*TEMP+COSN*Q(I,JP)
      IF (X(I)-ABS(Q(I,JP))) 400,530,530
  400 X(I)=ABS(Q(I,JP))
      IH(I)=JP
      GO TO 530
C
  420 IF (I-JP) 430,530,480
  430 TEMP =Q(IP,I)
      Q(IP,I)=COSN*TEMP+SINE*Q(I,JP)
      IF (X(IP)-ABS(Q(IP,I))) 440,450,450
  440 X(IP)=ABS(Q(IP,I))
      IH(IP)=I
  450 Q(I,JP)=-SINE*TEMP+COSN*Q(I,JP)
      IF (X(I)-ABS(Q(I,JP))) 400,530,530
C
  480 TEMP=Q(IP,I)
      Q(IP,I)=COSN*TEMP+SINE*Q(JP,I)
      IF(X(IP)-ABS(Q(IP,I))) 490,500,500
  490 X(IP)=ABS(Q(IP,I))
      IH(IP)=I
  500 Q(JP,I)=-SINE*TEMP+COSN*Q(JP,I)
      IF (X(JP)-ABS(Q(JP,I))) 510,530,530
  510 X(JP)=ABS(Q(JP,I))
      IH(JP)=I
  530 CONTINUE
C
```

```
C     NEXT 6 STATEMENTS TEST FOR
C            COMPUTATION OF EIGENVECTORS
C
      IF (JVEC) 540,40,540
  540 DO 550 I=1,N
      TEMP=V(I,IP)
      V(I,IP)= COSN*TEMP+SINE*V(I,JP)
  550 V(I,JP)=-SINE*TEMP+COSN*V(I,JP)
      GO TO 40
 1000 RETURN
      END
      SUBROUTINE JACOBI4(N,Q,JVEC,M,V)
C     SUBPROGRAM FOR DIAGONALIZATION OF MATRIX
C                Q BY SUCCESSIVE ROTATIONS
      DIMENSION Q(12,12),V(12,12),X(12),IH(12)
   13 FORMAT (2E15.5)
C
C     NEXT 8 STATEMENTS FOR SETTING
C            INITIAL VALUES OF MATRIX V
C
      IF(JVEC) 10,15,10
   10 DO 14 I=1,N
      DO 14 J=1,N
      IF(I-J) 12,11,12
   11 V(I,J)=1.0
      GO TO 14
   12 V(I,J)=0.
   14 CONTINUE
C
   15 M=0
C     NEXT 8 STATEMENTS SCAN FOR LARGEST OFF DIAG. ELEM.
C            IN EACH ROW X(I) CONTAINS LARGEST ELEMENT
C            IN ITH ROW IH(I) HOLDS SECOND SUBSCRIPT
C            DEFINING POSITION OF ELEMENT
C
      MI=N-1
```

```
      DO 30 I=1,MI
      X(I)=0.
      MJ=I+1
      DO 30 J=MJ,N
      IF (X(I)-ABS (Q(I,J))) 20,20,30
   20 X(I)=ABS (Q(I,J))
      IH(I)=J
   30 CONTINUE
C
C     NEXT 7 STATEMENTS FIND FOR MAXIMUM OF
C            X(I)S FOR PIVOT ELEMENT
   40 DO 70 I=1,MI
      IF(I-1) 60,60,45
   45 IF (XMAX-X(I)) 60,70,70
   60 XMAX=X(I)
      IP=I
      JP=IH(I)
   70 CONTINUE
C
C     NEXT 2 STATEMENTS TEST FOR XMAX,
C            IF LESS THAN 10**-8,GO TO 1000
C
      EPSI=1.E-12
      IF (XMAX-EPSI) 1000,1000,148
C
  148 M=M+1
C
C     NEXT 11 STATEMENTS FOR COMPUTING
C             TANG,SINE,COSN,Q(I,I),Q(J,J)
C
      IF (Q(IP,IP)-Q(JP,JP)) 150,151,151
  150 TANG =-2.*Q(IP,JP)/(ABS(Q(IP,IP)-Q(JP,JP))+
     1 SQRT((Q(IP,IP)-Q(JP,JP))**2+4.*Q(IP,JP)**2))
      GO TO 160
  151 TANG =+2.*Q(IP,JP)/(ABS(Q(IP,IP)-Q(JP,JP))+
     1 SQRT((Q(IP,IP)-Q(JP,JP))**2+4.*Q(IP,JP)**2))
```

```
  160 COSN=1.0/SQRT(1.0+TANG**2)
      SINE=TANG*COSN
      QII= Q(IP,IP)
      Q(IP,IP)= COSN**2*(QII+TANG*
     1 (2.*Q(IP,JP)+TANG*Q(JP,JP)))
      Q(JP,JP)= COSN**2*(Q(JP,JP)-
     1 TANG*(2.*Q(IP,JP)-TANG*QII))
C
      Q(IP,JP)=0.
C
C     NEXT 4 STATEMENTS FOR PSEUDO
C            RANK OF THE E1GENVALUES
      IF (Q(IP,IP)-Q(JP,JP)) 152,153,153
  152 TEMP=Q(IP,IP)
      Q(IP,IP)=Q(JP,JP)
      Q(JP,JP)=TEMP
C     NEXT 6 STATEMENTS ADJUST SIN, COS FOR
C            COMPUTATION OF Q(I,K),V(I,K)
C
      IF(SINE) 154,155,155
  154 TEMP=+COSN
      GO TO 170
  155 TEMP=-COSN
  170 COSN=ABS(SINE)
      SINE=TEMP
C
C     NEXT 10 STATEMENTS FOR INSPECTING  T8E IHS BETWEEN
C             I+1 AND N-1 TO DETERMINE WHETHER A NEW MAXIMUM
C             VALUE SHOULD BE COMPUTED SINCE THE PRESENT
C             MAXIMUM IS IN THE I OR J ROW
C
  153 DO 350 I=1,MI
      IF (I-IP) 210,350,200
  200 IF (I-JP) 210,350,210
  210 IF (IH(I)-IP) 230,240,230
  230 IF (IH(I)-JP) 350,240,350
```

```
  240 K= IH(I)
      TEMP=Q(I,K)
      Q(I,K)=0.
      MJ=I+1
      X(I)=0.
C
C     NEXT 5 STATEMENTS SEARCH IN DEPLETED
C            ROW FOR NEW MAXIMUM
C
      DO 320  J=MJ,N
      IF (X(I)-ABS(Q(I,J))) 300,300,320
  300 X(I)=ABS(Q(I,J))
      IH(I)=J
  320 CONTINUE
      Q(I,K)=TEMP
  350 CONTINUE
C
      X(IP)=0.
      X(JP)=0.
C
C     NEXT 30 STATEMENTS FOR CHANGING
C             THE OTHER ELEMENTS OF Q
C
      DO 530 I=1,N
C
      IF (I-IP) 370,530,420
  370 TEMP=Q(I,IP)
      Q(I,IP)=COSN*TEMP+SINE*Q(I,JP)
      IF (X(I)-ABS(Q(I,IP))) 380,390,390
  380 X(I)=ABS(Q(I,IP))
      IH(I)=IP
  390 Q(I,JP)=-SINE*TEMP+COSN*Q(I,JP)
      IF (X(I)-ABS(Q(I,JP))) 400,530,530
  400 X(I)=ABS(Q(I,JP))
      IH(I)=JP
      GO TO 530
```

```
C
  420 IF (I-JP) 430,530,480
  430 TEMP=Q(IP,I)
      Q(IP,I)=COSN*TEMP+SINE*Q(I,JP)
      IF (X(IP)-ABS(Q(IP,I))) 440,450,450
  440 X(IP)=ABS(Q(IP,I))
      IH(IP)=I
  450 Q(I,JP)=-SINE*TEMP+COSN*Q(I,JP)
      IF (X(I)-ABS(Q(I,JP))) 400,530,530
C
  480 TEMP=Q(IP,I)
      Q(IP,I)=COSN*TEMP+SINE*Q(JP,I)
      IF(X(IP)-ABS(Q(IP,I))) 490,500,500
  490 X(IP)=ABS(Q(IP,I))
      IH(IP)=I
  500 Q(JP,I)=-SINE*TEMP+COSN*Q(JP,I)
      IF (X(JP)-ABS(Q(JP,I))) 510,530,530
  510 X(JP)=ABS(Q(JP,I))
      IH(JP)=I
  530 CONTINUE
C
C     NEXT 6 STATEMENTS TEST FOR
C            COMPUTATION OF E1GENVECTORS
C
      IF (JVEC) 540,40,540
  540 DO 550 I=1,N
      TEMP=V(I,IP)
      V(I,IP)= COSN*TEMP+SINE*V(I,JP)
  550 V(I,JP)=-SINE*TEMP+COSN*V(I,JP)
      GO TO 40
 1000 AAM=FLOAT(M)
      WRITE (58,13) EPSI,AAM
      RETURN
      END
      SUBROUTINE JACOBI3(N,Q,JVEC,M,V)
C     SUBPROGRAM FOR DIAGONALIZATION OF MATRIX Q
```

```
C                    BY SUCCESSIVE ROTATIONS
       DIMENSION Q(3,3),V(3,3),X(3),IH(3)
   13 FORMAT (2E15.5,//)
C
C     NEXT 8 STATEMENTS FOR SETTING
C              INITIAL VALUES OF MATRIX V
C
      IF(JVEC) 10,15,10
   10 DO 14 I=1,N
      DO 14 J=1,N
      IF(I-J) 12,11,12
   11 V(I,J)=1.0
      GO TO 14
   12 V(I,J)=0.
   14 CONTINUE
C
   15 M=0
C     NEXT 8 STATEMENTS SCAN FOR LARGEST OFF DIAG. ELEM.
C              IN EACH ROW X(I) CONTAINS LARGEST ELEMENT IN
C              ITH ROW IH(I) HOLDS SECOND SUBSCRIPT DEFINING
C              POSITION OF ELEMENT
C
      MI=N-1
      DO 30 I=1,MI
      X(I)=0.
      MJ=I+1
      DO 30 J=MJ,N
      IF (X(I)-ABS (Q(I,J))) 20,20,30
   20 X(I)=ABS (Q(I,J))
      IH(I)=J
   30 CONTINUE
C
C     NEXT 7 STATEMENTS FIND FOR MAXIMUM OF
C              X(I)S FOR PIVOT ELEMENT
   40 DO 70 I=1,MI
      IF(I-1) 60,60,45
```

```
   45 IF (XMAX-X(I)) 60,70,70
   60 XMAX=X(I)
      IP=I
      JP=IH(I)
   70 CONTINUE
C
C     NEXT 2 STATEMENTS TEST FOR XMAX,
C            IF LESS THAN 10**-8,GO TO 1000
C
      EPSI=1.E-12
      IF (XMAX-EPSI) 1000,1000,148
C
  148 M=M+1
C
C     NEXT 11 STATEMENTS FOR COMPUTING
C             TANG,SINE,COSN,Q(I,I),Q(J,J)
C
      IF (Q(IP,IP)-Q(JP,JP)) 150,151,151
  150 TANG =-2.*Q(IP,JP)/(ABS(Q(IP,IP)-Q(JP,JP))+
     1 SQRT((Q(IP,IP)-Q(JP,JP))**2+4.*Q(IP,JP)**2))
      GO TO 160
  151 TANG =+2.*Q(IP,JP)/(ABS(Q(IP,IP)-Q(JP,JP))+
     1 SQRT((Q(IP,IP)-Q(JP,JP))**2+4.*Q(IP,JP)**2))
  160 COSN=1.0/SQRT(1.0+TANG**2)
      SINE=TANG*COSN
      QII= Q(IP,IP)
      Q(IP,IP)= COSN**2*(QII+
     1 TANG*(2.*Q(IP,JP)+TANG*Q(JP,JP)))
      Q(JP,JP)= COSN**2*(Q(JP,JP)-
     1 TANG*(2.*Q(IP,JP)-TANG*QII))
C
      Q(IP,JP)=0.
C
C     NEXT 4 STATEMENTS FOR PSEUDO
C            RANK OF THE E1GENVALUES
      IF (Q(IP,IP)-Q(JP,JP)) 152,153,153
```

```
  152 TEMP=Q(IP,IP)
      Q(IP,IP)=Q(JP,JP)
      Q(JP,JP)=TEMP
C     NEXT 6 STATEMENTS ADJUST SIN, COS FOR
C            COMPUTATION OF Q(I,K),V(I,K)
C
      IF(SINE) 154,155,155
  154 TEMP=+COSN
      GO TO 170
  155 TEMP=-COSN
  170 COSN=ABS(SINE)
      SINE=TEMP
C
C     NEXT 10 STATEMENTS FOR INSPECTING  T8E IHS BETWEEN
C             I+1 AND N-1 TO DETERMINE WHETHER A NEW MAXIMUM
C             VALUE SHOULD BE COMPUTED SINCE THE PRESENT
C             MAXIMUM IS IN THE I OR J ROW
C
  153 DO 350 I=1,MI
      IF (I-IP) 210,350,200
  200 IF (I-JP) 210,350,210
  210 IF (IH(I)-IP) 230,240,230
  230 IF (IH(I)-JP) 350,240,350
  240 K= IH(I)
      TEMP=Q(I,K)
      Q(I,K)=0.
      MJ=I+1
      X(I)=0.
C
C     NEXT 5 STATEMENTS SEARCH
C            IN DEPLETED ROW FOR NEW MAXIMUM
C
      DO 320  J=MJ,N
      IF (X(I)-ABS(Q(I,J))) 300,300,320
  300 X(I)=ABS(Q(I,J))
      IH(I)=J
```

```
  320 CONTINUE
      Q(I,K)=TEMP
  350 CONTINUE
C
      X(IP)=0.
      X(JP)=0.
C
C     NEXT 30 STATEMENTS FOR CHANGING
C             THE OTHER ELEMENTS OF Q
C
      DO 530 I=1,N
C
      IF (I-IP) 370,530,420
  370 TEMP=Q(I,IP)
      Q(I,IP)=COSN*TEMP+SINE*Q(I,JP)
      IF (X(I)-ABS(Q(I,IP))) 380,390,390
  380 X(I)=ABS(Q(I,IP))
      IH(I)=IP
  390 Q(I,JP)=-SINE*TEMP+COSN*Q(I,JP)
      IF (X(I)-ABS(Q(I,JP))) 400,530,530
  400 X(I)=ABS(Q(I,JP))
      IH(I)=JP
      GO TO 530
C
  420 IF (I-JP) 430,530,480
  430 TEMP=Q(IP,I)
      Q(IP,I)=COSN*TEMP+SINE*Q(I,JP)
      IF (X(IP)-ABS(Q(IP,I))) 440,450,450
  440 X(IP)=ABS(Q(IP,I))
      IH(IP)=I
  450 Q(I,JP)=-SINE*TEMP+COSN*Q(I,JP)
      IF (X(I)-ABS(Q(I,JP))) 400,530,530
C
  480 TEMP=Q(IP,I)
      Q(IP,I)=COSN*TEMP+SINE*Q(JP,I)
      IF(X(IP)-ABS(Q(IP,I))) 490,500,500
```

```
  490 X(IP)=ABS(Q(IP,I))
      IH(IP)=I
  500 Q(JP,I)=-SINE*TEMP+COSN*Q(JP,I)
      IF (X(JP)-ABS(Q(JP,I))) 510,530,530
  510 X(JP)=ABS(Q(JP,I))
      IH(JP)=I
  530 CONTINUE
C
C     NEXT 6 STATEMENTS TEST FOR
C            COMPUTATION OF E1GENVECTORS
C
      IF (JVEC) 540,40,540
  540 DO 550 I=1,N
      TEMP=V(I,IP)
      V(I,IP)= COSN*TEMP+SINE*V(I,JP)
  550 V(I,JP)=-SINE*TEMP+COSN*V(I,JP)
      GO TO 40
 1000 AAM=FLOAT(M)
      WRITE (58,13) EPSI,AAM
      RETURN
      END
```

```
      PROGRAM CUQ (INPUT,OUTPUT,TAPE5=INPUT,TAPE58=OUTPUT)
C     THIS PROGRAM ANALYSES EPR DATA WITH NUCLEAR HF
C     FORBIDDEN LINES WITH ELECTRON SPIN S=1/2 AND NUCLEAR
C     SPIN I=3/2 FOR  CU2+DOPED TUTTON'S SALTS ( A-SECOND
C     ORDER).
C
C     M  =NO. OF PARAMETERS
C     L4 =NO. OF ITERATIONS ALLOWED
C     Q1 =MIN. VALUE OF SUM OF SQUARES FOR FITS
C         (CHI-SQUARE TOLERANCE)
C     Z(I)=MAGNETIC FIELD VALUES FOR FITS
C     B  =PARAMETER MATRIX
C     N  =NO. OF  DATA POINTS USED IN LEAST-SQARES FITTING
C     Q1 =N/10
C     Q2 =TOLERANCE ON GRAD(CHI**2) =APPROX .01
C     FM(I) = MEASURED VALUES
C     FC(I) = CALCULATED VALUES
C     ERR(I)= STANDARD DEVIATION ON FM(I) = SQRT(FM(I))
C
C     DIMENSIONS OF A,B IN EXAM AND MATINV SUBROUTINES
C     SHOULD BE THE SAME AS THOSE OF B2,B1 RESPECTIVELY IN
C     THE MAIN PROOGRAM AND IN CURFIT
C
C     ENTER TEETA IN DEGREES
C     DIMENSIONS OF Q,V IN JACOBI1 SHOULD BE THE SAME AS
C     THOSE OF B3, B2 RESPECTIVELY IN CURFIT
C
C     PARAMETERS=I.GT IS G**2-TENSOR
C         (G**2ZZ,G**2ZX,G**2XX,G**2ZY,G**2YY,G**2XY)
C         GGT(J,NUMBER) REPRESENTS G-SQUARE TENSOR.
C               II.(AB(I),I=1,6)=AZZ,AZX,AXX,AZY,AYY,AXY
C               III.(B(I),I=1,5)=QXX,QXY,QYY,QXZ,QYZ
C     A=A-SQUARE TENSOR ABOVE
C                ENTER A WITH POSITIVE SIGN
C
C  DELANG(I,J),J=1,2,3 ARE ANGLE CORRECTIONS FOR ZX,ZY,XY
```

```
C    PLANES AS DETERMINED BY "KRDBLT" FOR VARIOUS CASES.
C
C     NUMBER=INDEX THAT CHANGES WITH EACH NEW CASE ITS
C       VALUE SHOULD BE THAT OF THE FIRST CASE CONSIDERED.
C     NCASES=NO. OF LAST CASE CONSIDERED.
C            ITS VALUE SHOULD BE ENTERED.
C
C     N1(J1,NUMBER)=NO.OF LINES(FOR VARIOUS ORIENTATIONS)
C     FOR J1 HYPERFINE LINE OF CASE NO.=NUMBER
C
C     ZZ(J,K,L)=LINE POSITIONS,J=WHICH ONE OF K=A SWITCH
C       CONTROL PARAMETER, WHEN K=1,4 CORRESPOND TO THE
C       FORBIDDEN TRANSITIONS M_M+-1, I.E., 3/2_3/2-1,
C       1/2_1/2+1, -3/2_-3/2+1 AND -1/2_-1/2-1,
C       RESPECTIVELY, WHILE K=5,8 CORRESPOND TO THE
C       FORBIDDEN TRANSITIONS M_M+-2, I.E., 3/2_3/2-2,
C       -1/2_-1/2+2, -3/2_-3/2+2 AND 1/2_1/2-2 RESPECTIVELY.
C      CASE NO.=L
C
      DIMENSION Z(400),FM(400),FC(400),DF(400),ERR(400),
     1B(12),B1(12),B2(12,12),DC(5000),ABC(2),Y(4),
     2HN(400),G(6,8),GG(6,8),SMD(9),AAA(3,3),QQQ(3,3),
     3AAV(3,3),QQV(3,3),IBB(400,2),THETA(400),D1(12),
     4D2(12,12),HHN(3,8),AADD(3,8),GGTT(6,9),AB(6),
     5FFACTR(3,8),TEETA(100,4,8),ZZ(100,4,8),NN(8),N1(8,5),
     6GGT(6,9),GT(6),ACOSZ(400),ACOSX(400),ACOSY(400),
      DIMENSION DELANG(8,3),AJ1(400),GGTL(8,3),
     1GGTM(8,3),GGTLL(8,3),GGTMM(8,3),GGTNN(8,3),
     2GGTN(8,3),DELHH(400,8),DELH(400),A4(3),
     3LZX(1),LZY(1),LXY(1),NCASES(1),NZERO(1)
      COMMON/DATA1/ABC,Y
      COMMON/DATA2/DC,ACOSZ,ACOSX,ACOSY,AJ1,GGTL,GGTM,GGTN
      COMMON/DATA3/DELH
      EQUIVALENCE (Z,DC),(FM,DC(401)),(FC,DC(801)),
     1(DF,DC(1201)),(ERR,DC(1601)),(HN,DC(2001)),
     2(THETA,DC(2401)),(IBB,DC(2801)),(B,DC(4101)),
```

```
     3(B1,DC(4125)),(B2,DC(4137)),(N,DC(4301)),
     4(L4,DC(4302)),(Q1,DC(4303)),(Q2,DC(4304)),
     5(M,DC(4305)),(I,DC(4306)),(L,DC(4307)),(BO,DC(4308)),
     6(SMD,DC(4309)),(SSMD,DC(4320)),(D1,DC(4321)),
     7(D2,DC(4333)),(NUMBER,DC(4100)),
     8(GT,DC(4093)),(AB,DC(4500))
C
      READ(5,*) NZERO,NCASES,LZX,LZY,LXY
      WRITE(58,5123) NZERO,NCASES,LZX,LZY,LXY
 5123 FORMAT(1X,6HNZERO=,I8, 7HNCASES=,I8,
     14HLZX=,I8, 4HLZY=,I8, 4HLXY=,I8)
      READ(5,*)(HHN(J,NCASES),J=1,3)
      READ(5,*)(FFACTR(J,NCASES),J=1,3)
      READ(5,*)(AADD(J,NCASES),J=1,3)
      READ(5,*)(GGT(J,NCASES),J=1,6)
      READ(5,*)(GGTT(J,NCASES),J=1,6)
      READ(5,*)(G(J,NCASES),J=1,5)
      READ(5,*)(DELANG(NCASES,J),J=1,3)
      READ(5,*)(GGTLL(NCASES,J),J=1,3)
      READ(5,*)(GGTMM(NCASES,J),J=1,3)
      READ(5,*)(GGTNN(NCASES,J),J=1,3)
      READ(5,*)(N1(J,NCASES),J=1,6)
      NSUM=0
      II=0
      NXY=0
      NSUM=LZX+LZY+LXY
      NSUM=6*NSUM
      READ(5,*)(DELHH(J,NCASES),J=1,NSUM)
      READ(5,*)(ZZ(J,1,NCASES),J=1,LZX)
      READ(5,*)(ZZ(J,2,NCASES),J=1,LZX)
      READ(5,*)(ZZ(J,3,NCASES),J=1,LZX)
      READ(5,*)(ZZ(J,4,NCASES),J=1,LZX)
      READ(5,*)(ZZ(J,5,NCASES),J=1,LZX)
      READ(5,*)(ZZ(J,6,NCASES),J=1,LZX)
      READ(5,*)(TEETA(J,1,NCASES),J=1,LZX)
      II=LZX+1
```

```
      NXY=LZX+LZY
      READ(5,*)(ZZ(J,1,NCASES),J=II,NXY)
      READ(5,*)(ZZ(J,2,NCASES),J=II,NXY)
      READ(5,*)(ZZ(J,3,NCASES),J=II,NXY)
      READ(5,*)(ZZ(J,4,NCASES),J=II,NXY)
      READ(5,*)(ZZ(J,5,NCASES),J=II,NXY)
      READ(5,*)(ZZ(J,6,NCASES),J=II,NXY)
      READ(5,*)(TEETA(J,1,NCASES),J=II,NXY)
      II=NXY+1
      NXY=NXY+LXY
      READ(5,*)(ZZ(J,1,NCASES),J=II,NXY)
      READ(5,*)(ZZ(J,2,NCASES),J=II,NXY)
      READ(5,*)(ZZ(J,3,NCASES),J=II,NXY)
      READ(5,*)(ZZ(J,4,NCASES),J=II,NXY)
      READ(5,*)(ZZ(J,5,NCASES),J=II,NXY)
      READ(5,*)(ZZ(J,6,NCASES),J=II,NXY)
      READ(5,*)(TEETA(J,1,NCASES),J=II,NXY)
C
C
  188 FORMAT(1H1)
    8 FORMAT(1X,4HQ1 = ,E13.5,5X,4HQ2 = ,E13.5)
  137 FORMAT (3X,I2,5X,E16.6/)
  136 FORMAT(10X,19H INITIAL PARAME
     1TERS//3X,1HJ,10X,4HB(J)//)
  135 FORMAT(1X,11H PARAME
     1TERS//3X,1HJ,10X,4HB(J),27X,6HERRORS//)
    9 FORMAT(2X,4H HN= ,F9.4)
  140 FORMAT(3X,I2,5X,E16.6,15X,E16.6/)
  138 FORMAT(5X,14H CASE NUMBER =,I2//)
  141 FORMAT(10X,6H SMD =,E13.5//)
  235 FORMAT (15X,5(E13.5,8X)/)
  236 FORMAT(15X,3(E13.5,8X)///)
  237 FORMAT(15X,*PRINCIPAL ELEMENTS OF Q TENSOR ARE=*,///)
  238 FORMAT(15X,*"Q" DIR. COS.(ROWS) ACC. TO E.
     1VALS. ABOVE=  *,///)
      PI2=2.*3.1415926
```

```
      RD=PI2/360.
      NZERO=1
      NUMBER=NZERO
      NCASES=1
      M=5
      L4=7
      Q1=1.E-8
      Q2=1.E-20
      MM=M
      WRITE(58,188)
    1 CONTINUE
      N11=N1(1,NUMBER)
C     DO 1188 J=1,8
      DO 1188 J=1,6
C
C      HERE J IN J=1,8 OR J=1,4 STATEMENTS HAS THE SAME
C      MEANING AS THE K IN ZZ(J,K,L), WHICH INDICATED IN
C      THE BEGINING OF THIS PROGRAM.
C
      DO 1188 J1=1,N11
 1188 TEETA(J1,J,NUMBER)=TEETA(J1,1,NUMBER)
      DO 9242 J1=1,3
      GGTL(NUMBER,J1)=GGTLL(NUMBER,J1)
      GGTM(NUMBER,J1)=GGTMM(NUMBER,J1)
9242  GGTN(NUMBER,J1)=GGTNN(NUMBER,J1)
      LINE=0
C     DO 150 J1=1,8
      DO 150 J1=1,6
      NN1=N1(J1,NUMBER)
      DO 150 I1=1,NN1
      LINE=LINE+1
      AJ1(LINE)=J1
      THETA(LINE)=TEETA(I1,J1,NUMBER)
      IF(THETA(LINE).GT.8000.) GO TO 155
      IF(THETA(LINE).LT.0.) GO TO 160
      TH=THETA(LINE)*RD+DELANG(NUMBER,1)*RD
```

```
      ACOSZ(LINE)=COS(TH)
      ACOSX(LINE)=SIN(TH)
      ACOSY(LINE)=0.
      HN(LINE)=HHN(1,NUMBER)
C     Z(LINE)=(ZZ(I1,J1,NUMBER)+
     1AADD(1,NUMBER))*FFACTR(1,NUMBER)
      Z(LINE)=(ZZ(I1,J1,NUMBER)*
     1FFACTR(1,NUMBER)+AADD(1,NUMBER))
      IF(ZZ(I1,J1,NUMBER).EQ.0.) Z(LINE)=0.
 9160 FORMAT(5X,*ACOSZ ETC=*,3E12.5)
      GO TO 165
  160 TH=-THETA(LINE)*RD + DELANG(NUMBER,2)*RD
      ACOSZ(LINE)=COS(TH)
      ACOSY(LINE)=SIN(TH)
      ACOSX(LINE)=0.
      HN(LINE)=HHN(2,NUMBER)
C     Z(LINE)=(ZZ(I1,J1,NUMBER)+
     1AADD(2,NUMBER))*FFACTR(2,NUMBER)
      Z(LINE)=(ZZ(I1,J1,NUMBER)*
     1FFACTR(2,NUMBER)+AADD(2,NUMBER))
      IF(ZZ(I1,J1,NUMBER).EQ.0.) Z(LINE)=0.
      GO TO 165
  155 TH=THETA(LINE)*RD+DELANG(NUMBER,3)*RD
      ACOSZ(LINE)=0.
      ACOSX(LINE)=COS(TH)
      ACOSY(LINE)=SIN(TH)
      HN(LINE)=HHN(3,NUMBER)
C     Z(LINE)=(ZZ(I1,J1,NUMBER)+
     1AADD(3,NUMBER))*FFACTR(3,NUMBER)
      Z(LINE)=(ZZ(I1,J1,NUMBER)*
     1FFACTR(3,NUMBER)+AADD(3,NUMBER))
      IF(ZZ(I1,J1,NUMBER).EQ.0.) Z(LINE)=0.
  165 CONTINUE
  150 CONTINUE
      NN(NUMBER)=LINE
      N=NN(NUMBER)
```

```
      N9=N
      DO 181 LL=1,12
  181 B(LL)=0.
      DO 210 LL=1,MM
  210 B(LL)=G(LL,NUMBER)
      WRITE(58,138) NUMBER
      WRITE(58,136)
      WRITE(58,137) (J,B(J),J=1,M)
      WRITE(58,6659)
      WRITE(58,6657) (Z(J),J=1,N)
      WRITE(58,6660)
      WRITE(58,6657) (HN(J),J=1,N)
 6660 FORMAT(5X,*FREQUENCY-KLYSTRON ARE=*,/)
 6659 FORMAT(5X,*MAG. FIELD VALUES ARE=*,/)
 6657 FORMAT(5X,7(E12.5,2X))
      DO 180 J1=1,6
      GT(J1)=GGT(J1,NUMBER)
  180 AB(J1)=GGTT(J1,NUMBER)
      DO 201 II=1,N9
      DELH(II)=DELHH(II,NUMBER)
  201 FM(II) = HN(II)
      CALL CURFIT
      SMD(NUMBER) = SSMD
      WRITE(58,188)
      WRITE(58,135)
      DO 220 LL=1,M
  220 GG(LL,NUMBER) = B(LL)
      WRITE(58,140)(J,B(J),B1(J),J=1,M)
      WRITE(58,188)
    3 CONTINUE
      SSS=0.
      SSS1=0.
      DO 555 ID=1,N
      SSS=DF(ID)**2
      SSS1=SSS1+SSS
      WRITE(58,656) ID,SSS
```

```
  555 CONTINUE
      WRITE(58,6656) SSS1
 6656 FORMAT(/,10X,*CHI-SQUARE=*,E13.5,/)
  656 FORMAT(10X,*LINE NUMBER = *,I3,5X,*SMD = *,E13.5)
      AAA(1,1) = B(1)
      AAA(1,2) = B(2)
      AAA(2,2) = B(3)
      AAA(1,3) = B(4)
      AAA(3,3) = -(B(1)+B(3))
      AAA(2,3) = B(5)
      DO 20 J1 = 1,2
      J4 = J1 + 1
      DO 20 J2 = J4,3
      AAA(J2,J1) = AAA(J1,J2)
   20 CONTINUE
      CALL JACOBI3(3,AAA,1,NR,AAV)
      WRITE (58,237)
      WRITE(58,236) (AAA(J1,J1),J1 = 1,3)
      WRITE (58,238)
      DO 25 J1 = 1,3
      WRITE (58,236) (AAV(J2,J1),J2 = 1,3)
   25 CONTINUE
      NUMBER=NUMBER+1
      IF(NUMBER-NCASES) 1,1,2
    2 CONTINUE
      DO 230 LL=NZERO,NCASES
      WRITE(58,138) LL
      WRITE(58,141) SMD(LL)
  230 WRITE (58,235) (GG(LM,LL),LM=1,MM)
      STOP
      END
      SUBROUTINE CURFIT
C
C     EXAM HANDLES ALL MATRICES OF DIMENSIONS UPTO THE
C     DIMS.MM OF A,B,C THAT IS M IS LESS THAN OR EQUAL TO MM
C     (SAME IS TRUE OF MATINV AND JACOBI)
```

```
C
C     EQUIVALENCE OF GRAD BEGINS AT DIMENSION OF B AFTER
C     THE EQUIV. OF B
C
C         F O R T R A N  4
      DIMENSION Z(400),FM(400),FC(400),DF(400),ERR(400),
     1B(12),B1(12),B2(12,12),DC(5000),ABC(2),Y(4),X(400),
     2GRAD(12),D1(12),D2(12,12),B3(12,12),SMD(9),HN(400),
     3ACOSZ(400),ACOSX(400),ACOSY(400)
      DIMENSION IBB(400,2),THETA(400),GT(6),AB(6)
      DIMENSION AJ1(400),GGTL(8,3),GGTM(8,3),GGTN(8,3)
      COMMON/DATA1/ABC,Y
      COMMON/DATA2/DC,ACOSZ,ACOSX,ACOSY,AJ1,GGTL,GGTM,GGTN
      EQUIVALENCE (Z,DC),(FM,DC(401)),(FC,DC(801)),
     1(DF,DC(1201)),(ERR,DC(1601)),(HN,DC(2001)),
     2(THETA,DC(2401)),(IBB,DC(2801)),(B,DC(4101)),
     3(B1,DC(4125)),(B2,DC(4137)),(N,DC(4301)),
     4(L4,DC(4302)),(Q1,DC(4303)),(Q2,DC(4304)),
     5(M,DC(4305)),(I,DC(4306)),(L,DC(4307)),(BO,DC(4308)),
     6(SMD,DC(4309)),(SSMD,DC(4320)),(D1,DC(4321)),
     7(D2,DC(4333)),(GRAD,DC(4113)),
     8(NUMBER,DC(4100)),(GT,DC(4093)),(AB,DC(4500))
C
      ABC(1)="NO"
      ABC(2)="YES"
      L1 = 0
      SA = 0.0
      MM=M
      I6=I
      NN=N
      DO 1000 J=1,MM
      B1(J)=0.0
      DO 1000 K=1,MM
 1000 B2(J,K)=0.0
      DO 100 I6 = 1, NN
      L=1
```

```
      I=I6
      CALL FUNC(2)
      X(I6)=ERR(I6)**2
 901  FORMAT(5X,10H FUNC2,210  )
      DF(I6) =FM(I6) - FC(I6)
      DO 101 J=1,MM
      B1(J)=B1(J)-(2.0*DF(I6)*D1(J))/X(I6)
      DO 101 K=1,MM
  101 B2(J,K)=B2(J,K)-(2.0*(DF(I6)*D2(J,K)-
     1 D1(J)*D1(K)))/X(I6)
  100 SA = SA + DF(I6)**2/X(I6)
      GMOD=0.0
      DO 102 J=1,M
  102 GMOD=GMOD+B1(J)**2
      WRITE(58,243)SA,GMOD
  243 FORMAT (1X,26H*INITIAL VALUE SUM OF SQ.=
     1E13.5,20X,17H*SQ MOD OF GRAD =E13.5)
      WRITE(58,1751)
 1751 FORMAT(14H0 DERIVATIVES-)
      WRITE(58,240)(B1(J),J=1,M)
  240 FORMAT (15X,5(E13.5,8X)/)
      IF (SA - Q1) 110, 110, 200
  110 LE = 1
      GO TO 600
  200 S = 0.0
      GMOD = 0.0
      BMOD = 0.0
      PROD = 0.0
      A2=ABC(1)
      DO 210 J = 1, MM
      B1(J) = 0.0
      DO 210 K = 1, MM
  210 B2(J,K) = 0.0
      WRITE(58,902)
      DO 220 I6 = 1, NN
      L=1
```

```
      I=I6
      CALL FUNC(2)
      X(I6)=ERR(I6)**2
 902  FORMAT(5X,10H FUNC2,210  )
      DF(I6) = FM(I6) - FC(I6)
      DO 220 J = 1, MM
      B1(J) = B1(J) - (2.0*DF(I6)*D1(J))/X(I6)
      DO 220 K = 1, MM
  220 B2(J,K) = B2(J,K) - (2.0*(DF(I6)*D2(J,K) -
     1 D1(J)*D1(K)))/X(I6)
       DO 230 J = 1, MM
  230 GRAD(J) = B1(J)
      L1 = L1 + 1
      CALL EXAM (B2,B1,M,LF)
      WRITE(58,903)
 903  FORMAT(5X,9H EXAM,230  )
      WRITE (58,914) LF
  914 FORMAT (5X,I3)
      IF (LF)  250, 250, 305
  250 DO 231 II=1,M
      DO 231 JJ=1,M
  231 B3(II,JJ)=B2(II,JJ)
      WRITE (58,904)
      CALL JACOBI4(M,B3,4,NR,B2)
 904  FORMAT(5X,12H JACOBI1,231  )
      WRITE(58,904)
      DO 235 I6=1,MM
  235 B1(I6)=B3(I6,I6)
      A2=ABC(2)
      DO 260 J = 1, MM
  260 D1(J) = 0.0
      DO 270 J = 1, MM
      DO 270 K = 1, MM
  270 D1(K) = D1(K) + B2(J,K) *GRAD(J)
      DO 275 J = 1, MM
      IF (B1(J))  280, 290, 285
```

```
 280 B1(J) = - B1(J)
 285 D1(J) = D1(J)/B1(J)
     GO TO 275
 290 D1(J) = 0.0
 275 CONTINUE
     DO 295 J = 1, MM
 295 B1(J) = 0.0
     DO 300 J = 1, MM
     DO 300 K = 1, MM
 300 B1(J) = B1(J) + B2(J,K)*D1(K)
 305 DO 310 J=1,MM
     GMOD = GMOD + GRAD(J)**2
     BMOD = BMOD + B1(J)**2
 310 PROD = PROD + GRAD(J)*B1(J)
     IF (GMOD - Q2)  315, 315, 320
 315 LE = 2
     WRITE(58,1761) GMOD
1761 FORMAT(5X,7H GMOD =,E13.5//)
     GO TO 600
 320 C=PROD/SQRT(BMOD*GMOD)
     IF (C) 335, 335, 400
 335 LE = 4
     GO TO 600
 400 LD = 0
     L3 = 0
     DO 410 J = 1, MM
 410 GRAD(J) = B(J) - B1(J)
 450 DO 420 I6 = 1, NN
     L=2
     I=I6
     CALL FUNC (1)
     X(I6)=ERR(I6)**2
 905 FORMAT(5X,10H FUNC1,450  )
     DF(I6) = FM(I6) - FC(I6)
 420 S = S + DF(I6)**2/X(I6)
     WRITE(58,905)
```

```
    IF (SA - S) 435, 500, 500
435 LD = LD + 1
430 DO440 J = 1, MM
    B1(J) = B1(J)/2.0
906 FORMAT(5X,16H BINARY CHOP,430  )
440 GRAD(J) = B(J) - B1(J)
    WRITE(58,906)
    S = 0.0
    L3 = L3 + 1
    IF(L3-5)450,460,460
460 LE = 5
    GO TO 600
500 IF (LD) 505, 505, 506
506 LD = 0
    GO TO 430
505 DO 510 J = 1, MM
510 B(J) = GRAD(J)
    SA = S
    IF (SA - Q1) 507, 507, 530
507 LE = 1
    GO TO 600
530 IF (L4) 200, 200, 900
900 WRITE(58,920)L1,A2,L3,S,GMOD,(B(J),J=1,M)
920 FORMAT(//,15H ITERATION NO.=I5,10X,43H   TRANSFORMA
   1TION MADE TO PRINCIPAL AXES = A4,10X,   18H BINA
   2RY CHOP USED=I3,6H TIMES/1X,27H WEIGHTED SUM OF SQU
   3ARES = E14.7,25X,32H   SQUARE MODULUS OF GRADIEN
   4T = E14.7/20H   PARAMETERS B(J) -/(6E17.8)/)
    IF (L1 - L4) 200, 910, 910
910 LE = 6
    GO TO 600
600 DO 710 J=1,MM
    B1(J) = 0.0
    DO 710 K=1,MM
710 B2(J,K) = 0.0
    L=1
```

```
      WRITE(58,907)
  907 FORMAT(5X,* FUNC(2),720 *)
      DO 720 I6 = 1, NN
      I=I6
      CALL FUNC(2)
      X(I6)=ERR(I6)**2
      DF(I6) = FM(I6) - FC(I6)
      DO 720 J = 1, MM
      B1(J) = B1(J) - (2.0*DF(I6)*D1(J))/X(I6)
      DO 720 K = 1, MM
  720 B2(J,K) = B2(J,K) - ((DF(I6)*D2(J,K) -
     1 D1(J)*D1(K)))/X(I6)
      WRITE (58,3029)
 3029 FORMAT(* I AM LOST IN MANTINV*)
      CALL MATINV(B2,M,B1,1,DETERM)
      WRITE (58,3029)
      DO 730 J=1,MM
      IF (B2(J,J)) 2001,2001,2002
 2001 B1(J) = -SQRT(-B2(J,J))
      GO TO 730
 2002 B1(J)= SQRT(B2(J,J))
  730 CONTINUE
      DO 740 J=1,MM
      DO 740 K=1,MM
  740 B2(J,K)=B2(J,K)/(B1(J)*B1(K))
      WRITE(58,551)LE,SA
  551 FORMAT(//,13H EXIT NUMBER=I3,20X,25H WEIGHT
     1ED SUM OF SQUARES=E15.8//)
      SSMD = SA
9999  CONTINUE
      RETURN
      END

      SUBROUTINE FUNC(LX)
C     SUBROUTINE FUNC
C
```

```
C
      DIMENSION DC(5000),B(12,2),D1(12),D2(12,12),FC(400),
     1Z(400),S(4,4),SIGN(400),HN(400),ST(4,4,16),FM(400),
     2DF(400),DELH(400),ERR(400),B1(12),B2(12,12),SMD(9),
     3ACOSZ(400),ACOSX(400),ACOSY(400),IBB(400,2),
     4THETA(400),DD(16),GT(6),AJ1(400),AL(400),AM(400),
     5AN(400),GGTL(8,3),GGTM(8,3),GGTN(8,3),AB(6),
     6C2(6),C3(6),CK(6),F4(6),JA1(400)
      COMMON/DATA2/DC,ACOSZ,ACOSX,ACOSY,AJ1,GGTL,GGTM,GGTN
      COMMON/DATA3/DELH
      EQUIVALENCE (Z,DC),(FM,DC(401)),(FC,DC(801)),
     1(DF,DC(1201)),(ERR,DC(1601)),(HN,DC(2001)),
     2(THETA,DC(2401)),(IBB,DC(2801)),(B,DC(4101)),
     3(B1,DC(4125)),(B2,DC(4137)),(N,DC(4301)),
     4 (L4,DC(4302)),(Q1,DC(4303)),(Q2,DC(4304)),
     5(M,DC(4305)),(I,DC(4306)),(L,DC(4307)),(BO,DC(4308)),
     6(SMD,DC(4309)),(SSMD,DC(4320)),(D1,DC(4321)),
     7(D2,DC(4333)),(NUMBER,DC(4100)),(GT,DC(4093)),
     8(AB,DC(4500))
      IF(Z(I).EQ.0.) GO TO 135
      BETA=92.732/66252.
      BETAN=.00054464*BETA
      RD=3.1415926/180.
      R2=SQRT(2.0)
      R3=SQRT(3.0)
      R5=SQRT(5.0)
      R7=SQRT(7.0)
      FACTOR=92.732/66252.
      AL(I)=ACOSZ(I)*GGTL(NUMBER,1)+ACOSX(I)*
     1 GGTL(NUMBER,2)+ACOSY(I)*GGTL(NUMBER,3)
      AM(I)=ACOSZ(I)*GGTM(NUMBER,1)+ACOSX(I)*
     2GGTM(NUMBER,2)+ACOSY(I)*GGTM(NUMBER,3)
      AN(I)=ACOSZ(I)*GGTN(NUMBER,1)+ACOSX(I)*
     3GGTN(NUMBER,2)+ACOSY(I)*GGTN(NUMBER,3)
      FCI=GT(1)*AL(I)**2+GT(3)*AM(I)**2+GT(5)*AN(I)**2
      ENELSP=Z(I)*BETA*SQRT(FCI)
```

```
      BB1=GT(1)*AL(I)**2
      BB3=GT(3)*AM(I)**2
      BB5=GT(5)*AN(I)**2
      BB2=2.*SQRT(GT(1)*GT(3))*AL(I)*AM(I)
      BB4=2.*SQRT(GT(1)*GT(5))*AL(I)*AN(I)
      BB6=2.*SQRT(GT(3)*GT(5))*AM(I)*AN(I)
      AEFF2=AB(1)*BB1+AB(3)*BB3+AB(5)*BB5+
     1 AB(2)*BB2+AB(4)*BB4+AB(6)*BB6
C     AMI=4.5-AJ1(I)
      IF(AEFF2.LT.(0.)) GO TO 109
      AEFF=SQRT(AEFF2/FCI)
C     HYPFEN=AEFF*(AMI-0.5)
      CC1=AB(1)**2+AB(2)**2+AB(4)**2
      CC2=AB(1)*AB(2)+AB(2)*AB(3)+AB(4)*AB(6)
      CC3=AB(2)**2+AB(3)**2+AB(6)**2
      CC4=AB(1)*AB(4)+AB(2)*AB(6)+AB(4)*AB(5)
      CC5=AB(4)**2+AB(6)**2+AB(5)**2
      CC6=AB(2)*AB(4)+AB(3)*AB(6)+AB(5)*AB(6)
      CKK=CC1*BB1+CC3*BB3+CC5*BB5+CC2*BB2+CC4*BB4+CC6*BB6
      AKK=SQRT(CKK/AEFF2)
      DETA=AB(3)*(AB(1)*AB(5)-AB(4)**2)+
     1 AB(6)*(AB(2)*AB(4)-AB(1)*AB(6))+
     2 AB(2)*(AB(4)*AB(6)-AB(2)*AB(5))
      DETA1=SQRT(DETA)/(4.*AEFF*ENELSP)
      AI=1.5
      AI1=AI*(AI+1.)
C     DELE3=(0.5*(AB(1)+AB(3)+AB(5))*(AI1-AMI**2+AMI-0.5)-
C    1 AKK**2*(AI1-3.*AMI**2+3.*AMI-1.5)/2.-
C    2 AEFF**2*(AMI**2-AMI+0.5))/(2.*ENELSP)
      QEFF=B(1,L)*BB1+B(3,L)*BB3-(B(1,L)+B(3,L))*BB5+
     1     B(2,L)*BB2+    B(4,L)*BB4+    B(5,L)*BB6
      QEF=QEFF/FCI
C     HYF=QEF*(2.*AMI-1)
C     FC(I)=ENELSP+HYPFEN+DELE3+DETA1+HYF
      JA1=AJ1(I)
 1001 GO TO (1111,2222,3333,4444,5555,6666),JA1
```

```
1111 AMI=1.5
     GO TO 1110
2222 AMI=0.5
     GO TO 1220
3333 AMI=-1.5
     GO TO 1220
4444 AMI=-0.5
     GO TO 1110
5555 AMI=-0.5
     GO TO 2211
6666 AMI=-1.5
     GO TO 2211
1110 HYPFEN=AEFF*(AMI-0.5)
     HYF=QEF*(2*AMI-1)
     DELE3=(0.5*(AB(1)+AB(3)+AB(5)-AKK**2)*
    1(AI1-AMI**2+AMI-0.5)+(AKK**2-AEFF**2)*
    2(AMI**2-AMI+0.5))/(2.*ENELSP)
     FC(I)=ENELSP+HYPFEN+DELE3+DETA1+HYF
     GO TO 8008
1220 HYPFEN=AEFF*(AMI+0.5)
     HYF=QEF*(2*AMI+1)
     DELE3=(0.5*(AB(1)+AB(3)+AB(5)-AKK**2)*
    1(AI1-AMI**2-AMI-0.5)+(AKK**2-AEFF**2)*
    2(AMI**2+AMI+0.5))/(2.*ENELSP)
     FC(I)=ENELSP+HYPFEN+DELE3-DETA1-HYF
     GO TO 8008
2111 HYPFEN=AEFF*(AMI-1)
     HYF=QEF*(4*AMI-4)
     DELE3=(0.5*(AB(1)+AB(3)+AB(5)-AKK**2)*
    1(AI1-AMI**2+2*AMI-2)+(AKK**2-AEFF**2)*
    2(AMI**2-2*AMI+2))/(2*ENELSP)
     FC(I)=ENELSP+HYPFEN+DELE3+2*DETA1+HYF
     GO TO 8008
2211 HYPFEN=AEFF*(AMI+1)
     HYF=QEF*(4*AMI+4)
     DELE3=(0.5*(AB(1)+AB(3)+AB(5)-AKK**2)*
```

```
     1(AI1-AMI**2-2*AMI-2)+(AKK**2-AEFF**2)*
     2(AMI**2+2*AMI+2))/(2*ENELSP)
      FC(I)=ENELSP+HYPFEN+DELE3-2*DETA1-HYF
      GO TO 8008
 8008 ERR(I)=SQRT(FCI)*DELH(I)*FACTOR
      ERR(I)=1.
      GO TO 136
  135 CONTINUE
      FC(I)=HN(I)
      ERR(I)=1.
  136 CONTINUE
      IF(LX-1)110,110,120
  120 CONTINUE
      DO  235 IZ = 1,12
      D1(IZ) = 0.0
      DO  235 JZ = 1,12
  235 D2(IZ,JZ) =0.0
      IF(Z(I).EQ.0.) GO TO 110
      DDD=(2.*AMI-1)/FCI
      D1(1)=DDD*(BB1-BB5)
      D1(2)=DDD*BB2
      D1(3)=DDD*(BB3-BB5)
      D1(4)=DDD*BB4
      D1(5)=DDD*BB6
      GO TO 110
  109 WRITE(58,108) I
  108 FORMAT(5X,*NEG AEFF2 FOR I*,I3)
      FC(I)=FM(I)
      DO 197 JJ=1,6
  197 D1(JJ)=0.
  110 CONTINUE
      RETURN
      END
      SUBROUTINE EXAM(A,B,M,LF)
C     SUBROUTINE EXAM
C       F O R T R A N  4
```

```
    DIMENSION A(12,12),B(12),C(12)
    DO 80 J=1,M
 80 C(J)=A(J,J)
    IF(A(1,1)) 60,200,70
 60 A(1,1) =-SQRT(-A(1,1))
    GO TO 300
 70 A(1,1) =SQRT(A(1,1))
    GO TO 100
100 IF(M-1)400,400,110
110 DO 115 K=2,M
115 A(1,K)=A(1,K)/(A(1,1)         )
    DO 120 J=2,M
    J1=J-1
    S=A(J,J)
    DO 125 L=1,J1
125 S=S-A(L,J)**2
    IF (S) 50,200,40
 50 A(J,J) =-SQRT(-S)
    GO TO 300
 40 A(J,J) =SQRT(S)
    GO TO 130
130 IF(J-M)135,400,400
135 J2=J+1
    DO 120 K=J2,M
    S=A(J,K)
    DO 145 L=1,J1
145 S=S-A(L,J)*A(L,K)
120 A(J,K)=S/A(J,J)
400 B(1)=B(1)/A(1,1)
    IF(M-1)420,420,405
405 DO 410 J=2,M
    S=B(J)
    J1=J-1
    DO 415 L=1,J1
415 S=S-A(L,J)*B(L)
410 B(J)=S/A(J,J)
```

```
  420 B(M)=B(M)/A(M,M)
      J=M-1
  435 IF(J)450,450,425
  425 S=B(J)
      J2=J+1
      DO 430 L=J2,M
  430 S=S-A(J,L)*B(L)
      B(J)=S/A(J,J)
      J=J-1
      GO TO 435
  450 LF=1
      GO TO 460
  200 LF=0
      GO TO 460
  300 LF=-1
  460 DO 465 J=1,M
      A(J,J)=C(J)
      IF(J-M)470,475,475
  470 J2=J+1
      DO 465 K=J2,M
  465 A(J,K)=A(K,J)
  475 RETURN
      END

      SUBROUTINE MATINV(A,N,B,M,DETERM)
C     SUBROUTINE MATINV
C       F O R T R A N   4
C     MATRIX INVERSION WITH ACCOMPANYING SOLUTION OF LINEAR
C            EQUATIONS
      DIMENSION IPIVOT(12),A(12,12),B(12,1),INDEX(12,2),
     1 PIVOT(12)
      EQUIVALENCE (IROW,JROW),(ICOLUM,JCOLUM),(AMAX,T,SWAP)
      DETERM=1.0
      DO 20 J=1,N
   20 IPIVOT(J)=0
      DO 550 I=1,N
```

```
    AMAX=0.0
    DO 105 J=1,N
    IF(IPIVOT(J)-1)60,105,60
 60 DO 100 K=1,N
    IF(IPIVOT(K)-1)80,100,740
 80 IF(ABS(AMAX)-ABS(A(J,K)))85,100,100
 85 IROW=J
    ICOLUM=K
    AMAX=A(J,K)
100 CONTINUE
105 CONTINUE
    IPIVOT(ICOLUM)=IPIVOT(ICOLUM)+1
    IF (IROW-ICOLUM)140,260,140
140 DETERM=-DETERM
    DO 200 L=1,N
    SWAP=A(IROW,L)
    A(IROW,L)=A(ICOLUM,L)
200 A(ICOLUM,L)=SWAP
    IF(M)260,260,210
210 DO 250 L=1,M
    SWAP=B(IROW,L)
    B(IROW,L)=B(ICOLUM,L)
250 B(ICOLUM,L)=SWAP
260 INDEX(I,1)=IROW
    INDEX(I,2)=ICOLUM
    PIVOT(I)=A(ICOLUM,ICOLUM)
    DETERM=DETERM*PIVOT(I)
    A(ICOLUM,ICOLUM)=1.0
    DO 350 L=1,N
350 A(ICOLUM,L)=A(ICOLUM,L)/PIVOT(I)
    IF(M)380,380,360
360 DO 370 L=1,M
370 B(ICOLUM,L)=B(ICOLUM,L)/PIVOT(I)
380 DO 550 L1=1,N
    IF (L1-ICOLUM)400,550,400
400 T=A(L1,ICOLUM)
```

```
      A(L1,ICOLUM)=0.0
      DO 450 L=1,N
  450 A(L1,L)=A(L1,L)-A(ICOLUM,L)*T
      IF(M)550,550,460
  460 DO 500 L=1,M
  500 B(L1,L)=B(L1,L)-B(ICOLUM,L)*T
  550 CONTINUE
      DO 710 I=1,N
      L=N+1-I
      IF(INDEX(L,1)-INDEX(L,2))630,710,630
  630 JROW=INDEX(L,1)
      JCOLUM=INDEX(L,2)
      DO 705 K=1,N
      SWAP=A(K,JROW)
      A(K,JROW)=A(K,JCOLUM)
      A(K,JCOLUM)=SWAP
  705 CONTINUE
  710 CONTINUE
  740 RETURN
      END

      SUBROUTINE JACOBI2(N,Q,JVEC,M,V)
C     SUBPROGRAM FOR DIAGONALIZATION OF MATRIX Q BY
C                SUCCESSIVE ROTATIONS
      DIMENSION Q(6,6),V(6,6),X(6),IH(6)
C
C     NEXT 8 STATEMENTS FOR SETTING
C            INITIAL VALUES OF MATRIX V
C
      IF(JVEC) 10,15,10
   10 DO 14 I=1,N
      DO 14 J=1,N
      IF(I-J) 12,11,12
   11 V(I,J)=1.0
      GO TO 14
   12 V(I,J)=0.
```

```
   14 CONTINUE
C
   15 M=0
C     NEXT 8 STATEMENTS SCAN FOR LARGEST OFF DIAG. ELEM.
C     IN EACH ROW X(I) CONTAINS LARGEST ELEMENT IN ITH ROW
C     IH(I) HOLDS SECOND SUBSCRIPT DEFINING
C     POSITION OF ELEMENT
C
      MI=N-1
      DO 30 I=1,MI
      X(I)=0.
      MJ=I+1
      DO 30 J=MJ,N
      IF (X(I)-ABS (Q(I,J))) 20,20,30
   20 X(I)=ABS (Q(I,J))
      IH(I)=J
   30 CONTINUE
C
C     NEXT 7 STATEMENTS FIND FOR
C            MAXIMUM OF X(I)S FOR PIVOT ELEMENT
   40 DO 70 I=1,MI
      IF(I-1) 60,60,45
   45 IF (XMAX-X(I)) 60,70,70
   60 XMAX=X(I)
      IP=I
      JP=IH(I)
   70 CONTINUE
C
C     NEXT 2 STATEMENTS TEST FOR XMAX,
C            IF LESS THAN 10**-8,GO TO 1000
C
      EPSI=1.E-12
      IF (XMAX-EPSI) 1000,1000,148
C
  148 M=M+1
C
```

```
C     NEXT 11 STATEMENTS FOR COMPUTING
C             TANG,SINE,COSN,Q(I,I),Q(J,J)
C
      IF (Q(IP,IP)-Q(JP,JP)) 150,151,151
  150 TANG =-2.*Q(IP,JP)/(ABS(Q(IP,IP)-Q(JP,JP))+
     1SQRT((Q(IP,IP)-Q(JP,JP))**2+4.*Q(IP,JP)**2))
      GO TO 160
  151 TANG =+2.*Q(IP,JP)/(ABS(Q(IP,IP)-Q(JP,JP))+
     1SQRT((Q(IP,IP)-Q(JP,JP))**2+4.*Q(IP,JP)**2))
  160 COSN=1.0/SQRT(1.0+TANG**2)
      SINE=TANG*COSN
      QII= Q(IP,IP)
      Q(IP,IP)= COSN**2*(QII+TANG*(2.*Q(IP,JP)+
     1 TANG*Q(JP,JP)))
      Q(JP,JP)= COSN**2*(Q(JP,JP)-TANG*(2.*Q(IP,JP)-
     1 TANG*QII))
C
      Q(IP,JP)=0.
C
C     NEXT 4 STATEMENTS FOR PSEUDO RANK OF THE EIGENVALUES
C      GO TO 897
      IF (Q(IP,IP)-Q(JP,JP)) 152,153,153
  152 TEMP=Q(IP,IP)
      Q(IP,IP)=Q(JP,JP)
      Q(JP,JP)=TEMP
C
C     NEXT 6 STATEMENTS ADJUST
C            SIN, COS FOR COMPUTATION OF Q(I,K),V(I,K)
C
      IF(SINE) 154,155,155
  154 TEMP=+COSN
      GO TO 170
  155 TEMP=-COSN
  170 COSN=ABS(SINE)
      SINE=TEMP
C
```

```
C     NEXT 10 STATEMENTS FOR INSPECTING  THE I"S BETWEEN
C     I+1 AND N-1 TO DETERMINE WHETHER A NEW MAXIMUM VALUE
C     SHOULD BE COMPUTED SINCE THE PRESENT MAXIMUM IS IN THE
C     I OR J ROW
C
  153 DO 350 I=1,MI
      IF (I-IP) 210,350,200
  200 IF (I-JP) 210,350,210
  210 IF (IH(I)-IP) 230,240,230
  230 IF (IH(I)-JP) 350,240,350
  240 K= IH(I)
      TEMP=Q(I,K)
      Q(I,K)=0.
      MJ=I+1
      X(I)=0.
C
C     NEXT 5 STATEMENTS SEARCH
C            IN DEPLETED ROW FOR NEW MAXIMUM
C
      DO 320  J=MJ,N
      IF (X(I)-ABS(Q(I,J))) 300,300,320
  300 X(I)=ABS(Q(I,J))
      IH(I)=J
  320 CONTINUE
      Q(I,K)=TEMP
  350 CONTINUE
C
      X(IP)=0.
      X(JP)=0.
C
C     NEXT 30 STATEMENTS FOR
C             CHANGING THE OTHER ELEMENTS OF Q
C
      DO 530 I=1,N
C
      IF (I-IP) 370,530,420
```

```
  370 TEMP=Q(I,IP)
      Q(I,IP)=COSN*TEMP+SINE*Q(I,JP)
      IF (X(I)-ABS(Q(I,IP))) 380,390,390
  380 X(I)=ABS(Q(I,IP))
      IH(I)=IP
  390 Q(I,JP)=-SINE*TEMP+COSN*Q(I,JP)
      IF (X(I)-ABS(Q(I,JP))) 400,530,530
  400 X(I)=ABS(Q(I,JP))
      IH(I)=JP
      GO TO 530
C
  420 IF (I-JP) 430,530,480
  430 TEMP =Q(IP,I)
      Q(IP,I)=COSN*TEMP+SINE*Q(I,JP)
      IF (X(IP)-ABS(Q(IP,I))) 440,450,450
  440 X(IP)=ABS(Q(IP,I))
      IH(IP)=I
  450 Q(I,JP)=-SINE*TEMP+COSN*Q(I,JP)
      IF (X(I)-ABS(Q(I,JP))) 400,530,530
C
  480 TEMP=Q(IP,I)
      Q(IP,I)=COSN*TEMP+SINE*Q(JP,I)
      IF(X(IP)-ABS(Q(IP,I))) 490,500,500
  490 X(IP)=ABS(Q(IP,I))
      IH(IP)=I
  500 Q(JP,I)=-SINE*TEMP+COSN*Q(JP,I)
      IF (X(JP)-ABS(Q(JP,I))) 510,530,530
  510 X(JP)=ABS(Q(JP,I))
      IH(JP)=I
  530 CONTINUE
C
C     NEXT 6 STATEMENTS TEST FOR
C            COMPUTATION OF EIGENVECTORS
C
      IF (JVEC) 540,40,540
  540 DO 550 I=1,N
```

```
      TEMP=V(I,IP)
      V(I,IP)= COSN*TEMP+SINE*V(I,JP)
  550 V(I,JP)=-SINE*TEMP+COSN*V(I,JP)
      GO TO 40
 1000 RETURN
      END
      SUBROUTINE JACOBI4(N,Q,JVEC,M,V)
C     SUBPROGRAM FOR DIAGONALIZATION OF MATRIX
C                Q BY SUCCESSIVE ROTATIONS
      DIMENSION Q(12,12),V(12,12),X(12),IH(12)
   13 FORMAT (2E15.5)
C
C     NEXT 8 STATEMENTS FOR SETTING
C            INITIAL VALUES OF MATRIX V
C
      IF(JVEC) 10,15,10
   10 DO 14 I=1,N
      DO 14 J=1,N
      IF(I-J) 12,11,12
   11 V(I,J)=1.0
      GO TO 14
   12 V(I,J)=0.
   14 CONTINUE
C
   15 M=0
C     NEXT 8 STATEMENTS SCAN FOR LARGEST OFF DIAG. ELEM.
C     IN EACH ROW X(I) CONTAINS LARGEST ELEMENT IN ITH ROW
C     IH(I) HOLDS SECOND SUBSCRIPT DEFINING
C     POSITION OF ELEMENT
C
      MI=N-1
      DO 30 I=1,MI
      X(I)=0.
      MJ=I+1
      DO 30 J=MJ,N
      IF (X(I)-ABS (Q(I,J))) 20,20,30
```

```
   20 X(I)=ABS (Q(I,J))
      IH(I)=J
   30 CONTINUE
C
C     NEXT 7 STATEMENTS FIND FOR
C            MAXIMUM OF X(I)S FOR PIVOT ELEMENT
   40 DO 70 I=1,MI
      IF(I-1) 60,60,45
   45 IF (XMAX-X(I)) 60,70,70
   60 XMAX=X(I)
      IP=I
      JP=IH(I)
   70 CONTINUE
C
C     NEXT 2 STATEMENTS TEST FOR XMAX,
C            IF LESS THAN 10**-8,GO TO 1000
C
      EPSI=1.E-12
      IF (XMAX-EPSI) 1000,1000,148
C
  148 M=M+1
C
C     NEXT 11 STATEMENTS FOR COMPUTING
C             TANG,SINE,COSN,Q(I,I),Q(J,J)
C
      IF (Q(IP,IP)-Q(JP,JP)) 150,151,151
  150 TANG =-2.*Q(IP,JP)/(ABS(Q(IP,IP)-Q(JP,JP))+
     1 SQRT((Q(IP,IP)-Q(JP,JP))**2+4.*Q(IP,JP)**2))
      GO TO 160
  151 TANG =+2.*Q(IP,JP)/(ABS(Q(IP,IP)-Q(JP,JP))+
     1 SQRT((Q(IP,IP)-Q(JP,JP))**2+4.*Q(IP,JP)**2))
  160 COSN=1.0/SQRT(1.0+TANG**2)
      SINE=TANG*COSN
      QII= Q(IP,IP)
      Q(IP,IP)= COSN**2*(QII+TANG*(2.*Q(IP,JP)+
     1 TANG*Q(JP,JP)))
```

```
      Q(JP,JP)= COSN**2*(Q(JP,JP)-TANG*(2.*Q(IP,JP)-
     1 TANG*QII))
C
      Q(IP,JP)=0.
C
C     NEXT 4 STATEMENTS FOR PSEUDO RANK OF THE E1GENVALUES
      IF (Q(IP,IP)-Q(JP,JP)) 152,153,153
  152 TEMP=Q(IP,IP)
      Q(IP,IP)=Q(JP,JP)
      Q(JP,JP)=TEMP
C     NEXT 6 STATEMENTS ADJUST
C            SIN, COS FOR COMPUTATION OF Q(I,K),V(I,K)
C
      IF(SINE) 154,155,155
  154 TEMP=+COSN
      GO TO 170
  155 TEMP=-COSN
  170 COSN=ABS(SINE)
      SINE=TEMP
C
C     NEXT 10 STATEMENTS FOR INSPECTING  T8E IHS BETWEEN
C     I+1 AND N-1 TO DETERMINE WHETHER A NEW MAXIMUM VALUE
C     SHOULD BE COMPUTED SINCE THE PRESENT MAXIMUM IS IN THE
C     I OR J ROW
C
  153 DO 350 I=1,MI
      IF (I-IP) 210,350,200
  200 IF (I-JP) 210,350,210
  210 IF (IH(I)-IP) 230,240,230
  230 IF (IH(I)-JP) 350,240,350
  240 K= IH(I)
      TEMP=Q(I,K)
      Q(I,K)=0.
      MJ=I+1
      X(I)=0.
C
```

```
C     NEXT 5 STATEMENTS SEARCH
C             IN DEPLETED ROW FOR NEW MAXIMUM
C
      DO 320  J=MJ,N
      IF (X(I)-ABS(Q(I,J))) 300,300,320
  300 X(I)=ABS(Q(I,J))
      IH(I)=J
  320 CONTINUE
      Q(I,K)=TEMP
  350 CONTINUE
C
      X(IP)=0.
      X(JP)=0.
C
C     NEXT 30 STATEMENTS FOR
C              CHANGING THE OTHER ELEMENTS OF Q
C
      DO 530 I=1,N
C
      IF (I-IP) 370,530,420
  370 TEMP=Q(I,IP)
      Q(I,IP)=COSN*TEMP+SINE*Q(I,JP)
      IF (X(I)-ABS(Q(I,IP))) 380,390,390
  380 X(I)=ABS(Q(I,IP))
      IH(I)=IP
  390 Q(I,JP)=-SINE*TEMP+COSN*Q(I,JP)
      IF (X(I)-ABS(Q(I,JP))) 400,530,530
  400 X(I)=ABS(Q(I,JP))
      IH(I)=JP
      GO TO 530
C
  420 IF (I-JP) 430,530,480
  430 TEMP=Q(IP,I)
      Q(IP,I)=COSN*TEMP+SINE*Q(I,JP)
      IF (X(IP)-ABS(Q(IP,I))) 440,450,450
  440 X(IP)=ABS(Q(IP,I))
```

```
      IH(IP)=I
  450 Q(I,JP)=-SINE*TEMP+COSN*Q(I,JP)
      IF (X(I)-ABS(Q(I,JP))) 400,530,530
C
  480 TEMP=Q(IP,I)
      Q(IP,I)=COSN*TEMP+SINE*Q(JP,I)
      IF(X(IP)-ABS(Q(IP,I))) 490,500,500
  490 X(IP)=ABS(Q(IP,I))
      IH(IP)=I
  500 Q(JP,I)=-SINE*TEMP+COSN*Q(JP,I)
      IF (X(JP)-ABS(Q(JP,I))) 510,530,530
  510 X(JP)=ABS(Q(JP,I))
      IH(JP)=I
  530 CONTINUE
C
C     NEXT 6 STATEMENTS TEST FOR
C            COMPUTATION OF E1GENVECTORS
C
      IF (JVEC) 540,40,540
  540 DO 550 I=1,N
      TEMP=V(I,IP)
      V(I,IP)= COSN*TEMP+SINE*V(I,JP)
  550 V(I,JP)=-SINE*TEMP+COSN*V(I,JP)
      GO TO 40
 1000 AAM=FLOAT(M)
      WRITE (58,13) EPSI,AAM
      RETURN
      END
      SUBROUTINE JACOBI3(N,Q,JVEC,M,V)
C     SUBPROGRAM FOR DIAGONALIZATION OF
C               MATRIX Q RY SUCCESSIVE ROTATIONS
       DIMENSION Q(3,3),V(3,3),X(3),IH(3)
   13 FORMAT (2E15.5)
C
C     NEXT 8 STATEMENTS FOR SETTING
C            INITIAL VALUES OF MATRIX V
```

```
C
      IF(JVEC) 10,15,10
   10 DO 14 I=1,N
      DO 14 J=1,N
      IF(I-J) 12,11,12
   11 V(I,J)=1.0
      GO TO 14
   12 V(I,J)=0.
   14 CONTINUE
C
   15 M=0
C     NEXT 8 STATEMENTS SCAN FOR LARGEST OFF DIAG. ELEM.
C     IN EACH ROW X(I) CONTAINS LARGEST ELEMENT IN ITH ROW
C     IH(I) HOLDS SECOND SUBSCRIPT DEFINING
C     POSITION OF ELEMENT
C
      MI=N-1
      DO 30 I=1,MI
      X(I)=0.
      MJ=I+1
      DO 30 J=MJ,N
      IF (X(I)-ABS (Q(I,J))) 20,20,30
   20 X(I)=ABS (Q(I,J))
      IH(I)=J
   30 CONTINUE
C
C     NEXT 7 STATEMENTS FIND FOR
C            MAXIMUM OF X(I)S FOR PIVOT ELEMENT
   40 DO 70 I=1,MI
      IF(I-1) 60,60,45
   45 IF (XMAX-X(I)) 60,70,70
   60 XMAX=X(I)
      IP=I
      JP=IH(I)
   70 CONTINUE
C
```

```
C     NEXT 2 STATEMENTS TEST FOR XMAX,
C            IF LESS THAN 10**-8,GO TO 1000
C
      EPSI=1.E-12
      IF (XMAX-EPSI) 1000,1000,148
C
  148 M=M+1
C
C     NEXT 11 STATEMENTS FOR COMPUTING
C             TANG,SINE,COSN,Q(I,I),Q(J,J)
C
      IF (Q(IP,IP)-Q(JP,JP)) 150,151,151
  150 TANG =-2.*Q(IP,JP)/(ABS(Q(IP,IP)-Q(JP,JP))+
     1 SQRT((Q(IP,IP)-Q(JP,JP))**2+4.*Q(IP,JP)**2))
      GO TO 160
  151 TANG =+2.*Q(IP,JP)/(ABS(Q(IP,IP)-Q(JP,JP))+
     1 SQRT((Q(IP,IP)-Q(JP,JP))**2+4.*Q(IP,JP)**2))
  160 COSN=1.0/SQRT(1.0+TANG**2)
      SINE=TANG*COSN
      QII= Q(IP,IP)
      Q(IP,IP)= COSN**2*(QII+TANG*(2.*Q(IP,JP)+
     1 TANG*Q(JP,JP)))
      Q(JP,JP)= COSN**2*(Q(JP,JP)-TANG*(2.*Q(IP,JP)-
     1 TANG*QII))
C
      Q(IP,JP)=0.
C
C     NEXT 4 STATEMENTS FOR PSEUDO RANK OF THE EIGENVALUES
      IF (Q(IP,IP)-Q(JP,JP)) 152,153,153
  152 TEMP=Q(IP,IP)
      Q(IP,IP)=Q(JP,JP)
      Q(JP,JP)=TEMP
C     NEXT 6 STATEMENTS ADJUST
C            SIN, COS FOR COMPUTATION OF Q(I,K),V(I,K)
C
      IF(SINE) 154,155,155
```

```
  154 TEMP=+COSN
      GO TO 170
  155 TEMP=-COSN
  170 COSN=ABS(SINE)
      SINE=TEMP
C
C     NEXT 10 STATEMENTS FOR INSPECTING  T8E IHS BETWEEN
C     I+1 AND N-1 TO DETERMINE WHETHER A NEW MAXIMUM VALUE
C     SHOULD BE COMPUTED SINCE THE PRESENT MAXIMUM IS IN THE
C     I OR J ROW
C
  153 DO 350 I=1,MI
      IF (I-IP) 210,350,200
  200 IF (I-JP) 210,350,210
  210 IF (IH(I)-IP) 230,240,230
  230 IF (IH(I)-JP) 350,240,350
  240 K= IH(I)
      TEMP=Q(I,K)
      Q(I,K)=0.
      MJ=I+1
      X(I)=0.
C
C     NEXT 5 STATEMENTS SEARCH
C            IN DEPLETED ROW FOR NEW MAXIMUM
C
      DO 320  J=MJ,N
      IF (X(I)-ABS(Q(I,J))) 300,300,320
  300 X(I)=ABS(Q(I,J))
      IH(I)=J
  320 CONTINUE
      Q(I,K)=TEMP
  350 CONTINUE
C
      X(IP)=0.
      X(JP)=0.
C
```

```
C     NEXT 30 STATEMENTS FOR
C                   CHANGING THE OTHER ELEMENTS OF Q
C
      DO 530 I=1,N
C
      IF (I-IP) 370,530,420
  370 TEMP=Q(I,IP)
      Q(I,IP)=COSN*TEMP+SINE*Q(I,JP)
      IF (X(I)-ABS(Q(I,IP))) 380,390,390
  380 X(I)=ABS(Q(I,IP))
      IH(I)=IP
  390 Q(I,JP)=-SINE*TEMP+COSN*Q(I,JP)
      IF (X(I)-ABS(Q(I,JP))) 400,530,530
  400 X(I)=ABS(Q(I,JP))
      IH(I)=JP
      GO TO 530
C
  420 IF (I-JP) 430,530,480
  430 TEMP=Q(IP,I)
      Q(IP,I)=COSN*TEMP+SINE*Q(I,JP)
      IF (X(IP)-ABS(Q(IP,I))) 440,450,450
  440 X(IP)=ABS(Q(IP,I))
      IH(IP)=I
  450 Q(I,JP)=-SINE*TEMP+COSN*Q(I,JP)
      IF (X(I)-ABS(Q(I,JP))) 400,530,530
C
  480 TEMP=Q(IP,I)
      Q(IP,I)=COSN*TEMP+SINE*Q(JP,I)
      IF(X(IP)-ABS(Q(IP,I))) 490,500,500
  490 X(IP)=ABS(Q(IP,I))
      IH(IP)=I
  500 Q(JP,I)=-SINE*TEMP+COSN*Q(JP,I)
      IF (X(JP)-ABS(Q(JP,I))) 510,530,530
  510 X(JP)=ABS(Q(JP,I))
      IH(JP)=I
  530 CONTINUE
```

```
C
C     NEXT 6 STATEMENTS TEST FOR
C             COMPUTATION OF E1GENVECTORS
C
      IF (JVEC) 540,40,540
  540 DO 550 I=1,N
      TEMP=V(I,IP)
      V(I,IP)= COSN*TEMP+SINE*V(I,JP)
  550 V(I,JP)=-SINE*TEMP+COSN*V(I,JP)
      GO TO 40
 1000 AAM=FLOAT(M)
      WRITE (58,13) EPSI,AAM
      RETURN
      END
```